NOVEL ROUTES TO POTENTIAL PACKED BED ABSORBENTS FOR THE DESULPHIDING REACTION

Tom Pringle

M. Phil.

University of Edinburgh

1999

Acknowledgements

I wish to thank the Eric Birse Family Trust for providing the funding for this research and both Prof. Brian F. G. Johnson and Dr. Mike Davidson for ideas, guidance, enthusiasm and support. Also, to IMS and LEELSTART for assistance in establishing 'Dr Bunhead's Science Education' business which has been successful enough to fund the latter days of my research work. I am also indebted to Dr. Jeremy Rawson for his invaluable and patient instruction on practical techniques and most of all for assistance in the interpretation of data in the early part of my work.

At times like this you know who your friends really are. I could not have got through the despair of lab work and the isolated gut-churning misery of writing up without the immense contribution of my friends. "Thanks you lot!" for all your invaluable support in keeping me (in)sane and getting me through this thing, thanks for: making me laugh; crap jokes; cash loans to endlessly bail me out of tight-spots with the bank; singing; dancing; cooking; consoling; counselling; kind words and encouragement; copy cut & pasting; proof-reading; photocopying and too many other things to mention. Huge thanks to (appearing in random order, except where it's non-random) Adam Harvey, Dimitri Mignard, Lucy Kirkham, Naomi Knights, Marc Wilkinson, Judith Procter, Andy Snell, Sophie Whitaker, Sophie Rippinger, Blandine Guillot, Bill Boddington, Gid (Squids) Freeman, Ali (Bongo) Brown, the edible Louise Gee, Riccy, Pants, Squirrel, Mum and all the people I've overlooked (sorry!). I'd need another thesis to individually acknowledge all the things you've done for me... so I shan't bother. I hope none of you ever ask me to repay my debt to you as I'd be here another five years.

Thanks also to Kenny Fee, Rab Kilgour, Tommy Murray, Bobbie Hogg, Matthew Rea in 'Chemeng' and, in 'Chemistry', David Priestley, Stewart Johnstone, Tim Calder, Raymond Borwick, Derek Burgess, Lorna Eades, Alan Taylor, John Millar, Elizabeth Stevenson, Drs Steve Henderson, Richard Winpenny, Andrew Harrison, Gordon McDougal, Simon Parsons and Lesley Yellowlees. Finally, the lovely, ever-smiling, most helpful librarian in the world Anne Pagan.

Abstract

Three interdependent areas of investigation were conducted in order to formulate a repeatable, reliable and simple set of procedures to synthesize, characterize and assess the potential desulphiding ability of the synthesized materials. The exclusion of atmospheric carbon dioxide throughout the sequence of preparation, characterization and assessment and the transfer processes between these stages was a key component of the design strategy and final success of these procedures.

The three areas of investigation were: (i) synthesis of precursor materials; (ii) development of air-free apparatus and regimes for the hydrolysis of precursors and the collection and transfer of hydrolysis products to air-free apparatus for analysis and; (iii) investigation of the properties of the products using purpose built equipment.

The aim of the syntheses was to prepare contaminant free samples of ZnO, $Zn(OH)_2$ or any other structurally modified compounds of zinc which may have activity as desulphiding reagents. The hydrolysis of zinc-based complexes containing oxygen-donor ligands was found to be a productive route to generating such structurally modified compounds of zinc. Basic zinc carboxylates (in particular hexakis(μ-2-acetato-O-O′)-(μ-4-oxo)-tetrazinc, $Zn_4O(O_2CCH_3)_6$) were found to be the simplest to prepare, with good yields and high levels of purity (ascertained by the absence of surface carbonate contaminants). These offered a rich source of structurally novel materials. The preparation of these materials led to the crystallographic determination of the structure of hexakis[μ-(propanato-O:O')]-μ_4-oxotetrazinc, $Zn_4O(O_2CCH_2CH_3)_6$. Two novel acetates of zinc were also discovered by sublimation of the neutral acetate. These have been assigned as the novel acetates $Zn_8O_3(O_2CCH_3)_{10}$ and $Zn_2(O_2CCH_3)_4$. In addition, mass spectral evidence supports the proposed existence of related multi-nuclear propionates.

Amongst other developments in apparatus design, a high-volume, rapid-evacuation glovebox was developed and evaluated. This was used for hydrolysis reactions and transfer to a purpose built air-free, high temperature environment cell (HTEC). The HTEC was designed to house the product for DRIFTS analysis. Consideration of the accuracy of the surface temperature measurement of such devices was made. A facility for near simultaneous analysis of surface spectra and desorbed gas spectra of samples was developed.

Contrary to the current view, that the hydrolysis of $Zn_4O(OAc)_6$ leads to the formation of ZnO, the formation of gelatinous materials other than ZnO was observed. Among the products was the novel material zinc (II) hydroxy acetate, $Zn(OH)(O_2CCH_3)$. A highly reactive absorbent material was also extracted from the product mixture.

Abbreviations Used

Ac ---------- Acetyl (CH_3CO-)
AcO ---------- Acetoxy, acetate or acetato (CH_3COO-)
Bz ---------- Benzoyl (C_6H_5-CO-)
Ct ---------- Crotonyl (CH_3CH=$CHCO$-)
DRIFTS ---------- Diffuse Reflectance Infra Red Fourier Transform Spectroscopy
DSC ---------- Differential Scanning Calorimetry
DTA ---------- Differential Thermal Analysis
EPR ---------- Electron Paramagnetic Resonance
EI ---------- Electron Impact
FAB ---------- Fast Atom Bombardment
Fo ---------- Formyl (HCO-)
FTIR ---------- Fourier Transform Infra Red
IR ---------- Infra-Red
LMCT ---------- Ligand to Metal Charge Transfer
MS ---------- Mass Spectroscopy
Pp ---------- Propionyl (CH_3CH_2CO-)
Pv ---------- Pivalyl ($(CH_3)_3CCO$-)
RCO ---------- Acyl
RCOO ---------- Acyloxy
TGA ---------- Thermogravimetric Analysis
upe ---------- unpaired electron

CONTENTS

CHAPTER 1: INTRODUCTION

Even very low levels of H_2S can poison industrial gas streams, such as natural gas. Natural gas is used extensively, e.g. in reformer feeds, in many domestic appliances and as methanol synthesis gas. On extraction from the earth it contains up to several per cents sulphur-bearing gases. Commercially, packed beds containing high surface-area zinc oxide granules (of approximately 3 mm diameter) are used for the removal of H_2S from such 'sour' gas streams. Zinc oxide is particularly useful in protecting catalysts (particularly nickel-based catalysts) used in the process industry, where total sulphur levels must be less than 1 ppm to prevent sulphur-deactivation of the catalysts. Zinc oxide beds are also suitable for use on off-shore production platforms, being favoured over conventional amine absorbers and regeneration systems. Whilst, ZnO based absorbents are more expensive than systems such as Fe_2O_3, which also have a much higher H_2S absorption capacity, the equilibrium partial pressure of H_2S over ZnO is much lower under similar temperature conditions.[1] Thus, whereas Fe_2O_3 reduces H_2S levels to *ca.* 10 ppm, ZnO removes H_2S to levels below 0.1 ppm. In addition to H_2S, other sulphur-bearing gases, such as COS, MeSH, higher thiols and thiophene, are often contained in sour gas streams . These are less reactive than H_2S and, consequently, more difficult to remove. Desulphurization of such organo-sulphur compounds from petroleum fractions is achieved by use of high temperatures and hydrogen in the presence of a catalyst; this process is known as hydrodesulphurization (HDS), hydrofining or hydrotreating and may be represented generally as below

$$C_xH_yS + nH_2 \rightarrow \text{hydrocarbons} + H_2S \qquad \text{Eqn. 1.1-A}$$

The catalyst usually used in hydrodesulphurization consists of a molybdenum disulphide phase, MoS_2, promoted by the addition of either cobalt or nickel.[2]

1.1 Desulphiding of Sour Gas Streams with ZnO

High surface area, commercial zinc oxide (produced by ICI) is available for a wide range of operating temperatures. For ambient operation the high surface area (30-

1) P. J. H. Carnell, *Catalyst Handbook*, M. V. Twigg ed., Wolfe Scientific, 1988, ch. 4.
2) H. Topsoe, B. S. Clausen, *Catal. Rev.-Sci. Eng.*, 1984, **26**, 395.

110 m^2g^{-1}) zinc oxide is required. The following reaction proceeds to 30-40% conversion for this material[3]

$$H_2S + ZnO \rightarrow H_2O + ZnS \qquad \text{Eqn. 1.1-B}$$

For ordinary catalytic systems the surface composition is fairly uniform throughout the reactor bed. However, for the gas-solid non-catalytic reaction in 1.1-B, which occurs with a progressing frontal zone, this is not the case. In fact, little is known of the kinetics of such gas-solid non-catalytic reactions. In order to develop systems for the removal of the less reactive organo-sulphur compounds (COS, MeSH etc.), it is beneficial to understand mechanistically, the behaviour of the more easily studied H_2S/ZnO system. On the basis of this understanding, it should be easier to develop a model of the behaviour of other organo-sulphur/absorbent systems.

To date, it has been shown that the reaction shown in eqn. 1.1-B is autocatalytic in water.[4] The reaction proceeds rapidly in the first instance, with high ZnO conversions even at 0 ^{O}C and H_2S concentrations of a few ppm. The high surface area of the absorbent is not sufficient to be solely responsible for this high reactivity. This evidence has been interpreted as supporting the working hypothesis that transport phenomena occur within the solid, in spite of the unfavourable increase in molar volume from ZnO to ZnS (increasing from 14.51 to 23.76 cm^3mol^{-1}).[5]

It has been shown that the concentration of H_2S has a negligible effect on the overall reaction rate, i.e. the reaction rate is close to zero-order in H_2S.[4] The variables of greatest importance appear to be surface area, porosity, alteration of the molar volume of the solid phase, defect structure of the solid and, in particular, the exposure of polar faces on ZnO (see section 2.5.1).

Whilst fresh ZnO samples were observed to react rapidly with H_2S, within 20-40 minutes the reactivity markedly decreased leading to a long-lasting pseudo-steady-

---

3) J. M. Davidson, P. J. Denny and C. H. Lawrie, "Autocatalysis by Water in the Reaction of Hydrogen Sulphide with Zinc Oxide", *J. Chem. Soc., Chem. Comm.*, 1989, **21**, 1695-6.
4) C. H. Lawrie, Ph.D. Thesis, Dept. Of Chemical Engineering, University of Edinburgh, 1989.
5) Values calculated from molar masses and densities of ZnO (zincite) and ZnS (blende) from Nuffield Advanced Science Book of Data, Longman Group Ltd., Essex, 1985.

state (PSS). During this PSS stage the differential reaction rate has been measured.[3] The H_2S consumed during the initial fast stage is *ca.* three times greater than that required for mono-layer coverage, and ZnO consumes water which is not stoichiometrically desorbed. It is clear from this that eqn. 1.1-B does not represent the reaction stoichiometry of the fast stage.

Surface hydroxyls observed on the faces of high surface area ZnO have been assigned by comparison with those observed on the low surface area material.[6] Using DRIFTS (see section 2.0.2), these have been shown to exhibit marked variation in their reactivity towards H_2S (at 125 ppm) in a water-free carrier stream.[7] The OH bands broaden and then coalesce with the peak of the product water, as it is transferred from polar to prism face. During sulphiding, a weak SH peak appears. If H_2S treatment is discontinued, OH frequencies slowly reappear and the thiol peaks disappear. It may be inferred from this that surface hydroxyls play a major role in the mechanism of the desulphiding reaction on ZnO surfaces. If this is the case, then a sample of pure $Zn(OH)_2$ should provide exceptionally high conversions of H_2S (above the current 20-35% obtained using commercial ZnO). Also, it should yield interesting information regarding the mechanism of the reaction. To test this theory, a pure sample of $Zn(OH)_2$, free of any surface contaminants, must be prepared.

The activity of ZnO for absorption of H_2S is well known. Screening tests have shown that a few other compounds, especially nickel basic carbonate, $Ni_5(CO_3)_2(OH)_6$, and lead carbonate, $PbCO_3$, also have high activity towards H_2S and COS; interestingly, the lead basic carbonate, $Pb_3(CO_3)_2(OH)_4$, *inter alia*, is inactive.[8] There is scope for synthesis of a wide range of potential absorbents in order to establish and understand the systematic behaviour of these materials. From these, it may be possible to develop versatile, multi-functional, low-temperature absorbents that would match the performance of high temperature HDS followed by H_2S

---

6) K. Atherton. G. Newbold and J. A. Hockey, *Disc. Farad. Soc.*, 1971, **52**, 33.
7) K. Sohail, Ph.D. Thesis, Dept. Of Chemical Engineering, University of Edinburgh, 1992.
8) J. M. Davidson and K. Sohail, "A Low Temperature Reaction of Metal Oxides, Carbonates and Basic Carbonates with Hydrogen Sulphide and Carbonyl Sulphide", IChemE Research Event, Edinburgh, 1995 **1**, 517.

removal. It has also been shown that multi-component oxides, such as doped ZnO, have promise as single-stage absorbents with low-temperature activity,[7] but at present there is little understanding of the chemical kinetics and transport mechanisms which must form the underlying basis for their development. Polydisperse ZnO surfaces always contain hydroxyl groups on the surface, and residual carbonates both on the surface and in the bulk.[6] A route to carbonate and hydroxyl-free ZnO would thus be of great benefit in furthering the study of the H_2S + ZnO reaction. To date, no preparative route has been shown that will yield carbonate-free ZnO surfaces.

1.2 Present Experimental Programme

The work conducted in this research project is part of a larger, on-going body of work conducted by a number of researchers. The overall aims and objectives of this body of research are wide-ranging and include the following projects.

(i) Development of new absorbents for gaseous substances, such as carbonyl sulphide, alkane thiols and thiophene. The objective is to achieve simultaneous decomposition and absorption in single beds at low temperature.

(ii) Investigating the mechanism and kinetics of H_2S absorption as a guide for work on less reactive gases such as COS and CH_3SH and as an aid in the design of new absorbents.

(iii) Improving the range of capabilities of present apparatus to yield further insight into the desulphiding of sour gas streams. For example, the DRIFTS cell would be improved by the implementation of a computer controlled mirror system to divert the infrared beam through a gas cell for H_2S, CO_2 and H_2O analysis.

The current work exists within this research programme. Its aim is to develop methodology and apparatus for the preparation, characterisation and testing of novel, potential packed-bed absorbents for the desulphiding reaction. More specifically, the objectives of this research were to:

- Develop routes for the preparation of impurity-free ZnO samples (preferably of high surface area), in which porosity, dispersion and surface area have been modified in a repeatable and characterisable manner.
- Devise a procedure for the synthesis of $Zn(OH)_2$ free of extraneous anions such as chloride, sulphide and carbonate.
- Develop apparatus for the preparation, handling and analysis of such ZnO and $Zn(OH)_2$ samples.

1.3 Preparation of Oxides

Reviewing the appropriate literature reveals that whilst routes exist for the formation of high surface area materials of definite porosity and dispersion it has not been possible to prepare entirely contaminant-free, high surface area materials. The reasons for this are discussed below.

For most practical purposes, where a large specific surface area is essential, polycrystalline or amorphous samples are desirable. Experience has shown that, in general, low-temperatures are necessary to obtain oxides of large surface-areas or small particle sizes. However, methods can be developed, such as in the preparation of aerogels,[9] in which high temperatures *are not* used. A low-temperature treatment does not necessarily lead to the formation of the thermodynamically most stable phase. Instead, depending on the details of the preparation procedure, metastable phases and/or amorphous samples may be obtained. Unfortunately, there is currently little understanding of the reasons behind the formation of a particular phase, and each case must be treated individually. A low-temperature treatment can lead to the formation of hydrous oxides, if the precursors were manufactured by an aqueous precipitation technique. The water in these hydrous oxides can be removed by treatment at elevated temperatures. However, this treatment is, *ipso facto*, no longer low temperature.

---

9) C. J. Brinker and G. W. Scherer, *Sol-Gel Science, The Physics and Chemistry of Sol-Gel Processing*, Academic Press Inc., Boston, 1990.

For many practical purposes, where the available surface area is critical, the oxides are commonly prepared by the decomposition, in air or oxygen, of precursor compounds containing the desired metal ion. Usually, preference is given to precursor compounds that decompose at low temperatures; this is to minimise sintering of the resulting oxide, which leads to low surface-area. Carbonates, bicarbonates, hydroxides, nitrates and oxalates are usually preferred over sulphates for this reason. The decomposition may also be carried out *in vacuo* to lower the decomposition temperatures. The desired precursor compounds can usually be obtained by precipitation from aqueous solutions of the readily available compounds. When the readily available compounds of some elements (such as titanium) are not soluble in water, hydrolysis of nonaqueous solutions or direct vapour-phase oxidation of some compounds may be employed.

ZnO may be prepared at high temperature by ignition of zinc in an oxidising atmosphere; a three dimensional crystalline sample of a low surface area is obtained.[10] Electron microscopy shows that the sample consists of crystallites of about 700 nm long and 300nm wide, exposing the prismatic face on the long side, and the polar faces on the short side. Small crystals grown from vapour transport take the form of needles of hexagonal cross section, about 0.1 cm long and 0.0001 cm in diameter. The long side exposes the prismatic face. A powder, prepared from $ZnCO_3$, precipitated from a nitrate solution with sodium carbonate, followed by washing and conversion to oxide by calcining, has a high surface-area of approximately $36 m^2 g^{-1}$. The resulting oxide contains hexagonal platelets about 15 mm across. The polar face represents about 33% of the exposed surface. A powder prepared by the decomposition of zinc acetate contains particles grown mostly along the (0001) orientation, while that prepared by the decomposition of zinc formate mostly contains particles grown along the $(11\bar{2}0)$ direction.[11] The surface area of ZnO prepared by the decomposition of $ZnCO_3$ precipitated from a nitrate solution depends on the calcination procedure. If the water trapped in the precipitate is removed efficiently during heating of the precipitate($ZnCO_3$), a high surface area

10) M. Bowker, H. Houghton, K. C. Waugh, *J. Catal.*, 1983, **84**, 252.
11) G. Djega-Mariadasson and L. Davignon, *J. Chem. Soc., Farad. Trans. 1*, 1982, **78**, 2447.

sample (above 30 m^2g^{-1}) is obtained. Otherwise, the surface area is much lower (10 m^2g^{-1} or lower). The calcining of hydrozincite, $Zn_5(CO_3)_2(OH)_6$, at 653 K in a dry nitrogen stream also yields high surface area ZnO.[12] Klissurski *et al.*[13] were able to attain a surface area of 62 m^2g^{-1} for zinc oxide produced by the decomposition of hydrozincite at 250-270^{O}C.

In all the above preparative routes, residual species (particularly carbonate and hydroxyl and, sometimes, other metal ions) are to be found on the surface and, usually, in the bulk of the ZnO sample. A different approach is, therefore, required if impurity-free polycrystalline samples are to be prepared. This research presents a novel attempt to the formation of contaminant-free, high surface area samples of materials such as ZnO.

1.4 The Specific Research Approach

An alternative approach is required for the preparation of high surface-area contaminant-free ZnO samples. A possible method is the hydrolysis of readily hydrolysed zinc salts which yield ZnO and a highly soluble salt. Two types of salt which behave in this manner are the basic carboxylates and alkoxides of zinc. For example, it has been reported that basic zinc acetate $Zn_4O(O_2CCH_3)_6$, also known as zinc oxyacetate, breaks down in water to yield ZnO and $Zn(OAc)_2.2H_2O$.[14,15,16]

$$Zn_4O(O_2CCH_3)_{6\,(s)} + xs\ H_2O_{(l)} \rightarrow ZnO_{(s)} + 3\ Zn(O_2CCH_3)_2.2H_2O_{(aq)} \qquad \text{Eqn. 1.4-A}$$

The preparation of $Zn_4O(O_2CCH_3)_6$ and other hydrolysable precursors provides the basis of this synthetic approach to creating new absorbents. Such methods benefit from the absence of other metal ions and the possibility of conducting air-free

12) J. M. Davidson and K. Sohail, "A DRIFTS Study of the Surface and Bulk Reactions of Hydrogen Sulphide with High Surface Area Zinc Oxide.", *Ind.Eng. Chem. Res*, 1995, **34**, 3675 - 3677.
13) D. Klissurski, I. Uzunov and K. Kumbilieva, "Preparation of Highly Dispersed Zinc Oxide by Thermal Decomposition of Basic Zinc Carbonate", *Thermochimica Acta*, 1985, **93**, 485 488.
14) H. Kunkely and A. Vogler, "Absorption and Emission Spectrum of $[Zn_4O(Acetate)_6]$",*J. Chem. Soc., Chem. Com.*, 1990, 1204-1205.
15) R. M. Gordon and H. B. Silver, "Preparation and Properties of tetrazinc μ_4-oxohexa-μ-carboxylates (basic zinc carboxylates)", *Can. J. Chem.*, 1983, **61,** 1218-1221.
16) H. Koyama and Y. Saito, *Bull. Chem. Soc. Jpn.*, 1954, **27**, 112.

hydrolysis experiments in which ambient CO_2 has been excluded, furthering the likelihood of achieving materials free of these contaminants.

In addition, the precursors themselves show interesting desulphiding activity. Neutral zinc (II) carboxylate, the precursor to $Zn_4O(OAc)_6$, has been shown to be a satisfactory preventative against H_2S contamination.[17] Furthermore, a brief examination of the desulphiding activity of the fresh hydrolysate from $Zn_4O(OAc)_6$ showed it to be more active than the commercially available ICI ZnO absorbent.[18] However, this activity declined rapidly over 24 hours, suggesting a high degree of reactivity. Such highly active compounds are usually difficult to handle but are interesting and may prove to be rewarding. Thus, developing air-free handling techniques for the hydrolysis of $Zn_4O(OAc)_6$ and the subsequent analysis of the hydrolysate was one of the key components of this research.

The choice of precursors was limited to those which were expected to yield the sparingly soluble (in water) ZnO or $Zn(OH)_2$ plus a by-product which should be readily soluble in water, to facilitate easy separation and purification of the desired product. The use of $Zn_4O(OAc)_6$ is ideal in this respect since its hydrolysis (eqn. 1.4-B) has been reported to yield the highly soluble neutral acetate, $Zn(O_2CCH_3)_2.2H_2O$. Thus, the use of basic carboxylates as precursors was restricted to acetic and propionic derivatives since zinc (II) butanoate and higher derivatives are water insoluble and basic zinc formate has not been prepared.

The alkoxides of interest were zinc (II) methoxide, $Zn(OMe)_2$, and zinc (II) ethoxide, $Zn(OEt)_2$. The hydrolysis of these materials was expected to yield $Zn(OH)_2$ (and methanol or ethanol, respectively). These materials were of particular interest due to the, anticipated, ready removal of the alcohol to yield impurity-free $Zn(OH)_2$. References to $Zn(OH)_2$ synthesis[19,20] provide no indication that atmospheric CO_2 has

---

17) *Compt. Rend. Congr. Ind. Gaz., Paris (Assoc. Tech. Ind. Gaz. France)*, 1948, **65**, 139-41.
18) J. M. Davidson and C. Lawrie, unpublished results, Dept. of Chem. Eng., University of Edinburgh, 1989.
19) G. Brauer, "Handbüch Präp. Anorg Chem." (English Version), 3rd Ed., Ferdinand Enke Verbg., 1975-1981.
20) A. N. Christensen, *Acta. Chem. Scand.*, 1969, **23**, 2016-2020.

been in any way excluded. Consequently, it was anticipated that the prepared samples would incorporate CO_2, thereby forming surface carbonate species; this expectation was confirmed by this research. The synthesis of carbonate-free $Zn(OH)_2$ would be of great interest, both in understanding the rôle of hydroxyl species in the $ZnO + H_2S$ reaction, and as a source of impurity-free ZnO by thermal dehydration of the hydroxide. In addition, the alkoxides, themselves, may have interesting desulphiding activity for species such as thiols.

The specific objectives of this research were, therefore:

(a) To use existing routes to known basic zinc carboxylates and alkoxides and to improve them, where possible.

(b) To attempt to prepare novel basic zinc carboxylates, both for their academic interest and for use as further precursors to potential novel absorbents.

(c) To develop apparatus specifically for the air-free hydrolysis of powdered samples of carboxylates and alkoxides.

(d) To hydrolyse these basic zinc carboxylates and alkoxides, to investigate whether this reaction could serve as a novel route to contaminant-free ZnO (or $Zn(OH)_2$ or other, zinc-based materials with potential desulphiding activity).

(e) To develop other novel routes to potentially contaminant free ZnO (or Zn(OH) or other, zinc-based materials with potential desulphiding activity).

(f) To refine the capabilities of the DRIFTS apparatus towards a system which permits simultaneous analysis of both the sample surface and the exiting gas stream. To enhance the ease of operation of the DRIFTS for conducting analysis of samples handled under air-free conditions.

These specific objectives have, on the whole, been met and, in some cases,extended. Additional research findings have also accrued from the pursuit of these objectives. The results are reported in chapters 3 and 4.

CHAPTER 2: LITERATURE REVIEW

The function of this chapter is to review the background literature for the methods and materials used in this research. To this end, this review will examine the pertinent chemistry of;

- The precursors used,
- The absorbent materials produced from these precursors and
- The surface species expected to interact with, and interfere with the behaviour of, precursors and absorbent materials.

The materials under examination are, principally, the following oxygen-donor zinc species: alkoxides, carbonates, carboxylates, oxides and hydroxides. The behaviour, as surface species, of carbon dioxide, carbonates and hydroxides will also be covered. Within this section, particular attention will be given to the characteristics of these compounds and species which enable them to be unambiguously distinguished and characterised. The main techniques used for characterising these materials are also reviewed (in this case, mostly infrared techniques). The use of non-contact infrared thermometry was explored during this research, hence this technique is also reviewed.

Examination of the structural variety of known examples of the above materials provides a useful platform for their introduction. Structural comparisons and predictions can then be proposed for any materials synthesised using the methodologies developed in this research. This will be of particular use where such materials elude characterisation by single crystal X-ray crystallography. To this end, the following section details the *physical properties* for each type of material under examination. Given that certain physical characteristics, such as high surface area and diffusivity, favour a substance's use as an absorbent in the desulphiding reaction, then a clear understanding of how to manipulate the precursors towards the desired structural form is also essential. Consequently, a *chemical properties* section is also included. Having produced a novel, potential absorbent material for the desulphiding reaction, some means of spectro-physio-chemical characterisation of

the absorbent is required. This will enable an absorbent's properties (chemical reactivity) to be related to its physical structure, so that a clearer understanding of the *modus operandi* of the absorbent may be achieved. Characterisation will also provide a means of ensuring repeatable results are obtained for any given route to an absorbent material. The most common means of such evaluation is through the use of readily available and amenable spectral techniques, such as infrared spectroscopy and mass spectrometry. Thus, a more in-depth analysis of the particular spectral properties of the individual groups of materials with regard to these techniques is given. This serves to show where, and how, unique characterisation of the materials may be achieved most readily. Thus, physical, chemical and spectral properties are addressed in each of the material sections in this chapter.

Although this study is primarily concerned with oxygen-donor zinc species, related complexes of other metals have also been used. Hence, where they serve to highlight areas of particular relevance to this study, they are also discussed. Since the majority of the research is centred on the preparation of zinc carboxylates, the following review contains a more detailed consideration of these, and related materials, than any other.

2.0 Analytical Techniques

2.0.1 Infra Red Spectroscopy of Bulk Materials

Almost every undergraduate-level general chemistry text contains a consideration of the basic principles of infrared spectroscopy. There are also numerous other texts and reviews available covering the subject in far greater depth.[1,2,3,4,5,6,7,8]

Consideration of the practical limitations and extensions to the basic method now follow. The following sections describe the practical manner by which the most useful information may be obtained from this technique. The sections examine detection of infrared spectra from bulk samples:

(i) Maximising the intensity of absorption bands

(ii) Preparing samples: the pressed salt method

For the analysis of surface species, more refined techniques are required. These are covered in section 2.0.2.

2.0.1(i) Maximising the Intensity of Absorption Bands

The ability to detect an absorption band in either transmission spectroscopy or reflection spectroscopy depends on the absolute magnitude of the intensity as the peak is scanned. If I_0 is the incident intensity and I the transmitted intensity at a particular frequency, the value of $\log_{10}(I_0/I)$ is termed the *absorbance* at that frequency. For homogeneous liquids or solids it is proportional to the path length (thickness), d. For substances in solution, or in the gas phase, it is also proportional to the concentration, c. A *molecular absorptivity* or *extinction coefficient*, ε, can be defined by the relation (Beer-Lambert law)

---

1) J. M. Hollas, *Modern Spectroscopy*, 2nd ed., Wiley, Chichester, 1992.
2) R. Chang, *Basic Principles of Spectroscopy*, McGraw-Hill, 1971.
3) L. H. Little, *Infrared Spectra of Adsorbed Species*, Academic Press, New York, 1966.
4) J. Pritchard and T. Catterick "Infrared Spectroscopy" in *Experimental Methods in Catalytic Research*, R. B. Anderson and P. T. Dawson Eds., **15-III**, Academic Press, New York, 1976, pp. 281-317.
5) R. P. Eischens and W. A. Pliskin "Infrared Spectra of Adsorbed Molecules" in *Advances in Catalysis and Related Subjects*, D. D. Eley, W. G. Frankenburg and V. I. Komarewsky Eds., **X**, Academic Press, New York, 1958, pp. 2-56.
6) C. N. Banwell, *Fundementals of Molecular Spectroscopy*, McGraw Hill, London, 1983.
7) K. Nakamoto, *Infrared and Raman Spectra of Inorganic Coordination Compounds*, 4th ed., Wiley, New York, 1986.
8) A. A. Davydov, *Infrared Spectroscopy of Adsorbed Species on the Surface of Transition Metal Oxides*, Wiley, Chichester, 1984.

$$\log_{10}(I_o/I) = \varepsilon cd \qquad \text{Eqn. 2.0.1-A}$$

with c expressed in mol litre^{-1} and d in cm. The peak values of ε vary widely, e.g. the very strong bands of the CO stretching vibrations in metal carbonyls give values of about 10^3 Lmol^{-1} cm^{-1}, while C-H bands of saturated hydrocarbons are considerably weaker, with ε in the range 10-10^{-2} Lmol^{-1} cm^{-1}.

Since absorption bands may be broadened by interactions with rotational transitions or with neighbouring molecules, as well as often being distorted in practice by inadequate spectrometer resolution, the peak extinction coefficient does not have as fundamental a significance as does the integrated intensity:

$$(1/cd) \int \log_{10}(I_0/I)dv \qquad \text{Eqn. 2.0.1-B}$$

The integration covers the full frequency range (cm^{-1}) of the band envelope. The integrated band intensities of particular groups are often remarkably constant, despite large variations in the bandwidth. Values for a number of adsorbed species have been collected by Little.[3] From the practical point of view of being able to detect a weak band, it is clearly more desirable to have a sharp band with a large extinction coefficient than a broad band of low coefficient even if the integrated intensity is the same.

The sensitivity of transmission experiments cannot be increased continuously by increasing the thickness of the sample. A limit is set by the absorption and scattering of radiation by the adsorbent itself, so that with increasing samples thickness the adsorbate absorption band becomes a larger and larger fraction of a smaller and smaller amount of available energy (*"law of diminishing returns"*). Thus, the absolute magnitude of a given absorption band passes through a maximum with increasing sample thickness. It can be shown that whenever the background absorption (or scattering) is large compared to the absorption band, the absolute signal is maximised when the thickness is sufficient to reduce the background level to 1/e, or 37%, of the initially incident level. Exactly the same consideration applies to reflection spectroscopy. Multiple reflections may improve the sensitivity of experiments with single-crystal surfaces , but only up to the point that reflection

losses reach 63% of the original radiation level.[9] In both transmission and reflection experiments, the ultimate sensitivity is likely to be determined by the noise inherently present in the detector.

An alternative to the extinction coefficient, ε, is preferred in physical optical calculations for absorbing media. The 'absorption index', k, is employed. Together with the refractive index, n, it defines the complex refractive index, $\mathbf{n} = n - ik$, where k is a measure of the attenuation of radiation per vacuum wavelength, λ, in a pathlength, d, and is related to I_0 and I by

$$I = I_0 \exp(-4\pi kd/\lambda) \qquad \text{Eqn. 2.0.1-C}$$

For the strong CO stretching bands of metal carbonyls in the 2000 cm^{-1} region, the value of k is around unity, whereas, for hydrocarbons in the C-H stretching frequency range ($\approx$ 3000 cm^{-1}), it is typically about 0.05.

2.0.1(ii) Preparing Samples: the Pressed Salt Method

The pressed-salt method has attained widespread application in studies of the transmission infrared spectra of solids. In this method, the solid sample is usually, but not always, mixed with a powdered halide salt such as KI or KBr, and the mixture is pressed into a disk at high pressures.[10,11,12] Inherent in this method are conflicting experimental considerations, in that a thick disk is required to make it self-supporting and a thin disk is required to permit the transmission of adequate infrared radiation through the sample to afford a reasonably intense spectrum. As a consequence the pressing of disks is, to a large degree, a matter of trial, error and experience.

Intensity losses are not only due to transmission phenomena, scattering also plays a large rôle. The intensity of transmitted light is also reduced by scattering phenomena. When infrared radiation is incident upon a particle it may undergo refraction, reflection and diffraction. If the wavelength of the radiation is

9) R. G. Greenler, *J Chem. Phys.*, 1969. **50**, 1963-1968.
10) E. S. Cooke, C. W. Kreke, E. B. Barnes and W. Motzel, *Nature*, 1954, **174**, 1144.
11) M. M. Stimson and M. J. O' Donnell, *J. Am. Chem. Soc.*, 1952, **74**, 1805.
12) U. Scheidt and H. Reinwein, *Z. Naturforsch*, 1952, **7b**, 270.

comparable to that of the particle size then these three processes become indistinguishable and are simply referred to collectively as scattering. The Beer-Lambert relationship (Eqn. 2.0.1-C) quantifies the extent of transmission through a sample but does not account for scattering by the sample. The degree of scattering, for a single component system, is given by:

$$S \propto r^3 \nu^a \qquad \text{Eqn. 2.0.1-D}$$

where S is the Rayleigh or Mie scattering undergone by a light beam impinging upon the surfaces of randomly oriented particles, which is dependant upon the cube of the particle radius, r, and the frequency of the light source, ν, to the power $a \leq 4$.[13] Examination of Eqn. 2.0.1-D reveals that scattering may be reduced by decreasing the particle size, by grinding the material under examination, for example. However, at higher wavenumbers the scattering losses are considerably increased. An alternative method to reduce scattering is to introduce a filler with a similar refractive index to that of the material under investigation; alkyl halides are most commonly employed for this purpose. This method reduces scattering because solid-gas interfaces are replaced by solid-salt interfaces. When this method is used, the particle size of the solid is no longer of critical importance. Unfortunately, alkyl halides can act as serious contaminants to some systems and are also susceptible to halide exchange with the anion of the salt under investigation.

Further disadvantages to the pressed disk method occur with *in situ* studies due to diffusional constraints. If an adsorbate's spectrum exhibits coverage dependant effects,[14,15] anomalous effects may occur due to unexpected local adsorbate concentration variations. Diffusion may also limit the effectiveness of pretreatments such as reduction and out-gassing. Although it is simple experimentally, the pressed salt method remains limited in its application in catalysis and related fields, because once the sample is embedded in the salt, it cannot be subjected to further treatment.

---

13) G. Kortüm, *Reflectance Spectroscopy; Principles, Methods and Applications*, Springer-Verlag, Berlin, 1969, p. 79.
14) W. Erley and H. Wagner, "Thermal Desorption of CO on a Stepped Ni Surface", *Surf. Sci.*, 1978, **74**, 337.
15) T. Engl and G. Ertl, *Adv. Catal.*, 1979, **28**, 1.

2.0.2 Infrared Spectroscopy of Surfaces

The use of infrared spectroscopy has been greatly extended in the last two decades to become a powerful technique in surface chemistry, where it is widely used to identify species at solid surfaces.[5] At one extreme it can be applied to single-crystal metal surfaces under ultrahigh vacuum conditions; at the other, it can be used to observe surface intermediates during catalytic reactions on porous oxides or supported metals. Although its experimental requirements have been modest in comparison with many other methods of surface investigation it is often capable of providing more insight into the chemical nature of the surface layer.

In many cases infrared spectroscopy may be effectively employed to study the surface properties of disperse oxide systems, such as those examined in this research. The main advantage of the method is the possibility of obtaining information on almost every possible state present on the surface: surface hydroxyl groups, oxygen and coordinatively unsaturated cations. Non-homogeneity of each type of centre (caused by oxide polydispersity), associated with the formation of multifarious exposed crystallographic planes, and even sample defects can often be reliably assigned using infrared spectroscopy.

In the surface infrared spectra of oxides, surface metal-oxygen vibrations, occurring in the region above the crystal lattice vibrations, are due to M-O bonds of different strength and reactivity. The presence of surface metal cations, which are coordinatively unsaturated to different extents, is highlighted by the appearance of different characteristic absorptions due to M-O group vibrations. This feature is beneficial when attempting to ascertain the presence of metal impurities in the prepared oxide/hydroxide material. These are, almost inevitably, present, due to the nature of most preparative routes; an example being the precipitation of $Zn(OH)_2$ by the addition of NaOH to $ZnSO_4$, which imparts the $Zn(OH)_2$ surface and bulk with traces of Na^+ SO_4^{2-} ions.

This technique is highly informative when applied to the description of surface hydroxyl-hydrate coverage of oxide systems due to their contact with water and

saturation of 'dangling bonds'[16] with hydroxyl groups. The resultant spectrum consists of several absorptions, due to both M-O bond vibrations and surface hydroxyl groups, reflecting the non-homogeneity of these surface sites. It should be noted, however, that criteria for comparative investigation during examination of the state of hydroxyl groups on oxide surfaces are still lacking. Nevertheless, molecules of different chemical nature, which specifically interact with certain surface sites and possess spectral parameters sensitive to the electronic properties of their adsorbate site, yield information on the chemistry of all manner of centre and their distribution.

The identification of surface species by infrared spectroscopy has been based, generally, on the recognition of group frequencies, or on what often amounts to the same thing, the matching of the surface spectra with one of those of known compounds. The frequencies in adsorbed molecules may be expected to parallel those of molecules in liquids and gases provided they are remote from the dense band of low-lying lattice vibrational frequencies of adsorbed molecules, producing an upward shift in certain frequencies clear of the lattice band. Relatively few spectra of adsorbed species have been recorded in the lower frequency ranges, however, because of experimental difficulties.

The exact position of a characteristic group frequency often provides evidence for the environment of the group. Frequency shifts due to substitution in adjacent environments are well documented for ordinary molecules. Similar effects may appear in the spectra of adsorbed species, either as an influence of the adsorbent itself or of the adsorbed groups.

The early work of Eischens and his collaborators[17] showed that conventional transmission infrared spectrophotometers could be used to record spectra of species at the surfaces of oxide powders or of metals dispersed on oxide powder supports. Thin layers of the finely powdered materials were sufficiently transparent in the infrared region. Such spectra provided very direct chemical information. For

16) J. A. Duffy, *Bonding, Energy Levels and Bands in Inorganic Solids*, Longman, Essex, 1990, p.192.
17) R. P. Eischens and W. A. Pliskin, *Advan. Catal.*, 1958, **10**, 1-56.

example, the acidic character, Lewis or Brønsted, of silica-alumina cracking catalysts could be inferred from the spectrum of adsorbed ammonia and was shown to depend on the degree of surface dehydration. Similarly, absorption bands in the range 1800-2100 cm^{-1} were observed in a study of chemisorbed carbon monoxide on platinum, palladium, nickel and copper. These bands were similar to those of transition metal carbonyl complexes and were assigned to terminal (linear) or bridging carbonyl groups with the carbon atom bonded to the surface metal atoms. Frequency shifts, or the growth of new bands with increasing coverage, provided evidence for interaction between adsorbed molecules and for the existence of alternative chemisorption states.

Sometimes, infrared bands that are forbidden for molecules in the gas phase on grounds of symmetry may appear when the molecule is adsorbed and perturbed by surface forces. In early studies of physical adsorption on porous glass, Sheppard and Yates[18] observed bands due to the stretching vibration of H_2 and the symmetric stretching vibration of CH_4. These vibrations produce no dipole oscillations in the gas phase and are, therefore, inactive in the infrared spectrum. This adsorption activity was attributed to dipoles induced by the electric fields associated with the partially ionic glass surface.

These early applications of surface infrared spectroscopy were successfully extended to cover a wide variety of adsorption and catalytic systems as attested by the many reviews and books on the topic [3,8,19,20,21] Of particular importance to this research project were those techniques which provide infrared data from powders, and other porous materials of high specific surface area, through to those which allow low-area samples, such as evaporated metal films, to be studied. Both areas have intrinsic problems. The surfaces of high-area materials are often very heterogeneous. A supported metal catalyst, for example, contains crystallites exposing a variety of

---

18 N. Sheppard and D. J. C. Yates, *Proc. Roy. Soc. London*, 1956, **A238**, 69-89.
19 M. L Hair, *Infrared Spectroscopy in Surface Chemistry*, Decker, New York, 1967.
20 A. T. Bell in *Vibrational Spectroscopy of Molecules on Surfaces*, J. T. Yates, Jr. And T. E. Madey Eds., Plenum Press, New York, 1987.
21) G. Kortüm, *Reflectance Spectroscopy; Principles, Methods and Applications*, Springer-Verlag, Berlin, 1969.

facets, edges, corners, steps and interphase boundaries. The spectra of molecules absorbed at all these sites may contribute to the measured spectrum and render it very difficult to interpret. On the other hand, low surface area materials present a problem of sensitivity. This is one reason why the majority of infrared studies continue to be based on transmission through porous materials. However, it is now possible to obtain highly informative spectra of surface species. The techniques of greatest interest in this area, for the research under discussion, were:

(i) Pressed disk method for obtaining surface spectra

(ii) Evaporated thin films

(iii) DRIFTS

of which, the DRIFTS technique proved to be the most useful and facile in the production of meaningful surface spectra.

The full potential of infrared spectroscopy for the study of practical catalyst surfaces will only be realised when reference spectra of well-defined systems are available. Spectra of adsorption states on individual faces of single crystals, for example, are now being obtained with the aid of reflection techniques. For the purposes of this research the spectra obtained were compared with those of other authors in order to attempt to define them.

2.0.2(i) Pressed Disk Method for Obtaining Surface Spectra

For strong chromophores, particularly hydroxyl and carbonyl, it is possible to observe surface species in the normal transmission infrared spectrum, without the use of any particularly elaborate refinements. Using such techniques, Anderson *et al.*[22], Peri and others[23,24,25] demonstrated that the infrared spectrum of the surface hydroxyls carried on oxide surfaces reflects the structure of the corresponding surface layers of the solid. This work was extended by Atherton *et al.*[26] to

22) P. J. Anderson, R. F. Horlock and J. F. Oliver, *Trans. Faraday Soc.*, 1965, **61**, 2754.
23) J. B. Peri, *J. Phys. Chem.*, 1965, **69**, 220.
24) J. B. Peri and A. L. Hensley, Jr., *J. Phys. Chem.*, 1968, **72**, 2962.
25) C. G. Armistead, A. J. Tylor, F. H. Hambleton, S. A. Mitchell and J. A. Hockey, *J. Phys. Chem.*, 1969, **73**, 3947.
26) K. Atherton, G. Newbold and J. A. Hockey, " Infrared Spectroscopic Studies of Zinc Oxide Surfaces", *Disc. Farad. Soc*, 1971, **52**, 3354.

demonstrate which specific surface hydroxyl vibrations corresponded to which particular underlying adsorption site. In spite of their crude infrared apparatus (by today's standards), Atherton *et al.* obtained detailed correlations of structure with infrared absorption frequency.

This simple technique has been extended to gain much useful information about the nature of surface species. For example, it has been used to estimate typical values for the adsorption of a single monomolecular layer. These may be obtained by employing Eqn. 2.0.1-A, in which the product, *cd*, is more conveniently expressed in units of molecules per unit area. The corresponding numerical values of ε in units of cm^{+2} $molecules^{-1}$ are obtained from the previous molar values by dividing by 6×10^{20}, giving $\varepsilon \approx 10^{-18}$ cm^2 $molecules^{-1}$ for carbonyls and 10^{-20} - 10^{-19} cm^2 $molecules^{-1}$ for CH bands, as examples. Similar values have been obtained for chemisorbed CO on metals (e.g., Pt/SiO_2 $\varepsilon = 2 \times 10^{-18}$ cm^2 $molecules^{-1}$ [27]) and oxides (e.g., ZnO $\varepsilon = 5.5 \times 10^{-18}$ cm^2 $molecules^{-1}$).[28]

These values may then be used to estimate typical values for the adsorption of a single monomolecular layer. For example, a complete chemisorbed CO layer on a metal surface and a complete layer of physically adsorbed ethane molecules will have similar densities of about 6 x 10^{14} molecules cm^{-2}. Using extinction coefficients of 2×10^{-18} and 9×10^{-20} cm^2 $molecules^{-1}$ gives absorptions of 0.28 and 0.013%, respectively. As it is desirable to have minimum adsorption levels of several percent in order to record good quality spectra with standard infrared spectrometers, it is common practice to employ porous absorbent samples such that the infrared beam may pass through hundreds or thousands of monolayers. Spectra can then be recorded at low fractional surface coverages. However, the detection of spectra from monolayer or submonolayer quantities of adsorbate on smooth single-crystal or polycrystalline surfaces is experimentally very demanding, and it is not surprising that most experiments directed to this end have involved strongly absorbing species such as CO or formic acid. For weaker chromophores the surface

---

27) H. J. Heyne and F. C. Tompkins, *Proc. Roy. Soc. London A*, 1966, **292**, 460-478.
28) D. A. Seanor and C. H. Amberg, *J. Chem. Phys.*, 1965, **42**, 2967-2970.

vibrations are usually too small to observe against the bulk spectrum of the pressed disk. To overcome this lack of surface sensitivity other techniques have been developed, two of which are now discussed.

2.0.2(ii) Evaporated Thin Films

The disadvantages of the pressed-disk method for metals led to the exploration of methods using evaporated films deposited on transparent substrates such as CaF_2 or NaCl. Eischens and Plisken[18] reported experiments with CO adsorption on platinum films, but their films were not prepared under ultrahigh vacuum conditions. Films may be produced by evaporating metal wires or beads and allowing the vapour to condense on a cool substrate in an ultra high vacuum. Whilst many other techniques exist for the preparation of thin films,[29] evaporation techniques have been extensively used for chemisorption investigations.[30]

Most materials to be evaporated are used in the molten state in order to attain reasonably high deposition rates. The support for the evaporant can be a filament of a high melting point metal. Attachment of evaporant to support is usually achieved by means of simply wrapping around the filament, forming into hooks or placing in a filament basket. Spot welding is also sometimes employed.[31] Boats of tungsten, tantalum or molybdenum are frequently employed[34,32] with special arrangements developed for the evaporation of low[33,34,35] and high[36] melting point metals. Filaments and boats are usually heated by resistance heating, while r-f induction or radiation is employed to heat the evaporant contained in ceramic crucibles. In all

---

29) K. H. Behrndt, "Preparation of Thin Films" in *Thin Films; Papers presented at a Seminar of the American Society for Metals*, Chapman and Hall, London, 1963, pp. 1-44.
30) J. R. Anderson, *Chemisorption and Reactions on Metallic Films*, Academic Press, New York, 1971.
31) L. Holland, *Vacuum Deposition of Thin Films*, John Wiley and Sons, New York, 1956.
32) W. Espe, *The Evaporation of Thin Films in High Vacuum*, Ergebn Hochvakuum Phys dünner Schichten, Wiss Verlagsges, Stuttgart, 1957, 67.
33) H. L. Caswell and J. R. Priest, *Vacuum Evaporator for the Fabrication of Multilayer, Thin Film Devices*, Trans. 9th Natl. Vacuum Symp. 1962, MacMillan Co., New York, 1962, 138.
34) E. M. Da Silva, "Evaporation Source with Controlled Characteristics", *Rev. Sci. Instr.*, 1960, **31**, 959.
35) A. L. Learn and R. S. Spriggs, "Vapor Sources for Vacuum Deposition of Superconductive Thin-Film Circuitry", *Rev. Sci. Instr.*, 1963, **34**, 179.
36) F. E. Hemmer and J. R. Piedmont, "Vacuum Evaporation Source with Double-Wall Cylindrical Graphite Heater and Nozzle Outlet", *Rev. Sci. Instr.*, 1962, **33**, 1355.

these techniques, the danger of the evaporation of the support material is inherent.[37,38] Sublimation from a wire reduces this possibility since the evaporant is in contact with the support merely at a few points.[39,40,41] However, this technique is feasible only for materials with relatively high vapour pressures in the solid state. Evaporation from the liquid state is possible by electron bombardment of the tip of the evaporant wire. The molten material, kept together by surface tension, is not in contact with any support, and contamination is entirely avoided.[42,43,44,45,46] However, thermal conduction and cooling of the evaporant wire must be high enough to prevent increasing the size of the liquid drop to a point where the surface tension could no longer keep it affixed to the wire. The correct selection of the diameter of the wire, rate of feed and electron bombardment current were shown to be critical parameters in achieving stable operation.

Having achieved stable operating conditions the repeatable creation of a defined surface film is required. In this context, the properties of the deposited film are known to vary depending upon the evaporation conditions used. In a high vacuum, say 10^{-6} Torr, the number of gas molecules arriving at the substrate would be sufficient to build a monatomic layer per second (if the sticking coefficient were one). However, at elevated substrate temperatures, the desorption probability is appreciably enhanced and only a fraction of the arriving molecules will adhere to the

---

37) K. H. Behrndt, "The Influence of the Deposition Parameters on the Properties of Thin Ferromagnetic Films", Trans. 8th Natl. Vacuum Symp. 1961, Pergamon Press, London, 1962, 912.
38) K. H. Behrndt, "Influence of The Deposition Conditions on Growth and Structure of Evaporated Films", *Vacuum*, 1963, **13**, 337.
39) K. H. Behrndt and R. A. Jones, "A Comparison Between the Evaporation Characteristics of a Crucible and A Ring Source", Trans. 5th Natl. Vacuum Symp. 1958, Pergamon Press, London, 1959, 217.
40) K. H. Behrndt, "An Evaporator for the Controlled Deposition of Films over Large Substrate Areas", Trans. 7th Natl. Vacuum Symp. 1960, Pergamon Press, London, 1961, 137.
41) K. H. Behrndt, "Large Area Sources and Two-Source Control", Trans. 6th Natl. Vacuum Symp. 1959, Pergamon Press, London, 1960, 242.
42) N. Milleron, "Continuous Evaporation of Refractory Metals by Elecrtron Bombardment Without Using Support Materials", Trans. 4th Natl. Vacuum Symp. 1957, Pergamon Press, London, 1958, 148.
43) D. M. Hart, "A Demountable Glass Vacuum System Using Electron Bombardment in the Vacuum Deposition of Ferromagnetic Films", Trans. 5th Natl. Vacuum Symp. 1958, Pergamon Press, London, 1959, 230.
44) D. W. Moore, "Research and Production Potentialities of Electron Bombardment Evaporation", Trans. 6th Natl. Vacuum Symp. 1959, Pergamon Press, London, 1960, 181.
45) J. C. Kelly, "Electron Bombardment Apparatus for Vacuum Evaporation", *J. Sci. Instr.*, 1959, **36**, 89.
46) O. S. Heavens, "Evaporation of Metals by Electron Bombardment", *J. Sci. Instr.*, 1959, **36**, 95.

surface. Since deposition rates of 10 As^{-1} can easily be attained and, depending upon the material, much higher rates are possible, the ratio of metal atoms to gas molecules on the substrate can be 10, 100 or even greater. Under common *glow discharge* conditions of 10^{-2} Torr or even higher pressures, with deposition rates of 10 As^{-1}, many more gas molecules than metal atoms arrive. Glow discharge differs from conventional *sputter coating* (a ballistic deposition technique where the metal sample is heated in a vacuum and as it evaporates the atoms "fly off" and settle on any available surface. The term glow discharge arises from the glow of the plasma formed under the given operating conditions. Since ions are now formed these may be electrostatically accelerated and directed towards the required surface. Although most of the gas molecules leave the surface again (the sticking probability of the noble gases must be orders of magnitude smaller than that of "reactive" gases), it is still possible that the surface migration of the metal atoms would be disturbed by collisions with the gas molecules, and this process could affect the thin film formation. It was observed by Baker *et al.*[47] that the structure of the thin film is likely to control the magnitude of the absorption spectrum. They showed that the infrared spectrum of carbon monoxide on thin vacuum-deposited metal films could be obtained by transmission through a single film, provided that the film was deposited at a low temperature, and that it was sufficiently thin.

It is known that small particle sizes and large surface areas are obtained when films are deposited on substrates at low temperatures, and so porous films of large specific surface area can be produced using evaporation techniques. Since the fresh surface is treated *in vacuo* the problems of reduction or of cleaning an initially contaminated surface are avoidable. Stringent vacuum conditions must be met for this to be true, however. The infrared cell must be fully bakeable. Glass cells with periclase or sapphire windows are convenient, but the windows restrict the wavelength range severely.

---

47) F. S. Baker, A. M. Bradshaw, J. Pritchard and K. W. Sykes ., "Infrared Spectra of Carbon Monoxide Adsorbed on Vacuum Deposited Metal Films", *Surf. Sci.*, 1968, **12**, 426-436.

Unfortunately, the large specific areas of porous films cannot be fully exploited in transmission spectroscopy. Only very thin films (≤ 10 nm) are suitable: thicker films absorb or reflect too strongly. The total surface area within the infrared beam is therefore limited to a small multiple of the beam area, resulting in a very poor sensitivity compared with supported metals. Harrod *et al.*[48] used a cell in which a stack of thin-film-coated plates could be assembled in order to enhance the sensitivity. Extending the work of Baker *et al.*,[50] Bradshaw and Pritchard used a simple glass cell with periclase windows to study CO and N_2 adsorption on nickel films under ultra-high vacuum conditions.[49,50] As in the earlier work of Baker *et al.*, under less satisfactory vacuum conditions, the best spectra were obtained with films deposited at low temperatures and sufficiently thin to give transmission of about 70% at 2000 cm^{-1}. Films of this thickness were found to be structurally discontinuous, consisting of a large number of nuclei beginning to connect into a continuous film. If the transmission was below 50% the absorption bands were small and difficult to observe against the spectrometer noise. Thicker films, although sufficiently transparent, gave no spectra with absorbed CO. This result was ascribed to the requirement that the oscillating dipole have a component in the direction of the electric vector of the radiation, a condition that would not be satisfied by linearly adsorbed CO on a smooth metal surface perpendicular to the infrared beam. In their experimental procedure the cell was evacuated for several hours via a trap at 77 K. The metal to be evaporated was then reduced in hydrogen at *ca.* 1 Torr for 30 minutes to remove surface oxides, and subsequently outgassed for one hour. Cooling of the infrared plate was achieved by conduction; the fluorite plate was attached to a liquid nitrogen well. By this means a plate temperature of 170 K was attained. The bare film spectra were recorded while the substrate was still cold. The effect of warming the films to room temperature was to lose some of the absorption at the high frequency end of the spectrum, leaving the lower CO band unchanged. Essentially the same procedure is commonly employed to this day.

---

48) J. F. Harrod, R. W. Roberts, and E. F. Rissman, *J. Phys. Chem.*, 1967, **71**, 343-352.

49) A. M Bradshaw and J. Pritchard., "Infrared Spectra of Carbon Monoxide on Evaporated Nickel Films", *Surf. Sci.*, 1969, **17**, 372-386.

50) A. M Bradshaw and J. Pritchard., " An Infrared Study of the Adsorption of Nitrogen on Thin Nickel Films", *Surf. Sci.*, 1970, **19**, 198-204.

Whilst far greater sensitivity, compared with the pressed disk method, is achieved by evaporation techniques there is a trade-off between that and the greatly increased requirements of the experimental set-up, in particular the need for good vacuum conditions and cryogenic operation.

2.0.2(iii) Theoretical Basis of Diffuse Reflectance Infrared Fourier Transform Spectroscopy (DRIFTS)

To take the DRIFTS spectrum of a powder, the sample is placed in a shallow cup and exposed to a beam of infrared radiation. The incident radiation passes into the bulk of the sample, undergoing reflection, refraction and absorption before emerging at the sample surface. In transmission spectroscopy, for thin samples, most of the light passes through with only small losses due to scattering and the additional (desired) losses due to the absorption of infrared radiation by the sample (Fig. 2.0.2-A).

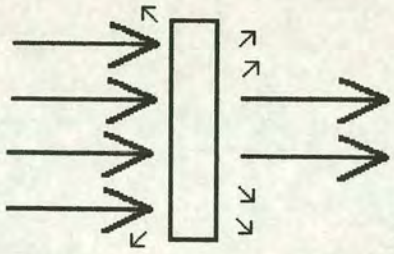

Figure 2.0.2-A Schematic representation of the passage of light through a 'thin' sample in transmission spectroscopy

The degree to which the scattered light is detected depends upon the sampling aperture of the detector and its optics. For a thicker sample, the transmitted beam will be reduced, and a higher proportion of the radiation will be scattered or absorbed. For a sufficiently thick sample, no radiation will reach the back surface, and, instead, will either be absorbed or exit via the front surface (Fig. 2.0.2-B). This diffusely scattered radiation is the detected quantity in DRIFTS. The diffusely reflected radiation from the sample is collected by a spherical or elliptical mirror and focused onto the detector of the spectrometer.

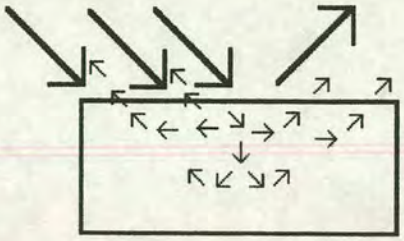

Figure 2.0.2-B Schematic representation of the passage of light through a 'thick' sample in diffuse reflectance spectroscopy

As previously stated, the fundamental equation describing the processes of transmission spectroscopy is the Beer-Lambert law (Eqn. 2.0.1-A). However, this does not account for other intensity losses due to phenomena such as diffuse reflectance. Thus, a different theoretical basis is required to model the behaviour of materials under diffuse reflectance conditions. The interpretation of diffuse-reflectance spectra is based on the phenomenological theory developed by Kubelka and Munk.[51] This approach assumes that all the radiation within the sample can be resolved into two fluxes taken to propagate in positive and negative x direction. Fluxes in all other directions of the (theoretically) infinitely extended sample are assumed to be returned to the $\pm$ x direction by scattering without absorption. Mathematical consideration of this model leads to the well-known Kubelka-Munk remission function:

$$K/S = F(R_\infty) = (1 - R_\infty)^2 / (2R_\infty) \qquad \text{Eqn. 2.0.1-E}$$

which relates the experimentally determined diffuse reflectance of a sample of "infinite" thickness, R_∞, to the parameters K and S, which account, respectively, for losses due to absorption and scattering of the incident radiation flux. This expression is useful for spectroscopy studies as long as S is independent of $\tilde{\nu}$, the absorption frequency, so that the only dependence on $\tilde{\nu}$ is through K. The condition of infinite sample thickness, R_∞, required for DRIFTS is approximated by samples of adequate thickness. Fuller[52,53] has shown that for samples greater than 2 mm in

51) P. Kubelka and F. Munk, *Z. Tech. Phys.*,1931, **12**, 593.
52) M. P. Fuller, PhD thesis, Ohio University, 1980.

depth the approximation holds, due to the rapid rise of $F(R_\infty)$ with sample thickness. For a comprehensive account of the mathematics involved in processing the DRIFTS signal, as well as all other fundamental aspects of this science, the book by Kortüm[24] is recommended.

2.0.2(iv) Diffuse Reflectance Infrared Fourier Transform Spectrometers

Due to the comparatively weak exiting signal of the DRIFTS system the signal-collectors used for DRIFTS must be orders of magnitude more sensitive than those for transmission spectroscopy. Signal to noise ratio is improved by using multiple scans (greatly facilitated by computer-based processing of Fourier transformed signals), resulting in much greater scanning times to obtain DRIFTS spectra than for ordinary transmission spectra. In older systems, this renders real-time spectra (e.g. for studying surface reactions which are complete in under 20 seconds or so) difficult to achieve. Older systems, such as the Digilab FTS-7 ex BioRad used for this research are also hindered by the mechanically mounted mirror systems. Newer systems employ air bearings for their mirror systems, greatly reducing scanning times, though increasing equipment costs. The most recent systems, such as the Digilab FTS 6000, employ air bearings and *dynamic alignment* of the mirror systems (using piezo-electric mirror-alignment compensating devices) which increase by a factor of *ca.* 100 the signal to noise ratio of otherwise identical FTIR devices. Coupled with increased computer capacity, such new systems are able to obtain single scan spectra in 10-15 ms. To obtain the equivalent spectra on older apparatus would require a factor of up to 10^4 times longer, using the same scanning frequencies. Thus, thermal desorption spectra are routinely collected on the newer devices. In spite of this, much useful information may be extracted from the careful use of older systems.

2.0.2(v) DRIFTS Signal Collectors

Two types of detector are available for mid-IR scanning use with DRIFTS. The first is the Deuterated Tri-Glycine Sulphate (DTGS) detector. This runs at room

---

53) M. P. Fuller and P. R. Griffiths in *Advances in Infrared and Raman Spectroscopy*, R. J. H. Clark and R. E. Hester Eds., 1982, **9**, 63.

temperature (cooled by an internal thermo-electric device) and only requires a normal purged-air environment. However, it is relatively slow to scan (maximum scanning frequency is 5 kHz), although it is, nominally, able to scan down to 200 cm^{-1} (though this requires special polythene windows due to spectral cut-off of the normal detector window). Although it does not require liquid nitrogen cooling, it is about 50-100 times less sensitive than MCT detectors, and so requires many more scans to observe weak surface absorptions, and may not be capable of detecting some surface adsorbed species.

The second type of detector for mid-IR scanning is the mercury cadmium telluride (MCT) detector, of which there are at least three types (referred to as A, B and C). This detector has a far greater sensitivity than the DTGS system due to improved signal to noise ratio and faster scanning frequency (maximum scanning frequency 20 kHz; about 4-12 times as fast as DTGS systems). The three MCT detector types have different scanning abilities such that low wavenumber cut-off is compromised against higher sensitivity at higher frequencies. All three types can scan up to 6000 cm^{-1} (and some up to 7500 cm^{-1}), although this may be limited by spectral cut-off from other system components. Type A detectors are capable of scanning down to 450 cm^{-1} and type C down to 750 cm^{-1}. MCT detectors must be liquid nitrogen cooled to operate satisfactorily.

2.0.2(vi) The Influence of Moisture on DRIFTS Spectra

It is generally observed that moist samples are darker than dried samples. Moisture also effects the nature of the observed spectra. The scattering power of a small particle is known to depend upon the ratio of the particle size to wavelength and on the ratio of the refractive indices of the particles, n, and the surrounding medium n_0.[24] This is also true for multiple scattering and so, if the pores of a dried powder are filled by water vapour and then by capillary condensed water, the ratio n/n_0 and the scattering coefficient decrease and $F(R_\infty)$ increases. In an experiment on K_2CrO_4 and NaCl (which are readily water soluble), and Cr_2O_3 and CaF_2 (which are only slightly water soluble), [54] it was found that highly dried samples of Cr_2O_3 diluted

54) G. Kortüm, W. Braun and G. Herzog, *Agnew. Chem.*, 1963, **75**, 653; Internat. Ed., 1963, **2**, 333.

with CaF_2 with water-vapour-saturated air for long periods enhanced the band intensities, but left the band positions unaltered. This effect was found to be almost completely reversible. The great difficulty in completely removing condensed water from the smallest pores may explain why the reversibility was not complete . However, when using K_2CrO_4 diluted with NaCl the analogous spectral changes were no longer found to be reversible. This may be the result of recrystallization effects causing grain enlargement (in order to minimize surface free energy). Such effects are not reversible by drying. Sometimes a powder pressed loosely into a DRIFTS cell forms a solid disk under the influence of moist air. This is an indication that such recrystallization has occurred.

These considerations present some practical problems when using DRIFTS. For example, water-insoluble diluents should be used wherever possible. For quantitative measurements, sophisticated experimentation is required to exclude moisture at every stage of sample preparation (grinding, loading etc.) and analysis. For qualitative measurements the use of flowing dried nitrogen in the DRIFTS cell cavity is sufficient precaution.

Whilst having some disadvantages, especially in set-up requirements, DRIFTS offers several advantages over pressed disk methods and evaporation techniques. Since DRIFTS does not require the compression of powder into a self-supporting disk, materials difficult to compress (e.g., TiO_2, certain zeolites, etc.) can be readily examined. The sensitivity of DRIFTS to surface species is far greater than that of transmission and evaporative techniques. It is also comparatively simple to set up, being several times faster than evaporation techniques to set up, but several times slower in general than the technique of transmission through pressed disks.

In the course of this research it was found that the pressed disk method was too insensitive to clearly observe the surface species of interest, although it was the simplest to set up and obtain repeatable results from. Evaporative techniques were found to be fraught with difficulties. Even obtaining a usable coating of metal proved to be non-trivial. However, this was, in large part, due to lack of experience

in this area. The necessary time investment to improve this method to a reliable, repeatable level was given over to other methods, where results were more readily forthcoming. On balance, the advantages of DRIFTS outweighed those of other methods for the purposes of this research, in spite of its labour intensive set-up and handling requirements. With persistence and application of rigorous and careful handling procedures, repeatable and useful results were obtained.

2.0.3 Temperature Measurement of Samples

The use of the DRIFTS cell required temperature measurements to be made of the material under test. It was important that the surface temperature measured corresponded with the temperature at the observed reaction site. This turned out to be less simple than anticipated and some development work was done on this problem. It is an inevitable consequence of heating a sample at any part of its surface that temperature changes, ΔT, will occur across the sample. Since the accurate measurement of temperature is an important component in the on-going interests of this research an appropriate review is included here, as an introduction to the development work conducted; reported in section 3.2.1.

The International Measuring System sets up independent standards for only four fundamental quantities: length, time, mass and temperature. Standards for all other quantities are derived from these. Temperature is fundamentally different in nature from length time and mass in that it is an *intensive* quantity whereas the others are *extensive*.[55] That is, if two bodies of the same length are combined the new length is twice the original, likewise for two time intervals or two masses. However, this is not true for two bodies of the same temperature being combined, since the result is that the bodies remain at the same temperature. Thus, the idea of a standard unit of mass, length or time that can be divided indefinitely to generate any arbitrary magnitude of these quantities cannot be carried over to the concept of temperature. Also, even though statistical mechanics relates temperature to the mean kinetic energies of molecules, these energies (which are dependent on only mass, length and

55) R. P. Benedict, *Fundamentals of Temperature, Pressure, and Flow Measurements*, 2nd ed., Wiley, New York, 1977.

time standards for their description) are not measurable at present. Thus, an *independent* temperature standard is required.

The fundamental meaning of temperature is not easily given. For most purposes the zeroth law of thermodynamics gives a useful concept: For two bodies to be said to have the same temperature, they must be in thermal equilibrium; that is, when thermal communication is possible between them, no change in the thermodynamic coordinates of either occurs. The zeroth law states that when two bodies are in thermal equilibrium with a third body, they are in equilibrium with each other. Then, by definition, the bodies are all at the same temperature. Thus, if a reproducible means of establishing a range of temperatures can be established, then unknown temperatures of other bodies may be compared with the standard by subjecting any type of "thermometer" successively to the standard and to the unknown temperatures and allowing equilibrium to occur in each case. That is, the thermometer is calibrated against the standard and afterward may be used to read unknown temperatures.

The thermodynamic temperature scale[56] proposed by Lord Kelvin in 1848 provides the theoretical basis for temperature scale independent of any material property and is based on the Carnot cycle. It can be shown that a temperature scale defined by a constant-volume or constant-pressure gas thermometer using an ideal gas is identical to the thermodynamic scale.[57] However, this scale is not a physically realisable temperature scale since real gases must be utilised in the gas-thermometers. This may be corrected for by using extremely tedious and time-consuming methods, which are impractical for everyday use. The situation has led to the acceptance in 1927 of the International Practical Temperature Scale which has been set up to conform to the thermodynamic scale as closely as possible; ITS-90 provides the latest version of this agreement. All temperature measuring methods are calibrated with respect to primary or secondary fixed temperatures (such as the triple-point of water). The actual instrument usually then requires the "thermometer" to be brought

56) F. W. Sears, *Thermodynamic, Kinetic Theory and Statistical Mechanics*, Addison-Wesley, Reading, Mass., 1950.
57) *Ibid.*, p. 116

into physical contact with the body whose temperature is to be measured. This has certain disadvantages such as thermal lag (especially in fast kinetic experiments) and temperature gaps across solids, a problem which occurred in the DRIFTS apparatus , as discussed in section 3.2.1. In order to overcome the problems of thermal lag and temperature gaps the use of non-contact temperature measurement, using infrared thermometry, was investigated. To appreciate the degree to which infrared thermometry may be capable of overcoming these problems an understanding of its basic operating principles is necessary. The following section addresses this need.

2.0.3(i) Radiation Temperature Sensors

In addition to the lack of thermal lag and temperature gaps when using non-contact radiation-temperature sensors, other advantages include the ability to span interfering atmospheres, "see around corners" and to isolate system electronics from hostile sensing environments by employing flexible fibre optics, although such systems work best at high temperatures (using silicon detectors, since fibre transmission is limited to the shorter wavelengths). Of the non-contact systems available infra red thermometry (more precisely '*radiometry*') was chosen for investigation due to its quoted, high levels of accuracy, ready availability and relatively modest costs. It was hoped that the infra-red thermometer would provide accurate and instantaneous measurement of a variety of solid samples in the DRIFTS cell.

There are three fundamental interferences which limit the accuracy of the infra-red thermometer. These are;

1) Sight path transmission,
2) Emissivity and
3) Background reflection,

each of which is considered separately below.

2.0.3(ii) Sight Path Transmission

This source of error occurs due to energy losses in transmitting the radiation from the measured object to the detector. Usually the optical path consists of some gas (often atmospheric air) and various windows, lenses or mirrors used to focus the radiation.

In atmospheric air the attenuation of radiation is due mainly to the resonance-absorption bands of water vapour, carbon dioxide and ozone, as well as the scattering effects of dust particles and water droplets. For a given concentration of light-absorbing species, shorter path lengths give narrower and weaker absorption bands. Since absorption varies with thickness of the gas traversed by the radiation, the effect is not an instrument constant and cannot be calibrated out. Fortunately, the absorption also varies with wavelength and so certain "windows" of negligible absorbency exist. Radiation thermometers are designed (usually) to respond only within one of these atmospheric windows, within which radiation is neither absorbed nor emitted, making them insensitive to these effects.

The lenses must also be made of special materials, since glasses normally utilised for the visible spectrum are almost opaque to radiation of wavelength longer than about 2 μm (the visible spectrum covers about 0.3 to 0.72 μm and the infrared spectrum covers from 0.72 to 1,000 μm). Common infra-red thermometer window materials are silicon, germanium and lead sulphide. Different windows are used for different temperature ranges, each of which utilises a different infra-red operating frequency.

2.0.3(iii) Emissivity

Radiation-temperature sensors operate with electromagnetic radiation whose wavelengths lie in the infrared and visible portions of the spectrum. Physical bodies (solids, liquids, gases) may emit electromagnetic radiation or subatomic particles for a number of reasons. As far as temperature sensing is concerned, only the part of radiation solely due to temperature is of interest. Every body above absolute zero in temperature emits radiation dependant upon its temperature. The ideal thermal radiator is called a *black body*. Such a body would absorb completely any radiation falling on it and, for a given temperature, emit the maximum amount of thermal radiation possible. The law governing this ideal behaviour is the Planck function, which defines W_λ, the amount of energy radiated at a given wavelength for a black body at a given temperature

$$W_\lambda = \frac{C_1}{\lambda^5 \cdot \left(e^{C_2/\lambda T} - 1\right)^{-1}}$$

Equation 2.0.3-A The Planck function

where C_1 = 37,413 W μm^4 cm^{-2} ; C_2 = 14,388 μm K ; W_λ = hemispherical spectral radiant intensity, W cm^{-2} μm^{-1} ; λ = wavelength of radiation, μm ; and T = absolute temperature of black body, K. C_1 and C_2 are derived from fundamental constants. The exact form of C_1 depends upon the geometrical specifications used in its calculation.

From Eqn. 2.0.3-A it can be seen that a black body emits some radiation per unit wavelength at every wavelength from zero to infinity, but not the same amount at each wavelength. For any given temperature a black body has a peak given by λ_{max}, as seen in Fig. 2.0.3-A below.

If the wavelength of light being observed is small, then the term $e^{C_2/\lambda T}$ is much greater than 1 and so the bracketed 1 in the denominator of Eqn. 2.0.3-A can be ignored. This reduces the equation to the simpler Wien Function (Eqn. 2.0.3-B).

$$W_\lambda = \frac{C_1}{\lambda^5 \cdot \left(e^{-C_2/\lambda T}\right)}$$

Eqn. 2.0.3-B The Wien Function

Provided the wavelength of interest is below λ_{max} of the target temperature, then Wien's Law applies and the simpler Wien function may be used. For example, a black body at 300K has $\lambda_{max} \approx 10\mu m$, so for calculation with $\lambda = 6\mu m$ the inaccuracies in the Wien function are negligible, as $\lambda << \lambda_{max}$. On the other hand, for a black body at 1,000K $\lambda_{max} \approx 3\mu m$ and a calculation using $\lambda = 6\mu m$ would require the use of the full Planck function. While the concept of a black body is a mathematical abstraction, real physical bodies can be constructed to approximate black body behaviour. However, some bodies are found to deviate considerably from such ideal behaviour. The deviation from black body radiation is expressed in terms of the *spectral emittance*, ϵ (or ε_λ), of the measured body, of which several types have been defined to suit particular applications. Strictly speaking, spectral

emittance (sometimes referred to as simply emittance) is the ratio of the radiance at wavelength, λ, emitted by a target, to that emitted by a black body at the same temperature. The measured signal is also lower than that predicted by Wien's Law due to attenuation by lenses and sight path interferences, such as the particular lens being used on the radiometer. This attenuation is a constant for the given set up and is expressed as the *emissivity*, ε, of the whole system. Emissivity may be defined as the ratio of the signal of a radiometer on a given target to that on a black target at the same temperature. Hence, emissivity is a "broadband" quantity related to the operating waveband of a particular radiometer, whereas emittance is monochromatic and relates only to the target. Consequently, for a very narrow band radiometer wavelength, λ, the emissivity is equal to the spectral emittance, ε_λ. Mathematically:

$$\varepsilon = \frac{\int \varepsilon_\lambda . \tau(\lambda).r(\lambda).B(\lambda,T).d\lambda}{\int \tau(\lambda).r(\lambda).B(\lambda,T).d\lambda} \qquad \text{Eqn. 2.0.3-C}$$

where $\tau(\lambda)$ is the spectral transmission of the radiometer optics, $r(\lambda)$ is the spectral responsivity of the radiometer detector and $B(\lambda,T)$ is the Planck Function (as given by Eqn. 2.0.3-A). In literature there is a tendency for the term emissivity to be used loosely for both emissivity and spectral emittance.

If a radiation thermometer has been calibrated against a black body source, knowledge of the appropriate emittance value allows correction of its readings for non-black body measurements. Unfortunately, emittance values are not simple material properties such as densities, but rather depend on size, shape, surface roughness, angle of viewing etc. This leads to uncertainties in the numerical values of emittance values, which are one of the main problems in radiation temperature measurement. Real objects are characterised by emittance $\in$, reflectance r and transmittance t, which are related by

$$\in = 1 - r - t \qquad \text{Eqn. 2.0.3-D}$$

When r or t, or both, are non-zero, there is non-black body behaviour and measurement errors are possible. Most commercial radiation thermometers include

an emissivity adjustment with a range from about 0.2 to 1.0. Thus, if material emissivity is known it can be compensated for.

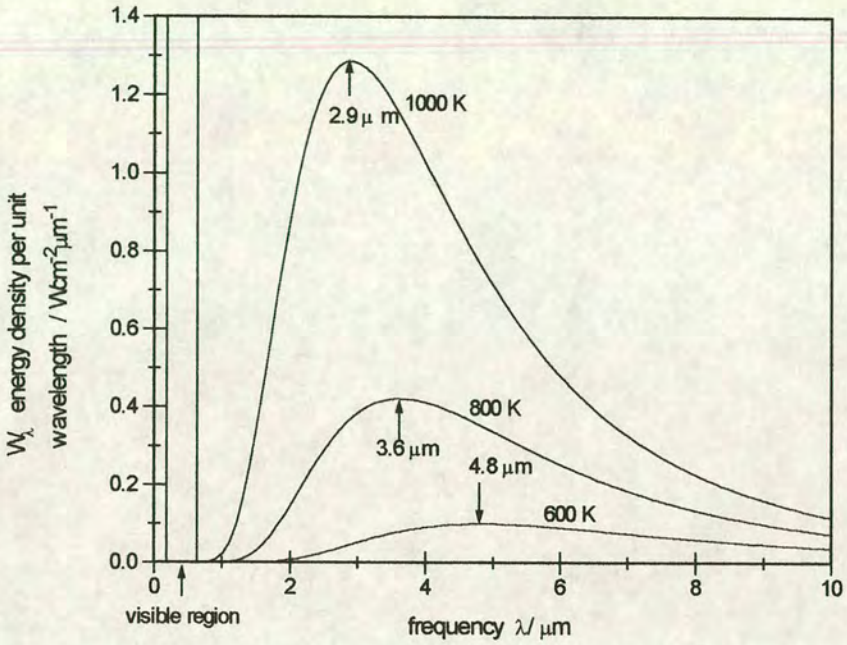

Figure 2.0.3-A Typical black body emission spectra[58]

2.0.3(iv) Signal Processing

The radiometer uses an algorithm to process the infrared beam intensity data. The nature of this algorithm greatly affects the outcome of the recorded temperature. Knowledge of this algorithm allows sensible application of infrared thermometric methods within the operational constraints of any given system.

The total signal entering the infrared thermometer comes from two sources. The first is the desired radiation emitted back from the target source, which subtends a solid angle ω (in units of hemispheres) at the lens of the infrared thermometer (Fig. 2.0.3-B). The second is the unwanted background radiation subtended by the solid hemispherical angle (1-ω). For high temperature measurements the background radiation (at ambient temperature of *ca.* 20 - 100 ^{O}C) is considered negligible and the thermometer signal, S, is defined by

$$S = \varepsilon.f(T) \qquad \text{Eqn. 2.0.3-E}$$

58) This plot was obtained using Microcal Origin 3.5, Microcal Software Inc., One Roundhouse Plaza, Northampton, MA 01060, USA.

where f(T) is the Wien function given by Eqn. 2.0.3-B. For use within the DRIFTS set-up, temperatures of up to *ca.* 400 ^{O}C will be measured. These are considered to be low temperature sources, in terms of the operational capacity of an infrared thermometer. In such cases a more complex model is required, as described below.

2.0.3(v) Low Temperature Signal Processing

For low temperature measurements (*ca.* < 400 ^{O}C) Eqn. 2.0.3-F is employed[59]

$$S = \omega.\varepsilon[f(T_t) - f(T_d)] + \omega.(1-\varepsilon)[f(T_b) - f(T_d)] + (1-\omega)[f(T_i) - f(T_d)]$$

(term 1) + (term 2) + (term 3) Eqn. 2.0.3-F

where T_t = the temperature of the target; T_d = detector temperature; T_b = background temperature and T_i = instrument temperature (see Fig. 2.0.3-B). In the processing two gross assumptions are made:

(i) $T_i = T_d$ and therefore term 3 drops out;

(ii) $T_b = T_d$ and therefore term 2 drops out;

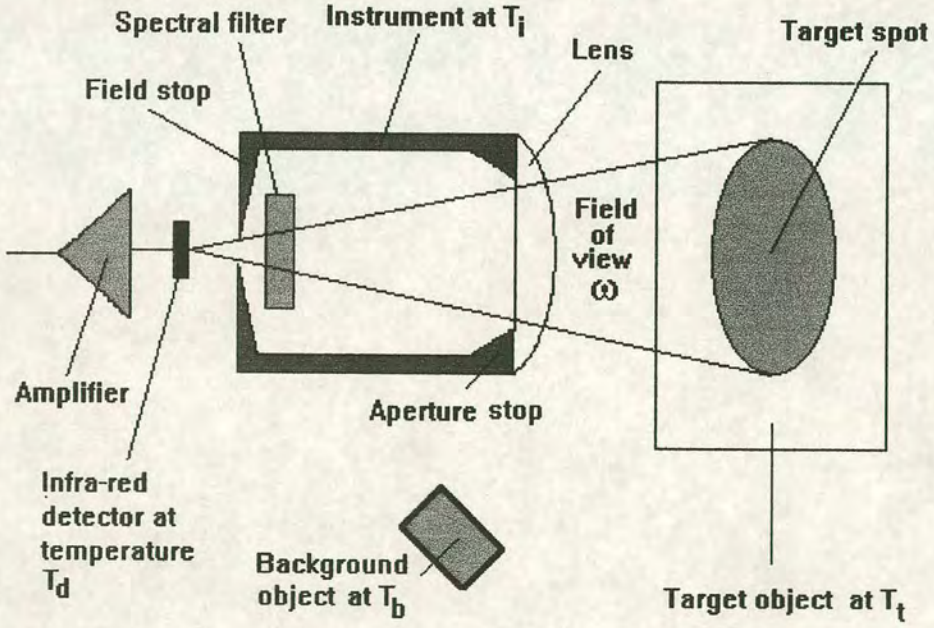

Figure 2.0.3-B Schematic representation of the basic infrared thermometer set-up

Assumption (i) presumes that the instrument is in complete thermal equilibrium. In the case of thermal shock (instrument brought into an environment hotter than itself)

59) Private correspondence, G. Bynon, Divisional Technical Director, Land Infrared, Dronfield, Sheffield S18 6DJ, England.

this is not the case and errors occur due to term 3. For isothermal instruments term 3 drops out, although, in most operating conditions a temperature gradient exists along the instrument. Assumption (ii) creates the biggest problem in signal processing. The background temperature is invariably unequal to the detector temperature. To compensate for this, some instruments allow the manual input of temperature T_b so that term 2 can be calculated. Another ramification of this assumption is that there must be a well-defined target area.

In conclusion, the major source of error in measuring low temperature systems is not discrepancies in emissivity values, but the interference by background radiation. If repeatability is to be ensured, then not only must ε be well defined over the temperature range of interest for the given target, but the same background and instrument temperature must be ensured each time. In practical terms, a short wavelength instrument (2.4μ) is more accurate than a long wavelength instrument (10μ). If long wavelength instruments are to be used then the set-up must be thermally controlled.

2.0.3(vi) Background Reflection

The operation of an infra-red thermometer may be simply visualised as that of an 'inverted' torch. With a torch, a beam of light leaves the instrument and strikes a target, whereas, with the infra-red thermometer a beam of infra-red 'light' leaves a target and strikes the instrument. Most importantly, the point at which the temperature is measured is not necessarily the point at which the infra-red beam is seen to strike (most infra-red thermometers have a visible laser pointer to sight the target). Instead, the point at which the temperature is measured occurs where the absorbency of the infra-red beam is greatest. Thus, if a background object is impinged upon by the infrared sightpath, and it has a sufficient absorbency, then it will add to the overall measured temperature, because the background reflections cannot be distinguished from emitted radiation in the sight path.

To illustrate the above point, consider a system set up to measure the temperature of platinum particles on a platinum alumina washcoat, supported on a stainless steel

block in contact with a heating element as shown in Fig. 2.0.3-C below. This particular example is chosen since it pertains to some of the research conducted by other members of this research group. It is desired that the surface temperature of the surface metal, T_2, be recorded rather than that of the substrate (washcoat), or any other part of the system. However, the actual temperature measured will be one of four defining cases, or some combination of these.

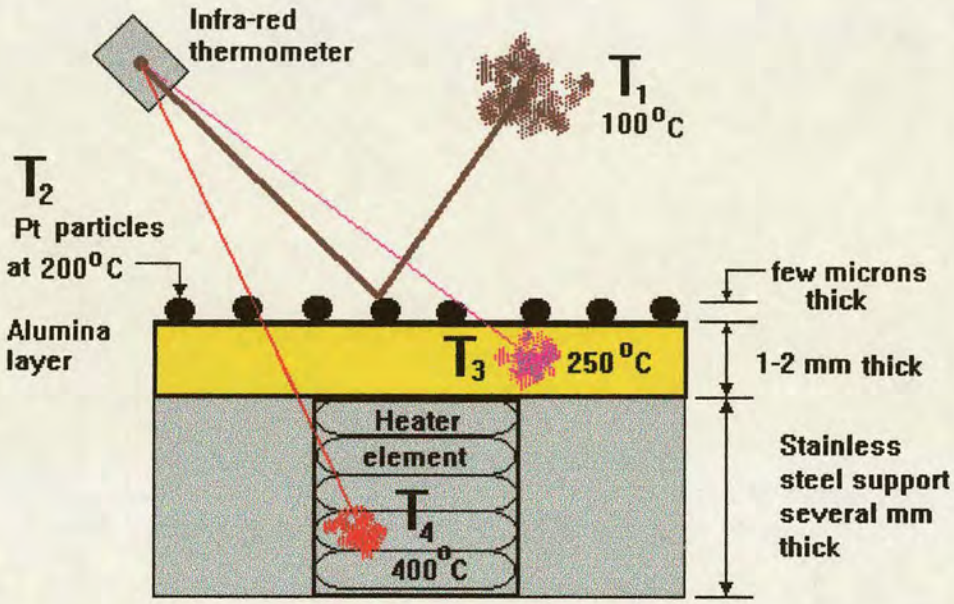

Figure 2.0.3-C Infrared temperature measurement in different scenarios

Case 1: If there is a high surface metal loading and the metal is highly reflective then virtually all of the infrared beam will be reflected back out to the atmosphere above the system under consideration with negligible absorbency at the metal surface. Instead, the majority of the infrared absorption occurs through the surrounding gas above the system, in this case at 100 ^{O}C. Consequently the temperature T_1 (100 ^{O}C) is measured.

Case 2: If there is a high surface metal loading and the metal is highly absorptive then virtually all of the infrared beam will be absorbed at the metal surface and the desired temperature, T_2 *ca.* 200 ^{O}C, will be recorded.

Case 3: If there is a low surface metal loading and the alumina washcoat is powdered, then there will be many internal reflections within the washcoat and infrared absorption will occur primarily in this region. Thus, temperature T_3 of *ca.* 250 ^{O}C will be measured.

Case 4: If there is a low surface metal loading and the alumina is in the form of single crystals (sapphire), then the infrared beam would penetrate into the heater apparatus and the maximum absorption would occur in this region giving T_4, *ca.* 400 ^{O}C, as the recorded temperature.

Clearly, from the above consideration, such a system would require the individual testing and emissivity measurement of each of its components in order to establish exactly what part of the system was being measured. Similar considerations will be required if any attempt is to be made at using infrared thermometry in the DRIFTS apparatus. These problems are discussed in section 3.2.1.

2.1 Alkoxides

The majority of work on alkoxides has been conducted by Bradley and co-workers.[1,2,3] The literature up to 1975 is well reviewed in the book by Bradley.[3] Mehrotra has reviewed the progress since then (up to 1982) of the alkoxide chemistry of 3d, 4d and 5d metals.[4]

2.1.1 Physical Properties of Alkoxides

The physical properties of the metal alkoxides generally show a dependency upon on the size and shape of the alkyl group and on the valency, atomic radius, stereochemistry and coordination number of the metal. The physical properties involve a balance between the tendency of the metal to expand its coordination number by utilizing the bridging property of alkoxo groups and the opposition to this by the steric effects of the alkyl group. This results in a wide spectrum of properties ranging from insoluble, non-volatile, ionic polymeric solids (of the form $[M(OR)x]_n$) of some of the alkali metals to volatile covalent alkoxides (often monomeric liquids) of the metals of valency three, four, five or six.

Of most interest in this research was the possibility of synthesising $Zn(OMe)_2$. In general, very little crystallographic data exists for alkoxides. No X-ray crystallographic data exists for $Zn(OMe)_2$, but ZnMe(OMe) has been shown to exist as a tetrameric crystal with the Zn and O atoms occupying the corners of two interpenetrating tetrahedra of different sizes, such that these atoms are four-coordinate and are situated on alternate corners of a distorted cube.[5] From the work of Mehrotra and Arora[6] it was suggested that zinc alkoxides are all highly polymeric compounds, but the coordination number of the zinc is not known. The thiolato

---

1) D. C. Bradley, "Metal Alkoxides" in *Prog. Inorg. Chem.*, 1960, **2**, 303-361; and references therein.
2) D. C. Bradley, "Metal Alkoxides and Dialkylamides" in *Adv. Inorg. & Radiochem.*, 1972, **15**, 259-321; and references therein.
3) D. C. Bradley, R. C. Mehrotra and D. P. Gaur, *Metal Alkoxides*, Academic Press, New York, 1978.
4) R. C. Mehrotra, "Transition Metal Alkoxides" in *Adv. Inorg. & Radiochem.* 1983, **26**, 269-333; and references therein.
5) H. M. M. Shearer and C. B. Spencer, "Tetrameric Methylzinc Methoxide", *Acta. Cryst.*, 1980, **B36**, 2046-2050.
6) R. C. Mehrotra and M. Arora, "Alkoxides and Double Alkoxides of Zinc", *Z. Anorg. Allg. Chem.*, 1969, **370**, 300-322.

analogue of zinc methoxide, $[Zn(SMe)_2]_n$[7], is known to be polymeric, but no crystal structure has been obtained. However, a crystal structure has been obtained for $[Zn(SPh)_2]_n$, which was shown to be polymeric with bridged thiolato ligands[8]

2.1.2 Chemical Properties of Alkoxides

2.1.2(i) Preparative Routes to Alkoxides

The alkoxides of zinc $Zn(OR)_2$ are insoluble, non-volatile compounds (including the *tert*-butoxide) for which several preparative methods have been devised. In 1853 Frankland found that dimethyl zinc inflames in air forming white fumes. In contact with pure oxygen an explosion occurs. Later work on the oxidation of diethyl zinc in ethereal solution led him to propose the formation of an alkoxide $Zn(OR)_2$ (R = Me, Et).[9] Subsequently, Butlerow[10] argued for the formation of a methyl-methoxy derivative in the oxidation of dimethyl zinc in MeI solution. Analysis of the crystalline product indicated methylmethoxyzinc, ZnMe(OMe), mixed with a little zinc methoxide, $Zn(OMe)_2$. Using the dialkyl zinc compound as a starting material, the dialkoxides (R = Et, Bu^n, Bu^t) have been obtained by Abraham[11] by the controlled oxygenation of solutions of ZnR_2 over several weeks. Coates and Roberts[12] obtained similar results by prolonged reaction with excess alcohol. $Zn(OMe)_2$ and $Zn(OPr^i)_2$ were prepared by Mehrotra and Arora[6] using the lithium alkoxide in its parent alcohol.

2.1.2(ii) Hydrolysis of Alkoxides

The chief chemical properties of metal alkoxides are their ease of hydrolysis (except for a few notable exceptions) and reactivity with hydroxylic molecules. A common characteristic of all metal alkoxides so far investigated is the ease with which they

---

7) K. Osakada and T. Yamamoto, "Formation of ZnS and CdS by Thermolysis of Homoleptic Thiolato Compounds $[M(SMe)_2]_n$ (M = Zn, Cd)", *J. Chem. Soc., Chem. Comm.*, 1987, 1117-1118.
8) J. C. V. Laurie, L. Duncan, R. C. Haltiwanger, R. T. Weberg and M. R. DuBois, *J. Am. Chem. Soc.*, 1986, **108**, 6234.
9) E. Frankland, *J. Chem. Soc.*, 1862, **15**, 363.
10) A. Butlerow, *Z. Pharm. Chem.*, 1864, 7, 402.
11) M. H. Abraham, "Autoxidation of Dialkyl Zincs", *Chem. & Ind.*, 1959, 750-751; and M. H. Abraham, "Organometallic Compounds. Part I. The Autoxidation of Dialkyl Zincs", *J. Chem. Soc.*, 1960, 4130-4135.
12) G. E. Coates and P. D. Roberts, "Some t-Butyl and t-Butoxy-derivatives of Zinc", *J. Chem. Soc. A*, 1967, 1233-1234.

are hydrolyzed. In many cases the alkoxides are so sensitive to traces of water that special precautions have to be adopted in order to study their properties. In the presence of excess water the ultimate product is the hydrated metal oxide or sometimes the metal hydroxide. It is this ready hydrolysis to form hydroxide materials which makes them of particular interest in this research. Little is known concerning the mechanism of the hydrolysis of metal alkoxides. It seems reasonable to suppose that the initial step involves the coordination of a water molecule through its oxygen to the metal, in a facile nucleophilic process.

2.1.3 Spectral Properties of Alkoxides

The observation of the characteristic vibration bands of the bonded alkoxide group (e.g., M-O and C-O stretching vibrations) has been used to support the identity of metal alkoxides. This has proven to be rather difficult due to the complex structure of the metal alkoxides, compounded by their often low molecular symmetry. Thus, the infrared technique has often not been definitive in structural assignment of the various types of M-O bands.

The infrared spectra of a number of alkoxides (*viz.*, aluminium, hafnium, niobium, tantalum, titanium and zirconium alkoxides) have been observed by Baraclough *et al.*[13] In most cases, ν(C-O)M bands appeared in the region 900-1150 cm^{-1} and the position of the band was seen to be determined by the nature of the alkoxy groups. For example, the ethoxide derivatives showed two bands around 1025 and 1070 cm^{-1} which were assigned to ν_s(C-O)M and ν_{as}(C-O)M stretching vibrations respectively. However, coupling of C-O and C-C complicates the interpretation.

The infrared spectra of methoxides and halide methoxides of first row transition metals such as manganese, iron, cobalt, nickel and copper were studied by Winter and co-workers[14,15,16,17,18]. They assigned the ν(C-O)M band in the region 1000-1100 cm^{-1} and the ν(M-O) stretching frequencies to below 600 cm^{-1} in these methoxides.

---

13) C. G. Barraclough, D. C. Bradley, J. Lewis and I. M. Thomas, "The Infrared Spectra of Some Metal Alkoxides, trialkylsilyloxides and Related Silanols", *J. Chem. Soc.*, 1961, 2601-2605.
14) A. G. Kruger and G. Winter, "Magnetism, Electronic Spectra and Structure of Transition Metal Alkoxides VIII. Nickel Halomethoxides", *Australian J. Chem.*, 1970, **23**, 1-14.

Bradley and Westlake[19] made a more detailed study of the infrared spectra of the polymeric metal ethoxides, following on from the earlier work of Barraclough *et al.* They attempted a definite assignment of bands to the C-O and M-O vibrations of terminal and bridging ethoxide groups. By measuring relative band intensities of terminal and bridging groups, they also attempted to assign structures to the polymeric alkoxides. Due to the structural complexity of these molecules and the possibility of coupling of vibrations, the simple criteria of comparison they attempted proved to be inadequate as a basis for the structural assignment of the alkoxides and more detailed criteria were developed.

Over all, the alkoxides exhibit a disappointing lack of adequate characterisation. Given the lack of recent work re-examining earlier results, it is quite feasible that equivocal conclusions have been drawn regarding some of the chemical structural assignments made.

---

15) L. Dubicki, G. A. Kakos and G. Winter, "Magnetism, Electronic Spectra and Structure of Transition Metal Alkoxides VI. Chromium III Chloro Alkoxides", *Australian J. Chem.*, 1968, **21**, 1461-1472.

16) R. W. Adams, C. G. Barraclough, R. L. Martin and G. Winter, "Magnetism, Electronic Spectra and Structure of Transition Metal Alkoxides V. Copper II Methoxides", *Australian J. Chem.*, 1967, **20**, 2351-2356.

17) R. W. Adams, R. L. Martin and G. Winter, "Possible Ligand Field Effect in Metal-Oxygen Vibrations of Some First Row Transition Metal Alkoxides", *Australian J. Chem.*, 1967, **20**, 773-774.

18) R. W. Adams, C. G. Barraclough, R. L. Martin and G. Winter, "Two Crystal Forms of Titanium IV Methoxide", *Australian J. Chem.*, 1967, **20**, 171-172.

19) D. C. Bradley and A. H. Westlake, *Proc. Symp. Coord. Chem., Tihany, Hungary*, Published by Hungarian Acad. Sci. Budapest, 1965, p. 309.

2.2 Carbon Dioxide and Carbonates

2.2.1 Physio-Chemical Properties of Carbon Dioxide

The presence of atmospheric carbon dioxide posed particular problems whilst preparing and handling the absorbent materials. To attempt to ascertain the function of the hydroxyl species on ZnO surfaces in isolation of interferences (of which CO_2 and related species were the most prevalent and pernicious), it is necessary to prevent contact of carbon dioxide with the absorbent surface. Thus, the handling of the adsorbents during synthesis and testing was performed in 'air-free' conditions, under a nitrogen atmosphere, using purpose-built apparatus to prevent ingress of CO_2 (see chapter 3). However, many of the preparative routes to the final absorbents involved solution chemistry. Since carbon dioxide is soluble in water and other solvents, the solutions used to prepare CO_2 free absorbents were, themselves, potential 'CO_2-carriers'. To quantify the extent to which CO_2 contamination could occur from this source, knowledge of the solution chemistry of CO_2 was required. The following section concerns those areas of the chemistry of CO_2 required to ascertain the extent to which CO_2 may be present in the solvent samples used (water, in almost all cases).

2.2.1(i) The Solubility of Gases in Water

The equilibrium between molecules of gas in the atmosphere and in the corresponding molecules of the same gas in solution,

$$G_{(g)} \rightleftharpoons G_{(aq)} \qquad \text{Eqn. 2.2.1-A}$$

is given by **Henry's Law,** which states that: *the solubility of a gas in a liquid is proportional to the partial pressure of that gas in contact with the liquid.*[1]

Thus, the solubility of a gas, G, in water may be expressed by the equation

$$[G_{(aq)}] = H_G \times P_G \qquad \text{Eqn. 2.2.1-B}$$

where H_G (sometimes referred to as K_H) is the Henry's Law constant for a specific gas at a given temperature and P_G is the partial pressure of that gas.

---

1) S. E. Manahan, *Environmental Chemistry,* 4th edn.,Lewis Pubs., London, 1990.

2.2.1(ii) The Behaviour of CO_2 in Water

The study of the properties and solution chemistry of carbon dioxide has been widely reported and reviewed.[1,2,3,4] Henry's Law is limited, in that it does not account for further chemical reactions of the gas in solution: it is much more complicated to calculate the solubility of CO_2 in water, than to calculate the solubility of a non-reactive gas like O_2 or N_2, because of carbon dioxide's acidic character. Consideration of the chemical interactions of carbon dioxide, in water is required.

Carbon dioxide is only a very small component of normal dry air, 0.314% by volume (see appendix A2.2.1-A). As a consequence of the low level of atmospheric CO_2, water totally lacking in alkalinity in equilibrium with the atmosphere contains only a very low level of carbon dioxide. However, initial absorption of carbon dioxide, following Henry's Law equilibrium, Eqn2.2.1-D, is rapidly followed by dissociation to form the bicarbonate and carbonate species, HCO_3^- and CO_3^{2-}, respectively, greatly increasing the solubility of carbon dioxide. Thus, for carbon dioxide, the general expression 2.2.1-A becomes

$$CO_{2\,(g)} \rightleftharpoons CO_{2\,(aq)} \qquad \text{Eqn. 2.2.1-C}$$

and the Henry's Law general expression 2.2.1-B becomes

$$H_{CO_2} = \frac{[CO_{2\,(aq)}]}{P_{CO_2}} = 0.0338 \text{ mol } L^{-1} \text{ atm}^{-1} \text{ at } 25^{O}C \,^{5} \qquad \text{Eqn. 2.2.1-D}$$

Substitution of $P_{CO_2} = 3.04 \times 10^{-4}$ atm into Eqn. 2.2.1-D gives the concentration of CO_2 dissolved in water as predicted by Henry's Law as 0.45 ppm (see appendix A2.2.1-E).

Since the carbon dioxide molecule has no protons associated with it, it is not an acid in and of itself (at least by the Brønsted-Lowry definition of 'a proton donor'[6]).

---

2) M. Radojevic, "Sea Changes", *Chem. In Brit.*, 1996, Nov., 47-49.
3) J. F. Pankow, *Aquatic Chemistry Concepts*, Lewis Publishers, Chelsea, 1991.
4) P. G. T. Fogg and W. Gerard, *Solubility of Gases in Liquids: A Critical Evaluation of Gas/Liquid Systems in Theory and Practice*, Wiley, Chichester, 1991.
5) *International Critical Tables of Numerical Data, Physics, Chemistry and Technology*, compiled by C. J. West, Pub. for the International Research Council (U.S.) by Mc Graw Hill Book Co., New York, 1993, vol. 3, p.260 and R. F. Weiss, *Marine Chem.*, 1974, **2**, 203.

However, dissolved carbon dioxide can equilibrate with water to form the diprotic species carbonic acid H_2CO_3 (Eqn. 2.2.1-E). There is controversy over the actual existence of the discrete molecular species H_2CO_3,[7] however, for the sake of convenience the historical term H_2CO_3 will be employed throughout to represent the species first formed by the association of carbon dioxide with water.

$$CO_{2\,(aq)} + H_2O \rightleftharpoons H_2CO_3\,; \qquad K = \frac{[H_2CO_3]}{[CO_{2(aq)}]} \approx 1.3 \times 10^{-3} \qquad \text{Eqn. 2.2.1-E}^{8}$$

As indicated in Eqn. 2.2.1-E both CO_2 and H_2CO_3 will be present in any solution containing carbon dioxide. Whatever CO_2 is present in a given solution has the capability to react with water according to Eqn. 2.2.1-E to form more H_2CO_3. Therefore, when, for example, counting how many acidic protons are present, or potentially present, in a solution of CO_2 those protons on the H_2CO_3 must be counted, as well as those that are available to be added by Eqn. 2.2.1-E using the CO_2 molecules present. Indeed, if a strong base were added to a solution of CO_2, then the equilibrium of Eqn. 2.2.1-E would be expected to be driven to the right to provide protons to react with the base. Thus, in effect, the total amount of diprotic acid in a CO_2 system will be given by the concentration of the hypothetical species H_2CO_3* where

$$[H_2CO_3^*] = [CO_2] + [H_2CO_3] \qquad \text{Eqn. 2.2.1-F}$$

Consequently, in this text, all non-ionised carbon dioxide in water will be designated as H_2CO_3* which, in subsequent discussion, will represent the total of dissolved molecular CO_2 and undissociated H_2CO_3, whilst $[H_2CO_3^*]$ will represent the combined molar concentrations of carbonic acid and dissolved CO_2, (not in the carbonic acid form).

The subsequent rapid dissociation equilibria give rise to the following mass action expressions;

---

6) R. J. Fessenden and J. S. Fessenden, *Organic Chemistry*, 3rd ed., Brooks/Cole Publishing Co., Monerey, California, 1986, p. 27.
7) M. Laing and M. Laing, "There is No Such Thing as H_2CO_3", *Ed. In Chem.*, 1993, 56.
8) D. C. Harris, *Quantitative Chemical Analysis*, W. H. Freeman & Co., New York, 1982, p. 168.

$$H_2CO_3^* \overset{K_1}{\rightleftharpoons} HCO_3^- + H^+; \quad K_1 = \frac{[HCO_3^-][H^+]}{[H_2CO_3^*]} = 4.45 \times 10^{-7} \quad \text{Eqn. 2.2.1-F}^9$$

Its behaviour as a diprotic acid appears anomalous when compared to other carboxylic acids. For example, for acetic acid, formic acid and cyanoacetic acid the K_1 values[8] are 1.75×10^{-5}, 1.80×10^{-4} and 3.37×10^{-3} respectively, i.e. *ca.* 10^2 to 10^4 times bigger than K_1 for carbonic acid. This arises from the convention that, for the carbonate system,[5] the term K_1 is normally reserved for the first dissociation constant of $H_2CO_3^*$. Thus the value commonly given for K_1 applies to the

$$K_1 = \frac{[HCO_3^-][H^+]}{[CO_{2\,(aq)} + H_2CO_3]} = 4.45 \times 10^{-7}, \quad pK_1 = 6.35 \quad \text{Eqn. 2.2.1-G}$$

From Eqn. 2.2.1-E, only about 0.13% of dissolved CO_2 is in the form H_2CO_3. When the true value of $[H_2CO_3]$ is used, instead of the value $[CO_{2\,(aq)} + H_2CO_3]$, the value of the equilibrium constant becomes

$$K_{H_2CO_3} = \frac{[HCO_3^-][H^+]}{[H_2CO_3]} = 2 \times 10^{-4} \quad \text{Eqn. 2.2.1-H}$$

which is now comparable to the values for analogous carboxylic acids. The second dissociation equilibrium is then given by

$$HCO_3^- \overset{K_2}{\rightleftharpoons} CO_3^{2-} + H^+; \quad K_2 = \frac{[CO_3^{2-}][H^+]}{[HCO_3^-]} \quad \text{Eqn. 2.2.1-I}^{10}$$

$$K_2 = 4.69 \times 10^{-11}, \quad pK_2 = 10.33$$

On the basis of the above it may be concluded that all aqueous solutions containing carbon dioxide will contain four dissolved species, *viz.*, CO_2, H_2CO_3, HCO_3^- and CO_3^{2-}. Also, the actual amount of gas taken up by the water may be a great deal larger than predicted by Henry's Law for carbon dioxide. However, the total concentration of dissolved carbon may still be related to the gaseous partial pressure of CO_2 using a pseudo-Henry's Law constant, K_1^*:

$$K_1^* = K_1[1 + \{K_1/a_{H^+}\} + \{K_1.K_2/(a_{H^+})^2\}] \quad \text{Eqn. 2.2.1-J}^4$$

---

9) H. S. Harned and R. Davis Jr., *J. Am. Chem. Soc.*, 1943, **65**, 2030.
10) H. S. Harned and S. R. Scholes, *J. Am. Chem. Soc.*, 1941, **63**, 1706.

where K_1 is the first dissociation constant of H_2CO_3* and K_2 is the dissociation constant for HCO_3^-, in terms of the activities of the various species.

Given the values of K_1 and K_2, a distribution of species diagram for the H_2CO_3*-HCO_3^--CO_3^{2-} system may be prepared as a series of plots of the fractions present as H_2CO_3*, HCO_3^- and CO_3^{2-} as a function of pH (see appendix A2.2.1-D).

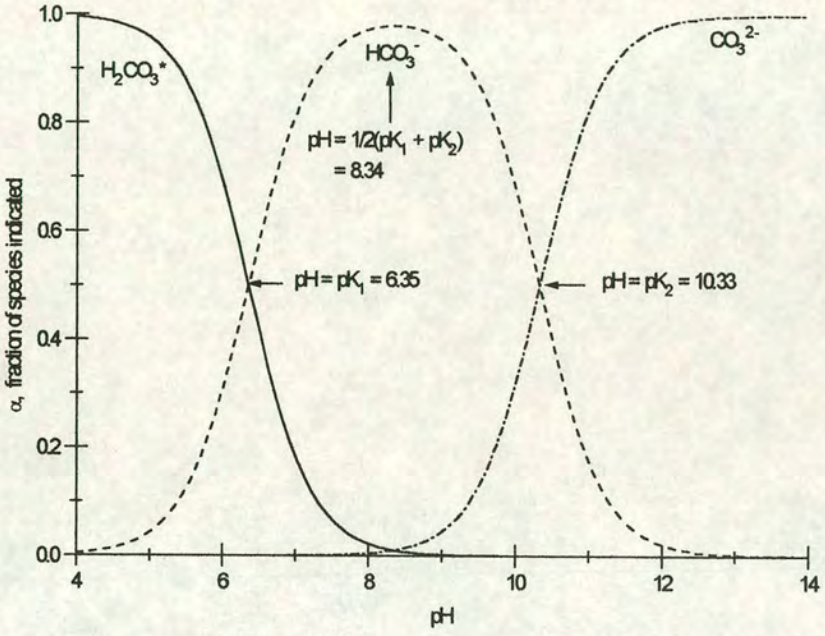

Fig. 2.2.1-A Distribution species for the H_2CO_3*-HCO_3^--CO_3^{2-} system in water[11]

The fractions, designated as α_x, are given by the following expression:

$$\alpha_X = \frac{[X]}{[H_2CO_3*] + [HCO_3^-] + [CO_3^{2-}]} \qquad \text{Eqn. 2.2.1-K}$$

where X = H_2CO_3*, HCO_3^- or CO_3^{2-}

Additionally, the actual changes in carbonate species concentration as a function of pH may be plotted. Rearrangement of Eqn. 2.2.1-D, using the defined term [H_2CO_3*] in place of [$CO_{2(aq)}$] and K_H to represent H_{CO_2} gives

$$[H_2CO_3*] = K_H . P_{CO_2} \qquad \text{Eqn. 2.2.1-L}$$

Substituting Eqn. 2.2.1-L into Eqn. 2.2.1-F gives

11) This plot was obtained using Microcal Origin 3.5, Microcal Software Inc., One Roundhouse Plaza, Northampton, MA 01060, USA.

$$\left[HCO_3^-\right] = \frac{K_H . P_{CO_2} . K_1}{\left[H^+\right]} \qquad \text{Eqn. 2.2.1-M}$$

and substitution of Eqn. 2.2.1-M into Eqn. 2.2.1-I yields

$$\left[CO_3^{2-}\right] = \frac{K_H . P_{CO_2} . K_1 . K_2}{\left[H^+\right]^2} \qquad \text{Eqn. 2.2.1-N}$$

Substitution of known values for K_H, K_1, K_2 and P_{CO_2} into Eqns. 2.2.1-L, M and N allows Fig. 2.2.1-B to be plotted, as below.

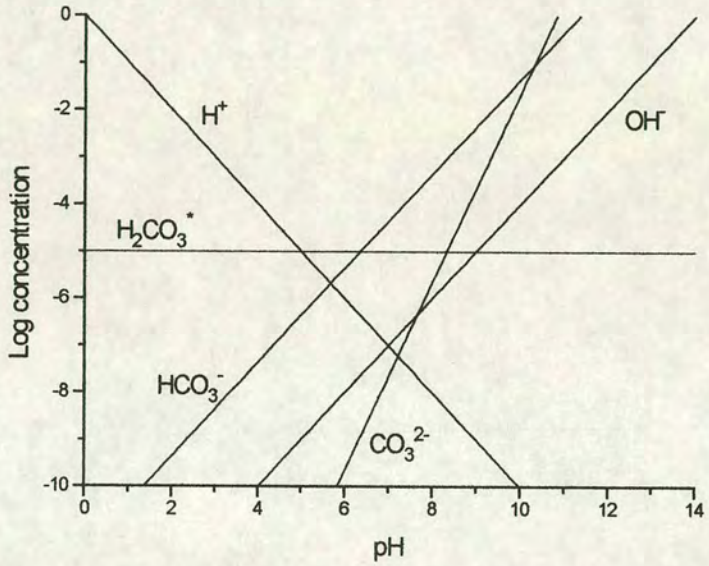

Figure 2.2.1-B Changes in carbonate species concentration as a function of pH [11]

From Fig. 2.2.1-A it can be seen that, at pH values less than 8, the total dissolved carbon dioxide is almost exclusively in the form of H_2CO_3 and HCO_3^-, and so the total amount of CO_2 from air dissolving in 1.00 litres of pure, neutral (pH 7) water, in equilibrium with air, is the sum of $[H_2CO_3^*]$ and $[HCO_3^-]$. The value for this sum is 1.242×10^{-5} mol L^{-1}, which corresponds to 0.55 mg L^{-1} or 0.55 p.p.m. (the derivation of these figures is given in appendix A2.2.1-E).

Carbon dioxide, bicarbonate ion and carbonate ion have an extremely important influence upon the chemistry of water. The equilibrium of dissolved CO_2 with the atmosphere,

$$CO_2 \text{ (atmosphere)} \rightleftharpoons CO_2 \text{ (water)} \qquad \text{Eqn. 2.2.1-O}$$

and the equilibrium of CO_3^{2-} ion between aquatic solution and solid carbonate minerals,

MCO_3 (slightly soluble carbonate salt) $\rightleftharpoons M^{2+} + CO_3^{2-}$ (water) Eqn. 2.2.1-P

have a strongly buffering effect upon the pH of water.

The solubility of carbon dioxide is greatly increased by the presence of a base. It is important to distinguish between high *basicity*, manifested by a high pH, and high *alkalinity*, a high proton-accepting capability. Whereas pH is an *intensity* factor, alkalinity is a *capacity* factor. For example, 10^{-3}M $NaOH_{(aq)}$ has pH 11 and will neutralise 10^{-3} mole of acid, whereas, 0.1M $NaHCO_{3\,(aq)}$ has a pH of only 8.34 but it will neutralise 100 times more acid (0.1 mole) than that of the more basic NaOH solution.

Highly alkaline water often has a high pH and generally contains elevated levels of dissolved solids. Alkalinity serves as a buffer and reservoir for inorganic carbon. Generally, the basic species responsible for alkalinity in water are bicarbonate (Eqn. 2.2.1-F in reverse direction), carbonate (Eqn. 2.2.1-I in reverse) and hydroxide ions:

$$OH^- + H^+ \rightleftharpoons H_2O \qquad \text{Eqn. 2.2.1-Q}$$

Other, usually minor, contributors to alkalinity are ammonia and the conjugate bases of phosphoric, silicic, boric and organic acids. Consideration of the above factors played an essential role in assessing the degree of carbonate contamination available to absorbents prepared using aqueous media.

2.2.2 Physio-Chemical Properties of Carbonates

Zinc carbonate, $ZnCO_3$, occurs naturally as the mineral smithsonite. It forms colourless, trigonal crystals which lose carbon dioxide at 300 ^{O}C, and is sparingly soluble in water; one part dissolving in 100,000 parts of water at ordinary temperatures[12]. It is usually prepared by passing carbon dioxide through a zinc oxide slurry which is then filtered, washed and dried. Of more interest is the basic

12) R. E. Kirk and D. F. Othmer, *Encyclopaedia of Chemical Technology*, 4th ed., Wiley, New York, Chichester, 1991, **6**,

carbonate of zinc (usually $Zn_5(CO_3)_2(OH)_6$), since the surface of zinc oxide and hydroxide materials are invariably coated with this material, unless stringent conditions have been applied to exclude normal atmospheric air. The term 'basic salt' is applied to a variety of compounds intermediate between the normal salt and the hydroxide or oxide. This broad definition includes compounds such as Be an Zn oxyacetates, oxy and hydroxy-halides and hydroxy-oxysalts.[13]

In the presence of carbon dioxide and water vapour the basic carbonate, $Zn_x(CO_3)_y(OH)_{2(x-y)}$, zinc hydroxycarbonate, is formed by their combined action on zinc oxide. Hydrozincite is also the usual corrosion product of zinc in moist air.[13] O'Connor[14] demonstrated that when the reaction conditions are optimized, zinc oxide can be completely converted to basic zinc carbonate according to Eqn. 2.2.2-A.

$$xZnO + yCO_2 + (x - y)H_2O \rightarrow Zn_x(CO_3)_y(OH)_{2(x-y)} \qquad \text{Eqn. 2.2.2-A}$$

O' Connor[15] also studied the kinetic parameters involved in its formation and found that water vapour pressures close to saturated water vapour pressure were necessary for the reaction to proceed. It was further postulated that the mechanism involved the diffusion of mainly HCO_3^- ions to the reaction interface, which then react with preformed intermediate zinc hydroxide layers to form the final basic carbonate.

2.2.3 Spectral Properties of Carbonates

Generally, the symmetry elements of the carbonates are congruent with those of the carboxylates. The bonding modes of carbonates (see Table 2.2.3-A) may, thus, be divided in a similar fashion to the manner in which those of the carboxylates have been organized (section 2.3.1). The following section reviews the infrared spectra of types of carbonate groups that have been identified for both surface and bulk carbonates.[16, 17,18]

---

13) A. F. Wells, *Structural Inorganic Chemistry*, 5th ed., Clarendon Press, Oxford, 1986.
14) M. F. O'Connor, *Z. Naturforsch*, 1974, **29b**, 202.
15) M. F. O'Connor, "A Study of the Kinetics of the Basic Zinc Carbonate Formation Reaction", *Z. Naturforsch*, 1975, **30b**, 665-668.
16) L. H. Little, *Infrared Spectra of Adsorbed Species*, Academic Press, London, 1966; and references therein.
17) A. A. Davydov, *Infrared Spectra of Adsorbed Species on the Surface of Transition Metal Oxides*, Wiley, Chichester, 1984.

In general, absorption bands at 1000-1700cm^{-1} characterize bond vibrations in surface carbonate compounds. Gatehouse and co-workers[19] studied the infrared spectra of a variety of carbonates. Where the carbonate group is covalently bonded to other groups, as in organic carbonates, or is coordinated to a metal ion by a bond that has some degree of covalent character, the symmetry of the group will be changed from that of the simple carbonate ion. As a result of the decreased symmetry, additional bands appear in the spectrum of the complex carbonate. The causes are as follows;

1. The appearance of a band that had previously been forbidden for reasons of symmetry.
2. The splitting into two of a band due to a doubly degenerate stretching vibration.

The assignment of bands has been made by Gatehouse *et al.*[18], although it is difficult to ascertain the nature of the vibrations from their tables. They, also, showed that the separation of the CO stretching bands increases along the series,

basic salt < carbonato complex < acid < organic carbonate

Using the delineation of bonding types shown in table 2.2.3-A, the infrared spectral details of the different carbonato complexes may now be considered. Complex type 1, $[CO_2]_n^-$ is analogous to ionized carboxylates (acetates, etc.) and could also be considered to be a CO_2 derivative, but is closer in structure to a carbonate, and so is considered in this section. This type of structure has three normal vibrations active in the infrared spectrum. Symmetric and antisymmetric stretching vibrations in this structure are usually found in the 1350-1420 and 1550-1630cm^{-1} regions, respectively. Analysis of the deformation vibrations of these types of compounds is a useful probe for their detection as surface species. An important feature of this structure, which distinguishes it from 'full' carbonate structures (types 2-6), which also have two absorption bands in the 1300-1700cm^{-1} region, is that it does not

18) K. Nakamoto, *Infrared and Raman Spectra of Coordination Compounds*, 4th ed., Wiley, New York, Chichester, 1986.
19) B. M. Gatehouse, S. E. Livingstone and R. S. Nyholm, *J. Chem. Soc.*, 1958, 3137.

Table 2.2.3-A Bonding Modes of Carbonate Ligands

Ionic or non-coordinated (Types 1 & 2)

Ionic (types 1 &2)	
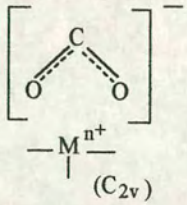	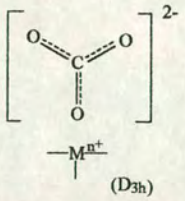
Type 1	**Type 2**

Covalent or co-ordinated (Types 3-6)

Unidentate (types 3 & 4)	
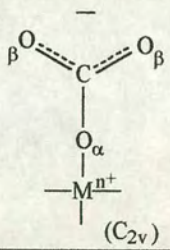	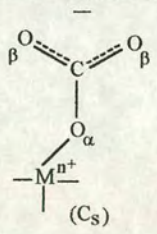
Type 3	**Type 4**

Bidentate (Types 5 & 6)	
Bridging	**Chelating**
syn-syn	4 mem. ring
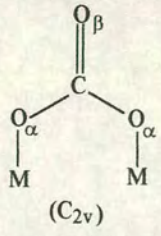	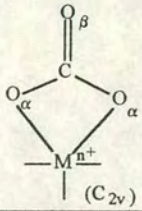
Type 5	**Type 6**

produce an absorbance in the 1000cm^{-1} region. Frequency values of the coordinated COO^- group depend on the metal character.[17] A higher degree of ionization depresses the stretching vibrations of this group.

The remaining carbonates may exist in free ion (type 2), monodentate (types 3 and 4) or bidentate (types 5 and 6) structures. In the process, the complex symmetry is lowered from D_{3h} in the free ion form to C_{2v} for the remaining types. The symmetry may be further lowered to Cs in certain cases of unidentate bonding (type 4). Accordingly, the selection rules are changed for each complex.

The free carbonate ion has six normal vibrations. Due to degeneracy, only four frequencies are observed in their spectra. The symmetric C-O stretching vibration, ν_1, is IR inactive (though Raman active at 1063 cm^{-1}).[15] Of the remaining three vibrations that are represented in the IR spectrum, only one, $\nu_3 \approx 1440$cm^{-1}, can be used for identification of free carbonate ions on oxide surfaces.[16] The remaining frequencies are below 900cm^{-1}. These are the out-of-plane carbon vibration (850-780 cm^{-1}) and the in-plane bending vibrations, which occur at yet lower frequencies.[15]

For the covalent bonding modes (C_{2v} and Cs) the selection rule changes (both unidentate and bidentate carbonate groups have the same C_{2v} symmetry if the metal atom is ignored). The ν_1 vibration, which is forbidden in the free ion, becomes infrared active and each of the doubly degenerate vibrations, ν_3 and ν_4, splits into two bands. The extent of splitting depends on the ligand type and number of ions in the M-0 bond.

For monodentate complexes (types 3 and 4) this splitting is smaller than in the bidentate complexes (types 5 and 6). Nakamoto[17] demonstrated that $\Delta\nu^*$ (the difference between $\nu(C\text{-}O_\alpha)$ and $\nu(C\text{-}O_\beta)$ is ca. 100 cm^{-1} for the monodentate complex and over 300 cm^{-1} for the bidentate complex. Another important factor in the analysis of differences between carbonate compounds is the covalent nature of

the M-O bond. It was found that the fully covalent bond, as in dimethyl carbonate, $(CH_3O_\alpha)_2CO_\beta$ increases the splitting toward 600cm^{-1}.[20] This effect is due to the strong covalency of the CH_3-O_α bond, whereby the CO_β stretching occurs at 1870 cm^{-1} and the CO stretching occurs at 1260 cm^{-1}. This consideration of the degree of covalency of the M-O bond is the key factor in determining the set of the carbonate compounds formed on the surface, particularly in oxides of similar nature. Higher values of $\Delta\nu^*$ indicate greater covalency of the surface M-0 bond, which is responsible for the formation of the carbonate in question. It is worth remembering, however, that the differences in the structure of the unidentate and bidentate carbonate complexes reflect, firstly, differences in the properties of surface oxygen which participates in their formation. In this light, the delineation of various forms of carbonate compounds is only a useful approximation, which indicates different surface oxygen properties on the oxide system.

20 T. A. Gordymova and A. A. Davydov, "Allyl complexes on the surface of the aluminium oxides and mechanisms of isomerization", *Kinet. Katal*, 1979, **20**, 733-740.

2.3 Carboxylates

There are comprehensive reviews covering the area of carboxylate complexes.[1,2,3] Most of the chemical elements form carboxylate complexes with monocarboxylic acids,[4] especially with acetic acid. Many of these have been known since the beginning of inorganic chemistry itself, and most are readily available from chemical suppliers. Consequently, the range of monocarboxylic acids available for review is large. Fortunately, the chemistry of acetic acid derivatives is generally similar to that of other monocarboxylic acid derivatives, and so, only these require description, except where notable deviations occur. Since this research focuses primarily on the use of carboxylate derivatives of zinc, the scope of this section has been further reduced. However, some non-zinc carboxylates are reviewed, where this enhances the perspective on the subject.

2.3.1 Physical Properties of Carboxylates

Due to the diverse manner in which the carboxylate ligand may bind to a metal centre, or centres, zinc carboxylates display a broad variety of structural forms. For example, when acting as a bidentate ligand, the oxygen atoms in the carboxylate ligand, RCOO, subtend an angle of as little as 60^0, in common with groups like nitrate (NO_3) and carbonate (CO_3). In comparison, undistorted square planar or octahedrally coordinated species subtend an angle of 90^0 and undistorted tetrahedrally coordinated, 109.5^0. This small bite-size of the bidentate carboxylate group results in insufficient filling of the space around the central metal atom. Consequently, these coordinating agents are often monodentate with respect to a single transition metal atom and the co-ordination sphere is often filled by co-ordinated water molecules, or by the coordinating agents bridging adjacent transition metal atoms to form dimeric or polymeric complexes. As a co-ordination centre, zinc also shows some flexibility. It may adopt either an octahedral or a tetrahedral

---

1) C. Oldham, "Complexes of Simple Carboxylic Acids", Prog. Inorg. Chem., F. A. Cotton ed., J. Weiley Interscience, 1968, **10**, 223-258.

2) J. Catterick and P. Thornton, "Structures and Physical Properties of Polynuclear Carboxylates", *Adv. Inorg. Chem. & Radiochem.*, 1977, **20**, 291-362.

3) R. C. Mehrotra and R. Bohra, *Metal Carboxylates*, Academic Press, London, 1983.

4) Monocarboxylic acids are those which contain only one carboxylic acid function, as opposed to those, such as glutaric acid (a.k.a. pentanedioic acid; $HO_2C(CH_2)_3CO_2H$) which contain more than one carboxylic acid function.

configuration, as in the neutral acetate $Zn(OAc)_2.2H_20$, or in the basic acetate $Zn_4O(OAc)_6$, respectively. Both of these examples illustrate the existence of bidentate carboxylates of zinc, in spite of the unfavourably small bite size of the carboxylate ligand. Since the carboxylate ligand demonstrates a diverse range of coordination geometries, it is convenient to create a scheme of classification which will allow novel structures to be compared and contrasted with known materials. It should be noted, however, that there are many carboxylate structures which have been deduced from spectroscopic or magnetic data, often quite speculatively. To provide a firm basis for classification only those structures which have been determined unambiguously by crystallographic methods will be considered in formulating this scheme of classification.

One manner in which the compounds of carboxylic acids may be categorised is by the number of co-ordinating metal centres they contain; either one (mononuclear), two (binuclear), three (trinuclear), four (tetra-nuclear) or in long chains (polymeric). In addition, there is some evidence (including crystal structures) for non-polymeric, higher-nuclearity carboxylate clusters with greater than four metal centres, e.g. six or eight metal centres, which will be discussed later. However, considering only the nuclearity of any complex proves to be limited in providing a comprehensive structural description. This may be overcome by additionally delineating the bonding modalities of the carboxylate ligands around the central metal(s). It is the ability of the carboxylate ligand to provide many bonding modes which essentially permits these various multi-nuclear complexes to be formed. Hence, this aspect of the structure provides an informative additional basis for categorising these materials.

In reviewing the carboxylate bonding modes eight distinct categories (types 1-8) may be described. The simplest characterisation defines the bonding type as either ionic or covalent. In the ionic group (type 1) the carboxylate species functions as a discrete, singly charged anion. In the covalent group (types 2-8) the carboxylate ligand acts as an oxygen donor and bonds through one or both of its carboxy oxygens. Within this covalent group there is a variety of possible structures. The

carboxylate ligand may attach itself in a *unidentate* (type 2) or *bidentate* (types 3-8) fashion. The bidentate characterisation may be further expanded into either *bridging* or *chelating* forms. The bridging mode may be still further expanded to include the four possible bridging geometries (types 3-6). Of these four structural types only the *syn-syn* configuration (type 3) brings the metal atoms close enough to form a clustered structure. The *syn-anti* (type 4) and *anti-anti* (type 5) configurations form polymeric structures. These three bridging geometries (types 3-5) involve both oxygens of the carboxylate group. The other type of bridging geometry (type 6) employs only one of its carboxylate oxygens to form a bidentate bridge. It is known as a *monatomic* bridge and is always accompanied by other bridges: it is never the only link between metal atoms. In some structures, ligands other than carboxylate help to form bridges between the metal atoms, but these are outside the scope of this review. As mentioned earlier, bridging complexes may be mono-, bi-, tri-, tetra- or poly- nuclear with regard to the central metal. In addition, the number of carboxylate bridges between any pair of metal atoms may also vary, examples being; singly bridged $Re_2(Ph_3)_2(O_2CCH_2CH_3)OCl_5$[5] doubly bridged $Re_2I_4(O_2CC_6H_5)_4$ [6]; triply bridged $[Re_2Cl_2(O_2CC_3H^i_7)_3]^+ ReO_4$.[7] Regarding the presence of carboxylate bridges, it should be mentioned that this does not necessarily imply the presence of metal-metal bonds. For example, in the trimeric palladium(II)acetate $Pd_3(OAc)_6$[8] (widely studied as a catalyst for vinyl acetate synthesis) Pd-Pd distances are *ca.* 3.15Å indicative of no direct metal-metal bonding. In contrast, the platinous analogue, $Pt_4(OAc)_8$ has Pt-Pt distances of 2.50Å consistent with the occurrence of single bonds between the metal atoms.[9]

Finally, when acting as a bidentate ligand, the coordinate links (from the carboxylate group to the central metal) may form a closed ring, i.e. a chelate compound may be formed. In this chelating mode two additional geometries have been observed, having either four or six-membered rings, types 7 and 8, respectively.

---

5) F. A. Cotton and B. M. Foxman, *Inorg. Chem.*, 1968, **7**, 1784.
6) W. K. Bratton and F. A. Cotton, Inorg. Chem., 1969, **8**, 1299.
7) C. Calvo, N. C. Jayadevan and C. J. L. Lock, Can. J. Chem., 1969, **47**, 4213.
8) F. A. Cotton and G. Wilkinson, *Advanced Inorganic Chemistry*, 4th ed., Wiley-Interscience, New York, 1980, ch. 30-14.
9) M. Corrondo and A. C. Skapski, *J. Chem. Soc., Chem. Comm.*, 1976, 410.

Table 2.3.1-A Bonding Modes of Carboxylate Ligands

Ionic or non-coordinated (Type 1)

Ionic **Type 1** e.g. Na(OFo)	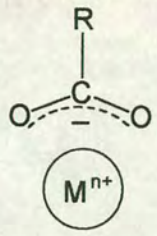

Covalent or coordinated (Types 2-8)

Unidentate **Type 2** e.g. $Li(OAc).2H_2O$ (mononuclear)	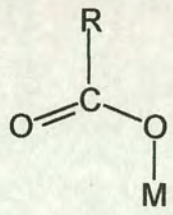

Bidentate (Types 3-8)					
Bridging (Types 3-6)				Chelating (Types 7-8)	
syn-syn	*syn-anti*	*anti-anti*	monatomic	4 mem. ring	6 mem. ring
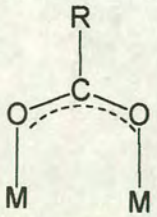	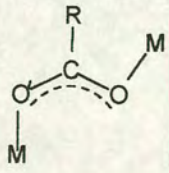	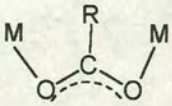	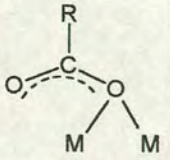	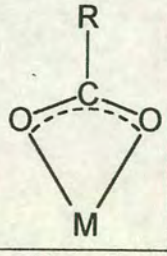	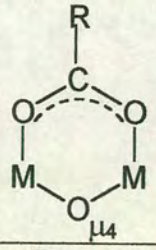
Type 3 e.g. $Cu(OAc)_2.H_2O$ (binuclear)	**Type 4** e.g. 1) $Zn(OAc)_2$ (2-D sheets) 2) $Zn(OAc)_2$ (3-D network) 3) $Zn(OPp)_2$ (2-D sheets)	**Type 5** e.g. $Cu(OFo)_2.4H_2O$ (polymeric)	**Type 6** e.g. 1) $Cu_2(OAc)_2$ (polymeric syn-syn) 2) $Cd(OAc)_2.2H_2O$ (syn-anti)	**Type 7** e.g. $Zn(OAc)_2.2H_20$ (mononuclear)	**Type 8** e.g. $Zn_4O(OAc)_6$ (tetra-nuclear)

It is the formation of a closed (chelate) ring which distinguishes type 3 (bidentate *syn-syn* bonding) from type 8, which, in all other regards, are structurally equivalent. Consequently, the usual enhanced stability of chelate systems would be expected from type 8 compounds and not from the non-chelated type 3 compounds. These 8 classifications provide a framework to describe any of the currently known examples of metal-carboxylate interactions.

This system of classification is illustrated with examples of each type in table 2.3.1-A. The crystal structures of the examples presented in table 2.3.1-A below are given in the following references; Na(OFo)[10], Li(OAc).$2H_2O$[11], $[Cu(OAc)2.H_2O]_2$[12], $Zn(OAc)_2$[13], $Zn(OAc)_2$[14], $Zn(OPp)_2$[15,16], $Cu(OFo)_2.4H_2O$[17], $Cu_2(OAc)_2$[18,19], $Cd(OAc)_2.2H_2O$[20], $Zn(OAc)_2.2H_20$[21] and $Zn_4O(OAc)_6$ [22,23,24]. Using this system the structural nature of carboxylates will now be examined more closely.

2.3.1(i) Types 1 and 2 Carboxylates

X-ray analysis of sodium formate shows it to be an example of the first classification, the ionic (type 1) structure. This structure is characterised by the equivalence of the two CO bond lengths (in the case of Na(OFo) they are both 1.27Å[10]). This equivalence of CO bond lengths is contrasted in the hydrated lithium

---

10) W. H. Zachariasen, *J. Am. Chem. Soc.*, 1940, **62**, 1011.
11) V. Amirlhalingam and V. M. Padmanabham, *Acta. Cryst.*, 1958, **11**, 896.
12) J. N. Niekerk and F. R. L. Schoening, *Acta. Cryst.*, 1953, **6**, 227.
13) W. Clegg, I. R. Little and B. P. Straughan, *Acta. Cryst.*, 1986, **C42**, 1701-1703.
14) A. V. Capilla and R. A. Aranda, "Anhydrous Zinc (II) Acetate $(CH3\text{-}COO)_2Zn$", *Cryst. Struct. Comm*, 1979, **8**, 795-798.
15) W. Clegg, I. R. Little and B. P. Straughan, "Orthorhombic Anhydrous Zinc (II) Propanoate ", *Acta. Cryst.*, 1987, **C43**, 456-457.
16) E. Goldschmied and A. D. Rae, "The Crystal Structure of Zn^{II} Propionate $(C_6H_{10}O_4Zn)_n$", Acta. Cryst., 1977, **B33**, 2117-2120.
17) R. Kiriyama, H. Ibamoto and R. Matsuo, *Acta. Cryst.*, 1954, **7**, 482.
18) R. D. Mounts, T. Ogura and Q. Fernando, *Inorg. Chem.*,1974, 13, 802.
19) M. G. B. Drew, D. E. Edwards and R. Richards, *J. Chem. Soc. Chem. Comm.*, 1973, 124.
20) W. Harrison and J. Trotter, *J. Chem. Soc. Dalton. Trans.*, 1972.
21) J. N. van Niekerk, F. R. L. Schoening and J. H. Talbot, "The Crystal Structure of Zinc Acetate Dihydrate, $Zn(CH_3COO)_2.2H_20$", Acta. Cryst., 1953, **6**, 720-723.
22) L. Hiltunen, M. Leskelä, M. Mäkelä and L. Niinistö, "Crystal Structure of μ_4-Oxo- hexakis(μ-acetato)tetrazinc and Thermal Studies of its Precursor, Zinc Acetate Dihydrate", *Acta. Chem. Scand.*, 1987, **A41**, 548-555.
23) J. Wyart, *Bull. Soc. Franc. Mineral.*, 1926, **49**, 148.
24) H. Koyama and Y. Saito, "The Crystal Structure of Zinc Oxyacetate, $Zn_4O(OAc)_6$", *Bull. Chem. Soc. Jpn.*, 1954, **27**, 112-114.

analogue (lithium acetate dihydrate $Li(OAc).2H_2O$), where the carboxylate group now functions as a unidentate (type 2) ligand. In this case, the inequivalent CO bonds are 1.33Å for the metal bonded CO, and 1.22Å[11] in the free CO unit.

2.3.1(ii) Type 3 Carboxylates

There is an increasing number of complexes, particularly within the transition series, which are found to contain bridging acetate cage structures. These arise from the *syn-syn* (type 3) configuration of the carboxylate ligand. It has been observed that such structures appear to be favoured by metals with octahedral stereochemistry which have one upe in the e_g orbitals, such as d^9 Cu^{2+}.[25] Much interest has been aroused by these structures, a prevailing postulate being that metal-metal interaction or, in some cases, bonding occurs between the metal centres. A point in case, much exploited for its richness in possibilities for both theoretical and empirical research, is the binuclear species $[Cu(OAc)_2H_2O]_2$.[26] As early as 1915 Lifschitz and Rosenbohm[27] measured the room temperature magnetic moment of copper (II) acetate monohydrate as 1.4 μ_B, appreciably lower than the spin-only value of 1.8-2.2 μ_B usually found for copper (II) compounds. Subsequently, Bleaney and Bowers,[28] having studied its anomalous EPR spectrum, suggested that this peculiar magnetic susceptibility arose from the coupling of isolated pairs of copper atoms by exchange forces. They proposed that the electron spins interact to form two energy levels. These are a singlet state, where the spins are antiparallel, and a triplet state, which is at a slightly higher energy. The characteristic shape of the susceptibility-temperature curve of this material reflects the thermal distribution of the molecules over these energy states. At the lowest temperatures the singlet state is more abundant, but as the temperature rises the triplet state becomes increasingly populated. This creates a rise in the susceptibility to a maximum, after which the expected Curie Law is followed and the susceptibility decreases with increasing temperature. Since these early investigations of copper (II) acetate monohydrate,

25) J. Lewis and R. S. Nyholm, *Sci. Progr.*, 1964, **52**, 577.
26) F. A. Cotton, *Rev. Appl. Chem.*,1967, **17**, 24.
27) J. Lifschitz and E. Rosenbohm, *Z. Electrochem*, 1915, **21**, 499.
28) B. Bleaney and K. D. Bowers, *Proc. R. Soc. London*, 1952, **A214**, 451.

there have been ample studies of other compounds of the type $Cu_2L_2(O_2CR)_4$; these are thoroughly listed by Jotham *et al.*[29]

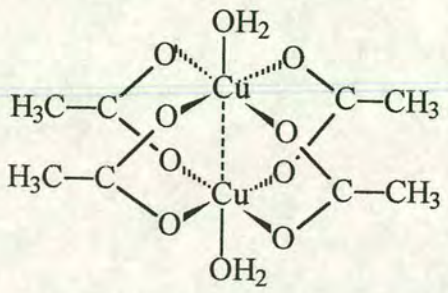

Figure 2.3.1-A Schematic representation of the structure of the dimeric copper (II) acetate $[Cu(O_2CCH_3)_2.H_2O]_2$

One outcome of these numerous studies is that the possession of a low and temperature-dependant magnetic moment is now used as the principal criterion for assigning a dimeric structure to copper (II) carboxylates. However, when considering metal-metal interactions of type 3 structures, it is important to distinguish between direct bonding and the loose coupling of spins. Recalling that acetic acid exists as a hydrogen bonded dimer, these dimeric complexes may be simply regarded as the replacement of the acidic proton of the carbonyl function with a metal. The dimeric acetic acid structure then serves as a template to locate the metal ions with sufficient proximity to one another that metal-metal bonding may be inferred. In such cases the metal atoms are only in close proximity by virtue of the steric constraints imparted by the bridging acetate ligand. However, there are some cases where the metal-metal distance is sufficiently short that there is a distortion from the hydrogen-bonded dimer dimensions. In such a case metal-metal bonding should be considered as part of the structural description of the material.

From the above discussion it is clear that to achieve substantial co-operative effects in physical properties the metal centres must be brought close enough together for adequate metal-metal interactions to occur. Additionally, the electronic configuration of the central metal must also be considered, for example, in zinc-based type 3 structures the electronic interactions that occur in copper (II) systems (such as copper (II) acetate monohydrate) would not occur, since Zn^{2+} possesses a

29) R. W. Jotham, S. F. A. Kettle and J. A. Marks, *J. Chem. Soc. A*, 1972, 428.

d^{10} outer electron configuration, and therefore has no upe's in its e_g orbital available to interact.

2.3.1(iii) Types 4 and 5 Carboxylates

The possibility of substantial co-operative effects in physical properties is a result of bridging in the type 3 *syn-syn* configuration. In contrast, in the type 4 *syn-anti* and type 5 *anti-anti* configurations, there are long metal-metal separations and only slight co-operative effects occur. The structural chemistry of copper (II) formate complexes provides examples of carboxylate systems in which metal-metal interaction is made untenable by the *syn-anti* (type 4) or *anti-anti* (type 5) bridging of the ligand. An illustration is afforded by the polymeric, tetrahydrated copper formate[17], in which the *anti-anti* (type 5) configuration of the ligand results in the closest approach of the copper atoms being 5.80Å. In the royal blue anhydrous copper (II) formate[30] the *syn-anti* configuration of the ligands results in the copper atoms having a closest approach of 3.44Å, as shown in figure 2.3.1-B. The tetragonal-pyramidal co-ordination around each copper atom requires one of the oxygen atoms to be 'shared'; this is reflected in the bond lengths. In both these cases the metal-metal bond lengths are a good deal greater than those which occur in the *syn-syn* bridged copper (II) acetate (which has a separation of only 2.615 Å between its copper atoms).[31]

The type 5 structure of polymeric copper (II) formate is known to be isomorphous with zinc (II) formate, as well as with the monoclinic formates of manganese (II), magnesium(II), cadmium(II) and strontium (II), where metal-metal separations are also large[1,32,33], as would be expected for this structure type.

2.3.1(iv) Type 6 Carboxylates

The final type of bidentate bridging of the carboxylate ligand is the type 6 monatomic configuration. In this instance the ligand bridges two metal centres, as is

30) G. A. Barclay and C. H. L. Kennard, *J. Chem. Soc.*, 1961, 3289.
31) G. M. Brown and R. Chidambaran, Acta. Cryst. B, 1973, **29**, 2393.
32) P. Groth, *Chem. Krystallographie*, **3**, Engielman, Leipzig, 1909.
33) "The Dictionary of Inorganic Compounds", **1-5**, Chapman and Hall, London, 1992.

2.3.1(iv) Type 6 Carboxylates

The final type of bidentate bridging of the carboxylate ligand is the type 6 monatomic configuration. In this instance the ligand bridges two metal centres, as is the case for types 3 to 5, but is distinctly different in that it does so through only one of its carboxylate oxygens. On its own such bonding, by necessity, would lead to longer metal-oxygen distances and weaker interactions compared with those of types 3 to 5. However, this type of bond is inadequate to support such structures, and so they always occur with other bonding types to provide greater structural rigidity for the compound, as in the case of $Cu_2(OAc)_2$[18,19] which has additional *syn-syn* bridging (type 3) carboxylates. Another example is that of $Cd(OAc)_2(H_2O)_2$[20] as illustrated in figure 2.3.1-C.

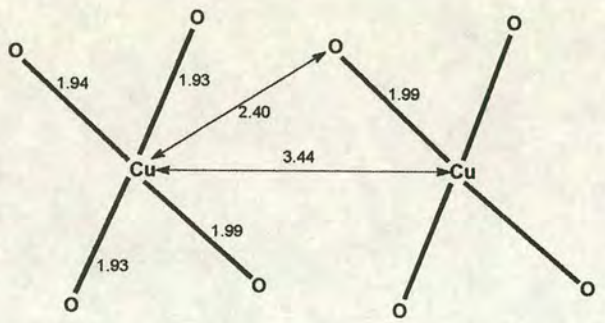

Figure 2.3.1-B Anhydrous Copper (II) Formate[30], bond lengths in Å

2.3.1(v) Type 7 and 8 Carboxylates

It is the chelating ability of carboxylate ligands which leads to the last two bonding categories. Lowry and French[34] were the first to postulate that the acetate group may function as a bidentate chelate giving a four-membered ring (type 7). This mode of bonding leads to mononuclear complexes. There are, however, only a few examples confirmed by X-ray crystallography of such an arrangement, zinc acetate dihydrate[21] being one of them. In this compound the zinc occupies a central octahedral environment with trans-diaxial water ligands and two bidentate chelating acetoxy groups, as shown in figure 2.3.1-D. The crystals are monoclinic with space group C2/c. Examples where 6-membered rings are produced are the more common of theses two types and are reviewed in the following section.

34) J. Lowry and W. French, *Proc. Roy. Soc. (London) A*, 1924, 106, 489.

The type 8 bonding mode provides arguably the most structurally fascinating examples of all the bonding categories. Where six-membered rings are present multi-nuclear complexes are most often found. Multi-nuclear carboxylates are known for other bonding modes such as type 3, for example, in the anhydrous acetates of palladium $Pd_3(OAc)_6$ and platinum $Pt_4(OAc)_8$.[5,9] It is these multi-nuclear complexes which are at the heart of the synthetic routes utilised in this research and as such they demand the greatest attention. The remainder of this section is devoted to these "high-nuclearity" materials, in particular to high-nuclearity zinc carboxylates.

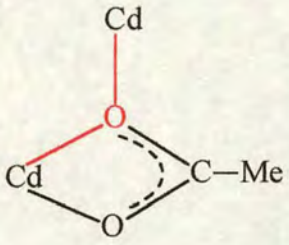

Figure 2.3.1-C Schematic representation of the structure of $Cd(OAc)_2(H_2O)_2$. The monatomic *syn-anti* bridge of the acetate oxygen is highlighted in red

In the case of type 8 zinc carboxylates, tetra-nuclear complexes occur. There are six different types of structure which have been reported for carboxylates containing a cluster of four metal atoms[2]. Of these, zinc[22], cobalt[35] and beryllium[36] form the only oxygen-centred versions (metallo complexes). They have the general formula $M_4O(LL)_n$, where LL represents a bidentate ligand and n = 6. These are the hexakis[μ-(carboxylato-O-O′)]-μ_4-oxotetrametal complexes, which are more commonly referred to as oxycarboxylato complexes, oxocarboxylates or basic carboxylates.

Throughout this work the archaic, but ubiquitous, term basic carboxylate will be used. These complexes may be classified as two-shell compounds because, in addition to the M_4O entity, there are chelating ligands co-ordinating to the metal.

---

35) J. Charalambous, R. G. Copperthwaite, S. W. Jeffs and D. E. Shaw, "Mass Spectra of Tetracobalt(II) and Tetrazinc(II) μ_4-hexa-μ-carboxylates (Basic Cobalt and Zinc Carboxylates)", *Inorg. Chim. Acta*, 1975, **14,** 53-58 and references therein.
36) A. Tullinsky, C. R. Worthington and E. Pignataro, *Acta. Cryst.*, 1959, **12**, 623.

Other $M_4O(LL)_n$ complexes, composed solely of carboxylate bridges (with $n \neq 6$), have been claimed, such as $Fe_4O(OAc)_{10}$.[2] However, no X-ray data was provided, although there was evidence of some form of cluster in the molecular structure.

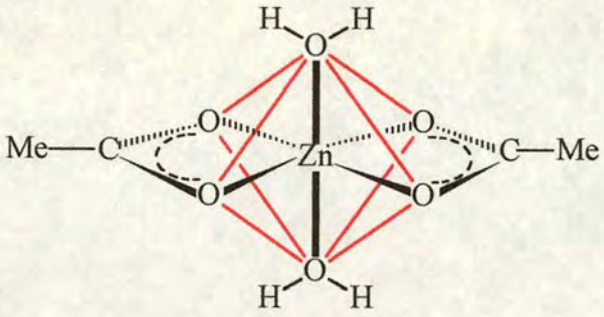

Figure 2.3.1-D Schematic representation of the structure of zinc (II) acetate dihydrate. The red lines show the octahedral arrangement of the oxygen donor set around the central zinc atom, they do not represent bonds. The formation of four membered rings by the ligation of the acetate group to the central zinc atom can also be seen.

These basic acetates possess some physical properties which are uncommon for simple metal carboxylates, viz. high volatility without decomposition and solubility in organic solvents, but not in water. Their exceptional characteristics aroused interest at the turn of the century.[37] The basic acetate $Zn_4O(O_2CCH_3)_6$ was first prepared by Auger and Robin[38] by the vacuum distillation of the neutral acetate $Zn(O_2CCH_3)_2.2H_2O$. The covalent nature of the basic acetates has been attributed to their unusual co-ordination. The early structural predictions[39,40] were later confirmed by Saito *et al*[24,41,] who showed that in the isomorphous beryllium and zinc compounds, the tetrahedral arrangement is rather regular, with Be-O and Zn-O distances ranging from 1.61 to 1.65 Å and from 1.96 to 1.98 Å, respectively. The accuracy of Saito's X-ray determinations was low (R = 0.18) by present day standards. Hiltunen *et al*[22] in 1987, obtained the following data (with an R-factor of only 0.037) for zinc oxyacetate; a = 16.402(1) Å, V = 4412.6(8) $Å^3$ and Z = 8, cubic space group *Fd3m*. Additional X-ray analysis of related basic carboxylates

37) G. Urbainand H. Lancombe, *Compt. Rend.*, 1901, **133,** 874.
38) V. Auger and I. Robin, *Compt. Rend*, 1926, **178,** 1546.
39) W. Bragg and G. T. Morgan, *Proc. Royal. Soc. (London)* , 1923, **A104**, 437.
40) W. H. Bragg, *Nature (London)*, 1923, **111,** 532.
41) T. Watanabe and Y. Saito, *Nature (London)*, 1949, **163,** 225.

complexes[36,42,43,] has repeatedly shown them to consist of six intersecting 6-membered rings formed by bidentate chelation of carboxylate ligands. In this arrangement the six carboxylate ligands edge-bridge a metal tetrahedron with a μ_4 oxygen atom at the centre (a feature first suggested in 1923).[40] Hence, all four zinc atoms are tetrahedrally co-ordinated to four oxygen atoms leading to an environment similar to that found in the lattice of bulk zinc oxide. Indeed, the emission properties of $Zn_4O(O_2CCH_3)_6$ have been used to demonstrate that it behaves as if it were the smallest zinc oxide particle.[44] The Zn-O and Zn-Zn distances for both compounds are almost identical (Zn-O ca. 1.97 Å in ZnO c.f. 1.94 Å in $Zn_4O(O_2CCH_3)_6$) and Zn-Zn ca. 3.20 Å in ZnO c.f. 3.16Å in $Zn_4O(O_2CCH_3)_6$.

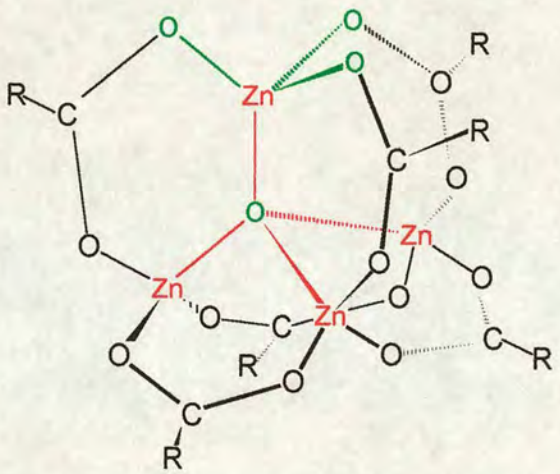

Figure 2.3.1-E Schematic representation of the structure of $Zn_4O(O_2CR)_6$. Part of the structure is coloured green to show the tetrahedral arrangement of oxygen atoms around a central zinc atom. Another part is coloured red to show the tetrahedral arrangement of zinc atoms around a central oxygen atom. This arrangement is analogous to that found in ZnO.

Besides the $M_4O(LL)_6$ type oxygen-centred metal complexes discussed above, there are related M_4O species. These have been discussed by Bergerhoff and Paeslack[45]

42) W. Clegg, D. R. Harbron, C. D. Homan, P. A. Hunt, I. R. Little and B. P. Straughan, "Crystal Structures of Three Basic Zinc Carboxylates together with Infrared and FAB Mass Spectrometry Studies in Solution", *Inorg. Chim. Acta*, 1991, **186**, 51-60.

43) W. Cen, K. J. Haller and T. P. Fehlner, "Transition-Metal Clusters as Substituents. Synthesis, Structure, and Thermal Decomposition of $Zn_4O[(CO)_9Co_3(\mu_3\text{-}CCO_2)]_6$", *Inorg. Chem.*, 1991, **30**, 3120-3121.

44) H. Kunkely and A. Vogler, "Absorption and Emission Spectrum of $[Zn_4O(Acetate)_6]$",*J. Chem. Soc., Chem. Com.*, 1990, 1204-1205.

45) G. Bergerhoff and J. Z. Paeslack, *Kristallogr.*, 1968, **126,** 112.

and, more recently, by Kauffman *et al.*[46] There are several M_4O compounds for which X-ray structural data are available[22]. In all cases M is a relatively small divalent cation. The majority of the compounds contain Cu^{2+} as the metal co-ordinating to the central oxygen, other divalent ions being Be^{2+}, Zn^{2+} and Mg^{2+}. The Cu_4O arrangement is, apparently, a stable configuration, as indicated by the existence of the oxide Cu_4O.[47] However, there are no purely carboxylate bridged μ_4-oxo complexes of copper, nor of magnesium. In virtually all copper and magnesium cases the metal atoms are 5-coordinate (with trigonal bipyramidal arrangement) and a complex of general formula $[M_4OL_nX_{10-n}]^{n-4}$ is formed, where X represents a halide ion and L a Lewis base ligand, e.g. $Mg_4Br_6.4(C_4H_{10}O)$[48] and $Cu_4OCl_6(2\text{-mepy})_4$[49] (see Fig. 2.3.1-F).

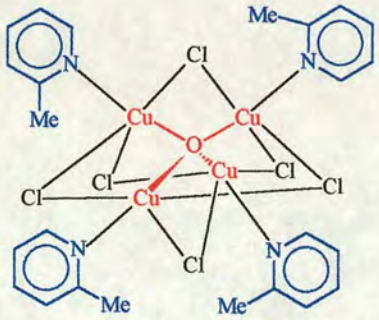

2.3.1-F Schematic representation of the structure of $Cu_4OCl_6(2\text{-mepy})_4$. The central tetrahedral arrangement of copper atoms around the μ_4-oxy-atom is shown in red. Six chloride bridges span the six tetrahedral edges formed by the copper atoms. The copper atoms are then each further bonded to a single 2-mepy moiety, shown in blue, gaining an overall trigonal bipyramidal co-ordination.

However, Teipel *et al.*[50] recently synthesised the first examples of this type of complex where the ligands are chelating. Of particular interest within their report

46) G. Kauffman, M. Karbassi and G. J. Bergerhoff, *Chem. Educ.*, 1984, **61,** 729.
47) R. Guan, H. Hashimoto, K. H. Kuo and T. Yoshida, Acta. Cryst., 1987, **B43,** 343.
48) G. Stucky and R. E. Rundle, *J. Am. Chem. Soc.*, 1964, **86,** 4821.
49) N. S. Gill and M. Sterns, "title re $Cu_4OCl_6(2\text{-mepy})_4$", *Inorg. Chem.*, 1970, **9**, No.7, 1619.
50) S. Teipel, K. Griesar, W. Haase and B. Krebs, "A New Type of μ_4-Oxo-Bridged Copper Tetramer: Synthesis, X-ray Molecular Structure, Magnetism and Spectral Properties of (μ_4-Oxo)tetrakis(μ-bromo)bis(μ-2,6-bis(morpholinomethyl)-4-methylphenolato)tetracopper(II) and (μ_4-Oxo)tetrakis(μ-benzoato) bis(μ-2,6-bis(morpholinomethyl)-4-methylphenolato)tetracopper(II)", *Inorg. Chem.*, 1994, **33**, 456-464.

was the synthesis of $[Cu_4O(OBz)_4(bmmk)_2].H_2O$[51] which demonstrates that Cu-Cu edges may be bridged in a bidentate chelating fashion by carboxylato ligands, in this case benzoate bridges. This bridging leads to significant perturbation of the $[Cu_4O]$ framework. The copper centres are no longer trigonal bipyramidally co-ordinated. Two atoms show square pyramidal co-ordination, the third copper atom is square planar and the fourth shows octahedral co-ordination. Nevertheless, a (slightly distorted) tetrahedron of four copper (II) atoms is still observed around the central oxygen. This very unsymmetrical co-ordination of the metal centres is due to the nature of the $\mu_{1,3}$-benzoate bridge bonding. It does not seem unreasonable, therefore, that a copper oxycarboxylate analogue of the zinc and beryllium oxycarboxylates may be prepared, although it would be anticipated to contain additionally coordinated monodentate ligands to provide a 5-coordinate environment for the copper atoms, e.g. something of the type $Cu_4O(O_2CR)_6(L)_4$, where L could be water or some other neutral donor ligand, in order to preserve electro-neutrality

Finally, mention should be made of the ability to form bi and trinuclear carboxylates, as well as polynuclear carboxylates with greater than four metal centres.

2.3.1(vi) Binuclear Carboxylates

The most well known binuclear carboxylate is copper (II) acetate which received much attention due to the debate over the nature of its Cu-Cu interactions.[2,52,53] This was reviewed earlier in this section as an example of type 3 carboxylate bonds. Whilst there is no known purely carboxylate bridged binuclear zinc complex, the existence of $[Zn_2(CH_3CO_2)_3(OCH_3)]$,[54] a three-dimensional polymer, comes close.

---

51) bmmk = the tridentate ligand 2,6-bis(morpholinomethyl)-4-methylphenolate 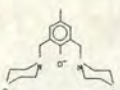

52) R. J. Doedens, "Structure and Metal-Metal Interactions in Copper (II) Carboxylate Complexes", *Prog. Inorg. Chem.*, 1976, **21,** 209-231.

53) M. Kato, H. B. Jonassen and J. C. Fanning, "Copper (II) Complexes with Subnormal Magnetic Moments", *Chem. Rev.*, 1964, **64,** 99-128.

54) C. D. Chandler, G. D. Fallon and B. O. West, "Synthesis and Molecular Structure of $[Zn_2(CH_3CO_2)_3(OCH_3)]$", *Polyhedron*, 1993, **12,** 2001-2004.

Another example of a binuclear carboxylate is formed by trivalent boron in tetra-acetyl diborate, $B_2O(OAc)_4$.[55]

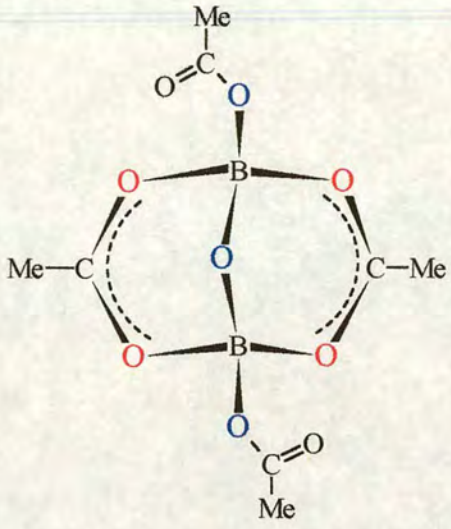

Figure 2.3.1-G Schematic representation of tetra-acetyl diborate, $B_2O(OAc)_4$, $C_8H_{12}O_9B_2$

$B_2O(OAc)_4$ consists of two distorted boron-oxygen tetrahedra, sharing a vertex, with all other oxygen vertices being connected to carbon atoms of the four acetoxy groups. The two tetrahedra are arranged so as to have two edges parallel (as indicated by the oxygen atoms coloured red) and two edges nearly linearly aligned (shown by the oxygen atoms coloured blue). The angle formed by the these near linear edges is 173.8^{O} and is conditioned by the two bridging acetoxy groups. In fact, the O_1 to O_2 separations of the two bridging acetoxy groups (i.e. O_1-C-O_2) are arranged so that the two B-O tetrahedra have a B_1 to B_2 separation of only 2.265Å, far shorter than those found in other borates. This example highlights the influence that bridging carboxylates may exert over the structures of materials. It is also interesting in that it demonstrates both type 2 and type 8 bonding in the same compound, since two acetoxy groups are linked *via* their oxygen atoms to both boron atoms (type 8), and each of the other two acetoxy groups has only one oxygen bonded to a boron atom (type 2). However, in spite of the anticipated added stability

55) A. D. Negro and L. Ungaretti, "Crystal and Molecular Structure of Tetra-acetyl Diborate", *J. C. S. Dalton*, 1972, 1639-1643.

due to having two chelating acetoxy groups (type 8), the crystals are relatively unstable and immediately decompose in air (m.p. 147-148^{O}C).

2.3.1(vii) Tri-nuclear Carboxylates

Trinuclear oxy-carboxylate complexes are formed most commonly by trivalent cations[2,22,56], although trinuclear carboxylates (those without central oxygen atoms) may be formed by divalent cations, an example being palladium in trimeric palladium (II) acetate, $Pd_3(OAc)_6$.[5]

Regarding the trinuclear oxycarboxylates, most structures take the form of the triangular cluster $[M_3L_3O(RCO_2)_6]^+$ in which an oxygen atom is situated at the centre of an equilateral triangle of metal atoms. Two carboxylate groups bridge each pair of metal atoms and a monodentate ligand is coordinated to each metal atom, thus providing the metals with an octahedral configuration. This planar trigonal arrangement of metal ions is exemplified by $[Fe_3O(OAc)_6(H_2O)_3].ClO_4$, $[Cr_3O(OAc)_6(H_2O)]ClO_4.6H_2O$ and $[Ru_3O(OAc)_6](OAc)$.[56] Only one complex of carboxylate shows a linear array of 3 metal atoms. This is the compound $Co_3(quinoline)_2(OBz)_6$, which, whilst it is not a pure carboxylate, is of interest due to this structural feature.

2.3.1(viii) Polynuclear Metal Carboxylates of the form $M_xO_y(O_2CR)$ where x>4

The first reported description of basic carboxylates with greater than four metal centres was given by Novoselova in 1956 for the compound $Be_5O_2(OAc)_6$[57] For the purpose of taxonomy these materials (where $x > 4$) will be referred to as "higher nuclearity carboxylates". A plethora of papers on many new higher beryllium oxoacetates followed Novoselova's report,[58,59,60,] particularly by Grigor'ev and

56) W. P. Griffith, "Tri- and Tetra- nuclear Oxy-complexes", *J. Chem. Soc. (A)*, 1969, 2270-2273.
57) A. V. Novoselova, K. N. Semenenko, N. N. Krasovskaya and Yu. P. Simanov, *Vest. Mosk. Univ. Khim.*, 1956, **N3**, 8. (In Russian).
58) A. I. Grigor'ev and V. I. Nefedov, "X-ray Electronic Spectra on Complex Compounds of Beryllium", *Dokl. Akad. Nauk. SSSR*, 1973, **210(2)**, 434-344. (In Russian)
59) A. I. Grigor'ev, L. N. Reshetora and A. V. Novoselova, "Compounds of Dioxo-octaacetatohexaberyllium with Ammonia", *Russ. J. Inorg. Chem.*, 1974, **19(8)**, 1093-1096.
60) V. A. Sipachev and A. I. Grigor'ev, "Vibrational Spectra of Beryllium Oxide Carboxylates", *Russ. J. Inorg. Chem.*, 1972, **17(2)**, 176-182.

Sipachev. They were the first to report the formation of $Be_6O_2(OAc)_8$ in 1970,[61] which they claimed to be polymorphic, having both α and β modifications.[62] Their characterisation of this structure was based upon elemental analyses, X-ray powder diffraction patterns and, especially, infrared spectra. The elemental analysis gave the formula $Be_3O(OAc)_4$ to within a maximum of 1% error (for acetate analysis). From this the beryllium dioxoacetate formulation $Be_6O_2(OAc)_8$ was made by inference from the low frequency infra red (200-900 cm^{-1}) metal-oxygen (Be-O) framework vibrations. Sadly, none of the work, which covers many exotic structural descriptions was supported by X-ray crystallographic data, although the case argued on the basis of the infra red data was highly plausible. All the work produced by these authors followed the same format of infra red, elemental analysis and X-ray powder diffraction based structural deteminations, without X-ray crystallographic structural determinations. However, in 1974 Atovmyan[63] confirmed the predicted structure of $Be_6O_2(OAc)_8$ with the low temperature X-ray crystallographic study of the triclinic α modification of $Be_6O_2(OAc)_8$. The results showed (R = 0.084) that the material consisted of two edge-shared OBe_4 tetrahedra joined by a common edge (fig. 2.3.1-H). There are consequently two types of beryllium atom present; four terminal and two bridging with respect to the oxygen tetrahedra, as was predicted by Grigor'ev and Sipachev. In this respect, there are also two forms of type 8 bridging acetate groups; four are bridging terminal beryllium atoms and the other four bridge one bridging, and one terminal, beryllium atom. Mass spectra of $Be_6O_2(OAc)_8$ as well as $Be_5O_2(OAc)_6$ and $Be_7O_2(OAc)_8(OH)_2$ were subsequently reported.[64] A remarkable feature of the mass spectrum of $Be_5O_2(OAc)_6$ is the presence of ions with *m/z* above the molecular weight of the parent compound.

---

61) A. I. Grigor'ev, V. A. Sipachev and A. V. Novoselova, "Synthesis and Characterisation of a New Oxyacetate of Beryllium: $Be_6O_2(OCOCH_3)_8$", *Dokl. Akad. Nauk. SSSR*, 1970, **194(4)**, 808-809. (In Russian).

62) A. I. Grigor'ev, V. A. Sipachev and A. V. Novoselova, "The Polymorphism of Beryllium Dioxide Acetate $Be_6O_2(OCOCH_3)_8$ ", *Russ. J. Inorg. Chem.*, 1972, **17(2)**, 297-298.

63) L. O. Atovmyan, O. N. Krasochka, A. I. Grigor'ev and V. A. Sipachev, "X-ray Structural Investigation of Beryllium Dioxoacetate", *Dokl. Akad. Nauk. SSSR*, 1974, **225**, 99-100. (In Russian).

64) A. I. Grigor'ev and L. N. Reshetova, "Mass Spectra of Beryllium Dioxoacetates", *Inorg. Chim. Acta*, 1977, **25**, L81.

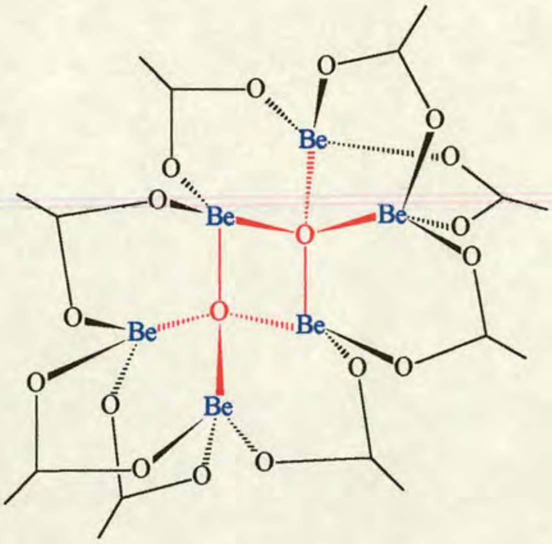

Figure 2.3.1-H Schematic representation of beryllium dioxoacetate $Be_6O_2(OAc)_8$. The two central μ_4-oxygen atoms are shown in red surrounded by the tetrahedrally coordinated beryllium atoms, shown in blue.

Beryllium carboxylates offer a richness of structural diversity unmatched by the carboxylates of any other element. The chemistry of beryllium acetato derivatives is, in general, governed by the preference of the divalent beryllium atom for the formation of coordination tetrahedra. Six membered cycles, a characteristic feature of beryllium stereochemistry, provide the most favourable conditions for charge redistribution and the formation of coordination tetrahedra. Thermodynamic stability of these cycles is probably responsible for the stability of such unusual molecular compounds as basic beryllium acetate and its structural analogues containing four-coordinate oxygen atoms. Given the similarity of neutral and basic zinc carboxylates to their beryllium analogues, the question arises as to whether the formation of zinc based structures analogous to the higher nuclearity basic beryllium carboxylates may be feasible.

For zinc there is, at least, one higher nuclearity basic carboxylate for which a crystal structure has been obtained. This was prepared by Clegg *et al.*[65] in the form of the basic crotonoate $[Zn_5(OH)_2(O_2CCHCHCH_3)_8]_n$ which exists as a chain polymer

65) W. Clegg, D. R. Harbron, C. D. Homan, P. A. Hunt, I. R. Little and B. P. Straughan, "Crystal Structures of three basic zinc carboxylates together with infra red and FAB mass spectrometry studies in solution", *Inorg. Chim. Acta*, 1991, **186**, 51-60.

consisting of five zinc atoms (four of which are tetrahedrally coordinated, the other being octahedrally coordinated); these are linked by two hydroxy groups and six *syn-syn* bridging (type 3) crotonoates. The mass spectra of this compound and others referred to in the same paper was of great interest. This is discussed in more detail in section 2.3.3. In brief, species such as $[Zn_6O_2(OCt)_7]^+$ and others with m/z values greater than that of the parent ion were observed. Many of the fragmentation patterns mirrored those observed for the beryllium analogue $Be_6O_2(OAc)_8$. This mirroring of mass spectral behaviour further supports the notion that zinc higher nuclearity basic carboxylates may be synthesised as stable compounds. Investigating this possibility forms one of the challenges of the experimental work conducted here.

2.3.2 Chemical Properties of Carboxylates

Of the large range of carboxylates it is only the basic carboxylates which are of interest as potential sources of hydrolysable materials for use as potential H_2S absorbents. Consequently, only these materials and their precursors, the neutral salts, are considered in the following account.

Generally, formate and acetate ions form many stable co-ordination complexes. Propionates and derivatives of higher acids show the same chemical tendencies as acetates, coupled with a decreasing tendency to coordinate as chain length increases.

2.3.2(i) Preparative Routes to Carboxylates

Zinc oxyacetate, $Zn_4O(O_2CCH_3)_6$, exists as white, octahedrally shaped crystals which melt at 252.3 ^{0}C and are soluble in a variety of solvents such as benzene, CH_2Cl_2, methanol and ethanol.[1] Koyama and Saito[2] noted that, when freshly formed, the crystals are transparent, but, on prolonged exposure to moist air, they are hydrolysed and become opaque. The product of this hydrolysis has been reported to be ZnO.[1,3] Due to this slight sensitivity to atmospheric moisture, solvents used in preparative routes have to be completely dry in order to avoid hydrolysis.

In an account by Gordon and Silver[4] several preparative routes to basic zinc carboxylates were outlined. They found that basic zinc acetate and propionate could only be prepared by the vacuum pyrolysis of the neutral salts, with yields of 55% and 49%, respectively. However, Hardt and Stavenow[5] reported yields of 55% of basic zinc acetate by reacting saturated $Zn(OAc)_{2(aq)}$ with ZnO (in 3:1 ratio respectively) under aqueous reflux. Given the previous observation regarding the sensitivity of the

---

1) *Dictionary of Inorganic Chemistry*, Chapman and Hall, London, 1992, **1-5**.
2) H. Koyama and Y. Saito, "The Crystal Structure of Zinc Oxyacetate, $Zn_4O(CH_3COO)_6$", *Bull. Chem. Soc. Jpn.*, 1954, **27**, 112-114.
3) H. Kunkely and A. Vogler, "Adsorption and Emission Spectrum of $[Zn_4O(Acetate)_6]$", *J. Chem. Soc., Chem. Comm.*, 1990.
4) R. M. Gordon and H. B. Silver, "Preparation and Properties of tetrazinc μ_4-oxohexa-μ-carboxylates (basic zinc carboxylates)", *Can. J. Chem.*, 1983, **61**, 1218-1221.
5) H. D. Hardt and F. Stavenow, *Z. Anorg. Allg. Chem.*, 1959, **301**, 267-270.

desired product to water, this method seems flawed. Hiltunen *et al.*[6] found that when a sufficiently low heating rate was applied, using the vacuum sublimation technique, only a small fraction of the zinc acetate, oxyacetate or both decomposes to zinc oxide and, hence, that zinc acetate may be almost quantitatively sublimed.

2.3.2(ii) Thermal Behaviour of Carboxylates

The thermal behaviour of carboxylates is of particular interest in its relation to the vacuum sublimation of neutral salts to form its basic salt. Understanding the mechanism of these reactions enables one to tailor the experimental set-up to maximize the yield and quality of basic salts formed.

Zinc acetate has a considerable vapour pressure above 180^0C. Hardt and Stavenow[5] claimed that $Zn(OAc)_2$ decomposes at 150^OC to form ZnO and Ac_2O and that at 300^OC it decomposes to give ZnO and Me_2CO. They neglected to mention the necessary formation of CO_2 in order to balance the equation for the reaction at 300^OC. Subsequent authors have observed that in the region 250-252^OC zinc acetate decomposes, but also forms the basic salt $Zn_4O(OAc)_6$. [4,6,7]

Hiltunen *et al.*[6] observed that when zinc (II) acetate dihydrate is slowly heated in air or nitrogen it first dehydrates, after which almost complete volatilization follows. The sequence and extent of thermally induced reactions were found to be strongly influenced by experimental conditions such as sample size, heating rate and crucible shape.[8] The last-mentioned factor influences the self-generated atmosphere and may have a significant effect on the decomposition on $Zn(OAc)_2.2H_20$. Thermal decomposition of zinc acetate, and the formation of oxyacetate, have also been studied in detail by McAdie,[7] who used a thermoanalyzer for simultaneous TGA and DTA measurements, as well as a separate instrument for DTA curves. He concluded

---

6) L. Hiltunen, M. Leskelä and L. Niinistö, "Crystal Structure of μ_4-oxo-hexakis(μ-acetato)tetrazinc and Thermal Studies of its Precursor, Zinc Acetate Dihydrate", *Acta. Chem. Scand.*, 1987, **A41**, 548-555.

7) H. G. McAdie, *J. Inorg. Nucl. Chem.*, 1966, 2801.

8) J. Catterick and P. Thornton, "Structures and Physical Properties of Polynuclear Complexes", *Adv. Inorg. Chem. & Radiochem.*, 1977, **20**, 291-362 and references there-in.

that in dynamic nitrogen atmosphere anhydrous zinc (II) acetate may decompose via two alternative routes [Eqn.(2.3.2-A) or Eqn.(2.3.2-B)]:

$$Zn(CH_3COO)_{2(s)} \xrightarrow{A1} Zn(CH_3COO)_{2(l)} \xrightarrow{A2} ZnO_{(s)} + CH_3COCH_{3(g)} + CO_{2(g)} \quad \text{Eqn. 2.3.2-A}$$

or

$$4\ Zn(CH_3COO)_{2(s)} \xrightarrow{B1} Zn_4O(O_2CCH_3)_{6(s)} + (CH_3CO)_2O_{(g)} \xrightarrow{B2} Zn_4O(O_2CCH_3)_{6(l)}$$

$$\xrightarrow{B3} 4\ ZnO_{(s)} + 3\ CH_3COCH_{3(g)} + 3\ CO_{2(g)} \quad \text{Eqn. 2.3.2-B}$$

In the first process (2.3.2-A) the neutral salt liquefies (step A1) then decomposes (A2). Alternatively, in the second process (2.3.2-B), the neutral salt tetramerizes to form the basic acetate in the solid state with the evolution of acetic anhydride (B1). It is debatable whether the degree of molecular mobility required for the internal rearrangement, causing bulk volume and ordering changes, and the evolution of gaseous materials in this proposed step, could all occur in the solid phase. However, as a rule of thumb, when it reaches 80% of the melting point value in Kelvin (where materials begin to sinter) a solid may become sufficiently mobile to allow internal rearrangement. It is also feasible that there is sufficient void space within the $Zn(OAc)_2$ structure to allow these rearrangements to occur. This effect would be enhanced if the dihydrate were used, because it would have dehydrated during the thermal sequence, creating increased internal void space.

McAdie proposed that, subsequent to the above step, the basic acetate then liquefies (B2) and subsequently decomposes, (B3) with the formation of zinc oxide, carbon dioxide and propanone (acetone, dimethyl ketone). Hiltunen *et al* [6] differed on their interpretation of the effects associated with the doublet endothermic peak around 250 ^{0}C at which the sublimation process occurs. They summarised the sequence of reactions in nitrogen as follows:

$$4\ Zn(CH_3COO)_{2(s)} \xrightarrow{C1} 4\ Zn(CH_3COO)_{2(l)} \xrightarrow{C2} Zn_4O(O_2CCH_3)_{6(s)} + (CH_3CO)_2O_{(g)}$$

$$\xrightarrow{C3} Zn_4O(O_2CCH_3)_{6(l)} \xrightarrow{C4} Zn_4O(O_2CCH_3)_{6(g)} \quad \text{Eqn. 2.3.2-C}$$

Initially the neutral salt liquefies (C1), which is in agreement with McAdie's step (A1). The liquefied neutral salt then tetramerizes (C2). This corresponds with McAdie's formation step (B1), although it is a far more plausible formation step since the process now occurs in the liquid phase, allowing the ready volume changes etc. required for the tetramerization to occur. Further heating of the tetramer then causes clean melting (C3) and evaporation (C4), with no decomposition. This disagrees with McAdie's observation of the decomposition of the basic salt (B3). However, at heating rates of $5^{O}C\ min^{-1}$, Hiltunen *et al.* found that only a small fraction of the zinc acetate or its basic salt decomposed to zinc oxide, leaving very little unvolatilized residue, i.e. at sufficiently low heating rates the zinc acetate may be almost quantitatively sublimed to form the basic acetate. Even at heating rates of $200^{O}C\ min^{-1}$ the amount of residue was found to account for only 15% of the original weight (complete conversion of zinc acetate dihydrate to ZnO would lead to a residue of 37 weight%. These observations are tantamount to accepting that the decomposition stages proposed by McAdie do, in fact, occur.

The thermal decomposition of the homologous neutral zinc propionate has also been studied.[9,10] Panevchik *et al.*[9] made a detailed study of the thermal decomposition of zinc propionate in inert media, vacuum and air monitored by thermal analysis, X-ray diffraction, gas chromatography and mass spectrometry. They concluded that the reaction occurs in two parallel directions with the formation of zinc oxide and the oxide salt $Zn_4O(OPp)_6$ as solid decomposition products. The primary decomposition products were found to be propionic anhydride and zinc oxide. The DTA curve for zinc propionate in argon showed three endothermic peaks with minima at 210, 310 and $330^{O}C$. The first endothermic effect was followed by fusion of the salt and accompanied by mass loss. X-ray analysis showed the product of the first endothermic event to be the basic propionate according to the proposed reaction:

$$4\ Zn(C_2H_5COO)_2 \rightarrow Zn_4O(C_2H_5COO)_6 + (C_2H_5COO)_2O \qquad \text{Eqn. 2.3.2-D}$$

---

9) V. V. Panevchick, V. M. Goryaev and V. G. Guslev, "The Thermal Decomposition of Zinc Propionate", *Russ. J. Inorg. Chem.*, 1982, **27**, 1241-1244.

10) P. S. Bassi, H. S. Jamwal and B. S. Randhawa, "Comparative Study of the Thermal Analysis of Some Transition metal (II) Propionates. Part 1", *Thermochimica Acta*, 1983, **71**, 15-24.

Panevchik does not specify the states of the materials in the equation given, but it is possible to infer them from the anecdotal description of the reaction sequence and the final proposed reaction summary. From this Eqn. 2.3.2-D can be expanded to read:

$$4\ Zn(C_2H_5COO)_{2(s)} \xrightarrow{E1} 4\ Zn(C_2H_5COO)_{2(l)} \downarrow E2$$
$$Zn_4O(C_2H_5COO)_{6(s)} + (C_2H_5COO)_2O_{(g)} \qquad \text{Eqn. 2.3.2-E}$$

where steps E1 and E2 correspond exactly with Hiltunen's steps C1 and C2. Panevchik observed that not all the neutral salt decomposed by this pathway, in fact only about 20% of the neutral salt was converted to the basic propionate.

Analysis of the volatile decomposition products of zinc propionate at 130^{O}C showed the chief product to be propionic anhydride, the concentration of which decreased with increase in the decomposition temperature (130-300^{O}C). The concentrations of propionic acid and diethyl ketone were observed to increase; the latter becoming the principal decomposition product at 280-300^{O}C. In the gas phase CO, CO_2, water and ethane were detected. In addition, zinc oxide was found to catalyse the secondary decomposition products (propionic acid its anhydride). Propionic acid may be obtained both by the hydration of the anhydride by water formed during all stages of the propionate decomposition and, apparently, according to Eqn. 2.3.2-F:

$$(C_2H_5CO)_2O \rightarrow C_2H_5COOH + \underset{\text{methylketene}}{CH_3\text{-}CH{=}CO} \qquad \text{Eqn. 2.3.2-F}$$

The acid was shown to begin decomposing at 120^{O}C according to Eqn. 2.3.2-G:

$$2\ C_2H_5COOH \xrightarrow{ZnO} \underset{\text{diethyl ketone}}{C_2H_5COC_2H_5} + CO_2 + H_2O \qquad \text{Eqn. 2.3.2-G}$$

Whilst the anhydride dissociated at the higher temperature of 180^{O}C, also yielding diethyl ketone, according to Eqn. 2.3.2-H:

$$(C_2H_5CO)_2O \xrightarrow{ZnO} C_2H_5COC_2H_5 + CO_2 \qquad \text{Eqn. 2.3.2-H}$$

Further temperature increase caused further decompositions:

$$C_2H_5COC_2H_5 \rightarrow C_2H_6 + CH_3\text{-}CH{=}CO \qquad \text{Eqn. 2.3.2-I}$$

$$CH_3\text{-}CH{=}CO \rightarrow 2\,C + 2\,H_2 + CO \qquad \text{Eqn. 2.3.2-J}$$

In conclusion, they postulated the mechanism of the thermal decomposition of zinc propionate could be represented as below:

$$\begin{array}{ccccc} Zn_4O(C_2H_5COO)_{6(s)} + (C_2H_5CO)_2O_{(g)} & \longrightarrow & & & 4C_2H_5COC_2H_{5(g)} + 4CO_{2(g)} \\ \uparrow K2 & & & K4 \downarrow & \uparrow K5 \\ \uparrow & & & \downarrow & \uparrow \\ 4\,Zn(C_2H_5COO)_{2(s)} & \xrightarrow[K1]{} & 4\,Zn(C_2H_5COO)_{2(l)} & \xrightarrow[K3]{} & 4\,ZnO + 4\,(C_2H_5CO)_2O \end{array}$$

Eqn. 2.3.2-K

Where the first process (K1) is the liquefaction of the neutral salt, which corresponds to steps A1 of McAdie and C1 of Hiltunen. The next process (K2) is the formation of the basic salt from the liquefied neutral salt. Whilst the resulting state of the basic salt was not specified, this step agrees in all other manner with that of Hiltunen's proposed second step (C2). After this point Panevchik *et al.* observed decomposition phenomena, in line with McAdie's observations rather than Hiltunen's observation of near decomposition free melting and evaporation. They proposed additional secondary pathways, whereby both the liquefied neutral salt (K3) and the basic salt (K4) decompose to form zinc oxide and propionic anhydride, which itself further decomposes (K5) to diethyl ketone and CO_2. Given that McAdie did not study decomposition products at intermediate temperatures it is feasible that he missed the intermediate formation of the carboxylic anhydride in steps A2 and B2. If it is assumed that these processes do occur, then Panevchik's steps K3/K5 correspond with McAdie's step A2, via intermediate carboxylic anhydride, and Panevchik's steps K4/K5 correspond with McAdie's step B2, via intermediate carboxylic anhydride formation also.

The use of air in place of nitrogen had a profound effect upon the reaction outcome. The double endothermic peak (310 and 330 ^{O}C) was found to be masked by a series of exothermic peaks due to the oxidation of the decomposition products by atmospheric oxygen. It was found that when the removal of volatile thermal decomposition products was restricted by diffusion (for example, by using conical sample holders), they underwent various secondary exothermic transformations.

When vacuum conditions were applied the basic salt, $Zn_4O(OPp)_6$, sublimed and the quantity of normal salt decomposing according to Eqn. 2.3.2-E increased sharply, accounting for up to 50% of the reaction pathway. This contrasts with the results in dynamic nitrogen atmosphere, where only about 20% of the neutral salt was converted to the basic propionate, i.e., vacuum conditions facilitate the production of the basic salt. The effect of the vacuum is to remove gaseous by-products, but these are also removed (through flushing) when a dynamic nitrogen environment is applied. So, it seems unlikely that this is the cause of the observed effect, although the rate of removal of gaseous products could alter the reaction outcome where competing processes occur. A likelier explanation is that the decreased pressure facilitates the sublimation of the basic salt (removing it from the reaction), which, by Le Chatelier's Principle, favours the further production of the basic salt. If entropy considerations are ignored, then out of the two competing processes (K2 and K3) K2 will be favoured, since it yields only 1 mole of gaseous products from 1 mole of neutral salt, whereas K3 yields 4 moles of gaseous products from 1 mole of neutral salt. Thus, if, hypothetically, 1 mole of gaseous products were removed from each of the reaction schemes then in K2 four moles of the neutral salt would be converted to products (in this case the desired basic propionate). On the other hand, in K3, only one mole of neutral salt would be converted to products (in this case the undesired decomposition products). Thus the generation of the basic salt over decomposition products would be favoured in the ratio 4:1. Of course, given the number of variables in the reaction set-up, other plausible explanations for the increase in basic salt formation under vacuum conditions could be postulated.

In any thermal analysis multiple parameters, such as heating rate, geometry of sample holder and of furnace/heat source, amount, volume, size of particles, packing, density and thermal conductivity of the sample affect the reaction outcome. This may present difficulties when interpreting results of differing authors, leading to equally valid, and yet contradictory conclusions. In spite of these difficulties, the results and conclusions of the authors correlate well. To some degree, these areas of common agreement provide an effective basis for the interpretation of thermal data obtained in the present research.

2.3.3 Spectral Properties of Carboxylates

In section 2.3.1 the broad range of physical structures exhibited by zinc and some other metal carboxylates was reviewed. When synthesising novel materials crystals suitable for X-ray analysis are sometimes difficult to obtain. Infrared spectroscopy provides a useful tool in predicting certain structural features of metal carboxylates, although caution must be exercised in so doing. The carboxylate ligand is the most amenable portion of the structure for infrared analysis. Since the various bonding modes of the carboxylate ligand have been delineated already it is now possible to examine the extent to which infrared techniques may be employed to corroborate structural assignments.

2.3.3(i) Infrared Spectroscopy of Carboxylates

Detailed reviews in this field, up to 1983, have been presented by Mehrotra and Bohra[1] and up to 1986 by Nakamoto.[2] More detailed infrared analyses of zinc (II) acetate dihydrate[3] and zinc oxyacetate[4] have also been made, which relate directly to the work conducted herein. The following section presents an overview of the salient issues concerning this form of analysis as it pertains to the assignment of carboxylate bonding modes.

In the infrared spectrum of carboxylates the O-C-O stretching modes are usually the most prominent features. When a ligand coordinates to a metal, its symmetry is usually lowered and many infrared and Raman active vibrations that are degenerate in the spectrum of the free ligand are split in the spectrum of the complex. Thus, a study of the vibrational spectra can often yield useful information about the symmetry and structure of a complex. As a basis for this review the structural classifications used in section 2.3.1 will be used. It is worth bearing in mind, however, that these categories are not entirely distinct. It can be difficult to decide

---

1) R. C. Mehrotra and R. Bohra, *Metal Carboxylates*, Academic Press, London, 1983.
2) K. Nakamoto, *Infrared and Raman Spectra of Inorganic Coordination Compounds*, 4th edn., Wiley, New York, Chichester, 1986, ch. 3.
3) M. K. Johnson, D. B. Powell and R. D. Cannon, "Vibrational Spectra of Carboxylato Complexes - I. Infrared and Raman Spectra of Beryllium (II) Acetate and Formate and of Zinc (II) Acetate and Zinc (II) Acetate Dihydrate", *Spectrochim. Acta*, 1981, **37A (10)**, 899-904.
4) M. K. Johnson, D. B. Powell and R. D. Cannon, "Vibrational Spectra of Carboxylato Complexes - II. Some Oxo-tetranuclear Complexes", *Spectrochim. Acta*, 1982, **38A (2)**, 125-131.

whether or not a ligand is coordinated, and, in a few compounds, the two oxygen atoms of a bidentate carboxylate group may be at different distances from the metal ion, giving unsymmetrical coordination leading to a unidentate configuration. Nevertheless, the simple classification provides a useful working model.

For convenience, the characteristic features of the vibrational spectra of the carboxylic acids are examined first, much work has been done on these materials and the bonding modes within the spectra have been assigned in numerous cases. Following this, the ionic carboxylates (type 1) are discussed, followed by the unidentate carboxylate group (type 2), since the characterisation of these two types by infrared techniques is more reliable than for the groups. The remaining bonding modes of the carboxylate ligand are included in the bidentate types 3 to 8. Within this group the clear delineation of bonding type on the basis of infrared characteristics proves to be intractable. This area is covered in the final section of this part of the review.

Infrared spectroscopic data of the carboxylic acids reveal that its carboxyl group has an unsymmetrical structure; the proton, owing to its small size, is located within the electron shell of one of the oxygen atoms.[5,6] A band due to the carbonyl group, C=O, has, therefore, been found in all free carboxylic acids. Detailed studies of these acids[7,8,9,10,11,12] indicate that the carboxyl group shows five characteristic frequencies at:

(i) 2500-2700 cm^{-1} (O-H stretching vibrations,

(ii) $\approx$ 1700 cm^{-1} (C=O stretching vibrations),

---

5) C. Duval, J, Lecomte and M. F. Douville, *Ann. Physique*, 1942, **17**, 5.
6) M. F. Douville, C. Duval and J. Lecomte, *Bull. Soc. Chim. Fr.*, 1942, **9**, 548.
7) M. S. C. Flett, *J. Chem. Soc., Farad. Trans.*, 1948, **44**, 767.
8) D. Hadzi and N. Sheppard, *Proc. Roy. Soc.*, 1953, **216A**, 247.
9) W. J. Potts and W. Wright, *Anal. Chem.*, 1956, **28**, 1255.
10) R. C. Gore, R. B. Barnes and E. Peterson, *Anal. Chem.*, 1949, **21**, 382.
11) L. J. Bellamy, "Advances in Infrared Group Frequencies", Methuen, London, 1968.
12) M. S. C. Flett, *J. Chem. Soc.*, 1951, 962.

(iii) and (iv) 1400, 1200-1300 cm^{-1} (C-O stretching vibrations or O-H deformations and

(v) $\approx$ 900 cm^{-1} (O-H deformation vibrations (non-planar) in COOH).

The most characteristic of these are the O-H stretching vibrations (2500-2700 cm^{-1} of carboxyl groups present in dimers) and the C=O stretching bands at $\approx$ 1700 cm^{-1}.

Ionic Carboxylates (Type 1)

Ionic carboxylate ions have a symmetrical structure, in which the metal atom is associated equally with the two oxygen atoms and the O-C-O angle is in the range 100-130°.[5,6] These carboxylates show no carbonyl band at *ca.* 1700cm^{-1}, but depict characteristic bands in the range 1510-1650cm^{-1} and 1280-1400cm^{-1}, along with a series of other characteristic bands due to the COO^- moiety.[5,6,10,11] Many ionic carboxylates have a very intense antisymmetric stretching frequency within the range 1560-1600 cm^{-1}. The alkyl bending modes are also found in this region of the spectrum, but these are generally weak and can easily be distinguished. An example of the spectral details of type 1 carboxylates is afforded by the work of Itoh and Bernstein[13] who studied the solution and solid state spectra of sodium acetate. Nakamura (Table 2.3.3-A)[14] also made a complete calculation of the frequencies and forms of the normal vibrations of the acetate ion, using the Urey-Bradley potential energy function. All 15 modes[15] were identified, except that of the torsional oscillation; C_{2v} symmetry was assumed, implying free rotation of the CH_3 group around the C-C axis. For the purpose of characterisation the most useful bands are the intense antisymmetric carboxylate stretch at 1578cm^{-1} and the symmetric stretch at 1414cm^{-1}, which have a separation, $\Delta\nu$, of 164cm^{-1}, where ($\Delta\nu = [\nu(CO)_{antisym} - \nu(CO)_{sym}]$). Separations between these bands and the trends in the position of these bands have been very widely used in assigning structures from infrared spectra. An investigation[16] of the infrared spectra of some carboxylate ions of the type $RCOO^-$

13) K. Itoh and H. J. Bernstein, *Can. J. Chem.*, 1956, **34**, 170.
14) K. Nakamura, *J. Chem. Soc. Japan*, 1958, **79**, 1411.
15) For CH_3COO^-, the number of atoms in the moiety, n, is 7 thus, the total number of expected vibrations, given by 3n-6, is 15)
16) E. Spinner, *J. Chem. Soc.*, 1964, 4217.

(where R = Me, Et, Bu^t, CF_3, CCl_3, CBr_3, $CHCl_2$, $CHBr_2$, CH_2CN, CH_2F, CH_2Cl, CH_2Br and CH_2I) showed that the separation between the two carboxylate stretches is highly dependant on the nature of the substituent. However, it was also reported that the band at about $1400cm^{-1}$, which is usually designated as the symmetric carboxylate stretch, is, in fact, due to the mixing of the C-O with the C-C symmetric stretching modes. Despite this, the COO stretches still prove to be the most useful observations to make in predicting the structure of metal carboxylates from infrared spectra.

When the complex contains other ligands beside the carboxylate, overlapping of the bands from the new ligands often makes the assignment of O-C-O stretching frequencies difficult. This problem is not of concern in this work, since complexes containing solely carboxylate ligands were used.

Table 2.3.3-A Assignment of frequencies in the infrared spectrum of sodium acetate

		Band (cm^{-1})	
Assignment	Type of vibration	Itoh[14]	Nakamura[15]
CH_3 sym. str.	A_1 ν_1	2936	2924
CH_3 sym. def.	A_1 ν_2	1344	1339
C-O sym. str.	A_1 ν_3	1414	1425
C-C sym. str.	A_1 ν_4	924	—
COO sym. def.	A_1 ν_5	646	647
COO torsion	A_1 ν_6	—	—
C-H antisym. str.	B_1 ν_7	2989 or 3010	2985
C-O antisym. str.	B_1 ν_8	1578	1582
CH_3 def.	B_1 ν_9	1430	1440
CH_3 rock	B_1 ν_{10}	1009	1007
COO rock	B_1 ν_{11}	460	670
C-H antisym. str.	B_2 ν_{12}	3010 or 2989	2985
CH_3 def.	B_2 ν_{13}	1443	1484
CH_3 rock	B_2 ν_{14}	1042	1045
COO out of plane	B_2 ν_{15}	615	616

Unidentate Carboxylates (Type 2)

When acting as a unidentate ligand the carboxylate has a lower symmetry (C_s) than those of ionic carboxylates (C_{2v}) and may be expected to show similarity in their spectra to those of the monomeric undissociated carboxylic acids mentioned earlier,

(although these are complicated by the presence of hydrogen-bonding). Derivatives with unidentate carboxylate ligands have all modes allowed in both the infrared, and Raman, spectra. It has been observed by many workers that complexes known to have unidentate carboxylate groupings show an increase in the antisymmetric COO stretching frequency, together with a decrease in the symmetric COO stretching frequency, leading to a large value of $\Delta\nu$ relative to that of ionic, type 1, carboxylates.[2,17,18] This often serves as a useful criterion to distinguish between these bonding types. The reason for this dissimilarity has been ascribed to the break-down in equality of the carbonyl groups. The antisymmetric stretching frequency increases from its free ion value as the vibration takes on more ketonic character, whereas the symmetric stretching frequency decreases, producing large values of $\Delta\nu$. Hence, a large splitting of the O-C-O stretching frequencies is often an indication of unidentate coordination.

This situation is unique to the unidentate form of coordination. However, in several cases the situation is complicated by the occurrence of hydrogen bonding between the non-coordinated oxygen atom of a unidentate carboxylate ligand and a solvent molecule leading to a reduction of antisymmetric COO stretching frequency.[19] As already stated, a large splitting of the COO stretching frequencies, $\Delta\nu$, is often an indication of unidentate coordination which is a result of the large increase in the COO antisymmetric stretching and a similar decrease in the COO symmetric stretching frequencies. These frequencies correspond approximately to ν(C=O) and ν(C-O), respectively. However, small splittings have been observed for structures known to have unidentate carboxylate groups. For example, in nickel acetate tetrahydrate the carboxylate stretching frequencies occur at 1520 and 1413cm^{-1} ($\Delta\nu$ = 107cm^{-1}).[19] The X-ray structural analysis shows both acetate groups to be unidentate.[20] This small separation was assumed to be due to the strong intermolecular hydrogen bonding between the uncoordinated carboxylate oxygen

17) C. B. Anderson and B. J. Burreson, *J. Organometal. Chem.*, 1967, **7**, 181.
18) T. A. Stephenson, S. M. Morehouse, A. R. Powell, J. P. Heffer and G. Wilkinson, *J. Chem. Soc.*, 1965, 3632.
19) K. Nakamoto, J. Fujita, S. Tanaka and M. Kobayshi, *J. Am. Chem. Soc.*, 1957, **79**, 4904.
20) T. C. Downie, W. Harrison, E. S. Raper and M. A. Hepworth, *Acta. Cryst. Part B*, 1971, **27**, 706.

atom and a water molecule, which tended to equate the two C-O bonds. The asymmetry produced by unidentate coordination can also be compensated by intermolecular hydrogen bonding between both carboxylate oxygen atoms and water molecules coordinated to other nickel atoms.

Since the symmetric and antisymmetric stretching frequencies are highly sensitive to: the structure of the carboxylate group, the nature of the accompanying ligands and the identity of the central metal ion, care should be taken when attempting to correlate the differences in these frequencies with the above parameters. For instance, Donaldson and co-workers[21] have shown that, for a number of acetate and formate complexes of metals possessing lone pairs of electrons, e.g. Tl(I), that the carbonyl group and the lone pair interact with a resultant lowering of stretching frequency in the infrared spectrum.

Bidentate Carboxylates (Types 3-8)

The purpose of part of this research was to synthesis novel basic carboxylates and improve the routes to existing ones. Therefore, the use of infrared spectroscopy to distinguish type 8 chelating carboxylate groups was of most interest in this study, since the presence of such groups is an indication that the compound present may be a basic carboxylate.

Although, in principle, infrared and Raman spectra could be used to distinguish various configurations, the symmetry of the free carboxylate ion is so low (C_{2v}) that the desirable splitting of the degenerate modes often is not observed and the assignment of structures from vibrational spectra becomes more difficult. Ignoring the nature of the group R, it can be seen that the carboxylate group retains C_{2v} symmetry when acting as a bidentate chelate or bridging group. From a symmetry viewpoint, the O-C-O stretching frequencies are not expected to be greatly different from the free ion spectrum, so that the same selection rules apply, with all vibrations being allowed in the infrared, except A_2, and all in the Raman, except A_1. However, there is likely to be some shifting, due to having a heavy atom attached to each

21) J. D. Donaldson, J. F. Knifton and S. D. Ross, *Spectrochim. Acta*, 1965, **21**, 1043.

oxygen. The effect of changing the metal on the COO stretching frequencies should be different for each type of structure. For example, the antisymmetric COO stretching frequency generally increases and COO symmetric stretching frequency decreases as the M-O bond becomes stronger. However, such a trend is not observed for a series of compounds having the bidentate bridging structure. Nakamoto *et al.*[22] reported that in the symmetrical structure both the COO stretching bands are shifted in the same direction upon changing the metal in some binuclear chloroacetate complexes. Thus, in practice, such changes are sometimes very small and therefore of limited application in establishing coordination.

Grigor'ev[23] reported a useful analysis of the spectra of bidentate acetates. He assumed that in the chelating acetates the O-C-O angle would be smaller than in bridging acetates. His premise is supported by observed structural evidence. For example, chelating acetate angles have been observed as 111^{O} in $Zn(OAc)_2.2H_2O$,[24] whereas the bridging angles in the basic zinc acetate, $Zn_4O(OAc)$,[25] are 125^{O}. Grigor'ev[22] also considered, theoretically, the effect of changing the O-C-O angle without changing the force constant on the C-O frequencies and found from his calculations that increasing this angle should decrease CO symmetric stretching (ν_3) and increase CO asymmetric stretching (ν_8) and hence increase $\Delta\nu$ ($= \nu_8 - \nu_3$). He also concluded that changing the force constant could alter the frequencies significantly, although it would have much less effect on $\Delta\nu$.

Infrared spectra of known crystal structures having only one type of acetate group support Grigor'ev's conclusions. For example, chelating acetates (types 7 and 8) show substantially smaller values of $\Delta\nu$ than bridging acetates (types 3-6). However, it is not easy to distinguish free acetate (type 1) from bridging acetate (types 3-6), as

---

22) K. Nakamoto, Y. Morimoto and A. E. Martell, *J. Am. Chem. Soc.*, 1961, **83**, 4528.
23) A. I. Grigor'ev, *Russ. J. Inorg. Chem.*, 1963, **8**, 409.
24) J. N. van Niekerk, F. R. L. Schoening and J. H. Talbot, "The Crystal Structure of Zinc Acetate Dihydrate, $Zn(CH_3COO)_2.2H_20$", Acta. Cryst., 1953, **6**, 720-723.
25) L. Hiltunen, M. Leskelä, M. Mäkelä and L. Niinistö, "Crystal Structure of μ_4-Oxo- hexakis(μ-acetato)tetrazinc and Thermal Studies of its Precursor, Zinc Acetate Dihydrate", *Acta. Chem. Scand.*, 1987, **A41**, 548-555.

both have smaller $\Delta\nu$. Indeed, Beattie and Gilson[26] concluded that there is ..."Clearly no *simple* way to distinguish between a discrete acetate ion and a bridging acetate group." The observation that, compared to bridging acetates the C-O antisymmetric stretch is generally lower for free acetate, may go some way toward mollifying this bleak perspective.

A slightly more useful predictor of molecular structure would be to identify the vibrations of the metal-oxygen units. These lie below the range of common infrared spectrometers. Low frequency infrared spectroscopy has been used[27] to examine metal-oxygen vibrations in a series of metal formates and acetates of known structure. Some correlations between spectra and structure were found but differences were such that the deduction of unknown acetate complexes by this method is still not foolproof. In spite of this, there have been assignments made in the 200-65 cm^{-1} region, sometimes without the necessary theoretical treatment or experimental confirmation. Examples of these speculative assignments are those of several beryllium carboxylates.[28,29,30,31] It is unfortunate that much of this work was unsupported by crystallography, as many tantalizing formulae were involved, such as $Be_5O_2(OAc)_6$, $Be_6O_2(OAc)_8$ and $Be_8O_3(OAc)_{10}$ with attractive structures proposed from the Be-O vibrations. The authors' bold conjecture was, however, partly vindicated by the subsequent X-ray crystal determination of $Be_6O_2(OAc)_8$ by Atovmyan.[32]

Since the formation and analysis of molecules of the form $M_4O(RCOO)_6$ is part of this research, a case study of these materials will serve to highlight some of the

---

26) I. R. Beattie and T. Gilson, "The Occurrence of Organotin Cations", *J. Chem. Soc.*, 1961, 2585-2586.

27) Y. Kuroda and M. Kubo, *Spectrochim. Acta,* 1967, **23A**, 2779.

28) A. I. Grigor'ev, L. N. Reshetora and A. V. Novoselova, *Russ. J. Inorg. Chem.*, 1974, **19,** 1093.

29) V. A. Sipachev and A. I. Grigor'ev, "Vibrational Spectra of Beryllium Oxide Carboxylates", *Russ. J. Inorg. Chem.*, 1972, **17(2),** 176-182.

30) A. I. Grigor'ev and V. I. Nefedov, "X-ray Electronic Spectra of Complex Compounds of Beryllium", *Dokl. Akad. Nauk. SSSR*, 1973, **210(2),** 343-344. *In Russian.*

31) A. I. Grigor'ev, V. A. Sipachev and A. V. Novoselova, "Synthesis and Characterisation of a New Oxyacetate of Beryllium: $Be_6O_2(OCOCH_3)_8$", *Dokl. Akad. Nauk. SSSR*, 1970, **194(4),** 808-809. *In Russian.*

32) L. O. Atovmyan, O. N. Krasochka, A. I. Grigor'ev and V. A. Sipachev, "X-ray Structural Investigation of Beryllium Dioxoacetate", *Dokl. Akad. Nauk. SSSR*, 1974, **225**, 99-100. (In Russian).

earlier observations. Consider the case of $Zn_4O(OAc)_6$ (which contains type 8 carboxylate ligands) and is formed from the neutral salt, $Zn(OAc)_2.2H_2O$ (which contain type 7 carboxylate ligands).

$Zn(OAc)_2.2H_20$ is octahedral with two *trans* water molecules and two chelate groups.[33] The spectrum in the region 4000-600cm^{-1} is essentially that of the acetate group, perturbed by the two water molecules in a planar arrangement. This creates an overall point group symmetry of D_{2h}. The presence of the two C_{2v} acetate groups under D_{2h} symmetry is expected to give splittings of the vibrational levels as follows:

$\underline{C_{2v}}$	$\underline{D_{2h}}$
A_1	$B_{1u} + A_g$
A_2	$B_{1g} + A_u$
B_1	$B_{2g} + B_{3u}$
B_2	$B_{3g} + B_{2u}$

Such splittings, although usually observed, are rather small. In the region below 600cm^{-1} the vibrations of the central 'ZnO_4' moiety of the coordinated acetate groups are observed. A full assignment for this compound was given by Johnson *et al.*[3] who ascribed the bands at 278, 195 and 115cm^{-1} to the infrared active modes of the central 'ZnO_4' unit.

With regards to $Zn_4O(OAc)_6$ this molecule is of the type $M_4O(RCOO)_6$ for which there are essentially three groups of vibrations;

1) vibrations of the carboxylate ligands
2) metal-oxygen vibrations of the metal carboxylate bonds and
3) vibrations of the central M_4O (μ_4) tetrahedron.

Considering point 1, comparison of the O-C-O stretching frequencies for a range of cluster carboxylates shows that the antisymmetric stretch varies appreciably in energy as different metals are coordinated. The symmetric stretching frequency is usually not shifted far from the free ion value. The positions of each of the O-C-O stretching frequencies may range across 180 cm^{-1} and their separation may be as

33) J. N. Van Niekerk, F. R. L. Schoening and J. H. Talbot, "The Crystal Structure of Zinc Acetate Dihydrate, $Zn(CH_3COO)_2.2H_2O$", *Acta. Cryst.*, 1953, **6**, 720-723.

small as 80 cm^{-1} or greater than 200 cm^{-1} within the bidentate configuration. Therefore, it is insufficient to use infrared spectroscopy of the carboxylate region alone to assign a cluster structure. Magnetic and EPR data are better criteria when appropriate metal ions are present. Nevertheless, infrared spectroscopy is often risked.

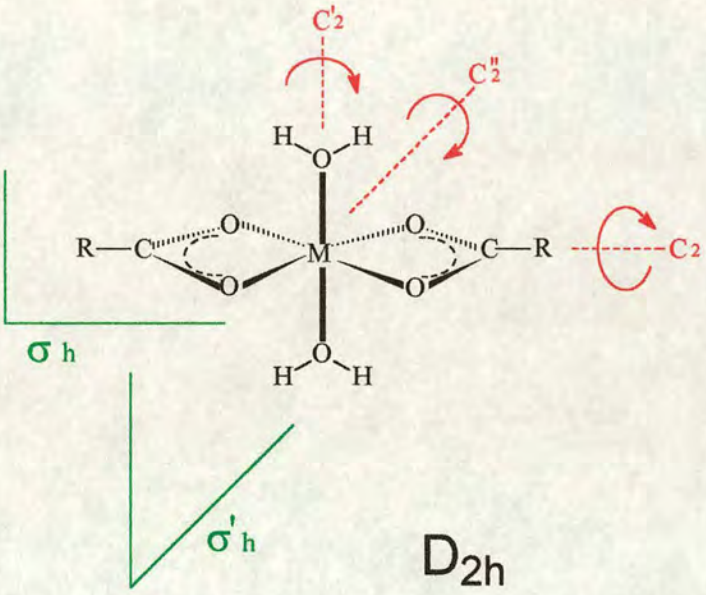

Figure 2.3.3-A C_{2v} acetate group under D_{2h} symmetry of $M(O_2CR)_2.2H_2O$ molecule. The D_{2h} rotational symmetry operations are shown in red and the reflection planes are shown in green.

Contrasting the spectra of the neutral and basic zinc acetates, the most obvious difference is in the value of $\Delta\nu$ for the symmetric and antisymmetric carboxylate stretches ν(COO). The $\Delta\nu$ value for the complex, $Zn_4O(O_2CCH_3)_6$ (in which the carboxylates are type 8 chelating) is 160 cm^{-1} and is greater than that for the neutral salt $Zn(OAc)_2.2H_2O$ (in which the carboxylates are type 7 chelating) with a value of 100 cm^{-1}, which is quite close to the ionic value for free carboxylate anions.[34] The difference in $\Delta\nu$(COO) between the modes has been attributed to changes in the M-O bond angle[35] between the two complexes. In addition, when considering the metal-oxygen vibrations, the basic salt is oxo-centred (MO_4) whereas the neutral salt

34) Nakamoto, "Infrared and Raman Spectra on Inorganic and Coordination Compounds", 4th Ed., J. Wiley and Sons Inc.,1978.
35) R. C. Mehrotra and R. Bohra, *Metal Carboxylates*, Academic Press, London, 1983.

is metallo-centred (M_4O). The basic salt shows two additional sharp absorptions due to Zn_4O 'metal framework' vibrations below 600cm^{-1}. These metal-framework vibrations are key guides to inferring the presence of a carboxylate cluster.

By way of further comparison, the beryllium analogue of basic zinc acetate, i.e. $Be_4O(OAc)_6$, as noted by Grigor'ev and Sipachev,[36] showed carboxylate vibrations in the region 4,000-900 cm^{-1} which were described as being only slightly perturbed by coupling effects. In the region 900-400cm^{-1} framework vibrations and carboxylate deformations were said to occur together and interact strongly. Below 400 cm^{-1} only framework vibrations were observed. In the case of $Zn_4O(OAc)_6$ these framework vibrations occur below 600 cm^{-1}, due to the heavier metal ions, and thus there is little interaction with the ligand vibrations. Overall, it may be said that, the presence of low frequency metal framework vibrations, 'M_xO_y', coupled with $\Delta\nu$(COO) values, along with the actual values of ν_{as}(COO) and ν_s(COO) provides the most useful handle in ascribing structures to cluster metal carboxylates by IR techniques.

The work of Deacon and Philips[37] serves as a summary of the above. They have arrived at the following conclusions through the examination of infrared spectra of many acetates and trifluoroacetates of known crystal structure:

1) Unidentate complexes (type 2) exhibit $\Delta\nu$ [$\nu_a(COO^-) - \nu_s(COO^-)$] values which are much greater than for the ionic complexes (type 1).
2) The $\Delta\nu$ values for bidentate chelating complexes (types 7 and 8) are significantly lower than the ionic values (type 1).
3) The $\Delta\nu$ values of bridging complexes (types 3-6) are greater than those of chelating complexes (type7 and 8), and close to the ionic values (type 1).

To summarise: the separation of CO stretching bands, $\Delta\nu$, decreases along the series,

unidentate > ionic ≈ bridging > bidentate

---

36) V. A. Sipachev and I. Grigor'ev, *Russ. J. Inorg. Chem.*, 1972, **17**, 176.
37) G. B. Deacon and R. J. Phillips, *Coord. Chem. Rev.*, 1980, **33**, 227.

Providing the above cautions are heeded this is a practical 'rule of thumb' in making preliminary structural assignments on the basis of infrared absorptions.

2.3.3(ii) UV Spectroscopy of Carboxylates

The study of the electronic spectra of metal carboxylates has so far been limited, often being confined to an empirical one-metal study. Kunkely and Vogler[38] examined the UV (200-500 nm) absorption and emission spectrum of $Zn_4O(O_2CCH_3)_6$ in ethanol solution, which was chosen because it is transparent above 200 nm. It was observed that solutions of $Zn_4O(O_2CCH_3)_6$ emitted an intense photoluminescence at room temperature (λ_{max} = 372 nm) and displayed an absorption minimum at λ_{max} = 216 nm (ε = 62 200 mol^{-1} dm^{-3} cm^{-1}). These were assigned to a LMCT transition which corresponds to the band-gap transition of the semiconductor ZnO. Mononuclear Zn^{2+} complexes such as $Zn(OAc)_2$ have not been observed to show any photoluminescence (with the exception of ligand-localised luminescence of Zn^{2+} complexes with ligands such as porphyrins).[39]

2.3.3(iii) Mass Spectroscopy of Carboxylates

The presence of five isotopes for zinc (^{64}Zn 48.89%; ^{66}Zn 27.81%; ^{67}Zn 4.11%; ^{68}Zn 18.56% and ^{70}Zn 0.62%[40]) makes assignment of *m/z* for some peaks difficult. This is, however, alleviated by the highly characteristic nature of the isotope patterns for zinc clusters (see Fig. 2.3.3-B).

It is known that the fragmentation pattern produced using the FAB technique depend upon the experimental conditions used.[24] Also, according to Catterick and Thornton,[41]

"Mass spectrometry is the most misleading technique available to the inorganic chemist seeking to characterise a non-crystalline carboxylate. 'Parent ions appear in

---

38) H. Kunkely and A. Vogler, "Adsorption and Emission Spectrum of [Zn_4O(Acetate)$_6$]", *J. Chem. Soc., Chem. Comm.*, 1990.

39) M. Gouterman, in "The Porphyrins", ed. D. Dolphin, Academic Press, New York, 1978, **3,** p.1.

40) *Nuffield Advanced science Book of Data*, Longman, Essex, 1984.

41) J. Catterick and P. Thornton, "Structures and Physical Properties of Polynuclear Carboxylates", *Adv. Inorg. Chem. & Radiochem.*, 1977, **20**, 291-362.

the spectrum indicating clusters bigger or smaller than those in the parent molecule, but only occasionally of the right size. The discrepancies may be caused by the necessity to use direct insertion methods for involatile samples and, perhaps, by using an excessively high ionising energy. (Workers in the field should check for sample pyrolysis[42] and rearrangement reactions)". An example may be afforded by considering the mass spectrum of $Zn_4O(O_2CCH_3)_6$. This has been studied by several authors. Each found that for this and other basic zinc carboxylates the most intense ion was that of $[(RCO_2)Zn_4O]^+$ and that fragments were observed for ions of mass greater than that of the parent ion.[24,43,44,45,46,47]

The problems of unambiguously identifying products from mass spectra is further compounded by the fact that the fragment ions of different substances have the same masses. For example ions with m/z = 27, 29 and 57 could equally well correspond to diethyl ketone, propionic acid or propionic anhydride, and the ion with m/z = 28, to propionic anhydride, CO or CO_2. Only the molecular ions can be taken as characteristic. Thus, for example, m/z = 86 for diethyl ketone, 56 for methylketene, 74 for propionic acid, 44 for CO_2 and 18 for H_2O. Whilst it may not be possible to state unambiguously the source of a particular fragment ion it is possible to assign the actual atomic composition of a particular fragment using its cluster pattern and exact peak mass matching. This is most easily achieved where the fragment contains atoms with a high abundance of isotopes, such as zinc.

---

42) Pyrolysis is the thermal fragmentation of large molecules into smaller molecules in the absence of oxygen.

43) J. Charalambous, R. G. Copperthwaite, S. W. Jeffs and D. E. Shaw, "Mass Spectra of Tetracobalt(II) and Tetrazinc(II) μ_4-hexa-μ-carboxylates (Basic Cobalt and Zinc Carboxylates)", *Inorg. Chim. Acta*, 1975, **14**, 53-58.

44) W. L. Mead, W. K. Reid and H. B. Silver, *J. Chem. Soc. Chem Comm.*, 1968, 573.

45) V. A. Sipachev, L. N. Reshetova, Yu. S. Nekrasov and S. Yu Sil'vestrova, *Org. Mass. Spectrom.*, 1980, **15,** 192.

46) R. M. Gordon and H. B. Silver, "Preparation and Properties of tetrazinc μ_4-oxohexa-μ-carboxylates (basic zinc carboxylates)", *Can. J. Chem.*, 1983, **61**, 1218-1221.

47) J. G. Vogel and B. G. Hobrock, 153rd Am. Chem. Soc. Meeting, Miami Beach, FL. April 1967.

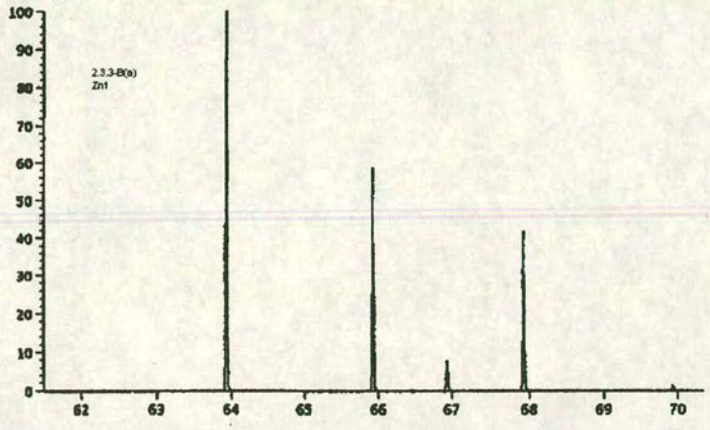

(a) "Zn_1"

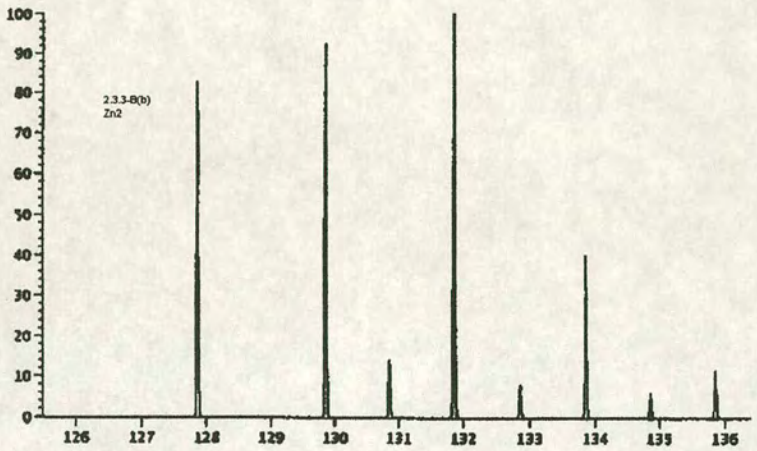

(b) "Zn_2"

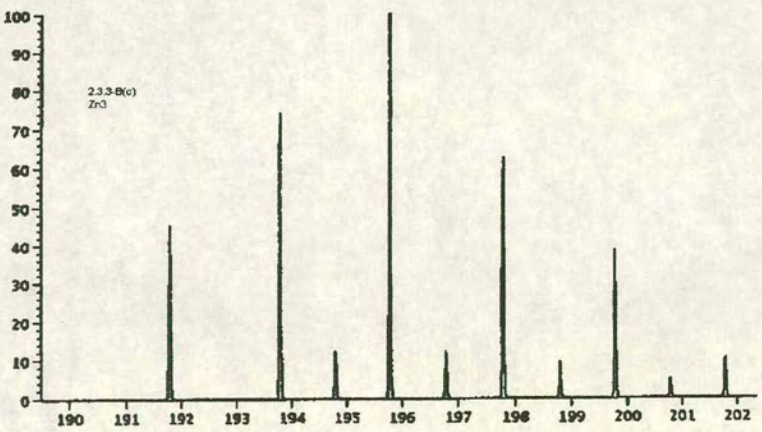

(c) "Zn_3"

Fig. 2.3.3-B MS distribution patterns for theoretical zinc molecules (a) Zn_1, (b) Zn_2, (c) Zn_3

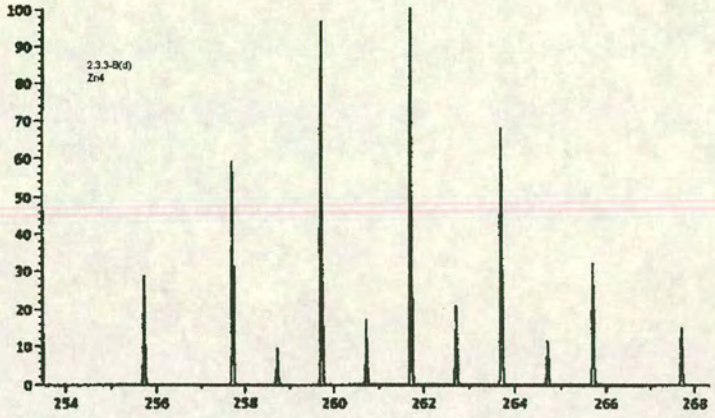

(d) "Zn_4"

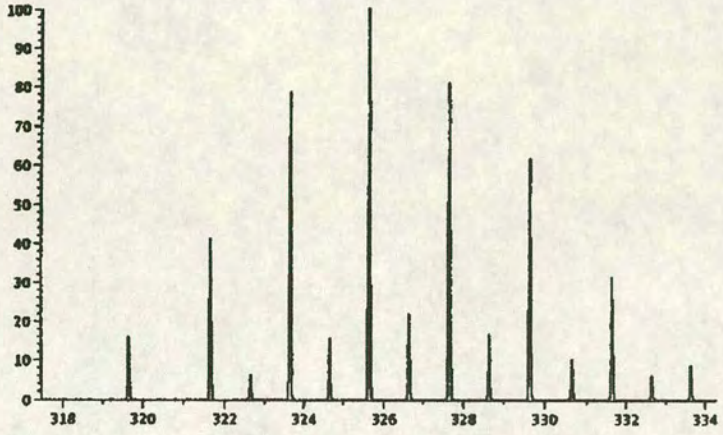

(e) "Zn_5"

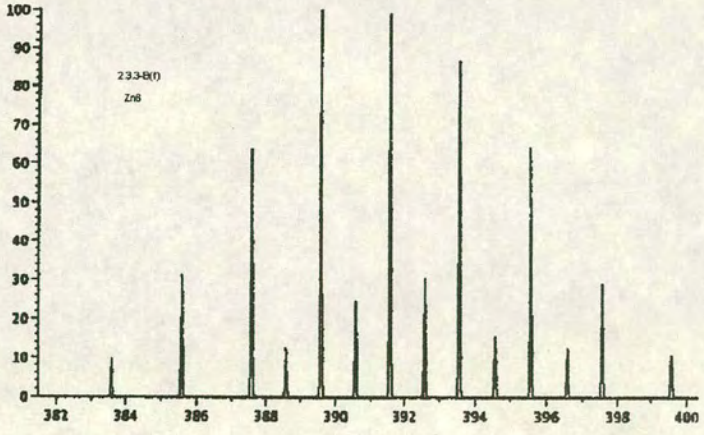

(f) "Zn_6"

Figure 2.3.3-B continued from previous page (c) Zn_3, (d) Zn_4, (e) Zn_5

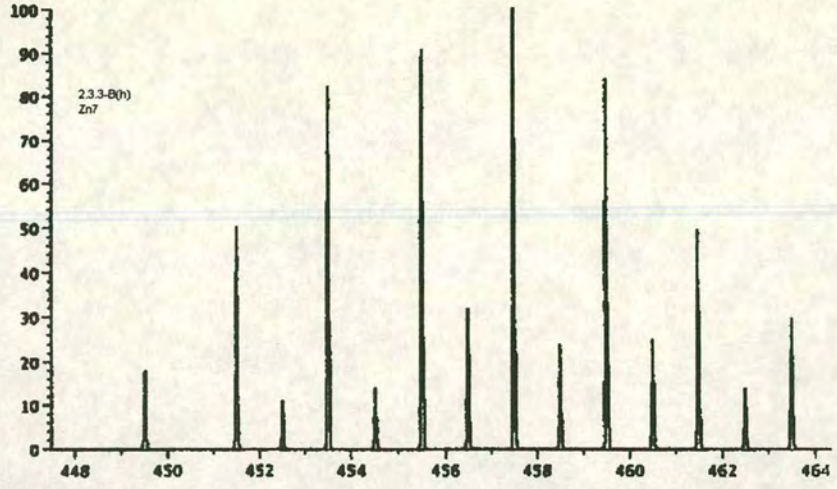

(g) "Zn_7"

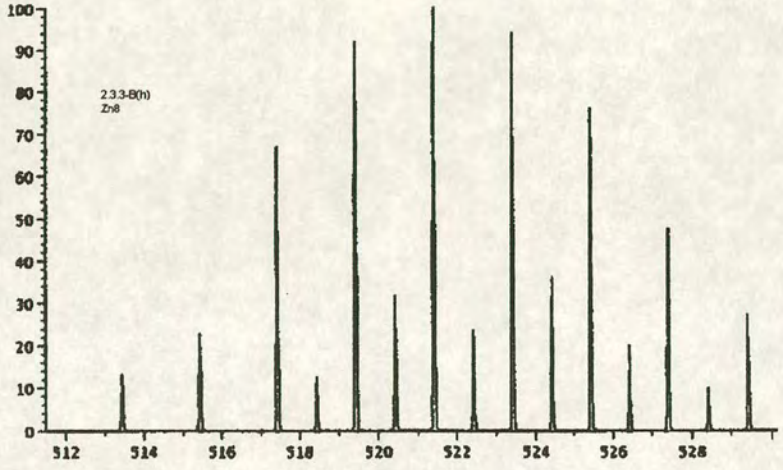

(h) "Zn_8"

Figure 2.3.3-B continued from previous page (f) Zn_6, (g) Zn_7, (h) Zn_8

By way of example, Clegg *et al*[48] studied the FAB mass spectra of the clusters of three different types of carboxylic acid: an α,β-unsaturated aliphatic (crotonic acid, $CH_3CH{=}CH\text{-}CO_2H$, CtOH); an aromatic (benzoic acid, $C_6H_5\text{-}CO_2H$, BzOH) and a saturated aliphatic (pivalic acid, $(CH_3)_3C\text{-}CO_2H$, PvOH). From these they synthesised the basic carboxylates; $[Zn_5(OH)_2(OCt)_8]$, $Zn_4O(OBz)_6$ and $Zn_4O(OPv)_6$. They found that the high ionisation energy involved in EI mass spectroscopy led to fragmentation patterns of the tetranuclear basic species, whilst the lower ionisation

48) W. Clegg, D. R. Harbron, C. D, Homan, P. A. Hunt, I. R. Little and B. P. Straughan, "Crystal Structures of Three Basic Zinc Carboxylates togehter with Infrared and FAB Mass Spectrometry Studies in Solution", *Inorg. Chim. Acta*, 1991, **186**, 51-60.

energies of FAB mass spectroscopy were more likely to show both the normal and tetranuclear species as found in solution by infrared spectroscopy measurements. They observed the presence of ethanol in one of the ions of basic zinc benzoate, which they took to suggest that the FAB technique produces ions which correspond closely to species found in solution. They also observed that the FAB mass spectrum of $[Zn_5(OH)_2(OCt)_8]$ showed peaks which were apparently due to both normal zinc crotonoate and the basic crotonoate in the form $Zn_4O(OCt)_6$, whereas the solution FT-IR spectrum of the hydroxy-species $[Zn_5(OH)_2(OCt)_8]$ was dominated by absorption bands which could only be assigned to $Zn_4O(OCt)_6$, although the presence of other species cannot be entirely ruled out. More interestingly, they found species in two of the basic carboxylates with *m/z* values higher than that of the parent ion. These were:

- $[Zn_5O_2(OPv)_5]^+$ (*m/z* 863), produced (possibly) by the fusion of normal and basic zinc pivalate, followed by loss of pivalic anhydride (PvOPv) and a pivalate ligand, and,
- $[Zn_6O_2(OCt)_7]^+$ (*m/z* 1017), possibly formed by the fusion of normal zinc crotonoate and basic zinc crotonoate, followed by the loss of two molecules of crotonaldehyde and a crotonoate ligand.

The assignment of these chemical formulae was based upon the correspondence of the matches observed for the exact peak measurements with those calculated for the same fragments.

Clearly, there is a general tendency for metal carboxylates to form many different multi-nuclear clusters under conditions of reduced pressure and elevated temperature, as found in mass spectrometers and as commonly used to synthesise basic carboxylate clusters by vacuum sublimation. In addition, there is supporting evidence that higher nuclearity basic carboxylates ($M_xO_y(O_2CR)_z$ where $x > 4$) are formed (the presence of daughter ions indicative of break-down fragments from such higher nuclearity carboxylates).

With the common formation of parent ions at *m/z* values greater than the parent ion and the known existence of higher nuclearity basic beryllium carboxylates,[32] it is enticing to speculate that other such species may be formed as isolable materials, given the appropriate conditions of temperature and pressure. If this is the case, then a great challenge exists: to synthesise, and isolate, the multinuclear carboxylates corresponding to those observed under MS conditions.

2.4 Zinc Oxide, $Zn_{(1+x)}O$

Because of their thermal stability and easy preparation as high surface area materials oxides have long been used as catalyst supports.[1] However, they also possess catalytic activity themselves. Many reactions are catalysed by transition metal oxides, ranging from dehydrogenations, selective oxidations and reductions, to the water-gas shift reaction.[2,3] Oxides are complex materials, generally polycrystalline in nature and consequently tend to have inhomogeneous surfaces. One of the features characteristic of disperse oxides is their enhanced surface area. The surface of a solid may be regarded as a lattice defect which disrupts its periodic nature. Hence, the crystalline structure in the surface layer deviates from that of the bulk structure. Atoms located at the surface have a smaller number of neighbours than the atoms within the crystal, hence, the forces applied to the atom in the surface layer are also different. This applies to both covalent and ionic lattices. In addition, the surfaces of disperse oxides contain defects, which can be enriched or depleted in an element and can vary in chemical state (e.g., hydroxylation). These, and other factors, underline the importance of well-controlled preparation conditions and subsequent, careful characterisation. Characterisation is essential for understanding the surface chemistry and, hence, the reactivity of oxides.

When a crystal of a binary oxide is cleaved to generate two new surfaces, the ions in the cleavage plane are partitioned into two separate solids in such a manner that charge neutrality is maintained in each solid. The structure of the two newly created surfaces, however, may or may not be identical. If they are identical, or if the surface plane contains a stoichiometric ratio of cations and anions, the surface will be dipoleless and is called a nonpolar surface. If they are not, the surface will probably (but not necessarily), possess a strong dipole and the surface is a polar one.

---

1) G. C. Bond, *Heterogeneous Catalysis: Principles and Applications,* Clarendon Press, Oxford, 1974, ch. 4, pp. 57-65.
2) H. H. Kung, *Transition Metal Oxides: Surface Chemistry and Catalysis, (Stud. Surf. Sci. Catal. 45),* Elsevier, Amsterdam, 1989, ch. 1, pp. 1-5.
3) V. E. Hendrich and P. A. Cox, *The Surface Science of Metal Oxides*, 1st ed., Cambridge University Press, Cambridge, 1994.

Examples of nonpolar surfaces are perovoskite (100) and corundum (047) surfaces. Examples of polar surfaces are wurtzite (0001) and $(000\bar{1})$ and rocksalt (111) surfaces. All other factors being identical, a polar surface is less stable than a nonpolar surface. The presence of a dipole moment increases the surface Gibbs energy. Comparing a metal-polar and an oxygen-polar surface, the latter is usually more stable because oxygen ions are more polarizable than metal ions. Polarization lowers the surface electric field and the surface energy.

2.4.1 Physical Properties of Zinc Oxide

ZnO possesses the wurtzite structure: a hexagonal close-packed structure with 4:4 coordination and tetrahedral bond direction, which presents three natural crystal faces. It exhibits two polar faces, one non-polar (prism) face and several stepped faces.

a) Polar face; Zn (0001) presenting a plane of zinc ions
b) Polar face; O $(000\bar{1})$ presenting a plane of oxygen ions
c) Prism face; $(10\bar{1}0)$ presenting an equal number of zinc and oxygen ions.

Due to the coordinative unsaturation of these three faces, they have enhanced reactivity towards reactant species when compared with the tetrahedrally coordinated ions in the bulk lattice. The different faces also have different reactivities towards different reactant species, due to their differing degrees of coordinative unsaturation, surface geometry and electrostatic interactions. The incoming species' bonding requirements also have an effect depending on whether it is anionic, cationic or neutral.[4] With ionic adsorbates or those with a significant dipole moment, different faces provide different coordination sites; the polar Zn (0001) face has alternating layers of Zn-O-Zn (A-B-A) and presents an outwardly directed dipole. It is more reactive than the prism face, due to increased coordinative unsaturation of the zinc atoms. The polar O $(000\bar{1})$ face presents an inwardly directed dipole. The non-polar

4) J. Akhter, K. Lui and H. H. Kung, *J. Phys. Chem.*, 1985, **89**, 1958-64.

$(10\bar{1}0)$ prism face has no net dipole. The presence of steps on the polar faces, exposing non-polar surfaces has also been observed.[1,5]

Non-stoichiometric systems in which the metal is reduced are rather rare and have a limited range of stoichiometry. One example of a reduced metal system is $Zn_{1+x}O$ (but x is very small, $\approx 10^{-5}$, and moderate values are found only at high temperatures where the formation of defects is favoured through entropy considerations). When zinc oxide is heated, the compound loses oxygen from the surface, forming $Zn_{1+x}O$; charge balance requires the zinc atoms to be reduced to Zn^+ or Zn^0. These ions migrate from the surface to interstitial positions within the lattice. As the concentration of these interstitial ions is so low, structural studies have been unable to locate their position, but consideration of the wurtzite structure adopted by ZnO and the larger size of these ions, Zn^+/Zn^0, would indicate that they occupy octahedral holes. The formation of lower-charged zinc ions/atoms permits an electron transfer process between the various zinc centres. The energy of these transitions occurs near to the visible region of the spectrum. On heating ZnO it changes colour from white to yellow. This colour change was ascribed, by Nicholl,[6] to a thermal shift of the ultraviolet absorption band of ZnO. Upon cooling, the number of the interstitial zinc ions decreases markedly and the colour of ZnO returns to white at room temperature.

A measurement by Miller,[7] of the shift in the absorption edge for a single crystal of ZnO in air with a change in temperature, shows a shift of about 1.44Å/^{O}C towards the red in the range 26-77^{O}C. An extrapolation of Miller's results on this basis places the absorption edge at about 4700Å at 425^{O}C, which produces the pronounced yellow appearance of the solid.

To prove that the colour change is of thermal origin, Coogan and Rees[8] heated ZnO *in vacuo* to 400-500^{O}C in a barium getter fire, to remove any oxygen evolved; the temperature was then allowed to fall. The oxide regained its white colour

---

5) J. Saussey, J. C. Lavalley and C. Bovet, *J. Chem. Soc., Farad. Trans. I*, 1982, **78**,.1457-63

6) F. H. Nicholl, *J. Opt. Soc. Am.*, 1948, **38**, 817.

7) P. H. Miller, *Semi-Conducting Materials,* Butterworth Scientific Publications Ltd., London, 1951, 172.

8) C. K. Coogan and L. G. Rees," The Nature of the thermal Color Change in Zinc Oxide", *J. Chem. Phys.*, 1952, **20**,

immediately. The reversible colour change of ZnO must, therefore, be ascribed to a thermal shift of the absorption band into the visible region and not to a stoichiometric defect. Only after prolonged heating under non-oxidizing conditions does ZnO attain a permanent yellow colour due to stoichiometric excess of Zn.

Similarly, Taylor and Amberg[9] found that the infrared transmission of ZnO is extremely sensitive to evacuation at elevated temperature. The treatment increases the defect structure of the solid and produces a higher concentration of conduction electrons. Heating with oxygen, which acts as an electron trap, restored the infrared transmission.

An array of coloured zinc oxides, including red, orange, yellow, green, and blue-green can be produced by the interaction of zinc oxide with varying amounts of CuO, MnO, MgO and CdO.[10]

2.4.2 Chemical Properties of Zinc Oxide

For all oxide systems, the following types of surface centres for adsorption can be distinguished: the hydroxyl-hydrate cover, electron-acceptor metal cations and electron-donating oxygen ions. The polydispersity of oxide catalysts and the resulting emergence of various facets of the lattice, together with possible oxide defects, condition the non-homogeneity of every type of adsorption differences in their reactivity.

Activation of an oxide by heating is needed because of the strong adsorption of water on oxides. Thus, an oxide surface becomes fully covered with adsorbed water and hydroxyl groups once it is exposed to the moisture in the atmosphere. This process is shown by Eqn. 2.4.2-A and Eqn. 2.4.2-B, where $*M^{n+}$ represents a coordinatively unsaturated metal centre:

$$*M^{n+} + H_2O \rightleftharpoons *M^{n+}OH_2 \qquad \text{Eqn. 2.4.2-A}$$

9) J. H. Taylor and C. H. Amberg, *Can. J. Chem.*, 1961, **39**, 535.
10) US Patent 2.579.020. 18 Dec. 1951 (Smith).

$$\begin{array}{c} O^{2-} \\ | \\ M^{n+}\ M^{n+} \end{array} + H_2O \rightleftharpoons \begin{array}{cc} H & H \\ {}^{-}O & O^{-} \\ | & | \\ M^{n+} & M^{n+} \end{array} \qquad \text{Eqn. 2.4.2-B}$$

In Eqn. 2.4.2-A water is adsorbed molecularly to satisfy the coordinative unsaturation of the metal ion. In Eqn. 2.4.2-B the coordinately unsaturated cation and anion pair adsorbs a water molecule dissociatively as OH^- and H^+. These surface ions become coordinately saturated and unable to adsorb other molecules. Heating causes the removal of water and formation of surface coordinative unsaturation. For example, Nagao and Morimoto[11] investigated the surface hydroxyl content of a ZnO sample evacuated at different temperatures. They observed that the extent of dehydroxylation depended upon the temperature. Water was lost continuously from ZnO when the temperature was raised. The water lost at low temperature was due to weakly adsorbed species; probably nondissociatively adsorbed water that is lost by a process similar to the reverse of Eqn. 2.4.2-A, as well as water held to the surface by hydrogen bonding. A rapid loss of water occurred around 200 to 350^{O}C which corresponds to dehydroxylation of the surface by the reverse of Eqn. 2.4.2-B. Further dehydroxylation of the remaining hydroxyl groups beyond 400^{O}C was slow, probably due to the removal of isolated (hence difficult to remove) hydroxyl groups. These results are representative of most oxides.

The heating *in vacuo* of oxides designed to remove admixtures and to form sufficiently pure oxide surfaces can disrupt the stoichiometric oxide composition. that the absence of agreed standards of preadsorptive oxide treatment hinders not only quantitative but, also in a number of instances, qualitative analysis of comparative data on molecule chemisorption, in addition to the nature of surface centres.

The chemisorption behaviour of ZnO is extremely complicated. The variety of polar and non-polar surfaces available, the presence of acidic Zn and basic O sites, the complex and imperfectly understood defect chemistry, and the possibility of

11) M. Nagao and T. Morimoto, *J. Phys. Chem.*, 1984, **84**, 2054.

electron and oxygen-atom transfer are factors that combine to enable all the types of chemisorption. Undoubtedly, these features are responsible for the activity of ZnO as a catalyst and a sensor. But, they make the elucidation of detailed chemisorption mechanisms very difficult. Many results, so far obtained, conflict with each other and with the expectations of simple models, and much more work needs to be done before a clear understanding can emerge.

2.4.3 Spectral Properties of Zinc Oxide

The chemical properties of adsorption centres are determined by the composition and structure of the solid. It is clear however, that the initial treatment and surface processes are certain to induce changes in both the hydroxyl-hydrate cover and the capacity for electron acceptance (cations) or electron donation (anions). This is particularly important for oxides of transition elements. For example, in the initial spectra of most oxides that have not been treated in any way, intense absorption bands are observed in the region over the fundamental absorption limit (lattice vibration region) in the 1200-1800cm^{-1} interval. This is due to admixtures adsorbed by the catalyst surface. These bands are caused by adsorption of CO_2 from the air or by other organic contaminants on the surface. This means that any real solid surface hosts a set of surface compounds, which are yielded by the interaction of coordinately or valently unsaturated surface atoms with molecules of the medium, and which are firmly bound to the solid. For example, early corrosion studies on zinc have shown that when zinc oxide is left in moist air it is completely converted to a basic zinc carbonate form,[12,13] according to the equation:

$$x\,ZnO + y\,CO_2 + (x-y)H_2O \rightleftharpoons Zn_x(CO_3)_y(OH)_{2(x-y)} \qquad \text{Eqn. 2.4.2-C}$$

Basic zinc carbonate is structurally quite complicated, its structure was first elucidated by Ghose.[14] This enabled Feitknecht and Oswald[15] to interpret observations made of other basic zinc carbonates and to conclude that basic zinc carbonate possesses the composition $Zn_5(CO_3)_2(OH)_6$ in most formation reactions

12) E. A. Anderson and M. L. Fuller, *Metals and Alloys*, 1939, 282.
13) M. F. Tabourt and E. Gray, *Séances Acad. Sci.*, 1937, **205**, 985.
14) S. Ghose, *Acta. Cryst. (Copenhagen)*, 1964, **17**, 1051.
15) W. Feitknecht and H. R. Oswald, *Helv. Chim. Acta*, 1965, **49**, 334.

but under different preparative conditions samples can exhibit small structural differences. Subsequently, O'Connor[16] investigated the effect that various conditions (gas pressure and reaction temperature) had on the reaction of water vapour and CO_2 on ZnO and the resulting composition and structure of the zinc hydroxide carbonate so formed. He observed that when water vapour and CO_2 were admitted to the zinc oxide surface simultaneously, the absorption process did not occur until the surface water layer had been constructed. On the other hand, when the oxide surface had been water pre-treated, the absorption began as soon as the CO_2 was introduced. The absorption rate was also found to decrease with increasing CO_2 pressure implying the greater competition between CO_2 and water molecules on the surface at higher CO_2 pressures.

The basic zinc carbonate produced by O'Conner[16] was found to be highly disordered, but became more ordered on ageing. Feitknecht and Oswald[15] prepared a similar strongly disordered highly basic zinc carbonate which also became more ordered on ageing, by treating amorphous zinc hydroxide with CO_2.

The advances achieved with infrared spectroscopy in the determination of hydroxyl-hydrate oxide coverage are well known. The infrared method is one of the few that make it possible to obtain a detailed picture of the spectral features of surface hydroxyl groups and of the nature of interactions with reacting molecules. Peri,[17] and others[18,19,20] were the first to show that the infrared spectrum of surface hydroxyls carried on oxide surfaces reflects the structure of the corresponding surface layers of the solid. Atherton *et al.*[21] were able to take this further and assign particular infrared absorptions with the location of hydroxyls on specific surface

---

16) M. F. O'Conner, "A study of Basic Zinc Carbonate Formation by the Action of Carbon Dioxide and Water Vapour on Zinc Oxide", *Z. Naturforsch*, 1973, **29b**, 202-205.
17) J. B. Peri, *J. Phys. Chem.*, 1965, **69**, 220.
18)P. J. Anderson, R. F. Horlock and J. F. Oliver, *Trans. Farad. Soc.*, 1965, **61**, 2751.
19) J. B. Peri and A. L. Hensley, Jr., *J. Phys. Chem.*, 1968, **72**, 2926.
20) C. G. Armistead, A. J. Tyler, F. H. Hambleton, S. A. Mitchell and J. A. Hockey, *J. Phys. Chem.*, 1969, **73**, 3947.
21) K. Atherton, G, Newbold and J. A. Hockey, "Infra-red Studies of Zinc Oxide Surfaces", *Disc. Farad. Soc.*, 1971, **52**, 33-54.

planes. This characterisation of surface hydroxyls has been put to use in assigning the presence of other adsorbates.

The surface OH can be considered as small probes sticking up from the surface. The position of the OH stretching band of surface OH groups is affected by the presence of adsorbed molecules. Thus, a study of the surface OH band position provides evidence on the nature of the adsorption process even though the spectrum of the adsorbed molecule may not be observed. This interesting effect was first reported by Yaroslavskii and Terenin[22] and Kurbatov and Neuiman.[23]

Another example of frequency shifts of hydroxyl groups found on oxide surfaces is that, after dehydration at high temperatures, a sharp band is commonly observed near $3700cm^{-1}$ due to isolated OH groups. In more extensively hydroxylated surfaces hydrogen bonding occurs. The typical hydrogen bonding effect is a shift to a longer wavelength ($3500\ cm^{-1}$) together with an increase in band width. Usually the integrated intensity is increased. In some cases the overtone OH band does not behave exactly the same as the fundamental when hydrogen bonding occurs.[24] Water molecules may also be hydrogen bonded to surface OH groups and they can be recognised by the band near $1600cm^{-1}$ due to the H_2O bending vibration.[25]

Isotopic substitution is often used to confirm such band assignments to a particular structural group. The force constant is unchanged but the altered mass causes a corresponding frequency change. The effect is, of course, particularly marked when deuterium replaces hydrogen.

Since the development of infrared analysis in surface chemistry has been applied mainly to surface hydroxyl groups, and since this subject is examined in detail elsewhere, no detailed descriptions will be given of the spectral characteristics of separate hydroxyl-hydrate oxide coverages. Most research attention has been

22) N.G. Yaroslavskii and A.N. Terenin., *Dokl. Akad. Nauk. S.S.S.R.*, 1949, **66**, 885.
23) L.N. Kurbatov and G.G. Neuiman., *Dokl. Akad. Nauk. S.S.S.R.*, 1949, **68**, 341.
24) E. Greinacher, W. Luttke, and R. Meeke, *Z. Electrochem.*,1955, **59**, 23.
25) M. L. Hair., "*Infrared Spectroscopy in Surface Chemistry*" Dekker, New York, 1967.

attached to systems such as silica gels, alumogels, and zeolites, i.e., materials whose spectral characteristics, if compared with those of transition metal oxides, are almost ideal in the ν_{OH} region. In contrast, most transition metal oxides are not favourable materials for the analysis of the spectra of surface hydroxyl group, primarily because of poor transmission in the 3100-3900cm^{-1} region, small surface areas and the possible proton delocalization on the oxide. This presents a serious challenge to the analyst whose aim is to record a complete spectrum of surface hydroxyl groups with the hydrogen bond method, which is widely used to investigate the acid-base properties of hydroxyl groups.

2.5 Zinc Hydroxide

In the last forty years very little work has been done on $Zn(OH)_2$. Most of the work conducted on $Zn(OH)_2$ was done prior to 1960.[1,2,3,4,5,6,7,8,9,10,11,12,13,14,15,16,17,18,19,20]

---

1) M. Farnsworth and C. H. Kline, *Zinc Chemicals*, 1st edn., Charles H. Kline and Co. Inc., Zinc Development Association, London, 1973.

2) W. Feitknecht, "Zur Kenntnis des β-Zinkhydroxyds (Preparation, physical appearance and powder diffraction pattern of β_1 and β_2 $Zn(OH)_2$)", *Helv. Chim. Acta*, 1949, **32**, 2294-2298.

3) W. Feitknecht, "Über die α-Form der Hydroxyde zweiwertiger Metalle" (The α-Form of the Hydroxides of Divalent Metals), *Helv. Chim. Acta*, 1938, **21**, 766-784.

4) R. Giovanoli, H. R. Oswald and W. Feitknecht, "Über die thermische Zersetzung der kristallinen Zinkhydroxide (The Thermal Decomposition of Zinc Hydroxide)", *Helv. Chim. Acta*, 1966, **49**, 1971-1983.

5) R. B. Corey and R. W. G. Wyckoff, "The Crystal Structure of Zinc Hydroxide", *Z. Krist.*, 1933, **86**, 8-18.

6) (i) G. F. Huttig and R. Mytyzek, *Z. Anorg. Allg. Chem.*, 1930, **190**, 353 and (ii) G. F. Huttig and H. Möldner, "Die spezifischen Wärmen des kristallisierten Zinkhydroxyds und die Berechnung der Affinitäten zwischen Zinkoxyd und wasser (The specific heat capacity of crystalline zinc hydroxide and the calculation of the affinities between zinc oxide and water)" *Z. Anorg. Allg. Chem.*, 1933, **211**, 368

7) A. F. Wells, *Structural Inorganic Chemistry*, 5th ed., Clarendon Press, Oxford, 1986, ch. 14, pp. 626- 652.

8) A. Nørlund Christensen, "The Crystal Structure of γ-$Zn(OH)_2$", *Acta. Chem. Scand.*, 1969, **23**, 2016-2020.

9) R. Scholder and G. Hendrich, "Das System ZnO-Na_2O-H_2O" (The ZnO-Na_2O-H_2O System), *Z. Anorg. Allg. Chem.*, 1939, **241**, 76-92.

10) (i) R. Scholder and H. Weber, *Z. Anorg. Allg. Chem.*, 1933, **215**, 355 and (ii) *Z. Anorg. Allg. Chem.*, 1969, **368**, 53.

11) O. K. Srivastava and E. A. Secco, "Studies on metal hydroxy compounds. II. Infrared spectra of zinc derivatives ε-$Zn(OH)_2$, β-$ZnOHCl$, $ZnOHF$, $Zn_5(OH)_8Cl_2$ and $Zn_5(OH)_8Cl_2.H_2O$", *Can. J. Chem.*, 1967, **45**, 585-588.

12) O. K. Srivastava and E. A. Secco, "Studies on metal hydroxy compounds. I. Thermal Analysis of zinc derivatives ε-$Zn(OH)_2$, $Zn_5(OH)_8Cl_2.H_2O$, β-$ZnOHCl$ and $ZnOHF$", *Can. J. Chem.*, 1967, **45**, 579-583.

13) R. Giovanoli, H. R. Oswald and W. Feitknecht, "Étude des Hydroxides de Zinc Cristallins Instables par Microscopie et Microdiffraction Électroniques et par Diffraction des Rayons X (Study of Unstable Crystalline forms of Zinc Hydroxide by Microscopy, Low Energy Electron Diffraction and X-Ray Diffracrion)", *J. Microscopie*, 1965, **4**, 711-724.

14) G. Bohnsack, "Die Auflösung von Zinkmetall und die Löslichkeit von Zinkhydroxid durch Messung der elektrischen Leitfähigkeit im System Zink/Wasser (The Disolution of Zinc and the Solubility of Zinc Hydroxide by measuring the Electrical Conductivity in the Zn/H_2O System)", *Ber. Bunsenges.*, 1988, **92**, 803-813.

15) H. G. Dietrich and J. Johnston, *J. Am. Chem. Soc.*, 1927, **49**, 1419.

16) W. Feitknecht, "Studies on the Influence of Chemical Factors on the Corrosion of Metals", *Chem. & Ind.*, 1959, 1102-1109.

17) T. F. Dirske, C. Postmus and R. Vandenbosch, *J. Am. Chem. Soc.*, 1954, **76**, 6022.

18) O. Glemser. H. G. Völz and B. Meyer, *Z. Anorg. Allg. Chem.*, 1957, **292**, 311.

19) P. Schindler, H. Althaus and W. Feitkneicht, "Löslichkeitsprodukte und Freie Bilungsenthalpian von Zinkoxid, amorphen Zinkhydroxid, β_1 -, β_2 -, γ -, δ - und ε - Zinkhydroxid (Solubility Product and ΔG Formation of ZnO, Amorphous $Zn(OH)_2$, β_1 -, β_2 -, γ -, δ - and ε - Zinc Hydroxide)", *Helv. Chim. Acta*, 1964, **47**, 982-991.

20) H. G. Schnering, "Zur Konstitution des ε - $Zn(OH)_2$ (The Structural Properties of $Zn(OH)_2$)", *Z. Anorg. Allg. Chem.*, 1964, **330**, 170-178.

2.5.1 Physical Properties

Zinc hydroxide exists in one amorphous and six crystalline forms.[1] The crystalline forms are designated as α, β_1, β_2, γ, δ and ε. Only the ε-form is stable (least energy content), the other forms revert to it in time. The overall picture of the structural chemistry of hydroxides is still very incomplete.

The very unstable α-$Zn(OH)_2$ has a hexagonal double layer lattice. Other unstable forms have been described with more complex layer sequences, some of which are stable only in the presence of foreign ions (such as carbonate and silicate).[2,3,4] The stable ε-crystals (rhombohedral) consist of $Zn(OH)_2$ tetrahedra sharing all corners with other similar groups.[5]

The lattice is basically a three-dimensional network of zinc atoms each linked to four others through the OH groups. The network is a distorted form of the diamond or crystabolite nets. Each OH is surrounded, roughly tetrahedrally, by two zinc atoms and two OH groups. The OH-OH distances are only 2.83Å, showing that hydrogen bonding is involved.

One of the less stable forms of $Zn(OH)_2$, the so-called γ form, has an interesting structure[8] consisting of rings of three tetrahedral $Zn(OH)_4$ groups which are linked through their remaining vertices into infinite columns. The upper vertices of the tetrahedra of one ring are the lower vertices of the ring above, so that all the vertices of the tetrahedra are shared within the column, which therefore has the composition $Zn(OH)_2$. Although zinc prefers tetrahedral coordination in $Zn(OH)_2$ itself, various hydroxy compounds with CdI_2-like structures appear to exist. In a number of basic salts Zn adopts a compromise, as in $Zn_2(OH)_2SO_4$, between the tetrahedral coordination in $Zn(OH)_2$ and the octahedral coordination in $ZnCO_3$ and other oxy-salts, by exhibiting both kinds of coordination in the same crystal.

Widely different values of solubility in water have been reported: even allowing for the presence of different polymorphs, the values appear inconsistent. Very low concentrations of other ions may be responsible. Understandably, the solubility

increases rapidly as the pH of the solution rises, because of the increasing importance of anionic complexes, mentioned below.

2.5.2 Chemical Properties

2.5.2(i) Preparation

$Zn(OH)_2$ is often described as the precipitate obtained by raising the pH of the solution of a zinc salt. Actually an oxyzinc salt forms or a flocculent zinc oxide precipitates, causing some investigators to doubt the existence of $Zn(OH)_2$. However, several methods have now been established for its preparation. In general, $Zn(OH)_2$ precipitates in the pH range 7-13 in the absence of ammonium salts. Ammonia precipitates zinc hydroxide from solution but re-dissolves it to form the $[Zn(NH_3)_4]^{2+}$ complex.

$Zn(OH)_2$ may be prepared by mixing an oxysulphate slurry with a sodium zincate solution at pH of about 13.3. A second method of preparation is to dilute a concentrated solution of sodium zincate. $Zn(OH)_2$ separates on standing for several days. Another method is to allow a strong ammoniacal solution of zinc oxide to stand in an open vessel. As the solution slowly loses ammonia, $Zn(OH)_2$ precipitates.[9] Preparation of amorphous $Zn(OH)_2$ occurs when a stoichiometric quantity of ammonia is added to a solution of $ZnSO_4$. Following washing, the precipitate is dissolved in concentrated ammonia and the solution slowly allowed to lose ammonia over one week.[15] It has also been shown that $Zn(OH)_2$ is formed as a volatile product when water vapour is passed over ZnO at about $1300^{O}C$; the quantity of vaporized solid is proportional to the pressure of water vapour.[18]

2.5.2(ii) Solubility

The ε form is the only phase that is stable in water below $39^{O}C$. Above that temperature the stable phase in contact with water is ZnO, although the transformation is exceedingly slow. $Zn(OH)_2$ is amphoteric. It reacts with acids to form zinc salts

$$Zn(OH)_2 + 2H^+ \rightarrow Zn^{2+} + 2H_2O \qquad \text{Eqn 2.5.2-A}$$

It dissolves in an excess of potassium or sodium hydroxide. The solubility in alkali is sometimes taken to indicate acidic properties. In fact the solubility is due to the formation of a series of readily soluble and highly hydrolysed anionic hydroxo-species, known as 'zincates'.[10] There is good evidence for the formation of $[Zn(OH)_3]^-$ and the dibasic zincate $[Zn(OH)_4]^{2-}$.[17] Although other ions, e.g., polynuclear $Zn_2(OH)_3^+$, $Zn_3(OH)_3^{3+}$ and six-coordinate $Zn_2(OH)_6^{4-}$, have been proposed, the evidence for them is not strong.

2.5.2(iii) Thermal behaviour

Very varying decomposition temperatures have been quoted. It appears that ε-$Zn(OH)_2$ loses water at an appreciable rate at 120°C, although the temperature must be raised to 900°C for complete conversion to ZnO. Evidently the migration of hydroxide through the lattice is a difficult process. Hüttig considered the thermodynamics of the zinc oxide/water system and asserts that there is a favourable decrease in ΔG for the formation of $Zn(OH)_2$ from this system at temperatures below 39°C.[6] Above 39°C only ZnO is stable. It is possible to heat ε $Zn(OH)_2$ *in vacuo* at 60°C without any appreciable loss of water.

2.5.3 Infra Red Spectral Properties of Hydroxy Species and Water

The presence of the hydroxyl group may be due to aquo species (HOH) or hydroxy species (OH) within the structure under examination. Aquo species are those which contain water. In inorganic salts these may be classified as lattice water or coordinated water. There is, however, no definite borderline between the two. The former term denotes water molecules trapped in the crystalline lattice, either by weak hydrogen bonds to the anion or by weak bonds to the metal, or both (fig. 2.5.3-A), whereas the latter denotes water bonded to the metal through partially covalent bonds. Although bond distances and angles obtained from x-ray and neutron diffraction data provide direct information concerning the geometry of the water molecule in the crystal lattice, studies of vibrational spectra are also useful for this purpose.

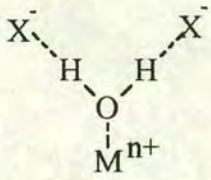

Figure 2.5.3-A Schematic representation of lattice water hydrogen bonded within a crystalline lattice

2.5.3(i) Lattice water

In general, lattice water absorbs at 3550-3200 cm^{-1} (antisymmetric and symmetric OH stretching frequencies) and at 1630-1600cm^{-1} (HOH bending)[21]. In the low frequency region, these crystals exhibit librational modes that are due to rotational oscillations of the water molecule restricted by interactions with neighbouring atoms.

2.5.3(ii) Aquo (H_2O) Complexes

In addition to the three fundamental modes of the free molecule, coordinated water is expected to show other modes. The rocking and the metal-oxygen stretching modes will become infrared active if the metal-oxygen bond is sufficiently covalent. The bands at 880-650cm^{-1} have been assigned to the rocking mode of coordinated water in inorganic salts.

2.5.3(iii) Bulk Water

As is well known liquid water possesses strong infrared absorption near 3300, 1640 and 800cm^{-1} as well as several other weaker absorption bands.[22,23] The presence of these intense bands means that little use of water solutions can be made in these regions. This is particularly unfortunate in the case of the 1640cm^{-1} deformation vibration, because it occurs in the centre of the extremely useful and interesting X=Y region (X, Y = C, O, N). It is possible to shift this angular vibration from 1640 to 1210cm^{-1} (*ca.* 74% of the hydrogenated value) by replacing the hydrogen atoms with deuterium. At the same time the 3300cm^{-1} O-H stretching vibration is shifted to

---

21) K. Nakamoto, "Infra Red and Raman Spectra of Inorganic Coordination Compounds", 4th ed., Wiley, New York, Chichester, 1986, *and references there-in.*

22) W. W. Coblentz, Carnegie Inst., Wash., 1905, **35**, pp. 56, 185, 331.

23) N. E. Dorsey, "Properties of Ordinary Water Substance", Reinhold Publishing Corp., New York, 1940, 341.

2500cm^{-1} (*ca.* 76% of the hydrogenated value). Leaving OH (and NH) vibrations free of solvent absorption. It is therefore possible through the use of two separate preparations using water and deuterium oxide as the solvents to cover the complete rock-salt infrared region.

When studying molecules in D_2O it is well to keep in mind the possibilities of exchange between the deuterium in the D_2O and any hydrogen atoms that may be present in the molecule under investigation. Many molecules containing OH (or NH) will undergo rapid exchange. Exchange between labile protons and deuterium in D_2O usually occurs rapidly and results in the appearance of new absorption bands at frequencies *ca.* 27% lower than the original hydrogenic frequencies.

This molecular change, however, is of little consequence when the major interest in the spectrum is centred in the double bond region of the carboxylic acids and their salts.

Adsorbed water has a deformation band near 1640 cm^{-1}. This band is due to the change in dipole moment associated with a change in the H-O-H angle. Its observation is proof that there are two hydrogens bonded to a single oxygen.

2.5.3(iv) Hydroxo (OH) Complexes

The infrared properties of OH species has previously been mentioned in the preceding chapter (section 2.4.3) in reference to their interaction with zinc oxide surfaces. The following section provides a more general account of their infrared spectroscopic properties.

The hydroxo group can be distinguished easily from the aquo group, since the hydroxo group lacks the HOH bending mode near 1600cm^{-1}. However, the M-O-H group exhibits the MOH bending mode below 1200cm^{-1}.

The earliest observations of infrared bands due to hydroxyl groups were made by workers who were primarily interested in the spectra of adsorbed molecules. Their interpretation of the hydroxyl bands is important to later studies of adsorption.

Buswell *et al.*[24] studied the effect of variation in drying conditions on the spectrum of montmorillonite-water systems. The use of infrared to study the state of water in minerals had previously been suggested and briefly exploited by Coblentz.[25] The spectral results of Buswell *et al.*[24] showed bands at 2.75μ (3636 cm^{-1}) and at 3.0μ (3333 cm^{-1}) which were attributed to free (non hydrogen-bonded) and hydrogen-bonded hydroxyl groups, respectively. This interpretation was based on work which showed that alcohols have strong bands at 2.75μ (3636 cm^{-1}) in dilute CCl_4 solution and bands in the 2.95-3.0μ (3636-3390 cm^{-1}) region in more concentrated solutions.[26] The shift from 2.75 to 3.0μ with increasing concentration of alcohol was attributed to hydrogen bonding.

The presence of two O-H stretching bands showed that there are at least two types of OH groups on the montmorillonite. On the simplest basis the OH bands can be separated into those due to adsorbed water and those due to surface OH groups. These species can be distinguished by the spectral region around 1600cm^{-1}. However, the real situation is more complex than this.

As mentioned in section 2.4.3, the OH group is a highly effective 'probe' species and small differences in the frequency of vibration of the hydroxyl group are capable of reflecting various changes in the species' environment.

---

24) A. M. Buswell, K. Krebs and W. H. Rodebush., *J. Am. Chem. Soc.* 1937, **59**, 2603.
25 W. W. Coblentz., *J. Franklin Inst.* 1911, **172**, 309.
26) A. M. Buswell, V. Deitz and W. H. Rodebush., *J. Chem. Phys.*, 1931, **5** , 501.

CHAPTER 3: EXPERIMENTAL

3.1 Analytical Procedures

3.1.1 Infra-Red (Transmission) Spectroscopy

Infra-red spectra were recorded as pressed KBr or CsI discs in a Perkin Elmer 1600 FTIR spectrometer. The KBr was FT-IR grade (99+%) and the CsI was 99.999%, both were supplied by Aldrich Chem. Co., The Old Brickyard, New Road, Gillingham, Dorset SP8 4JL, England. These were used from the bottle and pre-dried at 120°C for 3 hours and stored in an oven at 60^0C over zeolite 4A beads prior to use.

3.1.2 DRIFTS

A Digilab FTS-7 ex BioRad Fourier transform spectrometer was used, with an internal DRIFTS accessory. The infrared detector used was a liquid nitrogen-cooled, narrow band, mercury cadmium telluride (MCT) detector, capable of monitoring the spectral range 4000-700 cm^{-1} at a frequency of 20 kHz. At saturation the output signal was an interferogram of 12V peak to peak (maximum value 6V). This was slightly lower than its original maximum value (18V peak to peak), due to ageing effects. Samples were held and tested in a high temperature environmental cell (HTEC), see section 3.1.2(ii), which was itself mounted within a DRIFTS accessory referred to as the 'Collector', see section 3.1.2(i).

3.1.2(i) The DRIFTS Accessory (The Collector)

The DRIFTS accessory was manufactured by Spectra-Tech., Inc. (see Fig. 3.1.2-A and 3.1.2-B). It consists of a chamber which is roughly cubic in outline with an average edge of *ca.* 15cm. The Collector employs 4 plane and 2 aspherical mirrors. The aspherics are off-axis ellipsoids which focus and collect the infrared beam to and from the sample. The sample is accessed by sliding the aspherics apart.

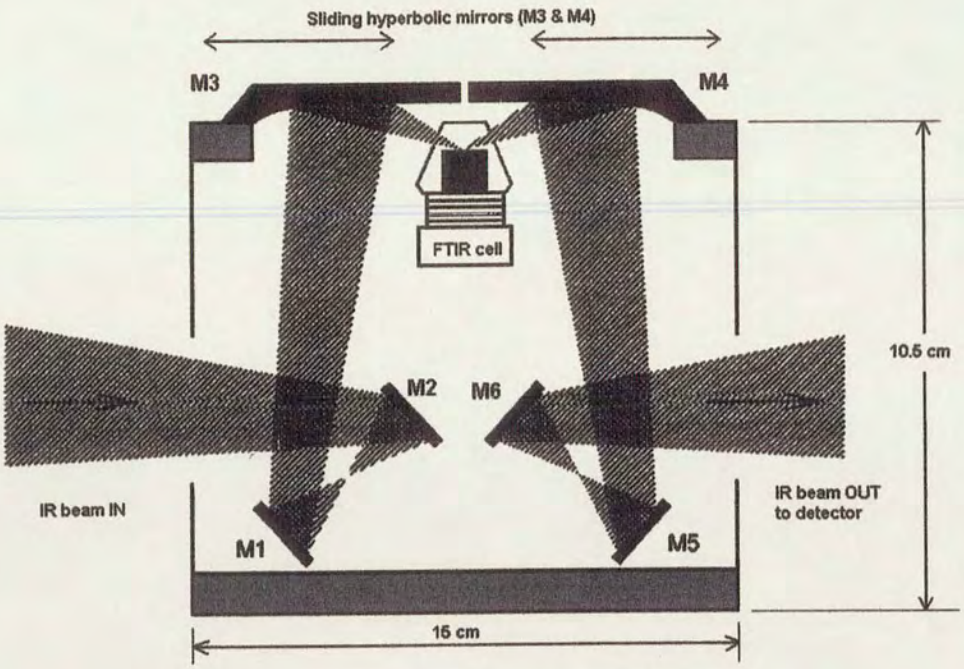

Figure 3.1.2-A Schematic representation of the optical layout of the Collector and the passage of the infrared beam across the mirrors M1-M7

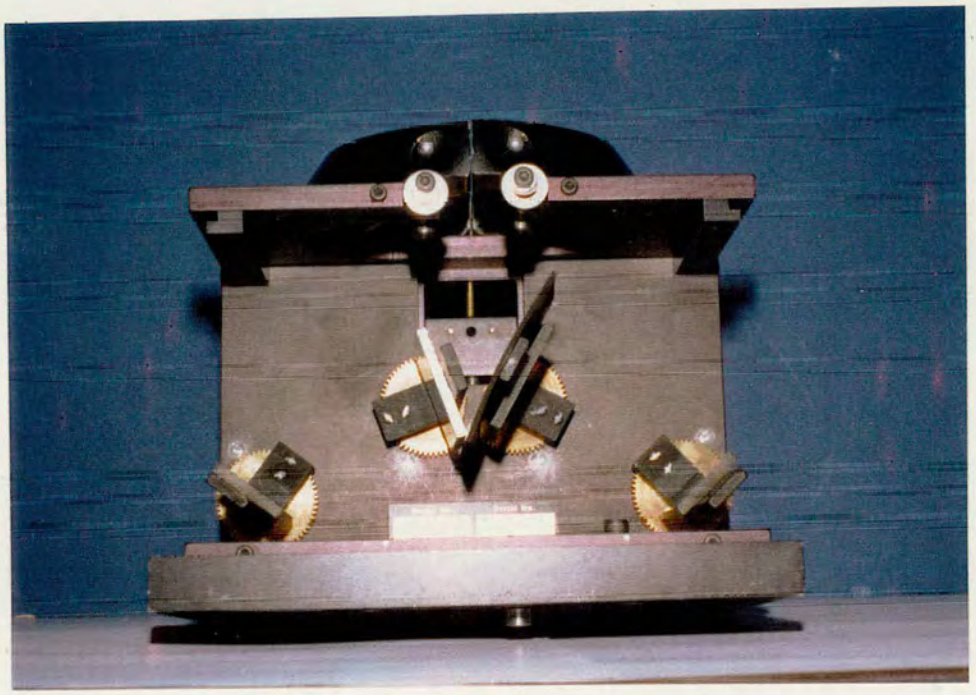

Figure 3.1.2-B Photograph of the Collector apparatus with the HTEC removed

3.1.2(ii) The High Temperature Environmental Cell (HTEC)

The HTEC consists of a shallow ceramic cup fixed onto a metal plate. The cup is 5mm in diameter and 2mm in depth and will hold *ca.*50mg of a powdered sample when levelled with the top (without compression). The cup is rendered air-tight by a dome, secured with screws to the plate, and via an O-ring (Fig. 3.1.2-C).

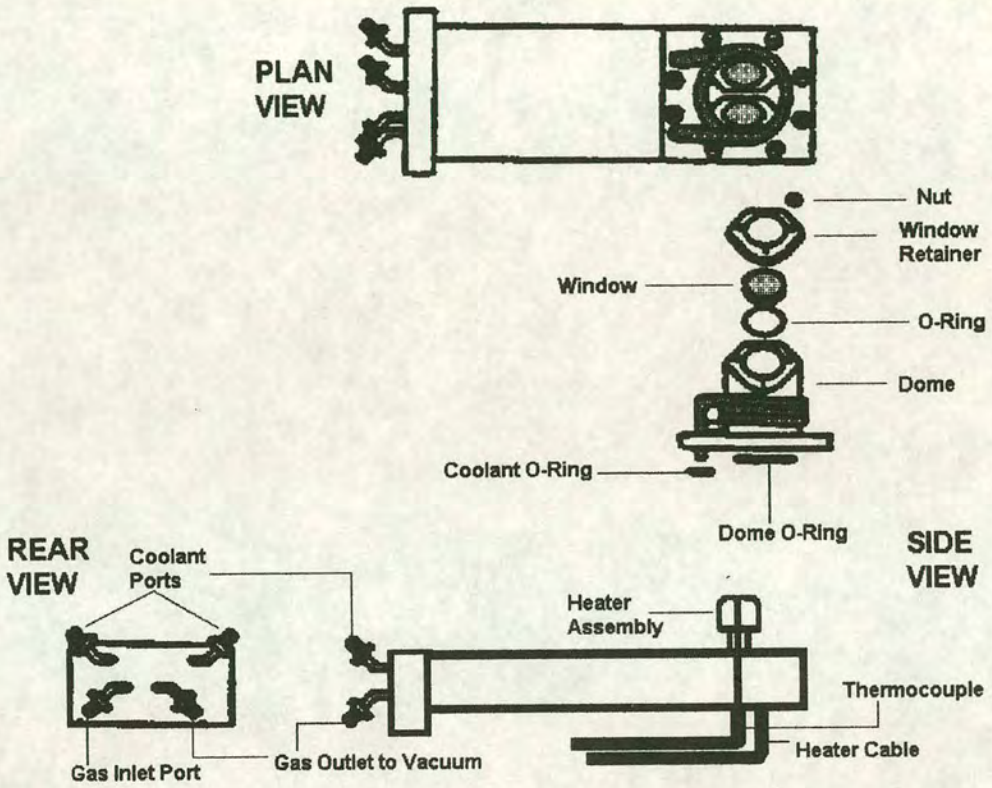

Figure 3.1.2-C Schematic representation of the high temperature environmental cell (HTEC)

The dome has zinc selenide cell windows to allow ingress and exit of the infrared beam. The sample within the cup may be heated between ambient and 1173K using a heating coil embedded within the sample cup. A chromel/alumel thermocouple, in contact with the sample, and connected to an electronic thermometer, is used to measure the sample temperature. Water is continuously circulated through a cooling coil when the cell is operated above *ca.* 120^{O}C. This prevents heat damage to the O-rings and cell windows. The water is ciculated at *ca.* 50mL min^{-1} using suction provided by a vacuum pump which aspirates water from an open tank through the

cooling coil and into an evacuated tank. Various gases may be passed over the sample using the gas supply system described by Sohail. [1]

3.1.2 (iii) DRIFTS Sample Preparation

DRIFTS samples are usually dispersed in an excess of a white standard, such as KCl or KBr, in order to fill in the voids between particles with a solid whose refractive index is close to that of the particles.[2] This practise helps increase spectra quality by eliminating scattering effects. However, due to concern over the possible influence of the diluent on the behaviour of the material and the risk of it presenting absorption bands of its own, which could be mistaken for surface species of the absorbent, the samples were prepared using the method of Sohail.[2] In this method the sample is finely ground without diluent. This was found to yield good spectra. In practice the best spectra are achieved when the particle size is below the wavelength of the incident radiation. With the apparatus described the lowest scanning wavelength was 2.5μm. All samples were, therefore, carefully ground in an agate mortar and pestle to give particle sizes in the range 1-40 μm. The fine grinding was to reduce Fresnel reflection, which occurs at crystal faces which are larger than the wavelength of the scanning radiation.

3.1.3 Mass Spectroscopy

Electron Impact and Fast Atom Bombardment mass spectra were obtained by Alan Millar of the Department of Chemistry, University of Edinburgh on a high resolution Kratos MS50TC. The instrument was run in positive mode using CsI as cal ibrant. For the FAB analysis, samples were dissolved in the least amount of acetone possible, prior to addition of 3-NOBA (3-nitrobenzaldehyde) liquid matrix. Xenon was used as the fast atom.

Accurate mass values, M_{AC}, and predicted peak distribution patterns obtained using either the Kratos MS50TC software package, the "Kratos Mach 3 Data System" or

---

1) K. Sohail, Ph.D. Thesis, Dept. Of Chemical Engineering, University of Edinburgh, 1992, p68.
2) J. T. Yates Jr. and T. E. Madey eds, *Vibrational Spectroscopy of Molecules on Surfaces*, Plenum, New York, 1987.

the "Molecular Mass Calculator 1.7" which is part of "Chem Window 3" supplied by Softshell International, 1600 Ute Ave., Grand Junction CO 81501.

3.1.4 Elemental (CHN) Analysis

The analyses of percentage carbon, hydrogen and nitrogen were obtained by Lorna Eades of the Department of Chemistry, University of Edinburgh using a Perkin Elmer 2400 Elemental Analyser, using a combustion temperature of 970^{O}C, reduction temperature of 640^{O}C and a detector oven at 80.6^{O}C, working at a pressure of 760 mm Hg. Predicted percentages were calculated using "Molecular Mass Calculator 1.7" which is part of "Chem Window 3" supplied by Softshell International, 1600 Ute Ave., Grand Junction CO 81501.

3.1.5 Atomic Absorption Spectrophotometry

The analyses of percentage chlorine, zinc, sodium and copper were obtained by Lorna Eades of the Department of Chemistry, University of Edinburgh. Zinc, copper and sodium analyses was obtained using the ATI Unicam 99 AA Spectrometer. The flame type was air/acetylene. For zinc, the wavelength used was 213.9 nm, bandpath was 0.5 mm, lamp current was 5 mA. For sodium, the wavelength used was 589.0 nm, bandpath was 0.5 mm, lamp current was 5 mA. For copper, the wavelength used was 324.8 nm, bandpath was 0.5 mm, lamp current was 3 mA. For chlorine analysis, micro-chemical oxygen flash combustion was used.

3.1.6 Nuclear Magnetic Resonance

Nuclear magnetic resonance spectra were recorded by Tony Taylor of the Department of Chemistry, University of Edinburgh using a Brüker WP200SY 200 MHz spectrometer. Dried, deuterated solvents for the samples were stored over zeolite beads (type 4A).

3.1.7 Thermal Analysis: Differential Scanning Calorimetry (DSC)

Before describing the DSC apparatus it is important to appreciate the many factors which may affect the outcome of any thermoanalytical study. A brief consideration of these variants follows.

The nature of the material (its degree of crystallinity and quality of structure) may have some effect on its thermoanalytical behaviour. In spite of identical chemical compositions, the variation with respect to structure, imperfections, grain boundaries etc. is almost unlimited. However, the variations do not necessarily produce noticeable changes.

Shape and particle size of the sample affect the surface area to weight ratio such that a sample with small surface area to weight ratio (large particles) will react more slowly than a sample of equal mass with finer particles. Smaller particles also allow closer packing which, in turn, may affect the thermal behaviour. A loosely packed, coarse material leaves voids which can act as air pockets, reducing thermal conductivity and rendering the sample more susceptible to settling during heating. Particle size distribution and packing density are both difficult to reproduce. Also, the weight and volume of the sample should be minimized so that the effects of inhomogeneous temperature distribution, retention of gaseous decomposition products etc. may be avoided.

The sample atmosphere may play an active rôle in certain decomposition reactions, especially oxidation and reduction processes. The pressure of the atmosphere is also important, since, combined with atmospheric composition, these factors determine whether a reaction will occur at a particular pressure.

The heating system used in thermoanalytical studies affects the temperature gradients within it. Within furnaces, for example, there always exists, to some degree, radial and vertical temperature gradients. The amount and shape of the sample can also add to this effect, as does the thermal conductivity of the sample holder and sample, which may cause temperature gradients of several ^{O}C, as described in section 3.2.1. The sample heating rate is also very important, especially in slow or complex reactions. Fast heating rates shift the reactions to higher temperatures and decrease the resolution when several reactions follow each other

closely. As a consequence the heating rate must not only be linear, but also adapted to the expected type of reaction.

The DSC technique monitors the amount of heat required to raise the temperature of a sample at a fixed rate. Normally, this would remain a fixed quantity, related to the heat capacity of the sample and DSC pan. However, when the sample undergoes an endothermic process, such as melting, boiling or endothermic reaction, more heat is required to raise the temperature at the steady rate and the DSC trace shows a higher power is required (the DVM reading is a digital voltmeter reading of the power supplied). In comparison, exothermic processes cause self-heating of the sample. Less power is, therefore, required from the heater and so the DSC trace shows a lower power requirement.

D.S.C. measurements were recorded by Simon Lawrence at Durham University using a Mettler FP85 thermal analysis cell coupled to a Mettler FP80 processing unit. Samples were hermetically sealed in aluminium capsules and pierced with a pin-hole to allow loss of volatile components. Heating was carried out in an inert argon shroud. Data collection and manipulation was carried out on an OPUS PCIII with in-house software (J. Rawson, 1991), and printed on an Epson LQ-850+ dot matrix printer.

3.1.8 X-Ray Powder Diffraction

Diffraction patterns were obtained by Graham Cruickshank of the Department of Chemistry, University of Edinburgh, using on a Philips Powder Diffractomer equipped with an automatic sample changer (PW1170/02). The goniometer (PW1050/80) was mounted on an X-ray generator (PW1730/10) which emits Cu Kα radiation of wavelength 1.541838 Å. A motor control (PW1390) and AMR focussing monochromator (AM3/202E) was fitted in front of a detector (PW1965/60). The tube voltage used was 40 kV and the tube current was 30 mA. The scanning angle used was 70^{O}-3^{O} 2θ, with a step angle of 1^{O} 2θ per minute. The range used was 4×10^{-3} counts per second. Samples were packed into specially constructed sample holders as described in section 3.2.4.

An internal silicon reference was used to improve the accuracy of peak position measurement. The 2θ values for the major silicon peaks are 28.470, 47.345 and 56.188^{O} 2θ. The position of the peaks was measured manually from the XRPD traces obtained. Traces were printed at 1^{O} 2θ cm^{-1} and the accuracy of peak position measurement was estimated to be ± 0.1^{O} 2θ, which corresponds to errors of ± 0.02 in d-spacing values. D-spacing values were calculated from the rearranged Bragg equation:

$$d = \lambda / (2 \sin \theta) \qquad \text{Eqn. 3.1.8-A}$$

3.1.9 Single Crystal X-Ray Diffraction

All X-ray measurements were collected on an Enraf-Nimbus CAD4 or Stoë Stadi 4 circle diffractometer, equipped with a graphite monochromator (Mo Kα radiation, λ = 0.71073 Å). An Oxford cryosystems device was used for data collection at low temperature.[3] The relevant crystal data, data collection and structure solution and refinement parameters are presented in the text where appropriate. All calculations were performed using the crystallographic programs SHELX86,[4] SHELX76,[5] and SHELX93.[6] Figures were produced using SHELXTL PC.[7] The data was collected by Simon Parsons of the Department of Chemistry, University of Edinburgh.

3.1.9(i) Crystal Quality Assessment

Crystals were assessed for suitability for 4-circle diffractometer data collection under low magnification microscope to check for quality of form and shape. They were then checked for their ability to transmit, and then sharply extinguish, polarised light through every 90^{O} rotation. Where ambiguity remained, crystals were mounted and photographed on a single-crystal Stoë Weissenberg camera operating with Cu-Kα

---

3) J. Cosier and A. M. Glazer, *J. Appl. Crystallogr.*, 1986, **19**, 105.
4) G. M. Sheldrick, *Acta. Crystallogr., Sect. A*, 1990, **46**, 467.
5) G. M. Sheldrick, "SHELX76; Program for Crystal Structure Refinement", University of Cambridge, U.K., 1976.
6) G. M. Sheldrick, "SHELX93 Program for Crystal Structure Refinement", University of Göttingen, Germany, 1993.
7) G. M. Sheldrick, "SHELXTL PC", University of Göttingen and Siemens Analytical X-Ray Instruments, Madison, 1990.

radiation. The resulting photographs were then assessed for clarity of spot-formation as a measure of crystal quality.

3.1.9(ii) Crystal Growth

Where re-crystallization was necessary, vapour and solvent diffusion techniques[8] were used (described below). 'Good' and 'bad' solvents were established using the criteria of Vogel,[9] whereby a solute is said to be soluble in a given solvent if 0.1g (for solids) or 0.2mL (for liquids) of the solute dissolves completely in 3.0 mL of the solvent under test. Solvents used, in order of preference, were:

1) water (protic, hydroxylic)
2) Dichloromethane (aprotic)
3) Acetone (aprotic)
4) Methanol (protic, hydroxylic)
5) Toluene (non-polar)
6) Ethyl acetate (polar)
7) Methyl cyanide (aprotic, polar)
8) Hexane (aprotic, non-polar)
9) Ether (polar)
10) Ethanol (protic, hydroxylic)

In cases where these failed, dimethyl formamide (DMF) or dimethyl sulphoxide (DMSO), both of which are very polar, were used, or the aprotic, cyclic ether tetrahydrofuran (THF).

Solvent Diffusion

The material required for recrystallization was dissolved in a 'good' solvent, which was then pipetted through a celite/cotton wool filter into a small (*ca.* 5mL) sample vial (see Fig. 3.1.9-A). A poor solvent (the precipitant; which must be miscible with the effective solvent) was then carefully injected (using a syringe and fine needle) into the bottom of the solution (when the precipitant was denser than the solution), or into the top of the solution (when the precipitant was less dense). Crystal growth normally occurs at the solvent interface. Vibration and movement must be minimized to prevent mixing of the solvents. Cooling the tube decreases solubility and diffusion rates thereby decreasing crystal growth rate and, generally, increasing crystal quality.

---

8) P. G. Jones, "Crystal Growing", *Chem. In Brit.*, 1981, **17**,222-225.
9) A. I. Vogel, *Practical Organic Chemistry*, 2nd ed., Longmans, London, 1966.

Vapour Diffusion

In this technique the rate of diffusion is minimized by allowing the precipitant to diffuse through the vapour phase into the solvent.

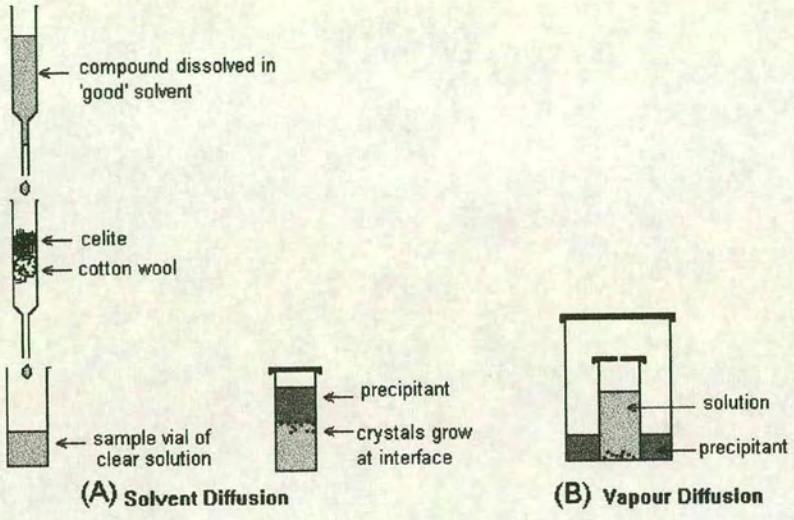

Figure 3.1.9-A Schematic representation of (A) solvent diffusion procedure and (B) vapour diffusion

3.2 Development of Apparatus

3.2.1 Glove Box

3.2.1(i) Design of Main Glove Box Unit

Commercially available glove boxes typically employ a main chamber which contains a static environment of nitrogen and an evacuable side-chamber in which samples to be handled are inserted. This side-chamber is then evacuated and refilled with nitrogen 2-3 times before opening the connecting door between the chambers and allowing the sample into the main glove box chamber. The main chamber is fitted with a gas pump which recalculates the nitrogen atmosphere through absorbent beds to trap out gaseous contaminants. For the purposes of this research there are problems inherent in using such a set up. Firstly, since the absorbent beds only trap out certain contaminants they can only be used for the same family of substances. Once a particular material is handled within the glove box traces of it will be recirculated indefinitely to potentially contaminate the samples of subsequent materials. Secondly, in spite of a positive pressure of N_2 maintained within the glove box, ambient gases diffuse into the glove box through the elastomeric material of the gloves. This process is driven by concentration gradient of a given gas between the external environment and the handling-chamber of the glove box. Ambient CO_2 was the most important contaminant to be avoided in the experimental procedures. The large surface area of elastomer presented by the gloves of the glove box ensures that CO_2 will diffuse into the glove box over time. The only way to remove the incoming CO_2 is to fit an effective CO_2 trap or to operate a flushable glove box. The problem with CO_2 traps is the difficulty in measuring whether or not they are functioning properly, especially at low gas concentrations. In addition, the CO_2 must spend some time in the glove box environment before being picked up by the trap. A preferable method is to evacuate the glove box and then flush it with a CO_2-free inert gas such as N_2. This is not practicable with standard glove boxes. A typical glove box window measures *ca.* 1.5m × 1.0m, presenting a surface area of 1.5 m^2. One atmosphere pressure corresponds to 1.01×10^5 Nm^{-2}, thus the force on an evacuated glass window would be 1.51×10^5 N, i.e., 15.4 tonnes; a force these devices are clearly not designed to withstand.

With the handling requirements of the materials being used the operational parameters of standard handling were found to be inadequate. It was therefore necessary to construct a system which would, repeatedly and reproducibly, provide a clean atmosphere of inert gas in a very short period of time (less than 30 minutes if possible) yet with sufficient space to handle bulky items like the DRIFTS assembly. Evacuable plastic bags, whilst offering brief down-times were not robust enough to use repeatedly with bulky cumbersome objects. They were also difficult to clean out in the event of sample spillage. Finally, being plastic they generated unacceptable amounts of static which caused powdered samples to cover the insides of the plastic chamber as attempts were made to transfer materials from preparation vessels to the DRIFTS cell.

The attempts to overcome such problems led to the development of a high volume, rapid evacuation glove box. (see Fig. 3.2.1-A). The main body of the box was constructed from a 1 cm thick QVF pipe-section of 24 cm diameter and 30 cm length. A sidearm, 16 cm long and of diameter 4 cm, is attached midway down the main body. The purpose of this tube was to allow for the introduction of samples etc. after the inert atmosphere has been established, with minimum danger of contamination (the sidearm essentially acted as an airlock). The QVF section was sealed at both ends to square polypropylene interfacing sections (referred to as 'end-blocks'). These square sectioned end-blocks had a diagonal portion cut from the presenting vertices (see Fig.3.2.1-A(b)) to facilitate access to the gloves. Butyl rubber O-rings set in grooves machined into these sections were used to seal the sections together. The right hand end-block (Fig. 3.2.1-A) was removable from the main body, whereas the left hand end-block was not. Removal of one end-block was necessary for loading and unloading the main chamber. Thick, neoprene rubber gloves[1] were attached through the centre of the end-blocks, and were secured to the outside of the end-blocks by large Jubilee clips.

---

1) Neoprene dry-box gloves (hand and sleeve), supplied by Aldrich, Catalogue number Z17,006-2. Hand: 0.018 in. thick (0.04572 cm), sleeve 0.022-0.025 in. thick (0.05969 cm). Total surface per glove = 776 cm^2, obtained by tracing outline onto graph paper and (1) counting squares, (2) weighing paper template.

The glove box is divided into three sections: the main chamber and two hemispherical sealing units (referred to as 'end-caps'). The end-caps join to main chamber via the end-blocks. Each transparent polythene end-cap was attached, via an isolation valve, to a rubber hose into the pumping system, such that all three sections pumped equally. Unequal vacuum, which is due to incorrect handling sequence or leaks, can lead to inflation of the rubber gloves, which can disturb samples etc. and, if left unattended, to glove rupture - a time-consuming and costly system failure.

To protect against over-pressure, when filling the box with nitrogen after evacuation, a butyl rubber pressure-buffer was attached to the main body of the box. A removable internal platform was constructed to provide a level surface for handling samples. When operating well the glove box could be evacuated to 0.1 torr (0.133 mbar) in under four minutes.

3.2.1(ii) Atmospheric Purity and Pumping Calculations

Glove box operation consists of evacuating the box and refilling with the desired atmosphere a number of times until the required purity criteria are met. Therefore, it was necessary to determine how many times, and to what degree of vacuum, the box had to be evacuated before the levels of ambient gases (principally carbon dioxide) still present in the glove box were low enough to be of negligible account as contaminants. The highest level of purity attainable would be that of the flushing gas (99.999% pure N_2, where $[CO_2] < 1$ppm). A target of within 10% of this level, i.e., $[CO_2] < 1.1$ppm, was set as an acceptably low level of CO_2 contamination.

Three factors were considered to be important in calculating the CO_2 levels within the glove box at any time.

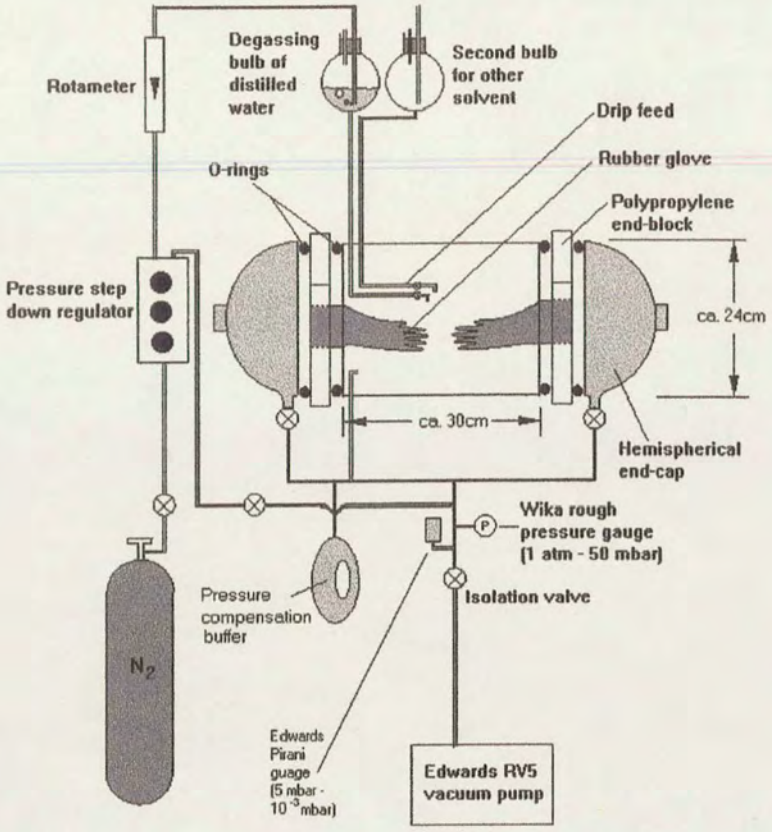

Figure 3.2.1-A(a) Schematic representation of the glove box system

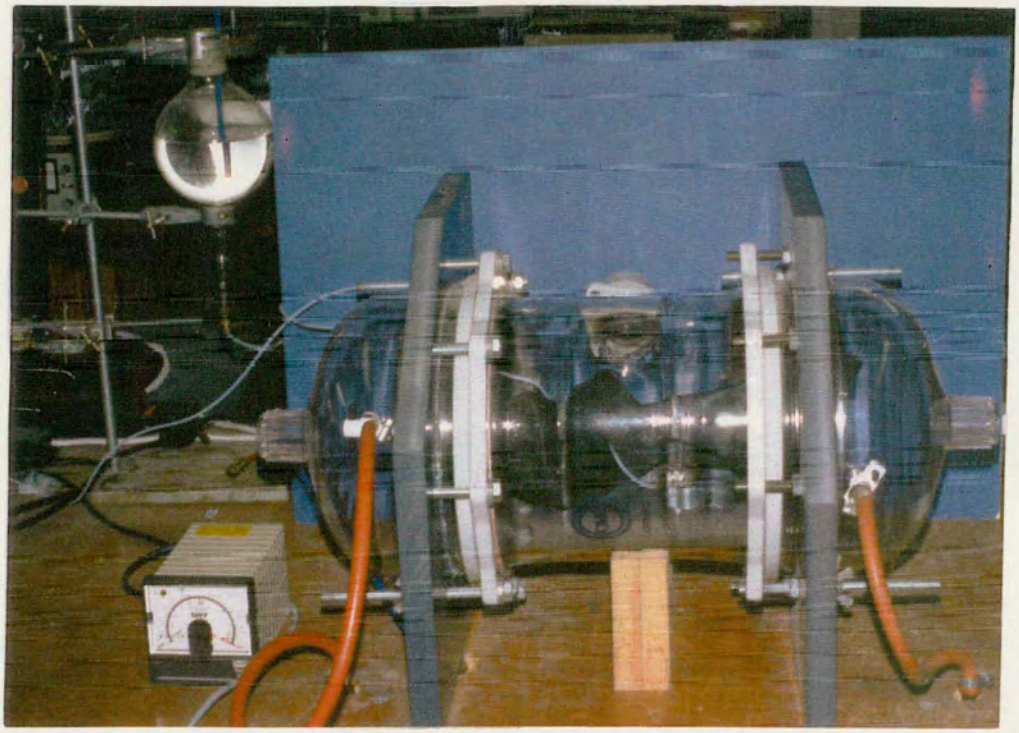

Figure 3.2.1-A(b) Photograph of the rapid-evacuation glove box system

Leak rate

Firstly the rate at which the glove box leaked air back into itself when under highest static vacuum must be established. The glove box was pumped down to its ultimate vacuum and the pressure measured. The vacuum was then isolated from the glove box and the internal pressure measured over a period of time. This was repeated several times. Two equations were found to fit the experimental data. For leak times less than one hour Eqn. 3.2.1-A best fitted the data but for leak times greater than one hour Eqn. 3.2.1-B provided a better fit.

$$P_L = 5 - 4.7 \exp\{-0.022\ T_{min}\} \qquad \text{Eqn. 3.2.1-A}$$

$$P_L = 5 - 4.7 \exp\{-0.025\ T_{min}\} \qquad \text{Eqn. 3.2.1-B}$$

Where P_L is the measured pressure in the glove box at time T_{min} (in minutes).

Diffusion rate

In trying to maintain partial pressures of CO_2 lower than the external environment, the permeability[2] of the elastomers present (in the gloves and the pressure buffer) must be considered. Permeability is the property which determines how readily gases will pass through a material - the higher the permeability value, the more readily gases pass through the material. The following points can be made with regard to the permeability of elastomers:[3]

1. Light gases (hydrogen and helium) pass through them more readily than heavy gases (oxygen, nitrogen, carbon dioxide etc.)
2. There is a time lag involved in the gas passing through the elastomer, the value depending on the thickness of the material. For a 3 mm thickness the time lag ranges from a few minutes for the light gases to an hour for heavier gases. This behaviour can complicate leak detection procedures.

---

2) Permeability is also called *permeability coefficient* and *permeability constant*, though these are not necessarily the same as permeability; permeability is sometimes used to mean the property, and the other terms its numerical value.

3) Guthrie, *Vacuum Technology*, John Wiley and Sons Inc., New York and London, 1963.

3. Neoprene and butyl are much less permeable than natural rubber (about ten times less), silicone rubber or Buna N.[4]

It was also necessary to calculate the diffusion rate of CO_2 back into the system through the neoprene gloves and the butyl rubber expansion bag. For this Eqn. 3.2.1-C was used.[5]

$$Q = P.a.t.\delta p/\delta x \qquad \text{Eqn. 3.2.1-C}$$

Where the quantity of gas (Q) passing in an interval of time (t) through a barrier of a measured area (a), with a difference of pressure - or of partial pressure- (δp), across the thickness (δx), and P is the proportionality constant of permeability.
Permeability may thus be regarded as the volume (at stp) - or the mass - of the permeating substance passing through a unit cube of the barrier in unit time under unit pressure difference, under steady state conditions. The permeability of a gas is largely independent of film thickness. With a vapour, however, the permeability may show considerable variation with thickness. Permeability measurements are quoted in the literature in various ways, and occasionally are incompletely defined. In order to avoid very small numbers the permeability of gases is often expressed in terms of $(10^{-10}\ cm^2)/(s\ cm\ Hg)$; which has the following values in other units: $76 \times 10^{-10}\ cm^2/(s\ atm)$ or $76 \times 10^{-10}\ cm^3/(cm^2\ s\ atm/cm)$.[6] Calculations were performed using an iterative programme (Table 3.2.1-A) which yielded the data plotted in Fig. 3.2.1-B.

---

4) Permeability of material at 20-30^{O}C, for CO_2, expressed as $(10^{-10}\ cm^2)/(s\ cmHg)$: nylon = 0.16-0.20; nylon 6 = 0.09; butyl rubber = 3.2; neoprene (polychloroprene) 26; natural rubber 130-135. Referenced from Roff and Scott, below.
5) Roff and Scott, *Fibres Films, Plastics and rubbers. A Handbook of Common Polymers*, Butterworth and Co. (Publishers) Ltd., 1971.
6) A table including additional conversion factors relating to volumes is given by W. M. Smith, *The Manufacture of Plastics*, New York and London, 1960, 172-173.

```
CLS
x = 0
pa = .0003
n = .00000073487509#
rt = 24.45135#
deltap = pa-p
qdot = .04118082657#
a$ = "co2diffn.dat"
SHELL "a:"
OPEN a$ FOR OUTPUT AS #1
10 vd = qdot*deltap
x =x + 1
deltap = pa - p
PRINT #1, p, x
nd = vd/ rt
n = n + nd
p = n*1.360775459#
k$ = INKEY$
IF k$<>"" THEN GOTO 20
REM IF x>5 THEN GOTO 20
IF pa/ p <= 1.05 THEN GOTO 20 ELSE GOTO 10
20 CLOSE#1
BEEP
END
```

Where **pa** = atmospheric pressure(atmospheres)
p = glove box internal pressure
n = number of moles of gas in glove box at T = 0
qdot = combined permeability term for CO_2 through given elastomers of given surface area (L atm^{-1} hr^{-1} in the above case and L $atm^{-1}s^{-1}$ for calculating plot 3.2.1-C(b)

Table 3.2.1-A Quick Basic programme for calculating partial pressure of gas diffusing into glove box through elastomers. In this case the gas is CO_2

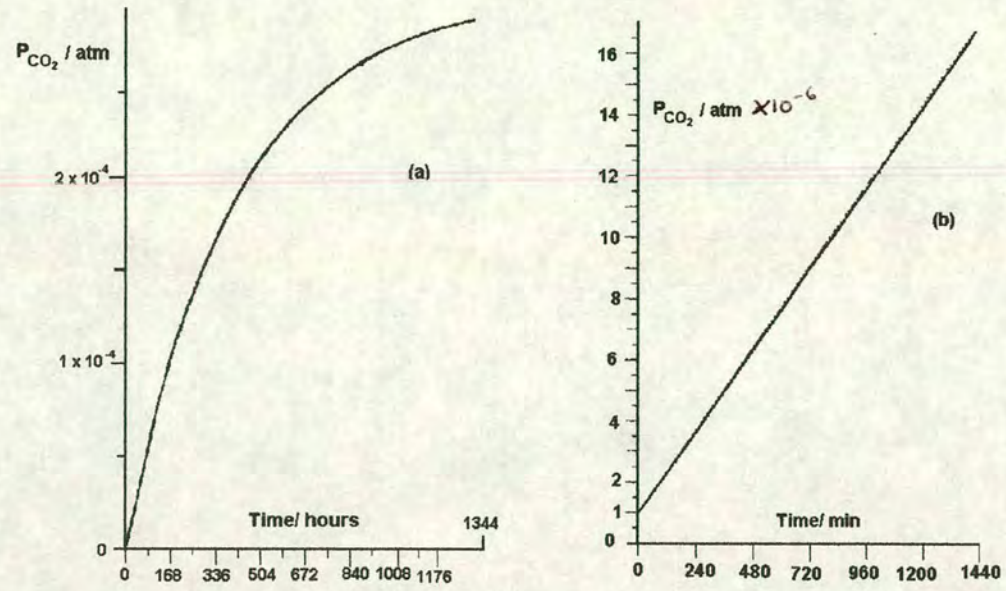

Figure 3.2.1-B Graph of partial pressure of CO_2 diffused into glove box vs. time (a) over time required to attain equilibrium with atmospheric CO_2, (b) over 24 hours

From the data it was observed that the CO_2 diffusion rate was almost linear over 24 hours, approximating to

$$P(CO_2)_{box} = 1.104 \times 10^{-8} .T + P(CO_2)_{t=0} \qquad \text{Eqn. 3.2.1-D}$$

Where $P(CO_2)_{box}$ is the partial pressure (atmospheres) of CO_2 passed into the glove box through diffusional processes over time T (minutes) and $P(CO_2)_{t=0}$ is the initial partial pressure of CO_2 within the glove box (atmospheres) after its pump-flush cycling. $P(CO_2)_{t=0}$ was usually 1.0×10^{-6} atm.

Pumping rate

Finally, in addition to the above, the pumping characteristics of the glove box were measured. In the Mk 1 version of the glove box end-caps were machined from 1 cm thick nylon. A circular plate was located onto an annulus via a butyl rubber O-ring. This formed the end-cap unit which was then placed onto the end of the glove box, via another butyl rubber O-ring. Thus, two O-rings were required per end-cap. The pumping and leaking characteristics of the glove box were greatly improved by replacing these machined end-caps with desiccator lids[7] and the included silicone O-

7) Nalgene desiccator, catalogue number 5311-0250, able to hold 711 mmHg of vacuum for 24 hours.

rings. These end-caps had the twin advantages of far greater lightness and ease of handling, and, more importantly, improved pump and leak characteristics. Since these end-caps were single piece the total number of O-ring seals in the glove box was reduced by one third. The pumping results, for the Mk 2 version are plotted below in Fig. 3.2.1-C. It can be seen in this plot that there is an obvious kink in the curve. This is due to the improved seating of the O-rings, leading to enhanced leak resistance, as the internal pressure drops below a critical value.

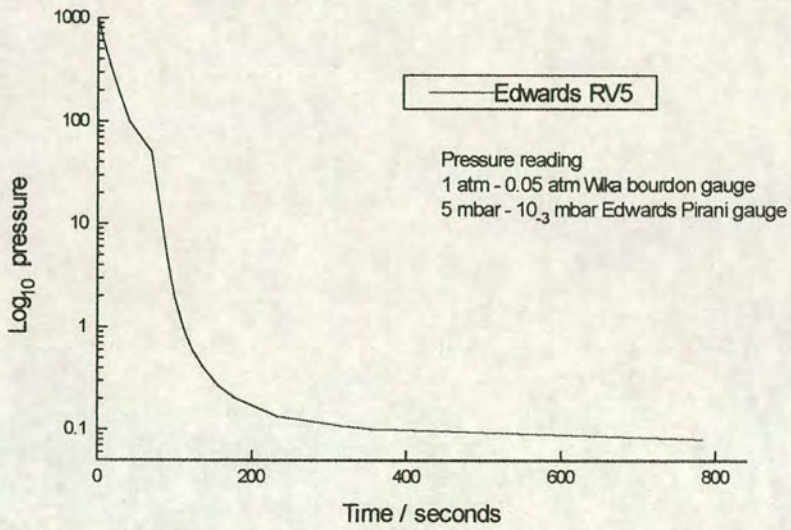

Figure 3.2.1-C Pumping characteristics of the glove box attached to an Edwards RV5 vacuum pump

Having established the equations which define the ingress and exit of CO_2 from the glove box, i.e., the permeability of CO_2 through the neoprene rubber gloves and the butyl rubber buffer; the pumping rate of the system; the leak rate of the system and the time required to reflush the system with N_2 once the system was evacuated, the shortest operating procedure was found. It was calculated that 2 pump-fill cycles (pumping down to 5 mbar each time) yielded a CO_2 concentration of 1.1 ppm and an O_2 concentration of 7.2 ppm. Three pump-fill cycles yielded CO_2 = 1.0 ppm and O_2 = 2.0 ppm. Various other combinations of final pumping pressure and number of pump-fill cycles were calculated. From these, the optimum pressure and number of pump-fill cycles to achieve the quickest clean atmosphere was found. Thus, the standard evacuation procedure consisted evacuation of the glove box to between 1

and 5 mbar followed by filling with N_2 back to atmospheric pressure. This was repeated three times. The calculated time to achieve this procedure was 7.5 minutes. In reality, due to time taken in switching valves, occasional leaks etc., 10-20 minutes was more usual.

Once a sample had been loaded into the glove box and it had been flushed to its operating level of purity it was then necessary to establish how long the samples could be maintained within the system before the internal atmosphere was again 'contaminated'. The only significant passage of CO_2 back into the box, once it had been set up, was through diffusion through elastomers in the system. Eqn. 3.2.1-D shows that after 1 hour $P(CO_2)_{box}$ is only 0.6% of $P(CO_2)_{amb}$ (where $P(CO_2)_{amb}$ is the partial pressure of CO_2 in normal air). After 4 hours $P(CO_2)_{box}$ = 1.25% $P(CO_2)_{amb}$ and is 3.02% of $P(CO_2)_{amb}$ after 12 hours and 5.67% after 24 hours. From this it was established that 4 hours (adequate for most operations) was a very safe working time for any sample within the glove box. For more involved manipulations, even 24 hours in the glove box still afforded a high level of CO_2 exclusion, being a factor of 20 times smaller than in normal air at this point.

3.2.1(iii) Exclusion of CO_2 from Water Supply

The main purpose of the glove box was to conduct hydrolysis experiments in CO_2 free environment. To this end a water feed was fitted to the apparatus with isolation and flow taps to regulate the entry of solvent into the main chamber. A second solvent bulb was also fitted for the use of other solvents, such as methanol or D_2O. The use of solvents within the glove box necessitated a consideration of the degree to which CO_2 could contaminate the solvent (water). From the calculations in section 2.2.1 it is clear that ordinary water, in equilibrium with the air, is highly contaminated with CO_2. CO_2 must, therefore, be thoroughly removed from the water used for hydrolysis purposes.

For simplicity of operation, bubbling nitrogen through water was the favoured means of stripping CO_2. Whilst the absorption of gases into water has been well studied,[8,9] the stripping of gases through desorption/bubbling processes is not well understood. Thus, in order to evaluate the effectiveness of this method in removing CO_2, from water, the system was tested as it would be used in the glove box set up. 500mL of ambiently aged, deionised water were placed in a vessel identical to the degassing bulb used in the glove box apparatus. In the absence of other contaminants the pH of water is directly related to the concentration of CO_2 in the water (section 2.2.1). Thus, by measurement of pH of deionised water, the degree of CO_2 absorption or removal may be calculated. Nitrogen was bubbled into the bulb of water, firstly with the system open to the atmosphere and then closed. The results are plotted below. In an open system equilibrium occurs between the rate of CO_2 stripped from the water and the rate at which it is reabsorbed from the atmosphere. The flow rate of N_2 must be increased substantially in order to strip the CO_2 faster than it is reabsorbed from the atmosphere.

It can be seen that the closed system is essential to effectively strip CO_2 from the system, taking ca. 4 hours to attain near pH neutrality and reasonably low level of CO_2 contamination. Whilst 4 hours was not deemed excessively time consuming for attaining CO_2 free water it was sometimes necessary employ more rigorous methods to ensure the purity of the sample.

In such cases the method of Albery and Calvo[10] was used. Alkaline, doubly deionised water, with added potassium permanganate to oxidize organic compounds, was refluxed for 2 hours and then distilled under dry nitrogen. The middle fraction (60%) of the distillate of bp. 100^{O}C was collected, producing CO_2 - free solvent. This was then decanted, under flowing nitrogen into the degassing bulb.

---

8) P. V. Danckwerts, *Gas-Liquid Reactions*, McGraw-Hill, New York, 1970.
9) P. G. T. Fogg and W. Gerard, *Solubility of Gases in Liquids*, J. Wiley, Chichester, 1991.
10) W. J. Albery and E. J. Calvo, "Ring-Disc Electrodes Part 21. - pH Measurement with the Ring", *J. Chem. Soc., Farad. Trans.*, 1983, **79**, 2583-2596.

Albery and Calvo[11] estimated that by using the above precautions to exclude CO_2 the concentration of unwanted buffer species was 1-10 μmol dm^{-3} which corresponds to 1-10 × 10^{-6} mol L^{-1} (c.f. normal CO_2 equilibrated with air = 1.24 × 10^{-5} mol L^{-1} which is *ca.* 10% equilibrium value at best).

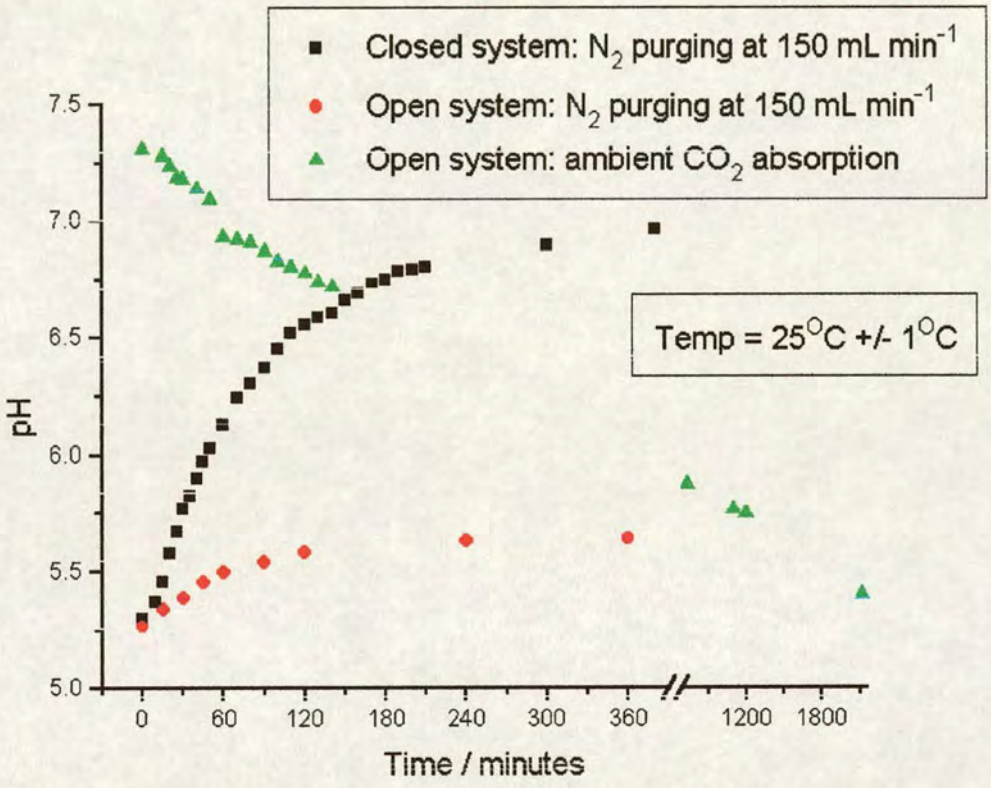

Figure 3.2.1-B Effect of N_2 purging on the CO_2 concentration of water (as indicated by pH) and the effect of standing in air on the amount of ambient CO_2 absorbed

Having attained near CO_2 free water it was of interest to ascertain the length of time it could be left before it re-attained equilibrium with atmospheric CO_2, once the purging effect of the bubbling N_2 had been ceased. House and Howard[11] have examined this area and found that the transport rate of CO_2 into aqueous solution was a complex function of the solution alkalinity, ionic strength, pH, temperature, gas-phase composition and flow rate. A chemical equilibrium model[12] was found to

11) W. A. House and J. R. Howard, "Kinetics of Carbon Dioxide Transfer across the Air/Water Interface", *Faraday Discuss. Chem. Soc.*, 1984, 77, 33-52.

12) In the chemical equilibrium model it is assumed that the hydration of CO_2 is reached at all points within the boundary layer. The theoretical maximum flux of CO_2 across the interface is attained and

suffice for low pH conditions. However, a finite-reaction-rate model was used to successfully predict the transfer velocity in different solution conditions at high pH. Given the complexity of this model[13] and the difficulty in controlling all the parameters affecting transfer rate it was more pragmatic to experimentally determine the rate of CO_2 uptake into the aqueous media the given reaction conditions.

This result is also plotted (Fig. 3.2.1-B) and shows that, initially, there is a rapid decrease in pH over the first 60 minutes of standing in air, i.e., rapid absorption of CO_2, as expected. Thus, it is essential to keep the system constantly under bubbling nitrogen once the water has been purged of CO_2 whilst hydrolysis experiments are in progress.

3.2.1(iv) Conclusion

The glove box system successfully performed the functions required of it to a greater level of performance than initially aimed for. It provided a sufficiently high volume working environment (*ca.* 18 L) to allow the handling of large pieces of apparatus, such as the DRIFTS collector. The use a of degassed water supply facilitated, *inter alia*, single step transfer of dried hydrolysates from their reaction vessel to the DRIFTS collector in air-free conditions. These conditions were not only rigorously free of CO_2 but, also, it was possible to calculate the level of CO_2 within the glove box at any time in its operation. Finally, the system provided excellent static hold times, over which the levels of CO_2 were known to be sufficiently low, of sufficient duration that even day-long handling procedures could be conducted in confidence.

---

may be simply calculated. This calculation is far simpler than when applying the finite-reaction-rate model.

13) The finite-reaction-rate model allows for the possibility that the hydration reaction is the rate limiting step leading to more complex calculations.

3.2.2 DRIFTS System

3.2.2 (i) Design of Demountable HTEC

Once the glove box had been designed, built, tested and optimized, the transfer of the hydrolysed materials to the HTEC could be conducted. In the original design of the HTEC (see section 3.1.2) the HTEC was permanently fixed to the DRIFTS collector system. In addition, part of the water cooling leads protruded from the front of the HTEC and part of the gas feed lines protruded from the rear. For the purposes of this type of research the design had a number of drawbacks:

1) As most samples in this research were air-sensitive, they had to be handled within the purpose-built glove box (described in section 3.2.1). The SpectraTech system had to be taken whole from the spectrometer. This resulted in an unwieldy and very sensitive piece of apparatus having to be handled within the confines of the glove box, which was only marginally larger than the whole DRIFTS assembly (collector plus HTEC with gas and water feed lines). This rendered operations within the glove box almost unmanageable at times and also labour intensive. As a result of the large size of the DRIFTS assembly, there was very little room to manoeuvre. Operations were already difficult enough, due to the handling of small implements such as micro-spatulas and the small allen keys required to seal the HTEC helmet whilst wearing the (necessarily) thick, rubber gloves within the glove box.

2) During transfer procedures, the sample was often, unavoidably, placed very close to the outer glass wall of the glove box. Internal static build-up (due to the dry N_2 atmosphere) during operation, caused high sample-loss levels, when the powdered samples were picked up by the static field and deposited across the interior of the glove box wall. This occasionally resulted in there being insufficient sample to run a spectrum.

3) Sample lost due to static or the difficulty of operation within the glove box, would also leave a thin coating on the ellipsoidal mirrors. This required that they were cleaned once outside the glove box, causing them to be displaced from their correct alignment. Thus also they required realignment each time this happened.

Mirror realignment could sometimes take 1-2 hours; particularly where the DRIFTS signal was not very strong, as the maximum component of the available signal had to be deflected into the signal detector cavity. This was achieved through optimizing the mirror alignment.

As a consequence of these problems, each sample took between 3 and 6 hours to be loaded ready for a DRIFTS spectrum to be taken. If the sample had been exposed to air at any time during the preparation, or the original sample had not been of a good enough quality, then it would only be at this stage that the problem would be revealed by the resulting spectrum.

To overcome the above problems a new HTEC was designed to reduce sample loading problems and, hence, reduce sample wastage and handling time. To achieve these objectives, the following changes were proposed and implemented.

1) The HTEC should be detachable from the DRIFTS collector mirror system, so that the mirror system could be permanently set up in the FTIR machine and there would be no need to realign its mirrors each time a sample was loaded. This would also mean that the mirror system would not need to be cleaned each time. The other main advantage of this feature would be that the apparatus handled in the glove box would be much smaller and therefore more manageable, resulting in less sample loss, greater ease of use and faster change-over of samples.

2) The design should have the facility for simplified preliminary testing of samples, prior to full, temperature-controlled experiments. This would save time by identifying unsuitable samples before the time-consuming process of preparation in the glove box had begun.

3) The HTEC should be easy to separate from the water and gas feeds and isolated from the air. The advantage of this modification would be, again, the reduction in size of the apparatus to be manipulated inside the glove box.

4) The new version should allow temperature controlled experiments up to 400^{O}C in changeable flowing gas environments.

The first attempt at implementing these changes was the Mk1 HTEC, described below.

Mark 1 HTEC (Preliminary Test Design)

A photograph and diagram of the Mark I design are shown in Fig. 3.2.2-A. The modifications evident in this design are:

- A detachable base plate, which sits on locating pins on the back of the DRIFTS mirror accessory. The pins ensure that the helmet is always in the correct repositioning of the HTEC within the collector. Thus, criterion 1, above, was fulfilled.
- The helmet is now screw-on, as opposed to the previous design where sealing required the tightening of 8 small allen key bolts, which had been a difficult operation inside the glove box. Sample loading is now rendered quick and facile. Thus fulfilling criterion 2.

As well as a step toward a full working design, the Mk 1 version acted as a simple device to test that adequate spectra could be obtained from new samples prior to conducting any more advanced experiments.

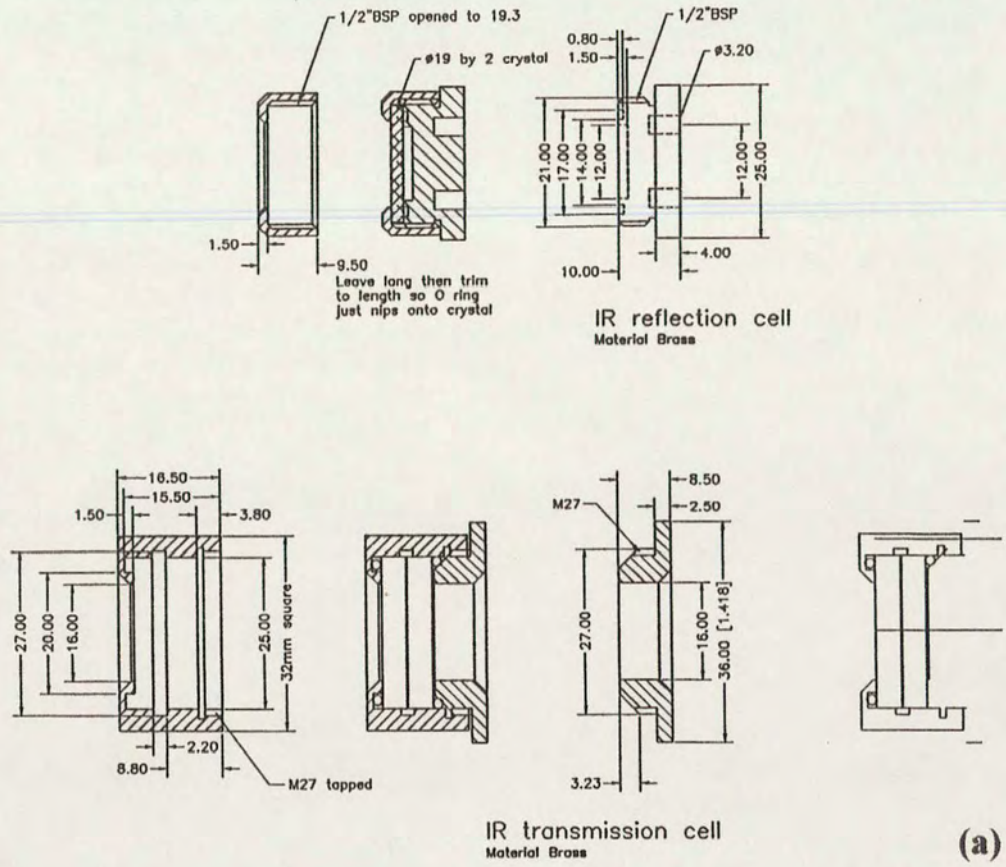

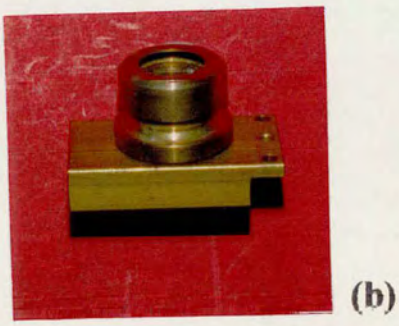
(b)


(c)

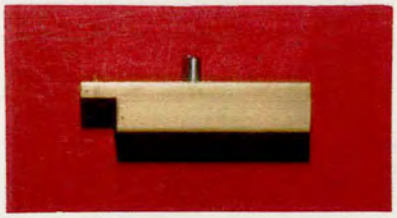
(d)

Fig. 3.2.2.-A: The Mark I HTEC: (a) technical drawing; (b) assembled cell - side elevation; (c) disassembled cell - plan view; (d) base plate - side elevation

To ensure, for the purposes of testing samples, that the helmet was air-tight, it was sealed using a rubber O-ring against a flat CaF_2 window (cover-glass). The effect of such cover-glasses on IR spectra has been studied by Kortüm and Oelkrug.[1] They measured the reflectance of Cr_2O_3 diluted with CaF_2 or MgO against MgO as standard, at various wavelengths, at various degrees of dilution and with directionally incident radiation ($\alpha = 45^{O}$); the same samples were used once with and once without quartz cover plates. There results showed that, whilst cover plates undoubtedly reduce the reflectance of the sample, the position of the maxima was maintained. Thus, the use over cover-glasses to exclude air was acceptable within the design criteria.

In summary, compared to the previous SpectraTech design, IR spectra were obtained much more rapidly, and the likelihood of wasting time on unsuitable samples was much diminished.

However, the design presented its own limitations:

1. The sample could not be heated;
2. The sample temperature could not be measured *in situ*;
3. There were problems with the sample lying so close to the position of the O-ring, since it was easy to spill sample onto it. Thus, the O-ring had to be cleaned frequently, since any sample on the O-ring adversely affected the seal, leading to the possibility of air contamination.
4. The internal gas environment could not be varied, i.e., there was no gas supply.

Some of these problems were addressed in the design of the Mk 2 HTEC, in which the improvements made in the Mk 1 HTEC design were integrated with the heating and water-cooling features of the SpectraTech design. The original SpectraTech water-cooled helmet was used in conjunction with further design modifications in

1) G. Kortüm and D. Oelkrug, *Naturwiss.*, 1966, **53**, 600.

order to minimize the amount of design and construction work necessary to provide coolant to the HTEC.

Mark 2 HTEC

The Mark 2 HTEC had the same successful detachable base as the Mark 1 design, but the screw-down assembly was replaced with a brass sample cup to be used under the original HTEC helmet. This helmet was water-cooled and sealed via an O-ring located on the base-plate. The Mk2 sample cup had a smaller diameter and greater depth sample cup. This cup was surrounded by sloping walls, resulting in easier sample loading with fewer spillages. Any spillages that did occur tended to stick to the sloping cup wall before reaching the O-ring below.

The advantages of this design over the Mark 1 were the greater ease of filling the sample cup, without fear of spillage onto a sealant O-ring. It was therefore decided to use this sample cup design, with the facility to perform flowing gas experiments, as the next stage in the design process.

Mark 3 HTEC

The Mk 2 version was modified to allow control over the sample's environment. A diagram and photograph of this design is provided in Fig. 3.2.2-B. Gas flowed in through the hole in the body of the sample cup into the space above the sample. It then flowed *through* the sample, and the sintered glass frit beneath, into the exit tube through the body of the sample cup, and then out through the baseplate.

The other advance made in the design of this model was that, unlike the original SpectraTech system, the one-eighth inch 'Swagelok' fittings (the gas inlets and outlets) were connected directly to the baseplate. The purpose of this modification was, once again, to reduce the size of the part of the system to be manipulated inside the glove box. The part is isolated at these fittings by the use of 2 end-caps. Previously the piping had protruded for *ca.* 15 cm from the fittings, making the piece more difficult to handle inside the glove box.

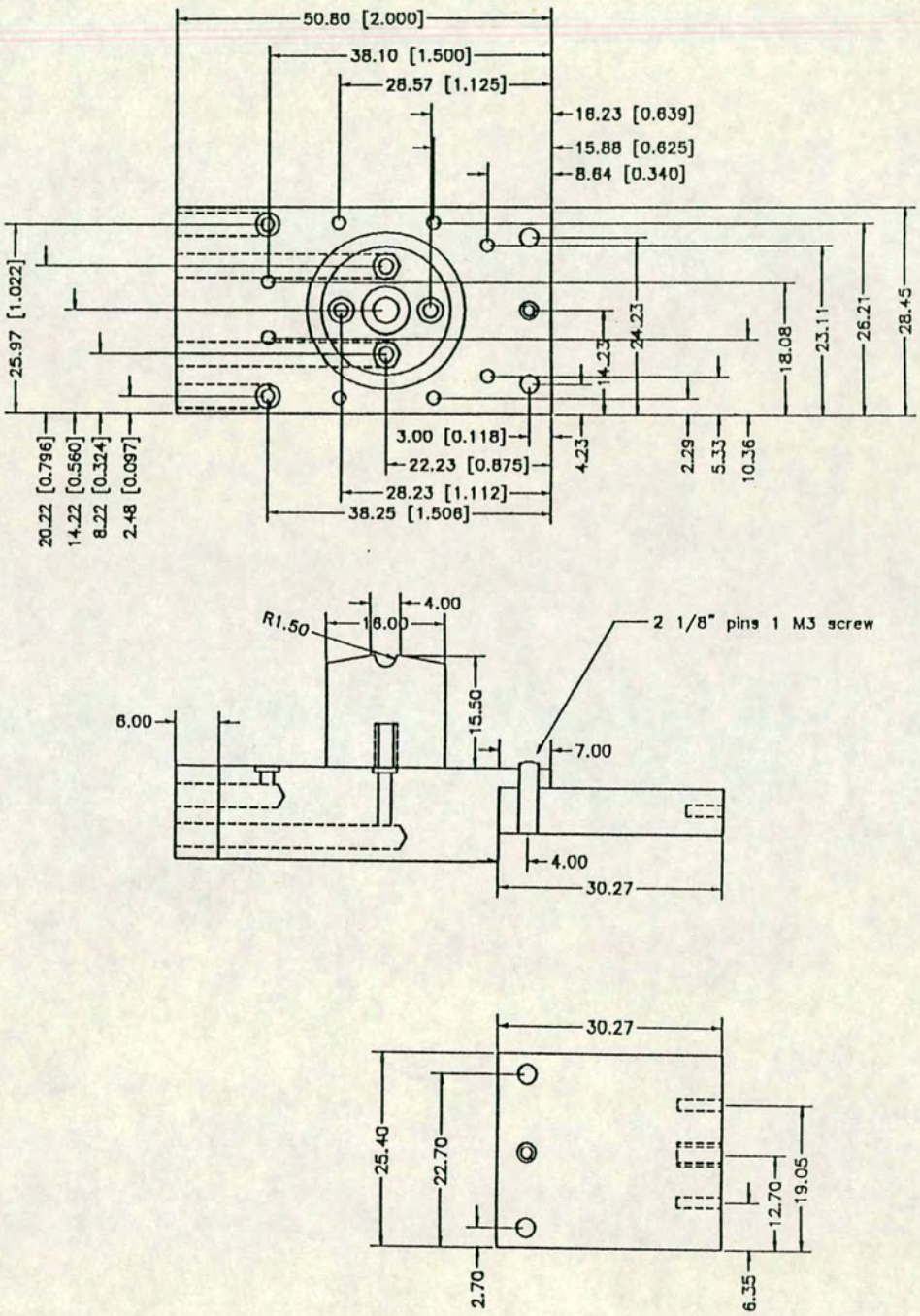

Fig. 3.2.2. -B(a): Mark III HTEC technical drawing, dimensions in mm (inches in brackets)

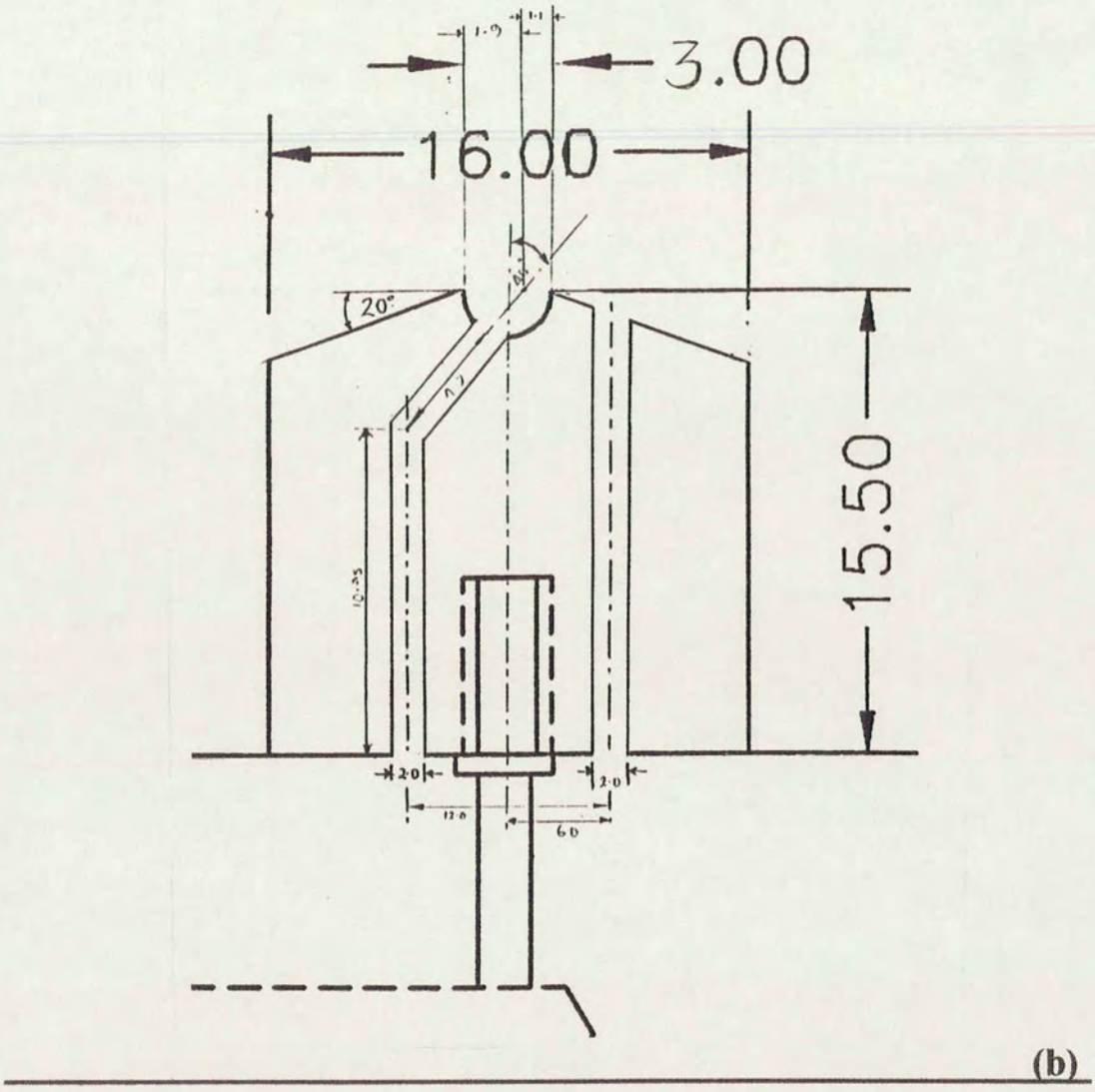

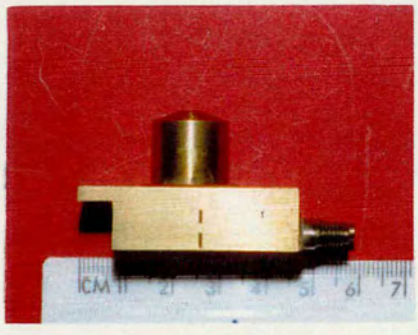

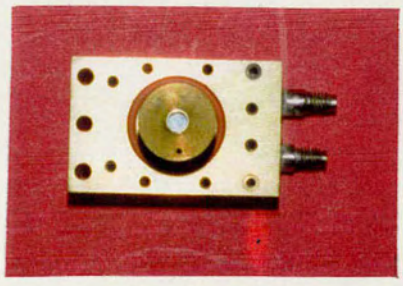

Fig. 3.2.2.-B: The Mark III HTEC: (b) technical drawing - close-up of brass sample holder, dimensions in mm; (c) assembled cell - side elevation; (d) assembled cell - plan view

There were found to be two main drawbacks to the Mk 3 design:

1) If the positioning of the cup was slightly wrong, then the spectra became very poor due to the brass sides of the cup giving a stronger signal than the sample.
2) The main design feature still missing was the facility for variable temperature work.

Mark 4 HTEC

See Fig. 3.2.2-C. This model has most of the operational capabilities found in the original SpectraTech system. The modifications over the Mark 3 version, and their functions, were as follows:

1. A wider sample cup was used, to prevent the problems of reflections from the brass experienced in Mark 3. (Cup dimensions: diameter 10 mm, depth 1.5 mm c.f. that of Mark 3: diameter 2 mm, depth 1.5 mm)
2. A cylindrical, internal cavity in the sample cup holder, designed to allow the insertion of a heater.
3. A thermocouple was now mounted.
4. Gas lines in and out were attached, with the gas now flowing across the surface of the sample rather than through it, as in previous models.
5. Water lines were now fitted to the water-cooled helmet, so that when the heater was fitted, the O-rings did not overheat.
6. A heater was constructed by winding 13 turns of 0.25 mm diameter nichrome resistance wire (3.7 ohm mm^{-1}) around a machined Makor cylinder of diameter 5 mm and height 12 mm. This heater was placed in the heater cavity and the dead space was filled with quartz wool. The heater cavity can be seen in Fig. 3.2.2-C(c).

Although this design had, theoretically, all the design features required, there were a number of unforeseen problems in its operation:

- Firstly, too large a cooling load was required from the water supply; the O-rings could not be kept at a low enough temperature to prevent damage. This was due to the metal sample cup conducting heat from the heater coil into the base plate and, hence, to the O-rings. The O-rings were observed to begin to volatilize when the sample was at *ca.* 300°C.
- The gas inlet and outlet lines interfered with the positioning of the mirrors of the DRIFTS collector which are located slightly below and on either side of the sample holder. This made alignment difficult.
- There was a large dead space above the sample. This would cause a number of problems: firstly, there would be stagnation points within this dead space, which would lead to the retention of gaseous decomposition products, thereby causing the wrong decomposition temperature to be recorded; secondly, the flow was not well characterised.

To address these problems, the solutions proposed were as follows:

- To reduce heat loss the cup was to be constructed of a ceramic material
- All lines in and out of the cup were to be attached at the front of the baseplate (this made handling easier too)
- To design the cup to fill as much of the helmet as possible.

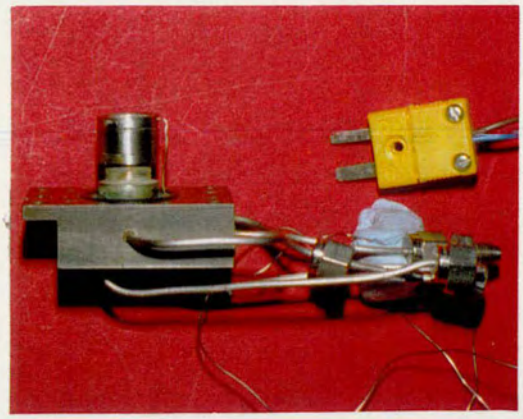

(a)

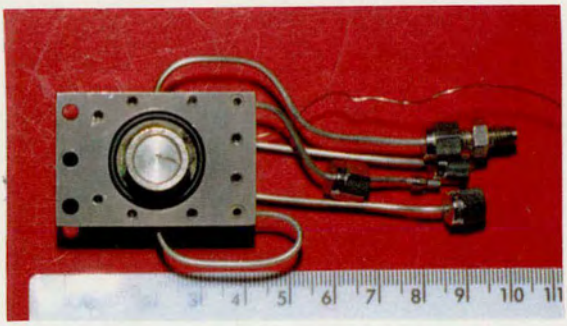

(b)

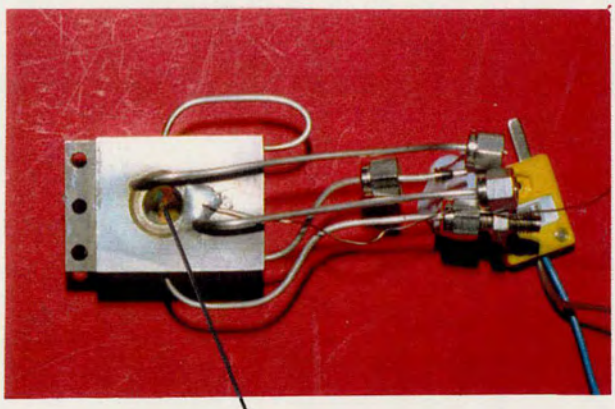

(c)

Fig. 3.2.2.-C: The Mark 4 HTEC technical drawing: (a) assembled cell - side elevation; (b) assembled cell - plan view; (c) assembled cell - plan view from below showing heater cavity

Mark 5 HTEC

(a) The first version of this design had the following features:

- A ceramic cup, constructed of a proprietary material known as 'Makor'. There was approximately 1 mm clearance between the cup and helmet. The gas flow in and out was now via deep grooves (1 mm deep and 2 mm wide) set into opposing sides of the cup, causing the gas to flow across the sample, with an improved, although still far from ideal, characterisation of flow.
- The thermocouple was held in position by a similar groove, although this was air-tight at the base (the thermocouple was soldered into position on the underside of the baseplate). The thermocouple's groove was at 90° to the other two, and the tip of the thermocouple was in contact with the sample at the centre of the bed.
- The same heating system as Mark 4 was used, which was plugged in place using quartz wool.

This design was beset by heating problems. These stemmed from the fact that the Makor has a much lower thermal conductivity than the previously used metal sample cup. This resulted in much higher temperatures required within the heater cavity, in order to raise the sample temperature to similar values obtained with the Mk 4 version. This required more power input to the heater resulting in the heater leads becoming red hot just to get the sample to 250°C. This caused concern due to the possibility of the red hot leads damaging nearby parts of the apparatus, and that the IR radiation from the red-hot wires may interfere with the IR beam signal.

It was decided to make two modifications:

1. To manufacture a heater which fitted into the cavity more closely, thereby maximising thermal contact between it and the cavity wall. This would lead to lower temperatures inside the cavity due to less heat being lost and, therefore, to lower power requirements.
2. To fill the end of the ceramic cup with ceramic filler, rather than with the quartz wool. This was intended to prevent stray radiation being emitted from the heater into the DRIFTS mirror system.

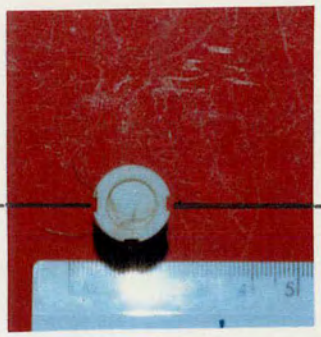

Fig. 3.2.2 -D The Mark 5 HTEC "Makor" sample cup: (i) side view. (ii) plan view. (iii) reverse plan view

The resulting design (see Fig. 3.2.2-D) achieved the desired results of cutting out stray IR radiation and lowering power input. Unfortunately, the ceramic filler had a greater rate of thermal expansion than the sample cup and caused the ceramic cup to crack apart on heating the sample to above 300^{O}C. It was decided to use a commercial cartridge heater instead, and to modify the heater cavity accordingly, with a small gap for expansion of the heater. This would negate the need for ceramic filler.

Mark 6 HTEC

This was the final version used in this research. A diagram and photograph are provided in Fig. 3.2.2-E. In summary, the main advantages of this final design were:

1. Easy loading and manipulation in the glove box.
2. Easy and quick loading into the DRIFTS sample holder, without needing to realign and clean mirrors each time.
3. Attainment of high temperatures (up to 500°C) reliably.
4. It generated good quality spectra, repeatably.

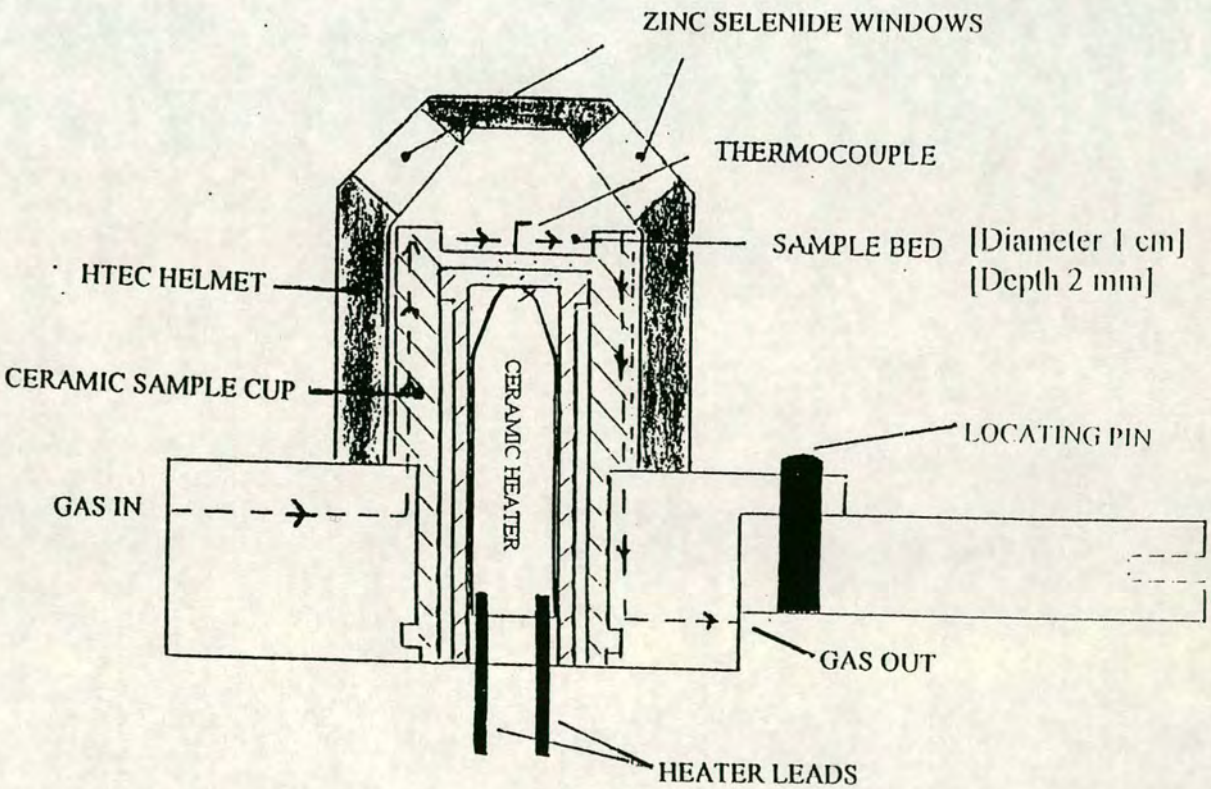

Fig. 3.2.2 -E(a) Schematic representation of the Mark 6 HTEC

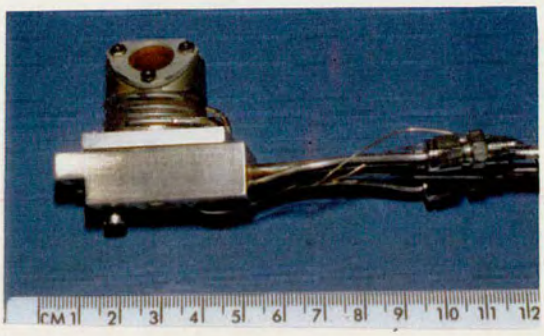

(b)

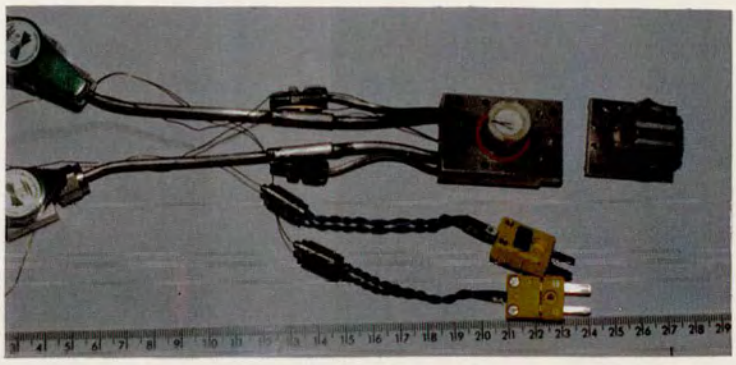

(c)

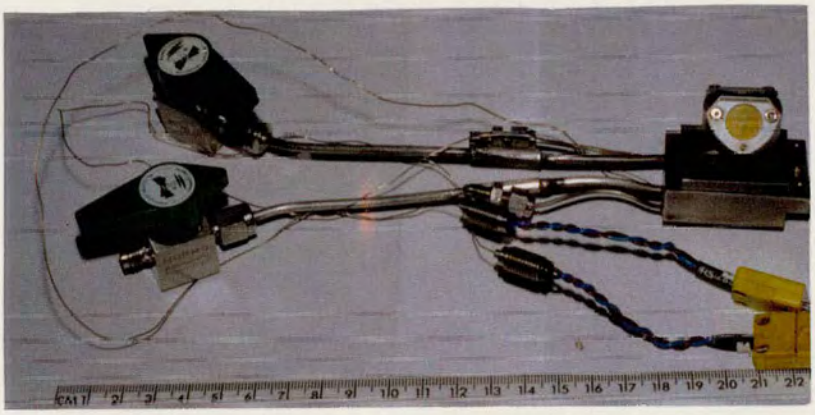

(d)

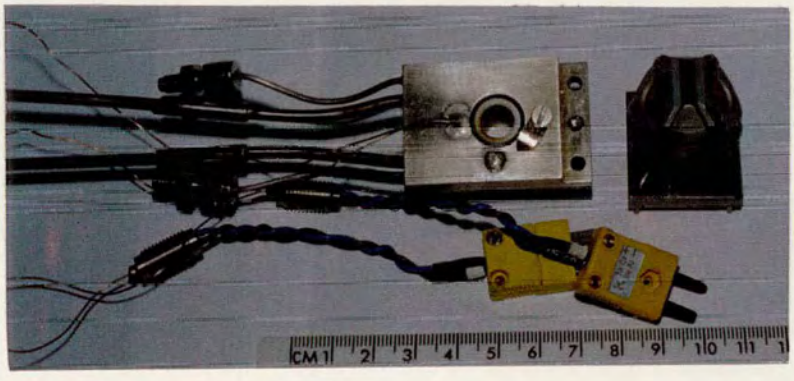

(e)

Fig. 3.2.2 -E Schematic representation of the Mark 6 HTEC: (b) side view; (c) plan view (helmet removed); (d) orthogonal view (helmet replaced); (e) reverse plan view (helmet removed)

3.2.2(ii) Investigation of Sample Temperature Measurement Using Thermocouples

During use of the Mk 6 HTEC another problem was detected which is addressed in the following section.

Tests on decomposition temperatures of known materials using the Mk 6 apparatus indicated discrepancies between those temperatures observed and quoted values.[2] Samples of hydrozincite were used, for which decomposition starts at about 240°C and ends at about 280°C. Sohail[3] observed that hydrozincite is completely converted to ZnO in one hour at 250°C and in 0.5 hours when held at 300°C. With the Mk 6 HTEC measuring 350°C no decomposition was observed, even after several hours heating. It was subsequently observed that small movements in the position of the thermocouple led to large changes in measured temperature. To establish the extent of this thermal variation the Mk 6 HTEC was modified to carry two thermocouples, one at the bottom of the sample bed, T_A, the other at the surface, T_B, with its tip just immersed in the sample, to avoid radiative heating from the IR beam.

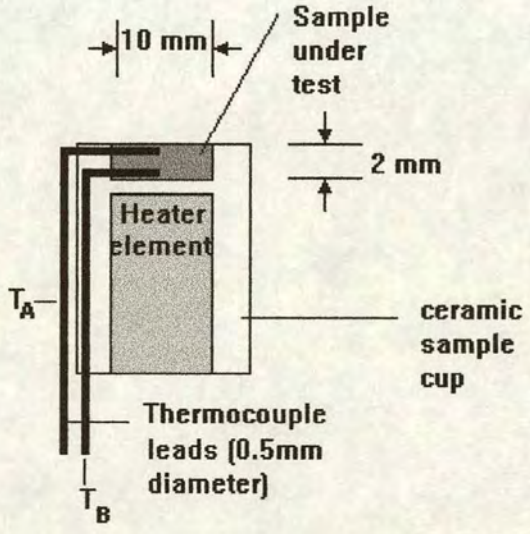

Figure 3.2.2-A DRIFTS cell set up to measure thermal gradient across sample bed

2) A. M. Khalil and S. Kolboe, "Surface Characterization of Some Selected Zinc Oxide Samples. IV Zinc Oxide Prepared by the Thermal Decomposition of Zinc Basic Carbonate", *Surf. Tech.*, 1983, **18**,249-262.

3) K. Sohail, Ph.D. Thesis, Dept. Of Chemical Engineering, University of Edinburgh, 1992.

The results of this investigation, which are plotted in Fig. 3.2.2-G, show how the recorded temperature varied for a given heater output with position of the thermocouple, for the two different thermocouple positions.

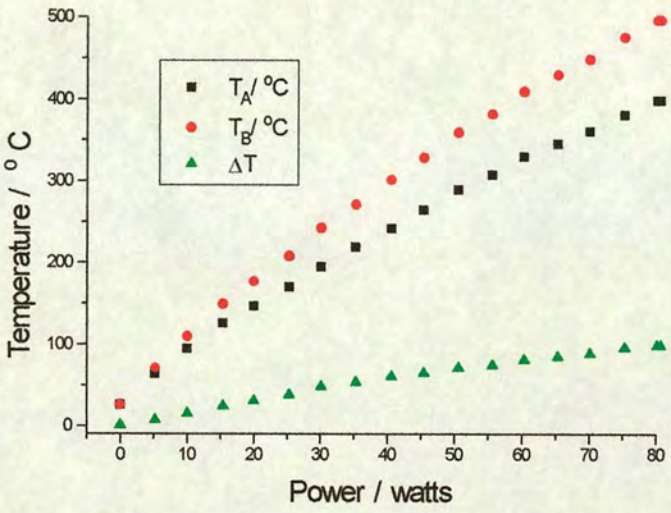

Figure 3.2.2-G Results of temperature measurement at different locations in Mk 6 HTEC

The sample used was hydrozincite. The helmet was flushed with bone-dry nitrogen (passed through an activated ZnO bed). The system was allowed to reach thermal equilibrium before the first readings were taken.

Clearly, the temperature differential is significant. In the kinetic experiments to be conducted as part of this on-going research, the temperature measurement is critical. In general, at least 1°C control is required for kinetic measurements at high temperatures, although 0.1°C is desirable. Further degrees of accuracy, e.g., to 0.01°C, would still reap rewards. The following table, 3.2.2-A, illustrates this point.

For a reaction with an activation energy of 150 kJ, there is nearly a 20 % change in the rate for every degree at 298 K, and approximately a 5 % change for every degree at 623 K.

Ratio of rate constants ($k_T/k_{(T+1)}$)			
	Activation Energy, E_A		
Temperature (K)	**80 kJ**	**100 kJ**	**150 kJ**
298	0.897	0.873	0.816
373	0.933	0.917	0.878
623	0.975	0.969	0.954

Table 3.2.2-A Comparison of change in rate constant for small variations in reaction temperature

It is difficult to conceive of a design of cup in which such a temperature differential could be avoided, particularly in light of the fact that Kubelka-Munk spectra require a certain bed depth and, in the range used here, tend to improve with increasing bed depth. Hence, consideration was made of alternative means of temperature measurement.

One method by which the correct surface temperature could be measured is infra-red thermometry. It is, after all, the surface that is of principal interest, and it is this part of the material that an infrared thermometer would detect the temperature from. There are other advantages to the IR method (see section 2.0.3) as well, particularly the fact that it does not rely on the contact between the sample and the thermometric device, thus decreasing the amount of design and machining required to produce the HTEC.

Using Non-Contact Radiation-Temperature Sensors

Infrared thermometers are radiometers which deduce the temperature of a target using the Planck function in conjunction with *a priori* assumptions. High accuracy at low temperatures is very difficult to achieve ('low' temperatures being typically those below 300^0C). Some of the problems relate to instrument design whilst others are more fundamental. An appreciation of these difficulties is essential in order that the best apparatus may be selected for the required task and in terms of "manipulating" the measurement to maximise the achievable precision. However, these devices have found application in kinetic studies.

Qin and Wolf[4] used infrared thermography to visualize the spatiotemporal oscillations on a Rh/SiO_2 washcoat catalyst supported on an aluminium disk. They used an Agema 782 thermal imager (quite an old instrument; available in both short wavelength, 3-5 μ, and long wavelength, 8-14μ versions). The paper did not state which version was used, nor did it report emissivity values, background temperature etc. Assuming that the experiments were reasonably sensible, that the target emissivity was known and that the instrument calibration was good to a couple of percent (these instruments are poor in terms of absolute calibration, but good at detecting temperature differences), then the temperatures should be accurate to ± $5^{O}C$. On the other hand, the temperature differentials, i.e., the "patterns" (which were of more interest in this instant) were probably quite reliable.

To examine the reliability and facility of infrared thermometry in measuring sample surface temperatures within the HTEC a Raytek[5] Raynger ST2 hand-held thermometer was tested. This instrument reads temperatures over the range -$18^{O}C$ to $400^{O}C$ with an accuracy of ± 2% of reading or ± $2^{O}C$, whichever is greater, at 18-$28^{O}C$ ambient temperature. Whilst not particularly accurate, if such accuracy could be achieved it would be a vast improvement over the current Mk 6 version. The maximum ambient working temperature was $50^{O}C$ for this model. The minimum spot-size was 20 mm diameter at 150 mm distance from target and 125 mm at 1 m from target. The spectral response was 7-18 μm, using a thermopile detector.

Firstly, as a test model, hydrozincite was used in order to establish its emissivity. The most reliable technique for determining emissivity utilises simultaneous, independent reading of temperature by thermocouple or similar device. The radiation emissivity dial is adjusted until the two temperatures agree. If there are no changes in conditions, this emissivity setting can be used for any future temperature measurements without the need of the thermocouple. Since emissivity can vary with

---

4) F. Qin and E. E. Wolf, "Infrared Thermography and Fourier Transform Infrared Spectroscopic Study of CO Oxidation over a Catalyst Washcoat Supported on a Metal Substrate", *Ind. Eng. Chem. Res.*, 1995, **34**, 2923-2930.

5) Raytek (UK), PO Box 120, Milton Keynes, Bucks. MK1 1ZU, UK. Tel: (+44 1908) 63 08 00.

temperature, such calibration may be necessary over the desired temperature range. In such a case leaving the ε setting fixed and producing a table of indicated versus true temperatures would be more useful for correction purposes.

Thus, a hydrozincite sample, set in 10 cm square container of 1 cm depth, was heated in a fan-assisted, thermostatically-controlled oven. Inside the oven it was heated from 25^{O}C to 365^{O}C and then allowed to cool back to 25 ^{O}C. The emissivity setting was altered at various temperatures as required, to cause the thermocouple-measured temperature to correlate with the infrared thermometer-measured temperature. It was found that the emissivity values on cooling were higher than those obtained at the same temperature on heating (pseudo-hysteresis). This is probably due to structural changes in the material on heating, decomposition of the material and, possibly, sintering affects. Various other experiments were conducted to try and establish a definitive standard by which the infrared thermometer could be calibrated. Attempts with heated brass or aluminium plates resulted in sinusoidal variation of emissivity values with increasing temperature. Similar results were obtained by Worner *et al.*[6] for iron surfaces. They found that bright metals, in general, oxidise on heating to build up surface oxide layers at ¼, ½, ¾ and 1λ values of the infrared thermometer scanning wavelength. This causes emissivity values to vary sinusoidally until the oxide layer is stabilized.

The brass and aluminium plates were observed to alter in lustre and colour on heating and cooling. After several heating and cooling cycles both metals began to remain constant in their appearance and also provided repeatable emissivity readings for the recorded temperatures.

This was repeated with the hydrozincite sample, which was cycled to 400^{O}C three times. Each time the emissivity values did not replicate one another. From this it was inferred that the emissivity values are sensitive to sample packing and that

---

6) B. Worner, G. Neuer and F. Güntert, Institut für Kernenergetik und Energiesysteme der Universitat Stuttgart, PRG, Emittance Measurements on Oxidising Metals and Application of the Results at Hot Rolling of Steel. In-house publication.

sample sintering must be responsible for this discrepancy. Subsequent heating, cooling cycles yielded repeatable data, suggesting that the sample morphology had stabilized.

Translating these observations to the measurement of samples of unknown materials within the HTEC leads to the following concerns. There would be no way of knowing, *a* prior, what ε setting would be required for a given sample, nor how this value might change on heating the sample.

Additionally, ensuring that the target sample area fully occupied the spot size of the infrared thermometer would also be problematic. This essential procedure was particularly difficult where hot samples (> 200^{O}C) were tested, since the infrared thermometer had to be sufficiently close to generate a small spot size but sufficiently removed from the hot sample to prevent thermal effects which would distort the temperature readings and possibly damage the infrared thermometer.

It is probable that a different infrared thermometer, such as the Raytek M4, would provide far more dependable and accurate results. This is a single spot instrument with a short operating wavelength. The beam path is sufficiently narrow to fit through the HTEC window, whilst being far enough removed so as not to be influenced by local temperature. However, this would require large capital investment without guaranteed performance.

Use of the HTEC also introduces a ZnSe window into the beam path of the infrared thermometer. The effect of the ZnSe window material is predictable and can be calibrated out (provided the window stays clean). However, guaranteeing that the window remains clean whilst running experiments where, for example, H_2O, CO_2 and H_2S may be generated or passed over the sample, would be a difficult exercise.

Conclusions

For the current purposes a portable infrared thermometer is far less reliable than the thermocouples used in the Mk 6 HTEC for determining the sample surface temperature. There is no guarantee that the surface temperature measured would be remotely close to the actual sample temperature when using anything less than well characterised materials. This would require much pre-evaluation of samples to establish ε values prior to IR study. This would be unfavourable due to the great increase in time requirements measuring ε values and in producing the extra sample needed (far greater volumes would be required than normally produced in a single hydrolysis experiment).

Future work

In light of the above, an alternative solution was sought to the problem of accurate temperature measurement within the HTEC. The next stage of development was to preheat the incoming gas stream to the same temperature as the sample bed. This would have the advantage of creating a near isothermal environment in which the position of the thermocouple within the sample bed should not affect the measured temperature. The major disadvantage of this set-up is that the cell windows could not be kept cool enough to prevent damage to the O-rings on which they are seated. The same problem affected the O-rings used in the baseplate of the HTEC. To circumvent these problems a system must be devised which does not rely upon O-rings to seal this system off from ambient gases. This development (Mk 7 HTEC) is currently in progress within this group's research programme.

For the purposes of the current research work the thermocouple lead was immersed *ca.* 0.5 mm below the sample surface. Whilst this arrangement meant that the exact surface temperature was not being measured it did allow for the sample shrinkage which occurred on heating. If the thermocouple was placed higher in the sample bed then it sometimes became exposed if sample shrinking occurred. This exposed it to the flushing gas which caused the temperature to drop a good deal below the actual temperature of the surface. This arrangement was essentially a trade-off between the two situations, neither of which was ideal.

3.2.2(iii) Development of simultaneous DRIFTS gas detection system: The Mk 2 collector

As part of the on-going improvements in the capabilities of the apparatus the ability to detect gas phase species during the analysis of solid samples was highly desirable. Ultimately, the system should have a computer controlled mirror system to switch between analysis of the solid and the gas phase at will.

The first working example of such a set up is shown in Fig. 3.2.2-H below. The system comprises the Mk 6 HTEC and DRIFTS collector system. The collector was modified to carry a set of guide channels on which a second mirror system, Fig. 3.2.2-H(a), could be inserted. This second mirror system was designed to divert the IR beam away from the solid sample and into a gas cell, Fig. 3.2.2-H(b). The gas cell then sat in the collector on a purpose built support, see Fig. 3.2.2-H(c). The second mirror system was attached to an arm (not shown) by which it could be slid into and out of the IR beam. Fig 3.2.2-H(d) shows the second mirror system placed in the 'in' position whereby the IR beam would be diverted through the gas cell.

The system was tested by decomposing $Zn_5(CO_3)_2(OH)_6$ and observing the evolution of H_2O and CO_2 in the gas phase.

Conclusions

This system proved to be an effective manually operated device for the near-simultaneous observation of related solid and gas phase phenomena within the HTEC environment.

Future work

The system could be automated by replacing the guide channels with a rack and pinion system for the second mirror system to slide into the collector. The movement of the second mirror system would be controlled by small, computer activated motors either side of the collector unit.

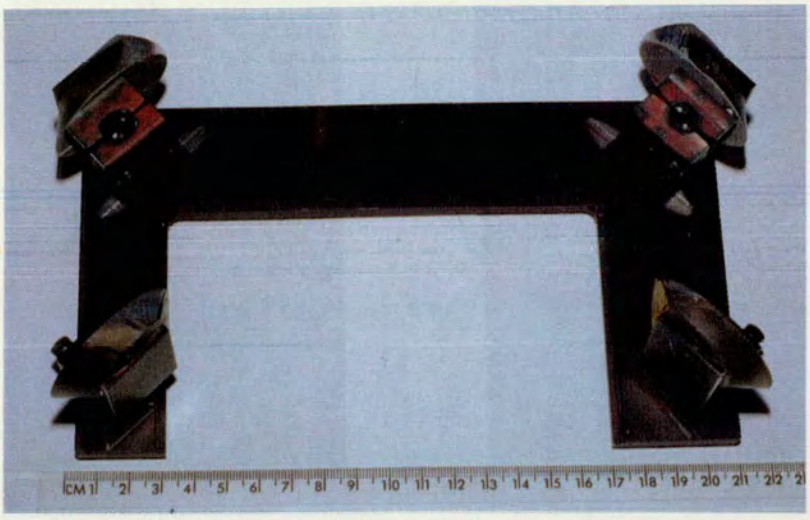

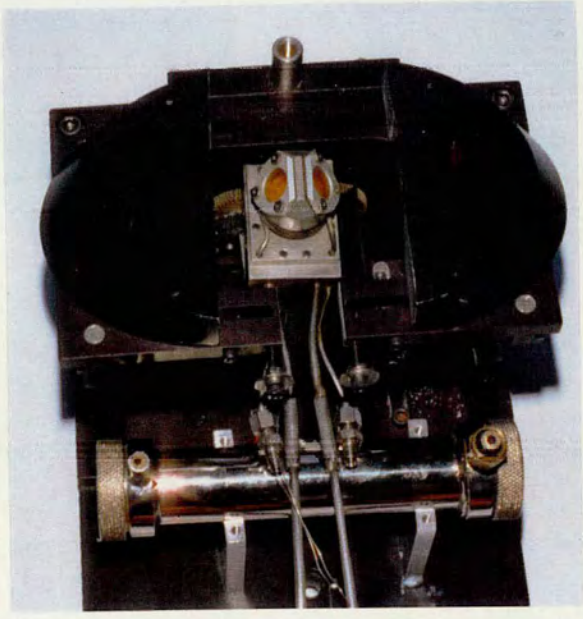

Fig. 3.2.2.-H: The Mark 2 collector system for simultaneous detection of gas phase materials: (a) sliding mirror system to divert IR beam away from HTEC and into gas cell; (b) gas cell; (c) Mk 2 collector with gas cell in place

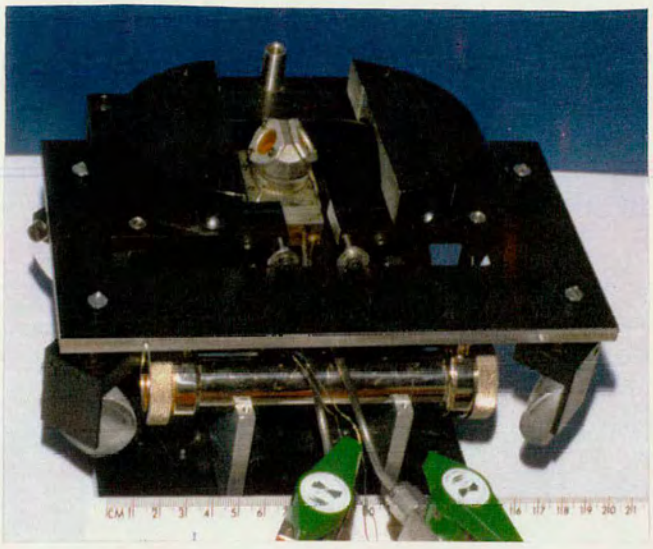

(d)

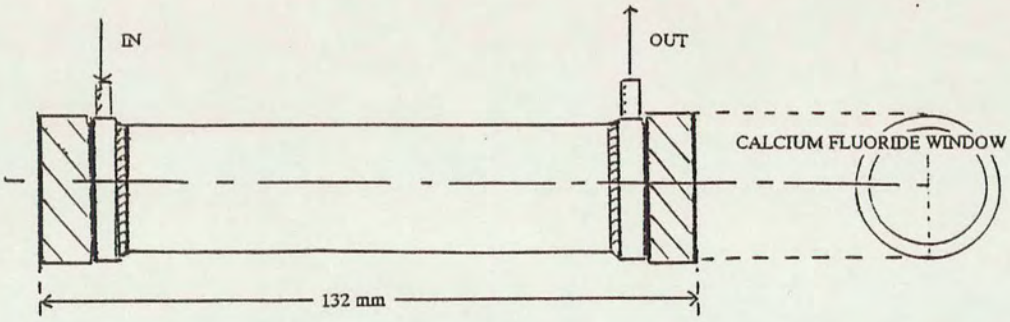

(e)

Fig3.2.2-H: The Mk 2 collector system: (d) Mk 2 collector with gas cell and mirrors system in place. (e) schematic representation of gas cell

3.2.3 Hydrolysis Apparatus

Having established methods and apparatus to handle air-sensitive materials and record their infrared spectrum, the final requirement was for an air-free method to hydrolyse the precursors that have been synthesised. Principally, two methods were used. These are described below.

3.2.3(i) Centrifuge Tube and Glove Box

In this method a sample of the precursor (usually $Zn_4O(OAc)_6$) was loaded into the glove box. This had been previously stored, under nitrogen, in sample vials sealed with 'Nesco' film. The sample was ground using an agate mortar and pestle within the glove box. The powdered precursor was then transferred to a centrifuge tube. Degassed water (*ca.* 30 ml.) was added to the precursor from the external water degassing bulb (as described in 3.2.1). The lid of the centrifuge tube was fastened and the sample shaken vigorously for *ca.* 5 minutes. This was allowed to stand for 15 minutes and then shaken for a further 5 minutes. This was repeated until all the precursor had been hydrolysed. For $Zn_4O(OAc)_6$ this was taken to be complete when only floating, white, gelatinous material was present above the water layer. This took up to 4 hours for $Zn_4O(OAc)_6$ samples.

The centrifuge tube was then sealed with 'Nesco' film and placed inside its air-tight centrifuge tube holder. This was then removed from the glove box and centrifuged for 5 minutes to separate the hydrolysate from the water. The centrifuge tube and holder were then reloaded into the glove box. The water was then removed from the mixture using suction through the second liquid line running into the glove box (this line was also used to deliver solvents). The damp cake was then submersed with a further *ca.* 30 ml. portion of distilled water and the above procedure repeated. The whole cycle was repeated three or four times to completely wash the hydrolysate. The final damp cake in the centrifuge tube, within the glove box, under nitrogen, was then placed inside the purpose-built large Schlenk tubes, for drying (see Fig. 3.2.3-A). Two of these drying tubes were constructed, one with a B34 socket and cone fitting, the other with a B50 socket and cone fitting, each fitted with Teflon sleeves.

the one that gave the lower dead-space when the container of hydrolysate was placed inside it.

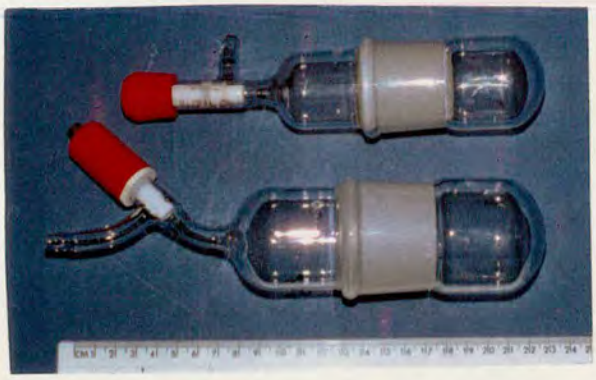

Figure 3.2.3-A Oversized Schlenk tubes: upper tube has B34 cone and socket, lower tube has B50 cone and socket

The hydrolysate, inside the open centrifuge tube, was sealed inside the drying tube, which, in turn, was sealed. All of these operations were performed within the glove box, under a nitrogen atmosphere. The Schlenk tube was then removed from the glove box and attached to a vacuum line and pumped down overnight to dry the sample. The dried sample, in the sealed sample tube, was then reloaded into the glove box, where it was removed from the drying tube and scraped out of the centrifuge tube into the HTEC, ready for DRIFTS analysis.

This method occasionally provided samples with surfaces free of carbonate frequencies (i.e. they had not been exposed to *any* CO_2). However, the routine was not sufficiently rigorous to repeatably exclude ambient air. This could be observed by the fact that, frequently, hydrolysate samples were observed, by DRIFTS, to be covered with surface carbonate species. To overcome this problem a more rigorous system of air exclusion was devised, as described below.

3.2.3 (ii) The Sealed Hydrolysis, Washing and Drying Unit (SHWADU)

The previous method used for hydrolysing zinc compounds by isolating the sample in a centrifuge tube was relatively quick, but did not yield repeatable results. After each washing, the sample was removed from the glove box in the centrifuge tube, centrifuged and returned to the glove box, requiring that the glove box be pumped down and refilled each time.

It would be preferable to develop a technique which absolutely guaranteed exclusion of carbon dioxide without constant opening and re-sealing of both centrifuge tube and glove box. The technique developed was the SHWADU.

The SHWADU technique is self-contained and does not require opening at any intermediate stage. Almost all of the handling can be performed outside the glove box.

SHWADU Mark 1

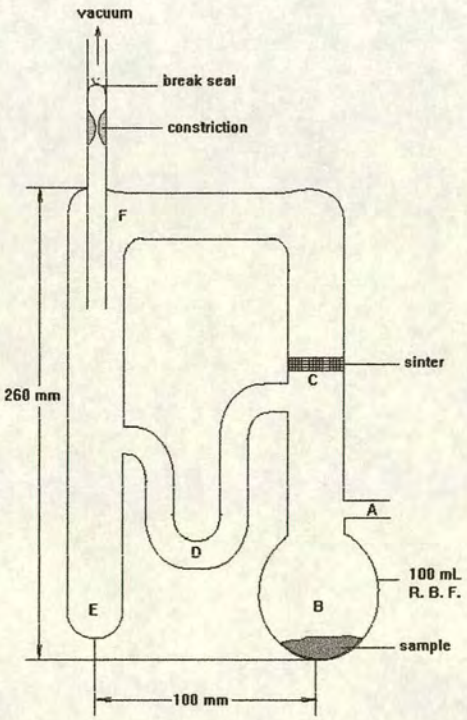

Figure 3.2.3-B Schematic representation of the SHWADU (sealed hydrolysis, washing and drying unit)

The procedure for its use was as follows:

1. The sample, in most cases (freshly opened and ground) $Zn_4O(OAc)_6$, was loaded through A into B, a round-bottomed flask.
2. A was then glass blown onto a glass vacuum line.
3. The SHWADU was then evacuated to 10^{-6} torr over the course of an hour.
4. The valve to the vacuum pump was then closed off. The valve to the bulb of pre-distilled water (distilled by undergoing a freeze-pump-thaw cycle three times) was then opened and the sample bulb (B) was immersed, slowly, in liquid nitrogen. This has the effect of drawing the water vapour into the sample bulb and onto the $Zn_4O(OAc)_6$.
5. The SHWADU was isolated by glass-blowing shut at A, leaving only the sample and the frozen water inside.
6. After removing the liquid nitrogen, the water thawed. The mixture of water and sample was then shaken vigorously to hydrolyse the $Zn_4O(OAc)_6$. The hydrolysis step took *ca.* 4 hours and was considered complete when there are two clearly defined layers. The top layer is the hydrolysate and is white and gelatinous, the lower layer being a solution of the $Zn(OAc)_2.2H_2O$.
7. The SHWADU was now tipped upside-down, such that the solids were captured by the filter, C, and the liquid (containing the dissolved $Zn(OAc)_2.2H_2O$) passed through it (some may be lost down the U-bend, D, but this was designed with the intention that material could be tipped back onto C).
8. The SHWADU was then rotated such that the liquid was trapped at E when it was tipped back. The net result of tipping the SHWADU back was that E contained a solution of $Zn(OAc)_2.2H_2O$ and B contained the filter cake from C, (the hydrolysate).
9. B was again immersed in liquid nitrogen. This has the effect of reducing the pressure, thereby causing water in E to evaporate, leaving behind a residue of $Zn(OAc)_2.2H_2O$ powder in E.
10. Steps 6 to 8 were repeated four times to wash the sample.
11. This entire operation took 8 - 10 hours. After the last washing, the water was distilled into E, by immersing it in liquid nitrogen.

12. The SHWADU was then evacuated via F. The tube was, firstly, glass-blown onto a vacuum line, then the seal was broken by releasing a metal 'slug' (using a magnet) down the tube at F. The water was then allowed to thaw or sublimed back into the vacuum line by use of a cold trap on the vacuum line. The whole system was evacuated. The result was that $Zn(OAc)_2.2H_2O$ powder was deposited in finger E and the hydrolysate in bulb B.
13. Before the SHWADU was placed in the glove box the surface was scratched, just above A. This enabled B to be broken off from the rest of the SHWADU inside the glove box, allowing the sample to be taken out of the bulb.
14. The SHWADU was put inside the glove box and the box filled with a nitrogen atmosphere. The hydrolysate-containing section was broken off. The sample was taken out and put into a DRIFTS cell for immediate analysis, and the remainder into vials, which were sealed air-tight with 'Nesco' film and kept for later use.

There were a number of problems with the operation of this device. The three main problems were as follows:

1. The U-tube between E and B was incorporated to ease the movement of the water vapour from E to B, in case the resistance due to the sinter was too great. It was a design fault in that, when the device was inverted to cause the mixture to move to C, some of it would go into this U-tube, and upon rotation move into E, rather than D as had been hoped. This led to a decrease in yield.
2. During distillation from E to B, bumping would occur (the rapid boiling of the water), and this would disperse the unevaporated portion of the solution around the device and back into B, thereby causing contamination and necessitating a time-consuming repetition of the washing stages. It seemed that, in this current design, bumping was unavoidable. All attempts to prevent it by keeping the distillation rate to a minimum were unsuccessful.
3. It was difficult to get all the $Zn_4O(OAc)_6$ to react, because the manner of mixing (shaking) was not very effective.

Numerous modifications were made to the device throughout a number of design stages. The final design ('Mark 7') is shown in Fig. 3.2.3-C. It was constructed from 20 mm internal diameter glass tubing, a 100 mL round-bottomed flask and side-arms of 10 mm internal diameter. Its use is illustrated in Fig. 3.2.3-C(c). The following advances in the design had been made:

- *No connecting U-tube.* It was found to be unnecessary for the return of water vapour to B. Also, it had been providing a route for the bumped solution back into B. In its absence, the route was much more difficult, requiring the solution to pass through the sinter (C).
- *Glass bead in round-bottomed flask.* This made agitation of the mixture much more effective and speeded up hydrolysis times two-fold.
- The receptacle for the solution, E, has been redesigned such that the bumped solution was no longer directed toward B.
- The effects of bumping were reduced by using optimal amounts of reagents. This optimum value, in practice, was found to be about 15 mL of water to 1g $Zn_4O(OAc)_6$. The main criterion was that there be just enough water for agitation to be effective (this was more than enough to dissolve the $Zn(OAc)_2$; 1g of $Zn_4O(OAc)_6$ was calculated to require 3mL of water to dissolve the $Zn(OAc)_2.2H_2O$ formed by its hydrolysis). The less water used, the less the effects of bumping were observed to be, but the more washing stages were required. The final value of 15mL was essentially a compromise between these two factors.

Contamination was now much less of a problem; normally all that was required was to tap the filter so that any powder would move back to E. The steps of its use are shown in Fig. 3.2.3-C(c).

1) The sample was loaded into bulb B via joint A using a pipette.

2) A was glass blown onto a vacuum line. 15mL of triply degassed water (by freeze/thaw process) was sublimed into B. Joint A was sealed off.

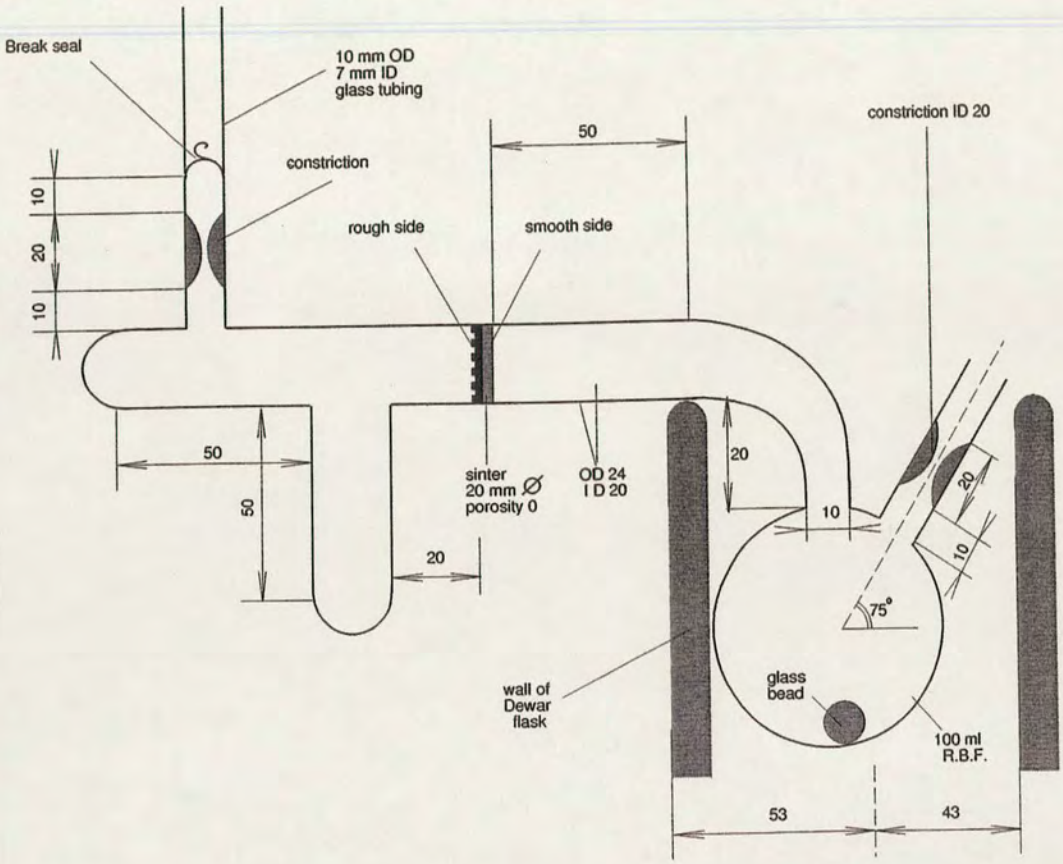

(a)

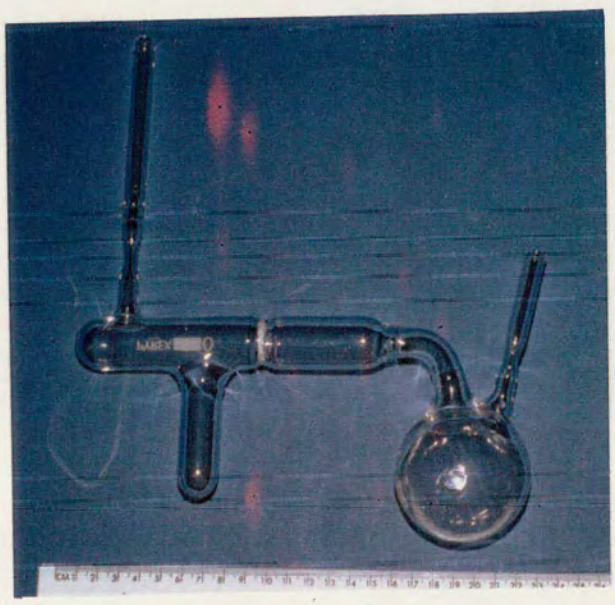

(b)

Fig. 3.2.3 -C The Mk 7 SHWADU: (a) Schematic representation of the Mk 7 SHWADU
(b) photograph of Mk 7 SHWADU

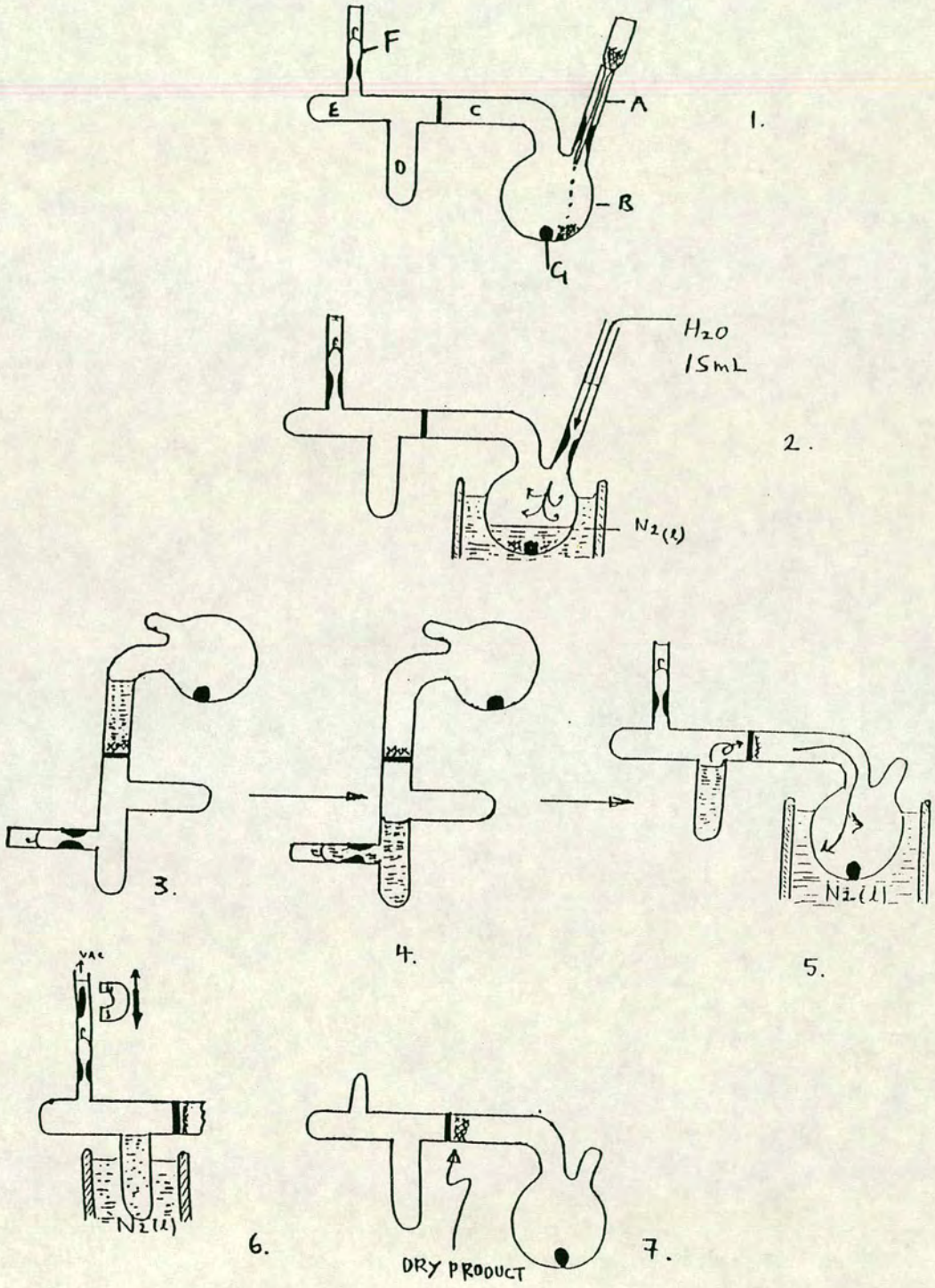

Fig. 3.2.3 -C (c) Sequence of operation of Mk 7SHWADU

3) The sample was shaken with the water and agitation was facilitated by the use of the glass bead G. The SHWADU was rotated anticlockwise 90^{O}.

4) The solution was allowed to pass into finger E. The SHWADU was rotated clockwise 90^{O} so that the solution passed into finger D.

5) The water was sublimed back into B leaving the solute behind in D and providing a clean sample of water with which to rewash the hydrolysate. This process (steps 3-5) was repeated at least three times to thoroughly wash the hydrolysate.

6) The water was sublimed into D. Joint F was glass blown onto a vacuum line with a metal slug in place. The break seal in joint F was broken.

7) The water was pumped off the system leaving the washed, dry hydrolysate cake on the sinter. From here it was loaded into the glove box and therein loaded into the Mk 6 HTEC.

The results from this set-up were found to be repeatable. Each experiment took *ca.* 24 hours in total (including 10-14 hours drying, usually overnight).

Conclusions

Using the Mk 7 SHWADU the hydrolysis, washing and drying of basic carboxylates was possible under stringent, air-free conditions, as required. Although very time-consuming, the method was virtually guaranteed to yield carbonate-free, highly reactive samples.

3.2.4 XRPD Air-Tight Sample Holder

In normal operation, X-ray powder samples are exposed to the atmosphere. This posed problems for the X-ray analysis of the type of materials used in this research. To overcome this, an air-tight sample holder was designed and constructed (see Fig. 3.2.4-A) such that it could be filled inside the glove box and transported to the X-ray machine without the sample being exposed to air. The sample-tray was held in position, within the unit by a locating 'pin' on its underside. The modifications made to ensure that the device was air-tight were:

- An O-ring seal in the main unit secured by a screw-top.
- X-ray-transparent film was secured in an air-tight fashion over the X-ray cavity.

(a)

(b)

Figure 3.2.4-A Air-tight XRPD sample holder: (a) holder disassembled showing screw top, base unit and sample tray (clockwise from centre left); (b) assembled unit

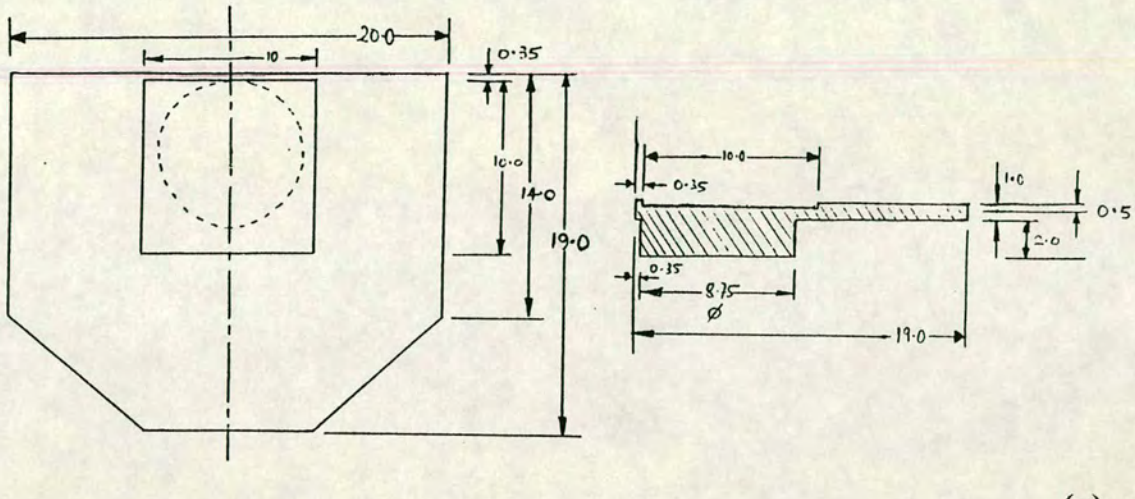

(c)

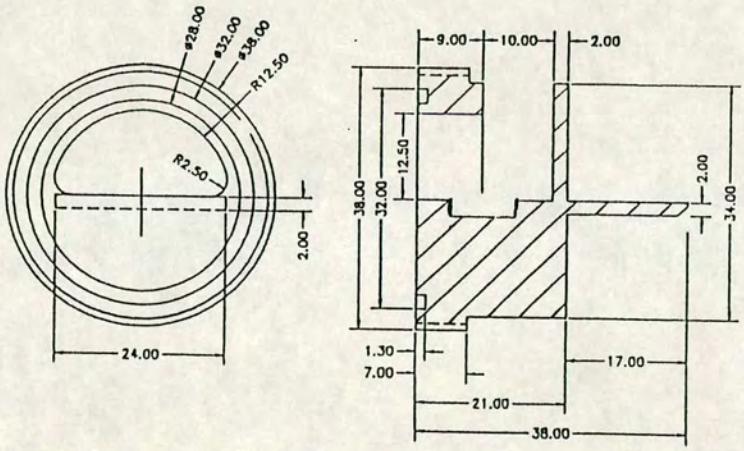

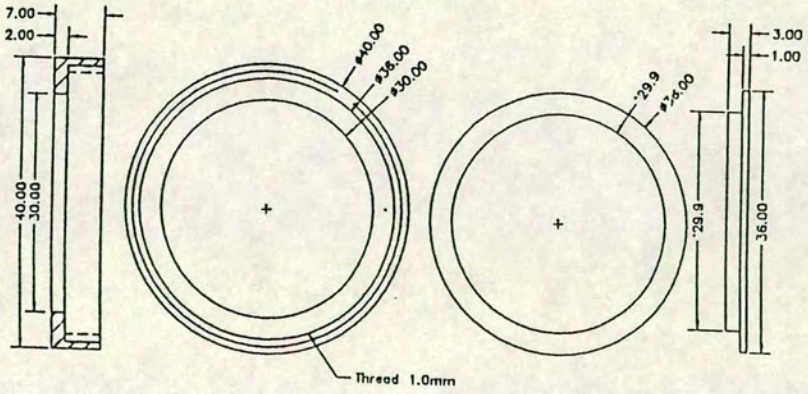

(d)

3.2.4 - A Technical drawing of the air-tight XRPD sample holder: (c): plan view and side elevation of sample tray; (d) plan view and side elevation of sample tray holder and screw-top lid.

3.2.5 Thin Film Deposition Apparatus

In further attempts to produce carbonate free ZnO or $Zn(OH)_2$ surfaces, amenable to DRIFTS study, the following approach was taken. An attempt was made to manufacture an evaporated thin film of zinc, thin enough to be IR radiation penetrable, on which the products of water oxidation could be formed and examined. The apparatus is shown in Fig. 3.2.5-A. The initial purpose at this stage was to evaluate whether an even film of zinc could be deposited upon an infrared-transparent window. Calculations were performed on the effect of temperature and pressure on the mean free path of zinc. Mean free paths were calculated using Eqn. 3.2.5-A:

$$\lambda = \frac{KT}{\sqrt{2}\sigma p} \qquad \text{Eqn. 3.2.5-A}^{1}$$

where λ is the mean free path, K, the Boltzmann constant, T, the temperature in K, p, the pressure and σ, the 'collision cross-section' ($-\pi d^2$–0.264 nm^2 for zinc). It was calculated that at 300°C zinc would have a mean free path of 8.26cm. Thus the apparatus was constructed such that the zinc source was less than 8cm from the CaF_2 window upon which the zinc vapour was to be deposited.

In the initial experiments, zinc wire was wound around a filament wire made of tungsten. The chamber was evacuated and a voltage put across the filament, causing it to heat up. If it reached a high enough temperature, the zinc in contact with it would melt and volatilize, and, ideally, uniformly coat the CaF_2 window, opposite the filament.

In the experiments conducted so far, results have been far from satisfactory. Early use of tungsten as the filament wire was to no avail, as the zinc was not volatilized. It was decided to try a platinum filament wire instead, and this led to better, but still, ultimately, unsatisfactory results. Use of the platinum wire *did* lead to zinc emission, but despite many variations in experimental variables, a thin, uniform coating could not be achieved. The best result achieved was a non-uniform, striated coating, in

1) P. W. Atkins, *Physical Chemistry*, 5th ed., Oxford University Press, Oxford, 1994, p. 38.

which the zinc layer varied between non-existent and too thick, and was therefore of no use.

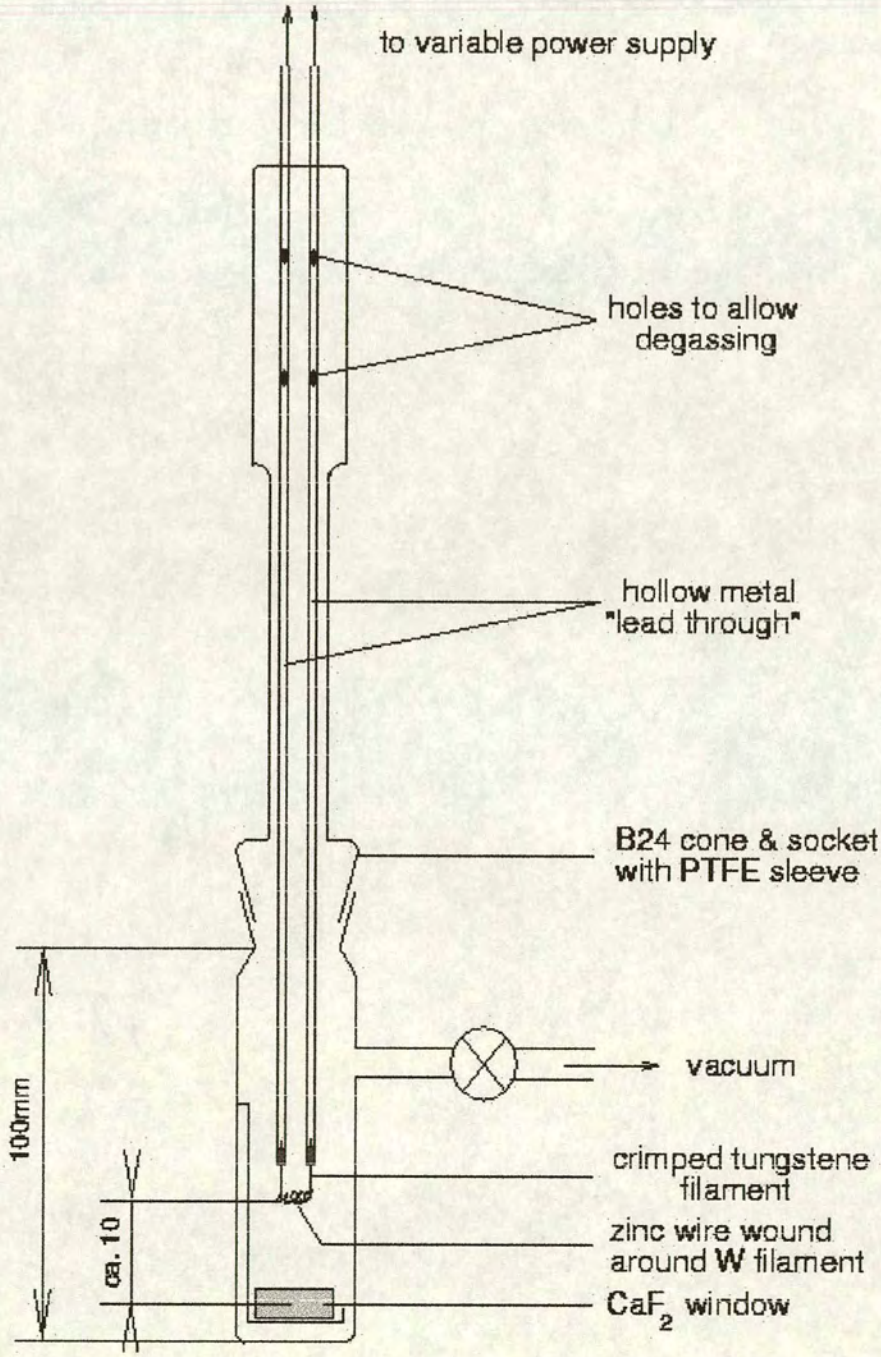

Figure 3.2.4-B Zinc film deposition apparatus

A possible avenue of advancement considered for this technique was to vary the window-filament distance. It was felt that greater distances may generate more uniform films, albeit more slowly. This theory was tested by heating zinc in an evacuated, enclosed glass tube (40cm long × 2cm diameter) inside a carbolite heater. It was found that thin films were deposited some 29 cm from the location of the zinc pellets, when a pressure of 10^{-5} torr was used. The films produced in this manner were far more even than had previously been obtained. It was also found to be possible to build them up very slowly and so control over film thickness was obtained, although no means of measuring this thickness was developed. Unfortunately, due to time constraints no further work was conducted in this area.

Conclusions

Some control over zinc film deposition had been obtained with the result that even, thin films of variable thickness could be achieved. No means of measuring film thickness was developed.

Future work

Firstly, the apparatus should be rebuilt with a greater path length (*ca.* 29cm for 10^{-5} torr operation) between the zinc source and the window upon which the zinc was deposited. To improve the quality of the deposited zinc film liquid nitrogen cooling of the CaF_2 window should be developed. Finally, a means by which resulting film thickness could be measured must be developed. With such a system the heating current and voltage settings for a given section of zinc wire used could be calibrated against resultant film thickness. This would allow films of a particular thickness to be grown in a repeatable fashion. The quality of the DRIFTS spectra for the water oxidation of these clean zinc film surfaces could then be related to known film thicknesses and the optimum thickness for these experiments established.

3.3 Preparation of Precursors

3.3.0 Reagents Used

Analar zinc oxide, zinc metal, granules and powder, copper acetate, dinitrogen tetroxide, glacial acetic acid were used as received from Fisher Scientific UK, Bishop Meadow Rd., Loughborough, Leics. LE11 0RG.

Solvents were also supplied by Fisher Scientific but those shown below were pre-treated to remove ambient moisture as following the methods described by Vogel[1] indicated.

Hydrozincite was used as prepared by Sohail[2]

Nitrogen was 99.999% pure (white spot) used as supplied by BOC. The total level of contaminants was *ca.* < 10 ppm made up as follows:

O_2	2 ppm	H_2O	3ppm	CO	<1 ppm
CO_2	<1 ppm	C_xH_y	<1ppm		

It was supplied as).0444m^3 cylinders at 175 bar pressure at 15^{O}C (corresponding to 7.77 m^3 at 15^{O}C and 1 bar pressure or 8.04 m^3 at 25^{O}C and 1 bar pressure; sufficient to flush glove box (section 3.2.1) 432 times, at 25^{O}C.

3.3.1 Preparation of Neutral Carboxylates

3.3.1(i) Preparation of Hydrated Zinc Acetate, $Zn(O_2CCH_3)_2.2H_2O$

Zinc(II) acetate crystallizes from dilute acetic acid. Its monohydrate may be crystallized from an ethanol-water mixture. The dihydrate is very soluble in hot ethanol (166g/ 100mL/ 79^{O}C), fairly soluble in water (30g/ 100mL/ 20^{O}C; 44.6g/ 100mL/ 100^{O}C) and nearly insoluble in glacial acetic acid. It loses both water molecules at 140^{O}C and has a melting point of 237^{O}C (with some decomposition).[3]

---

[1]) A. I. Vogel, *Elementary Practical Organic Chemistry. Part 2 Qualitative Organic Analysis*, 2nd ed., Longmans, London, 1966.

[2]) K. Sohail, Ph.D. Thesis, Dept. Of Chemical Engineering, University of Edinburgh, 1992, 61-65.

[3]) B. J. Aylett in, *Comprehensive Inorganic Chemistry*, Pergamon Press, Oxford, 1973, vol. 3, ch. 30, p 235.

The following preparation was conducted in a fume-hood.

$$ZnO_{(s)} + 2AcOH_{(l)} \xrightarrow{\text{boil}} Zn(OAc)_{2\,(aq)} + H_2O_{(l)} \xrightarrow{\text{cool}} Zn(OAc)_2.2H_2O_{(s)} \qquad (3.3.1\text{-A})$$

(glacial) (satd.) (precipitate)

Acetic acid (250mL) was added to ZnO (25g) in a 2L round bottomed flask to which a water-cooled reflux condenser was fitted. The mixture was heated, with stirring, to reflux (117^{O}C). Once the mixture was refluxing gently, water (*ca.* 45mL) was added drop-wise until a colourless solution, completely free of undissolved ZnO, was formed. Vigorous stirring was required to assist the dissolution process (*ca.* 15 min). The solution was then covered (to prevent ingress of aerial contaminants) and allowed to cool overnight. Large, white, 'flowers' of needle-shaped crystals of $Zn(O_2CCH_3)_2.2H_2O$ were formed in 82% yield. These were filtered off using a Buchner funnel, washed three times with 200mL portions of warm methanol (*ca.* 40^{O}C) and then dried *in vacuo* using a rotary vacuum pump until the odour of acetic acid no longer persisted (*ca.* 4 hours). The analytical results of this preparation are discussed in section 4.1.1.

3.3.1(ii) Preparation of Zinc Propionate Dihydrate, $Zn(O_2CCH_2CH_3)_2.2H_2O$

The following preparation was conducted in a fume-hood. 5g of ZnO was added to 80mL of propionic acid in a round-bottomed flask fitted with a magnetic stirrer. The mixture was heated to boiling (138-142^{O}C) at which point distilled water was added stepwise (*ca.* 35mL) during which the mixture was stirred vigorously whilst maintaining reflux. After *ca.* 15 minutes a clear, colourless solution was formed. This was then covered and allowed to cool. After 2 days a white microcrystalline solid was precipitated. This was washed with diethyl ether and then pumped down using Schlenk apparatus. The product was then recrystallized using vapour diffusion technique. The solvent used was dilute propanoic acid (50 v% water) and the precipitant was acetone. Hexane and diethyl ether were found not to yield any precipitate. The precipitate was formed as large (*ca.* 1-2mm edges), thin, square, plates in 44% yield. The analytical results of this preparation are discussed in section 4.1.4.

3.3.2 Preparation of Basic Carboxylates

The preparation of a large range of tetrazinc μ_4-oxohexa-μ-carboxylates by various techniques has been reported[4,5]. To ascertain the most convenient and highest yield routes to basic zinc carboxylates the reported methods were repeated and variations to these methods were attempted.

3.3.2(i) Preparation of Basic Zinc Acetate, Hexakis[μ-(acetato-O-O′)]-μ_4-oxotetrazinc, $Zn_4O(O_2CCH_3)_6$

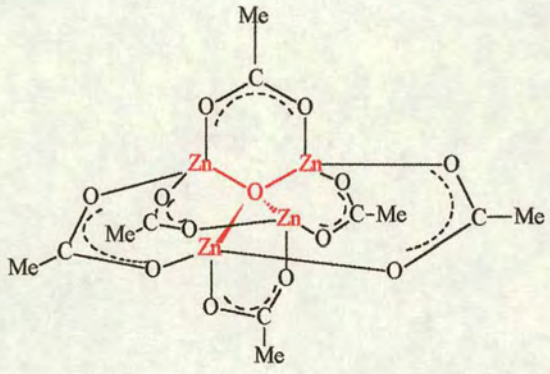

Figure 4.1.2-A Hexakis[μ-(acetato-O:O')]-μ_4-oxotetrazinc a.k.a. zinc acetate oxide, zinc oxyacetate and basic zinc acetate. Used as a virucide, bactericide and fungicide. Soluble in $CHCl_3$ and C_6H_c. mp 252-253°C. Dec. at 320°C.[6]

Method A

$$ZnO_{(s)} + 3\ Zn(O_2CCH_3)_{2\ (aq)} \xrightarrow{100^\circ C} Zn_4O(O_2CCH_3)_{6\ (aq)}$$

$$Zn_4O(O_2CCH_3)_{6\ (aq)} \xrightarrow{100^\circ C} Zn_4O(O_2CCH_3)_{6\ (s)} \qquad \text{Eqn. 3.1.2}$$

The following method of Hardt and Stavenow[5] was reported and said to give 55% yields of $Zn_4O(OAc)_6$.

---

4) R. M. Gordon and H. B. Silver, "Preparation and Properties of tetrazinc μ_4-oxohexa-μ-carboxylates (basic zinc carboxylates)", *Can. J. Chem.*, 1983, **61,** 1218-1221.
5) H. D. Hardt and F. Stavenow, Z. Anorg. Allg. Chem., 1959, **301**, 267-270.
6) *Dictionary of Inorganic Compounds*, Chapman and Hall, London, 1992, **1-5**.

The following method of Hardt and Stavenow[5] was reported and said to give 55% yields of $Zn_4O(OAc)_6$.

"...Octahedral crystals of $Zn_4O(OAc)_6$ mp. = 252 ± 1°C were obtained by adding ZnO (1 mol) to hot, saturated aqueous solutions of $Zn(OAc)_2$ (3 moles), evaporating to dryness, heating at 150 °C, and extracting the residue with C_6H_6 or $CHCl_3$ basic zinc acetate using the following procedure."

The method was repeated as follows. ZnO (0.8g, 0.01 mol) was added, with stirring, to a hot saturated aqueous solution of $Zn(O_2CCH_3)_2.2H_2O$ (6.6g, 0.03 mol). The reagents were heated under reflux until all the ZnO had reacted. The resulting solution was evaporated to dryness, heated to 150°C and the product was extracted with toluene.

Using this method the resulting products were always found to be insoluble in toluene. The reaction was repeated using benzene and $CHCl_3$ as solvents but these did not work either. Extraction was then attempted using a Soxhlet apparatus separately with benzene, toluene and chloroform run overnight or for 24 hours. The product solutions were evaporated to dryness using a rotary vacuum pump. The products always contained predominantly ZnO (explaining its insolubility in benzene, toluene and chloroform) with small amounts of $Zn(OAc)_2$ and $Zn_4O(OAc)_6$ and with some other minor, unidentified materials (observed through x-ray powder diffraction). Infra red analysis showed the product to contain carbonyl stretches characteristic of neutral and basic acetate. This mixture was subsequently worked up by dissolving it in dry methanol under nitrogen and filtering off the residual ZnO and $Zn(O_2CCH_3)_2.2H_2O$. The methanolic solution was then evaporated to dryness using a rotary vacuum pump to yield $Zn_4O(O_2CCH_3)_6$ as a fine white powder. This was collected and stored under nitrogen. The maximum $Zn_4O(OAc)_6$ yield obtained was *ca.* 4%.

This route was found to be highly unsatisfactory both in terms of yield and required effort. It is questionable how a yield of 55% could have been achieved using this method. It is known that $Zn_4O(OAc)_6$ is susceptible to hydrolysis and it has been reported that it breaks down in water to yield ZnO and $Zn(OAc)_2.2H_2O$.[4,7,8] Since this route involves aqueous reflux it seems inevitable that as the basic acetate is formed there is a competing back reaction in which it is hydrolysed back to the starting materials. Judging by the low yield for the reaction the equilibrium this could well be the case.

In addition the authors reported that:
"Analogous oxyformates and oxypropionates could not be prepared by this method or by sublimation of the neutral salts...Preparation of $Zn_4O(OAc)_6$ by sublimation of $Zn(OAc)_2$ gives low yields, owing to decomposition of $Zn(OAc)_2$ above 320°C."

However, it has been shown that zinc oxypropionate can be prepared by sublimation,[3,9] indeed the crystal structure has been obtained by the author (see section 4.1.5) using crystals obtained by this method.

Method B: Cold finger

$$4\ Zn(O_2CCH_3)_2.2H_2O_{(s)} \xrightarrow[in\ vacuo]{200^{\circ}C} Zn_4O(O_2CCH_3)_{6(s)} + 2\ CH_3COOH_{(g)}\ 7\ H_2O_{(g)} \quad \text{eqn.3.1.2}$$

Hydrated zinc acetate (2-3 g) was placed in a water-cooled 'cold-finger' apparatus attached to a vacuum line. The outer tube was heated in a silicone oil bath to 200°C. The sublimate produced by this method was a fine white powder. A grey amorphous residue was formed in the bottom of the outer tube.

Total yield was 54%.

---

[7]) H. Kunkely and A. Vogler, "Absorption and Emission Spectrum of $[Zn_4O(Acetate])_6$", *J. Chem. Soc., Chem. Comm.*, 1990, 1204-1205.

[8]) H. Koyama and Y. Saito, *Bull. Chem. Soc. Jpn.*, 1954, **27**, 112.

[9]) V. V. Panevchick, V. M. Goryaev and V. G. Guslev, "The Thermal Decomposition of Zinc Propionate", *Russ. J. Inorg. Chem.*, 1982, **27**, 1241-1244.

Method C: Round-bottomed flask and air-condenser

The procedure for method B was repeated except that the apparatus was replaced with a round-bottomed flask (100mL) fitted with an air-condenser connected to a vacuum line. The flask was heated in an isomantle. Efflorescence of the zinc (II) acetate dihydrate led to reagents and products being blown into the condenser and vacuum line. To prevent this, glass wool was placed in the neck of the round-bottomed flask. The sample was heated slowly to 200^{O}C and then held at 200^{O}C until no further sublimation occurred (*ca.* 2 hrs). During this period large (*ca.* 2mm side), white, octahedral crystals formed around the neck of the flask. The apparatus was allowed to cool to ambient temperature. The sublimate was then collected and stored under dry nitrogen.

These large crystals proved far easier to collect than the powdered form obtained from method B. Moreover, the crystalline form will *de facto* possess a lower surface area rendering it less susceptible to surface hydrolysis during storage. Increasing the mass of starting reagent was found to decrease the final percentage yield. This loss being accounted for by the formation of amorphous, grey, residual solids in the bottom of the round-bottomed flask.

Total yield was 88%.

The facile nature of this procedure and the high yield rendered sublimation the method of choice for the formation of $Zn_4O(O_2CCH_3)_6$. However, the final collection of the product from the round-bottomed flask, under flowing dinitrogen, proved to be a potential opportunity for air contamination of the product. To alleviate this difficulty the following apparatus was constructed from 15 mm section glass tubing.

Method D: Sublimation tube

A sublimation tube was constructed from 12 mm inner diameter glass of length *ca.* 30 cm. The upper section was separated from a vacuum line via a Young's vacuum tap. A thermocouple was attached to the side of the tube with the tip parallel with the base of the tube, where the sample was placed.

The use of heating tape incurred difficulties in measuring exact temperature of sublimation events and in observing reaction changes. Thus a thermostatically controlled, fan-assisted furnace was used. Using the above apparatus it was observed that small quantities of crystalline material were formed above the area of formation of $Zn_4O(O_2CCH_3)_6$ especially in the bends of the glassware. In addition, yellow and orange solids were deposited around the area of formation of the $Zn_4O(O_2CCH_3)_6$. These results are hitherto unreported in the literature concerning the preparation of $Zn_4O(O_2CCH_3)_6$. Consequently, further investigation was made. The results of this investigation are reported in section 4.1.2.

Total yield was 74%.

Method E: Sublimation tube with dry-ice trap

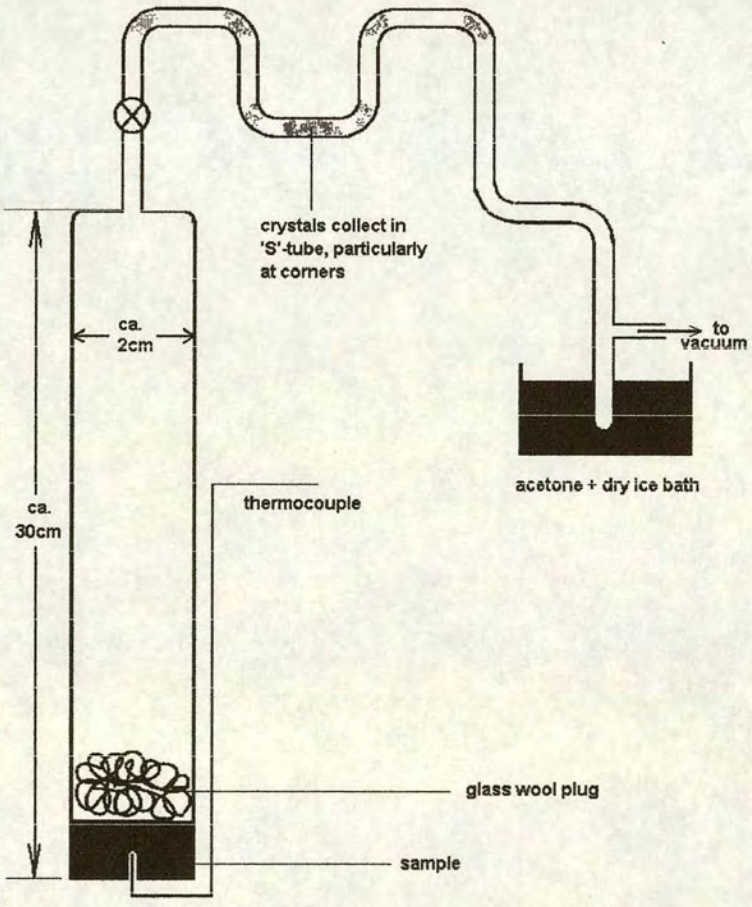

Figure 3.3.2-A Schematic representation of the apparatus used in method E

The difficulties in measuring temperatures of the sample were slightly alleviated by the inclusion of a 5mm deep hollow into the base of the previous design, see Fig. 3.3.2-A. The tip of the thermocouple was inserted into this hollow thereby increasing the thermal contact between the sample and the thermocouple. An acetone/dry-ice bath was also added to collect volatiles. Additional bends in the tubing above the vacuum tap were added to encourage the formation of the additional compounds observed in previous experiments.

Total yield was 76%.

3.3.2(ii) Preparation of Basic Zinc Propionate (hexakis(μ-2-propanato-O-O′)-(μ-4-oxo)-tetrazinc), $Zn_4O(O_2CCH_2CH_3)_6$

Method D, as described in section 3.3.2(i) was employed to synthesis basic zinc propionate. 1g of neutral zinc(II) propionate was used in each sublimation and heated at $2^{O}Cmin^{-1}$ to $190^{O}C$. The analytical results of the synthesis are discussed in section 4.1.5.

Total yield was 55%.

3.3.3 Preparation of Zinc (II) Methoxide, $Zn(OCH_3)_2$

The synthesis of zinc methoxide was attempted using the method of Mehrotra and Arora[10], "To a solution of anhydrous zinc chloride (3.94g) in methanol (50g) was introduced a solution of lithium methoxide (Li, 0.41g) in methanol. The reaction mixture was refluxed for about 7 hours and filtered hot through a closed system; the insoluble solid was washed repeatedly with hot methanol till it was free from chloride. The solid on drying under reduced pressure at $45^{O}C$/2 mm yielded a white powder (2.8g; yield 77%). Found: Zn 51.49; OMe 49.4%. $Zn(OMe)_2$ requires Zn 51.3; OMe 48.7%."

$$ZnCl_2 + 2\,LiOMe \xrightarrow[MeOH]{} Zn(OMe)_2\downarrow + 2\,LiCl \qquad \text{Eqn. 3.3.3-A}$$

The problems encountered in this preparation are described in section 4.1.6.

---

10) R. C. Mehrotra and M. Arora, "Alkoxides and Double Alkoxides of Zinc", *Z. Anorg. Allg. Chem.*, 1969, **370**, 300-309.

3.3.4 Preparation of Zinc (II) Hydroxide, $Zn(OH)_2$

Preparation of ε $Zn(OH)_2$ was by method of Scholder and Hendrich[11] as quoted by Brauer[12] "Analytical grade ZnO (160 g) is refluxed in a round-bottom flask containing a solution of 600g of NaOH in 300mL of H_2O. After the ZnO is dissolved, the solution is diluted with 300mL H_2O and cooled to 60°C. At this point, the volume of the solution is about 900mL. It is filtered and diluted 10 times with water. Crystalline $Zn(OH)_2$ separates out after 2-3 weeks. This is filtered, washed first with cold water, then several times with warm water, and dried over conc. H_2SO_4.

"Small needles are formed during the initial stages of crystallisation; however, standing converts them into the other crystal form."

The analysis of the product of this preparation is given in section 4.1.7.

---

[11]) R. Scholder and G. Hendrich, *Z. Anorg. Allg. Chem.*, 1939, **241**, 76.

[12]) G. Brauer, *Handbook of Preparative Inorganic Chemistry*, 2nd ed., Academic Press, New York, 1963-65, vol. 2, pp. 1074-1075.

CHAPTER 4: RESULTS & DISCUSSION

4.1 Precursor Materials

4.1.1 Analysis of Zinc(II) Acetate Dihydrate, $Zn(O_2CCH_3)_2.2H_2O$

The preparation of $Zn(O_2CCH_3)_2.2H_2O$ from zinc oxide and glacial acetic acid (see section 3.3.1) gave an 82% yield of a product which correlated well with infrared, mass spectrum and NMR data from the literature, and predicted CHN results.

4.1.1(i) CHN and AAS Data for $Zn(O_2CCH_3)_2.2H_2O$

$Zn(O_2CCH_3)_2.2H_2O$ = $C_4H_{10}O_6Zn$			M_{AC} = 217.976883610	
M_R = 219.50	C	H	N	Zn
Calculated	21.89	4.59	0.00	29.79
Found	21.99	4.49	0.00	29.65
% Error	0.45	2.23	0.00	0.47

Table 4.1.1-A CHN Analysis of $Zn(O_2CCH_3)_2.2H_2O$

The percentage error figure for this and all other elemental analyses was calculated using the formula:

$$\text{percentage error} = (|\text{Calculated} - \text{Found}| \div \text{Calculated}) \times 100\%.$$

The calculations were based upon the molecular mass, M_R, of the molecule. The molecular mass is denoted by M_R in the elemental analysis tables and the accurate mass (for use in mass spectroscopy) as M_{AC}.

4.1.1(ii) Infrared Data for $Zn(O_2CCH_3)_2.2H_2O$

The infrared spectrum is shown in Fig. 4.1.1-A and is in excellent agreement with the data of Johnson *et al.*,[1] from which band assignments have been taken and appended to Fig. 4.1.1-A. In the region 4000-600 cm^{-1} the spectrum of $Zn(O_2CCH_3)_2.2H_2O$ shows absorption values typical of acetate groups in a planar arrangement, although perturbed by coordinated water groups. In such an

1) M. K. Johnson, D. B. Powell and R. D. Cannon, *Spectrochim. Acta*, 1982, **38A, 2**, 125-131.

environment there are two C_{2v} acetate groups under D_{2h} symmetry. The RCOO bridging moiety provides the characteristic stretches for this compound; these being the symmetric ν_3(COO) at 1450cm^{-1} and the antisymmetric ν_8(COO) at 1558cm^{-1}.

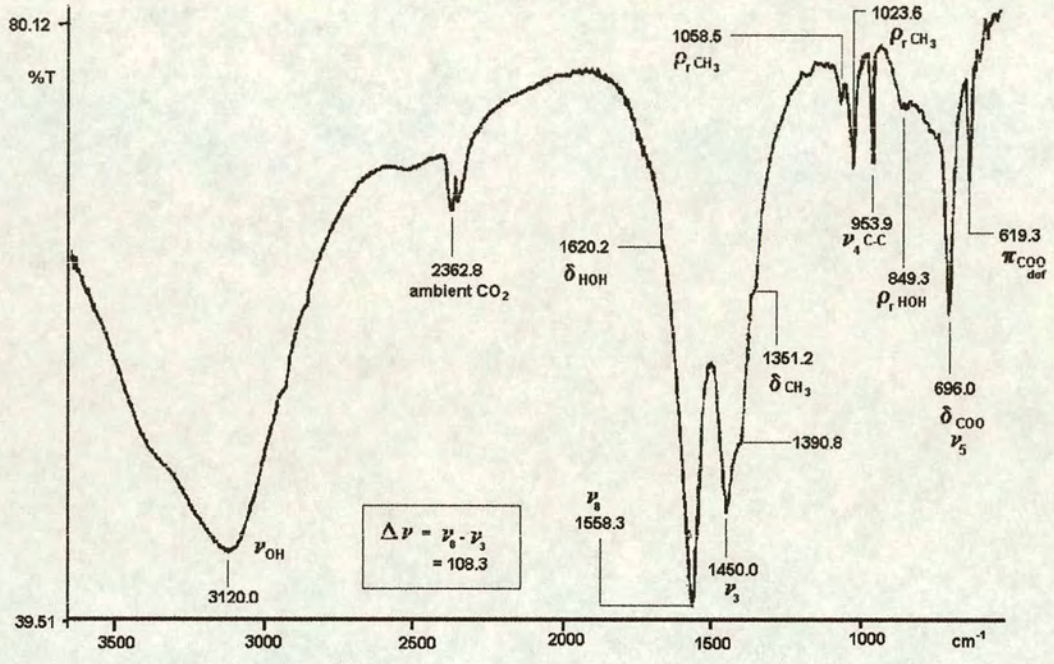

Figure 4.1.1-A The Infrared Spectrum of $Zn(OAc)_2.2H_2O$ in KCl

4.1.1(iii) Mass Spectral Data for $Zn(O_2CCH_3)_2.2H_2O$

The following mass spectral data are normalized to the largest peak in the spectrum and recorded as percentage intensity. The superscript c is used to denote when the recorded peak is part of a peak cluster.

The EI mass spectrum of $Zn(OAc)_2.2H_2O$ showed no significant peaks above *m/z* = 68 reflecting the destructive nature of this technique; the following main peaks were observed.

Mass	% intensity	assignment
28	17.3	$[CO]^+$
32	100	$[O_2]^+$
44	47.2	$[CO_2]^+$
60	23.0	$[CH_3COOH]^+$
64^c	1.9	$[Zn]^+$
66^c	1.0	$[Zn]^+$
67^c	0.5	$[Zn]^+$
68^c	0.9	$[Zn]^+$

Table 4.1.1-B The Major Peaks of the EI Mass Spectrum of $Zn(OAc)_2.2H_2O$

Mass	% intensity	assignment
32	62	$[O_2]^+$
44	100	$[CO_2]^+$
60	51	$[CH_3COOH]^+$
64^c	74	$[Zn]^+$
205	57	$[Zn_2O(OAc)]^+$
389^c	68	$[Zn_3O(OAc)_3]^+$
573^c	83	$[Zn_4O(OAc)_5]^+$

Table 4.1.1-C The major peaks of the FAB mass spectrum of $Zn(OAc)_2.2H_2O$

In the FAB mass spectrum of $Zn(OAc)_2.2H_2O$ and many other materials studied, the formation of peaks was found to be sensitive to the experimental set-up. In some cases the matrix peaks obscured all other peaks at *m/z* values < 100, and peaks above *m/z* = 100 were barely discernible from noise. Under the optimum conditions, peaks were observed at *m/z* values indicating breakdown products from a molecular mass greater than that of the parent ion, $[Zn(O_2CCH_3)_2.2H_2O]^+$, at *m/z* =219.50. The peaks

at *m/z* = 205, 389 and 573 are in agreement with those observed by Hiltunen *et al.*[2] and Charalambous *et al.*[3] Both papers proposed the formation of higher molecular weight clusters from neutral zinc acetate. Charalambous proposed that the peaks were due to the ions $[Zn_2O(OAc)]^+$, $[Zn_3O(OAc)_3]^+$ and $[Zn_4O(OAc)_5]^+$, and used exact molecular weight matching to confirm the identity of these and other fragments.

A feasible explanation for the formation of these higher molecular weight clusters from $Zn(OAc)_2.2H_2O$ is that the vacuum conditions of the mass spectrometer and the local heat generated by the bombardment of the sample with high velocity argon atoms is sufficient to cause the 'tetramerization' of neutral $Zn(OAc)_2.2H_2O$ to form $Zn_4O(OAc)_6$ within the mass spectrometer. This subsequently breaks down, yielding a pattern identical to that observed when $Zn_4O(OAc)_6$ is the sample.

4.1.1(iv) ^{1}H N.M.R. Data for $Zn(O_2CCH_3)_2.2H_2O$

The ^{1}H N.M.R. spectrum of $Zn(OAc)_2.2H_2O$ was obtained at 297 K using D_2O as solvent. It shows a singlet resonance, at 1.8529 ppm, due to the pair of equivalent methyl groups on the acetate ligands. A second singlet, at 4.8020 ppm, was also present, due to the protons associated with the two equivalent trans-diaxial water molecules (for water δ (^{1}H) = 4.8 at pH 7) in the $Zn(OAc)_2.2H_2O$ and also present in the solvent, due to its ready absorption of atmospheric moisture.

4.1.1(v) Thermal Analysis of $Zn(O_2CCH_3)_2.2H_2O$

DSC traces were obtained in order to ascertain the optimum heating rate required to produce the greatest amount of tetranuclear $Zn_4O(O_2CCH_3)_6$ from the thermal decomposition of neutral zinc(II) acetate and, also, in order to compare these results with literature data.[2]

---

2) L. Hiltunen, M. Leskelä, M. Mäkelä and L. Niinistö, "Crystal Structure of μ_4-oxo-hexakis(μ-acetato)tetrazinc and Thermal Studies of its Precursor, Zinc Acetate Dihydrate", *Acta. Chem. Scand.*, 1987, **A41**, 548-555.

3) J. Charalambous, R. G. Copperthwaite, S. W. Jeffs and D. E. Shaw, "Mass spectra of Tetracobalt(II) and Tetrazinc(II) μ_4-Oxo-hexa-μ-carboxylates (Basic Cobalt and Zinc Carboxylates)", *Inorg. Chim. Acta*, 1975, **14**, 53-58.

Samples of $Zn(OAc)_2.2H_2O$ (*ca.*5mg) were heated in inert argon atmosphere at three heating rates: 1, 5 and 10 $^{O}C\ min^{-1}$, across the temperature range 30-400^{O}C. In each case, three endothermic processes were clearly observed (see Fig. 4.1.1-B a, b and c), with a broad 4th endothermic feature occurring between 279 and 326^{O}C. These results compliment those of Hiltunen *et al.*[2] who used heating rates between 5 and 200^{O}C min ^{1} in a nitrogen atmosphere. In this author's results four endothermic processes were observed when a heating rate of 5^{O}C min^{-1} was employed (Fig. 4.1.1-B(b)). The first peak (peak 1, centred at 98^{O}C) correlates with that obtained by Hiltunen[2] (centred at 106^{O}C) and is attributed to dehydration:

$$Zn(O_2CCH_3)_2.2H_2O_{(s)} \rightarrow Zn(O_2CCH_3)_{2\ (s)} + 2\ H_2O_{(g)} \qquad \text{Eqn. 4.1.1-A}$$

The onset temperature of these dehydration peaks increases with increasing heating rate. This can be attributed to (i) the greater lag-time between the cell temperature (on the x-axis) and the sample temperature when employing the higher heating rates, and, (ii) the diffusional limitations experienced by out-going water molecules from $Zn(O_2CCH_3)_2.2H_2O$ particles when subjected to a heating rate greater than that which allows unhindered evolution of H_2O.

Peak 2, Fig. 4.1.1-B(b), with its maximum in the region 250^{O}C (c.f. Hiltunen *et al.*[2] 251^{O}C) is thought to be caused by melting of the anhydrous salt:

$$Zn(O_2CCH_3)_{2\ (s)} \rightarrow Zn(O_2CCH_3)_{2\ (l)} \qquad \text{Eqn. 4.1.1-B}$$

The third peak, centred at 259^{O}C (c.f. Hiltunen *et al.*[2] 257^{O}C) is thought to be associated with the formation and melting of $Zn_4O(O_2CCH_3)_6$:

$$4\ Zn(O_2CCH_3)_{2\ (l)} \rightarrow Zn_4O(O_2CCH_3)_{6\ (s)} + (CH_3CO)_2O_{(g)} \qquad \text{Eqn. 4.1.1-C}$$

$$Zn_4O(O_2CCH_3)_{6\ (s)} \rightarrow Zn_4O(O_2CCH_3)_{6\ (l)} \qquad \text{Eqn. 4.1.1-D}$$

Note that this peak was not present when the reaction occurred with a heating rate of 1 $^{O}C\ min^{-1}$. Hence, it was inferred that, with a heating rate of 1 $^{O}C\ min^{-1}$ the basic salt sublimes rather than liquefies. Such sublimation was also observed during *in*

vacuo studies conducted with a heating rate of $5^{O}C\ min^{-1}$, described later in this section.

On the $5^{O}C\ min^{-1}$ trace, the volatilization of the basic acetate is thought to occur above $260^{O}C$ (Eqn. 4.1.1-E). This process correlates with the broad endothermic feature (peak 4) centred at $315^{O}C$. Given the breadth of the endotherm, it is clear that this volatilization is a slow process.

$$Zn_4O(O_2CCH_3)_{6\ (s)} \rightarrow Zn_4O(O_2CCH_3)_{6\ (g)} \qquad \text{Eqn. 4.1.1-E}$$

On increasing the heating rate to $10^{O}C\ min^{-1}$, Fig. 4.1.1-B(c), this volatilization is succeeded by an endotherm (peak 6, $361^{O}C$) and an exotherm (peak 7, $373^{O}C$). These features may correspond with Eqn.2.3.2-J in which carbon is formed. This would explain the presence of grey material in the decomposition products of some *in vacuo* reactions conducted at higher heating rates.

Further differences, which were not observed by Hiltunen *et al.* [2] occur in the $10^{O}C$ min [1] trace. Firstly, the endothermic doublet now contains a shoulder at $246^{O}C$ (peak 5); this was observed as an even more obvious peak at $244^{O}C$ when a heating rate of $1^{O}C\ min^{-1}$ was used, Fig. 4.1.1-B(a). Other workers[4,5] have reported alternative secondary decomposition pathways, which may explain the presence of these peaks:

$$Zn(O_2CCH_3)_{2\ (s)} \rightarrow ZnO_{\ (s)} + (CH_3CO)_2O_{\ (g)} \qquad \text{Eqn. 4.1.1-F}$$

$$Zn(O_2CCH_3)_{2\ (s)} \rightarrow ZnO_{\ (s)} + CH_3COCH_{3\ (g)} + CO_{2\ (g)} \qquad \text{Eqn. 4.1.1-G}$$

However, when heated at $5^{O}C\ min^{-1}$, peak 5 was not present, yet it was present when heating rates of $1^{O}Cmin^{-1}$ and $10^{O}Cmin^{-1}$ were used. If peak 5 is due to decomposition pathways, then it is possible that numerous competing processes are in balance and that, at $5^{O}Cmin^{-1}$, their net effect is to inhibit the decomposition

4) H. D. Hardt and F. Stavenow, *Z. Anorg. Allg. Chem.*, 1959, **301**, 267-70.
5) H. G. McAdie, *J. Inorg. Nucl. Chem.*, 1966, **28**, 2801.

pathways. For example, Bowker *et al.*[6] studied the interaction of acetic acid with a ZnO surface. The major products, at temperatures up to 400^{O}C, were shown to be ketene ($H_2C=C=O$), acetic acid, CO_2, H_2 and H_2O. By the reasoning employed by Panevchik (section 2.3.2(ii); Eqn. 2.3.2-F), acetic acid would be expected to be present in the reaction mixture due to the presence of its anhydride. Since ZnO is also a known decomposition product, the reaction sequences observed by Bowker *et al.*[6] may also occur within the reaction mixture to yield, additionally, ketene and hydrogen. The presence of these materials may have a further effect on the decomposition pathway of $Zn(O_2CCH_3)_2.2H_2O$.

DSC traces were not available for vacuum conditions and so the reactions were repeated *in vacuo* using method E (section 3.3.3). Reactions were conducted at 5^{O}C min^{-1} with *ca.* 2g of powdered anhydrous zinc (II) acetate, held in place with a glass wool plug, which had been washed in acetone and oven dried at 300^{O}C to remove trace organic materials. This was held in a sublimation tube (evacuated to $<10^{-3}$ Torr) with a 16mm internal diameter and length of 30cm. Once at 120^{O}C, the samples were held for 15 minutes, and then for a further 15 minutes at each subsequent 10^{O}C increment, i.e. at 130, 140,...,270^{O}C. It was observed that no liquefaction occurred at any temperature within the observed range. Above 270^{O}C all the neutral salt had sublimed or formed involatile residues. Also, the condensation of $Zn_4O(OAc)_6$ began at 150^{O}C, well below the melting point of the neutral salt (237^{O}C) or the basic salt (252^{O}C). This condensate was observed as a fine white powder, *ca.* 6cm above the neutral salt. Above 170^{O}C the formation of large, transparent crystals of the basic salt $Zn_4O(OAc)_6$ (referred to as Z4) began to form on the surface of the amorphous deposits already laid down. The formation of the basic salt was confirmed by infrared, elemental and XRPD analysis. At 170^{O}C the first signs of the evolution of yellow/orange volatile products (referred to as ZL) appeared. These were collected in the acetone/dry-ice bath. As the temperature was increased to 250^{O}C, the quantity of sublimed $Zn_4O(OAc)_6$ increased to the point where it became an annulus *ca.* 5mm thick and 20mm high. Above this annulus a

6) M. Bowker. H. Houghton and K. C. Waugh, *J. Catal.*, 1983, **79**, 431-44.

band of yellow powder was deposited (referred to as ZY). As the temperature increased further ZY darkened towards the Z4 edge, being progressively lighter in colour away from Z4. By the end of the reaction there was a dark orange band fading into yellow above Z4. This band (ZY) contained poorly formed orange and yellow needle-shaped material (referred to as ZN), shown in Fig. 4.1.1-C. Simultaneously, the colour density of the liquids trapped in the acetone/dry-ice bath increased to dark orange in parts. These were observed as three bands, the first of which was pale yellow which merged with a pale orange band. These two bands were above a third band, which was dark orange and separated from the first two by a gap of *ca.* 3mm. On warming to room temperature the bands melted to form a homogeneous orange liquid with a ketonic odour, redolent of domestic TCP. Furthermore, small patches of white powder, *ca.* 5mm in diameter, containing up to *ca.* 20 small crystals were observed to condense *ca.* 10cm above the region where $Zn_4O(OAc)_6$ was condensing. These crystals were of three types (see Fig. 4.1.1-D). The first of these, 4.1.1-D(a), was identified by infrared spectroscopy as $Zn_4O(OAc)_6$. The remaining two could not be identified by infrared spectroscopy and are discussed in section 4.1.3, where they are referred to as Z2 and Z8.

The reaction was repeated with the same conditions, except for the use of narrower sublimation tubes. In the first instance a 7 mm inner diameter tube was used and in the second an 11 mm internal diameter tube was used. In each instance an annulus of $Zn_4O(OAc)_6$ would develop a yellow band at its uppermost point (as occurred with the 16mm inner diameter tube experiments). However, in addition, the reacting material in the base on the tube (reaction zone) would melt and then boil, whereas no liquefaction had been observed in the 16mm inner diameter tube. This liquefaction occurred at *ca.* 250^{O}C in the 7mm tube, and at *ca.* 255^{O}C in the 11mm tube. On further heating, the upper portion of the $Zn_4O(OAc)_6$ region would become distinctly yellow, and the material in the reaction zone would boil vigorously (this would occur at *ca.*253^{O}C in the 7mm tube and *ca.* 262^{O}C in the 11mm tube). In each case the same reaction products were observed as when the wider tube was used (16mm inner

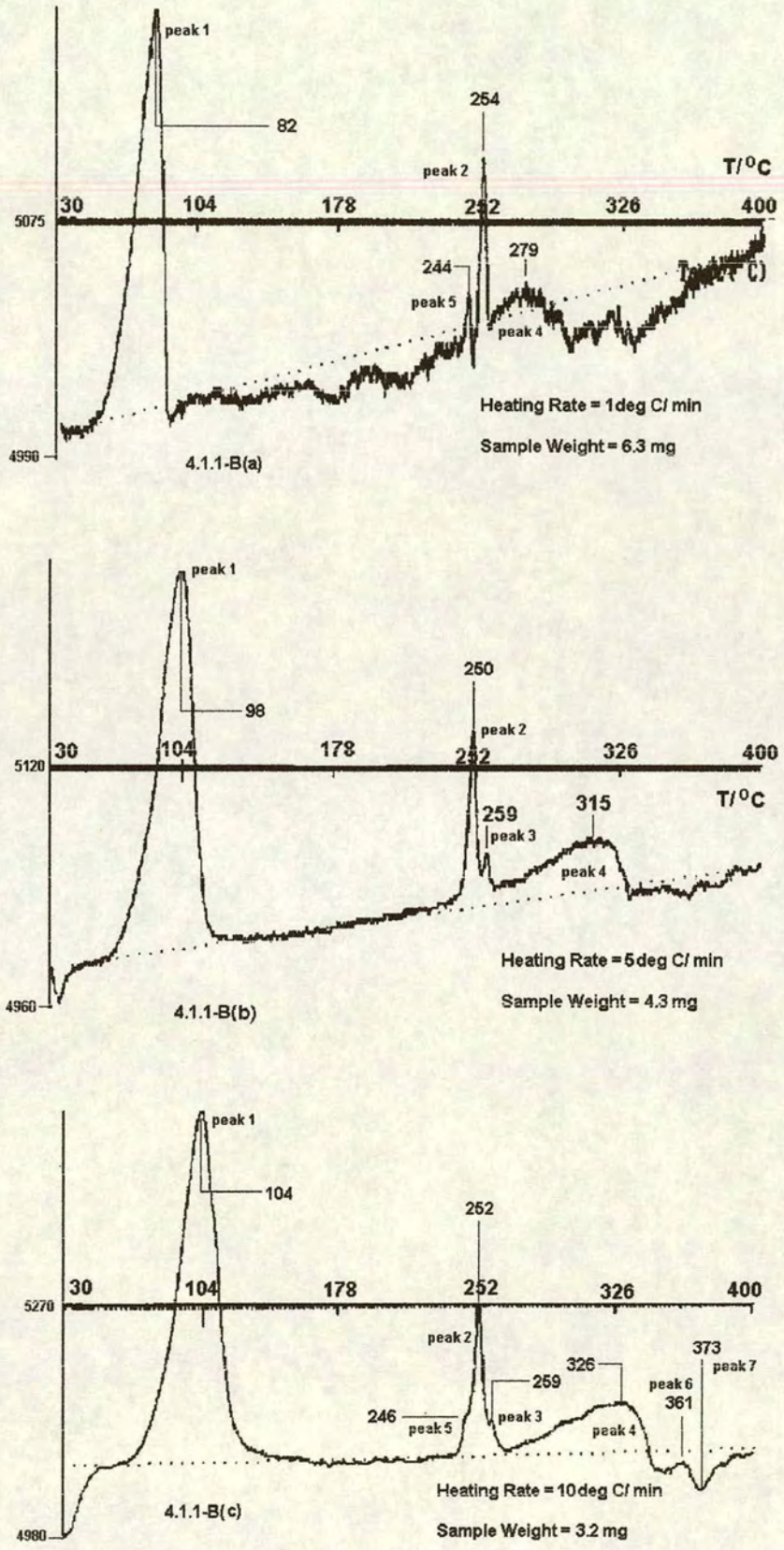

Figure 4.1.1-B DSC traces of $Zn(OAc)_2.2H_2O_1$ at (a) $1^{o}C\ min^{-1}$, (b) $5^{o}C\ min^{-1}$, (c) $10^{o}C\ min^{-}$

(a) (b)

Figure4.1.1-C Results of the pyrolysis of $Zn(OAc)_2.2H_2O$ (a) showing the whole apparatus, (b) close up of (a) showing the zone of $Zn_4O(OAc)_6$ formation

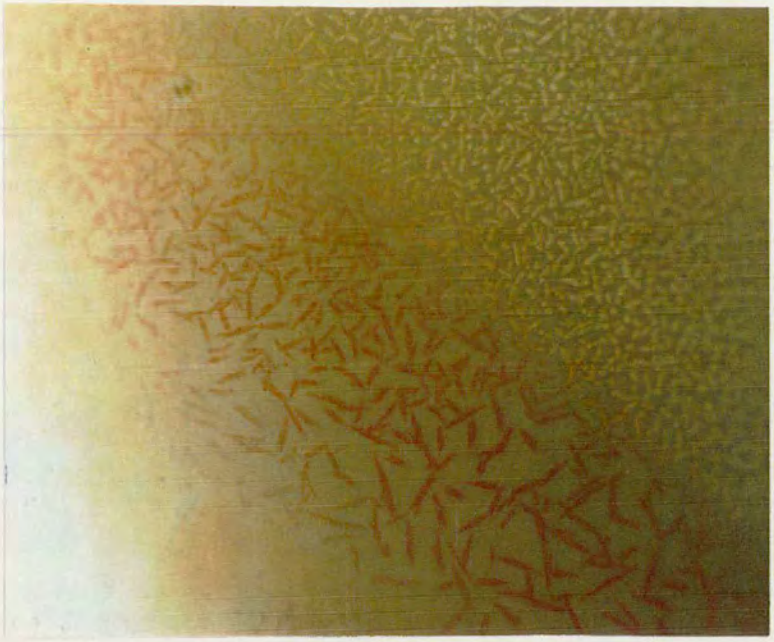

Figure 4.1.1-C(c) Close up of section shown in Fig. 4.1.1-C(b)

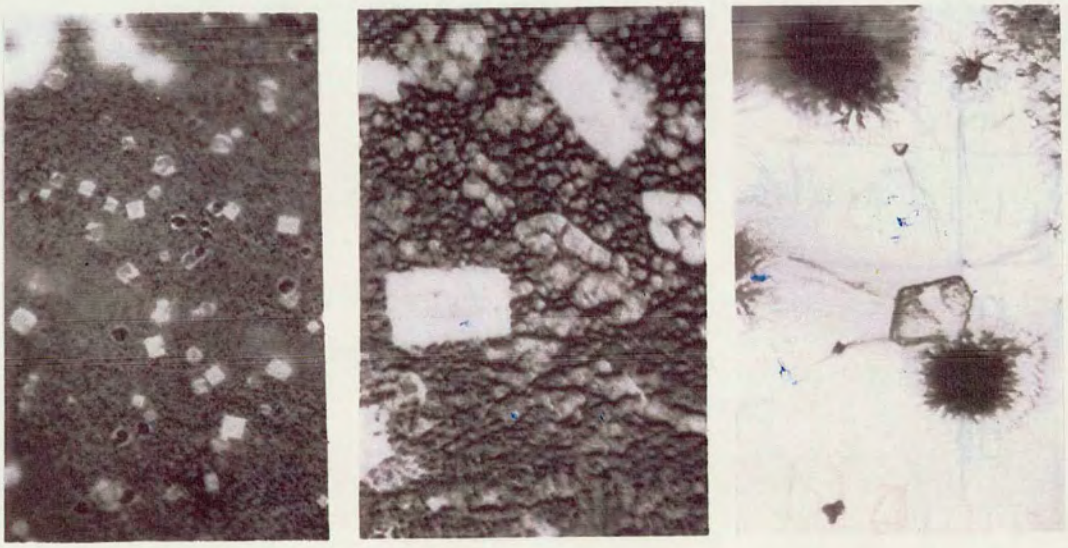

(a) (b) (c)

Figure 4.1.1-D Low magnification microscope images of crystals obtained from the pyrolysis of $Zn(OAc)_2.2H_2O$ (a) ×4 magnification negative image, (b) ×10 magnification negative image, (c) ×4 magnification positive image

Thus, the basic salt may be formed with or without observable liquefaction. The only factor definitely affecting whether or not boiling occurred was the diameter of the sublimation tube. The obvious effect that the tube diameter has, is on the diffusion rate of outgoing volatiles. From this it may be argued that, in narrow tubes, the rate of outward diffusion of gases is inhibited to such an extent that there is sufficient build-up of local pressure to cause the formation of the liquid phase of $Zn_4O(OAc)_6$.

This hypothesis provides a satisfactory explanation for differences in the observations of McAdie,[5] who witnessed sublimation of $Zn_4O(OAc)_6$ without liquefaction, and Hiltunen,[2] who witnessed the formation of $Zn_4O(OAc)_6$ with liquefaction prior to evaporation. It may simply be due to the differences in set-up of their respective sample holders and/or degree of operating vacuum (neither of which are commented upon by either author). This argument would also explain why, in this author's work, the highest yield of $Zn_4O(OAc)_6$ was obtained using method C, since this method used a round-bottomed flask which would have afforded the most facile release of volatiles from the reaction zone. When $Zn_4O(OAc)_6$ is allowed to sublime freely, no melting occurs and, when it is restricted, melting and boiling occur. It follows that $Zn_4O(OAc)_6$ has at least three pathways open to it, once it has formed in the solid state. Firstly, it may sublime and condense further up the reaction vessel, as observed with the 16mm tubes. Secondly, if its sublimation is inhibited (as with the tubes of internal diameter of 11mm or less) it may melt and then evaporate or, thirdly, it may melt and then decompose. It is proposed that the longer the basic salt is in the liquid state, the more opportunity it has to decompose and the lower the resulting yield. In contrast, once sublimed, the $Zn_4O(OAc)_6$ leaves the reaction zone and condenses in the cooler regions of the tube, where it is unlikely to decompose. Indeed, it was observed that the sublimate always formed around the region of the mouth of the oven where it was undoubtedly cooler than at the base of the oven where the reaction zone was centred. The hypothesis is further substantiated by the observation that, when 10g of $Zn(OAc)_2.2H_2O$ was used, the yield of $Zn_4O(OAc)_6$ was decreased from 74% (obtained when 2g samples were

used) to 48%. The increased reactant column height would have presented increased diffusion limitation to the outgoing gases, leading to higher internal pressure on the escaping $Zn_4O(OAc)_6$ and, hence, greater liquefaction and decomposition of the $Zn_4O(OAc)_6$ with, consequently, lower yields.

Since the reaction zone was taken to temperatures slightly above 260^{O}C, the temperature at the mouth of the oven may still have been sufficient to cause decomposition of $Zn_4O(OAc)_6$, as given by steps B2 and B3 in Eqn. 2.3.2-B. To determine if this was the case a 0.75g sample of $Zn_4O(OAc)_6$ was placed in an 11mm internal diameter tube, with remaining conditions as per method E (section 3.3.2). The purpose was to determine if, in the absence of other reactants, the basic salt would decompose when heated to the maximum reaction temperature of 260^{O}C. It was found that all the $Zn_4O(OAc)_6$ sublimed before the apparatus reached 250^{O}C. Only two products were formed, these being the resublimed $Zn_4O(OAc)_6$ in *ca.* 99% yield and a thin coating of brown residue in the base of the tube. Thus, virtually no decomposition of the $Zn_4O(OAc)_6$ occurred, in spite of using a narrow section tube. This supports the assertion that the difference in behaviour observed with $Zn(OAc)_2.2H_2O$ heated in different diameter tubes is simply due to the ease of escape of the outgoing gases and vapour, since, in the absence of decomposition, there would be no outgoing volatiles other than the $Zn_4O(OAc)_6$ vapour. Consequently, the amount of outgoing gases would be greatly reduced. The fact that no other products were observed, when the basic acetate was heated *in vacuo*, is in contrast to the numerous products formed when the neutral salt was heated under the same conditions. It is inferred that the production of these other materials is dependant upon the formation and interaction of decomposition products within the reaction zone. This result also confirms that, in the absence of other breakdown products, $Zn_4O(OAc)_6$ resublimes nearly stoichiometrically. Hence, once $Zn_4O(OAc)_6$ has condensed above the reaction zone, it is indeed far less susceptible to decomposition than if it were still present in the reaction zone. Finally, the fact that $Zn_4O(OAc)_6$ sublimes nearly stoichiometrically points to resublimation as an effective means of its purification.

4.1.2 Analysis of Basic Zinc(II) Acetate, $Zn_4O(O_2CCH_3)_6$

For analysis purposes the basic salt was synthesized using method E, without an acetone/dry-ice bath. The material obtained was then resublimed in an 11mm tube, for ease of breaking. The tube was scratched with a diamond blade and then snapped open in the glove box, where the sample was loaded into vials and sealed with 'Nesco' film for further analysis or hydrolysis experiments. For hydrolysis experiments, the samples were not ground until the moment they were required, in order to maintain as low a surface area as possible to inhibit surface reactions prior to experimentation.

4.1.2(i) CHN and AAS Data for $Zn_4O(O_2CCH_3)_6$

$Zn_4O(O_2CCH_3)_6 = C_{12}H_{18}O_{13}Zn_4$			$M_{AC} = 625.791322586$	
$M_R = 631.79$	C	H	N	Zn
Calculated	22.81	2.87	0.00	41.39
Found	22.88	2.87	0.00	41.29
% Error	0.31	0.00	0.00	0.24

Table 4.1.2-A CHN and AAS Analysis of $Zn_4O(O_2CCH_3)_6$

4.1.2(ii) Infrared Data for $Zn_4O(OAc)_6$

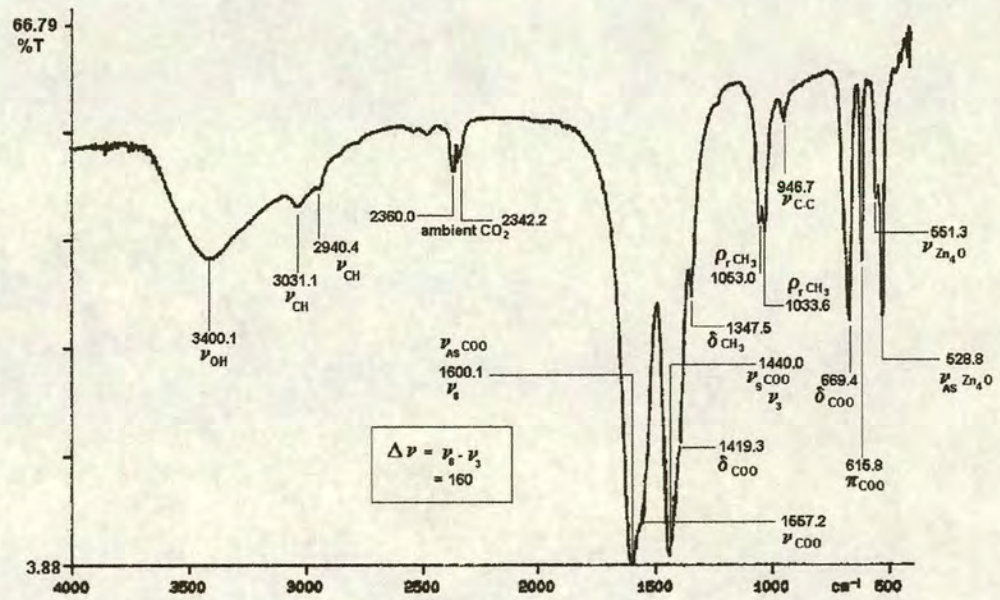

Figure 4.1.2-A Infrared spectrum of $Zn_4O(O_2CCH_3)_6$ in KCl. The absorptions at 551 cm^{-1} and 523 cm^{-1} are characteristic of the oxo-centred Zn_4O moiety

The infrared data for $Zn_4O(O_2CCH_3)_6$ agrees well with the results of Johnson *et al.*[1] and with earlier work by Beattie and Gilson[2] and Griffith.[3] The absorptions at 551 and 523 cm^{-1} are characteristic of the oxo-centred Zn_4O moiety, and the high $\Delta\nu$ value of 160 cm^{-1} is characteristic of the presence of type 8 chelating acetate ligands. These two features differentiate this spectrum from that of the neutral salt $Zn(OAc)_2.2H_2O$, in which there are no Zn_4O vibrations and $\Delta\nu$ is only 108 cm^{-1}. In the neutral dihydrate salt, the very strong, broad hydroxyl absorption, centred at 3120 cm^{-1}, further differentiates it from $Zn_4O(OAc)_6$. However, the basic salt readily absorbs and reacts with ambient water vapour (after standing in air for *ca.* one hour), also yielding a broad hydroxyl band. Fortunately, this feature is only of medium strength and is centred at a higher frequency (3400cm^{-1}), indicating weaker coordination of the hydroxyl-oxygen to the metal, and so it also serves to distinguish between the two materials.

4.1.2(iii) Mass Spectral Data for $Zn_4O(O_2CCH_3)_6$

The EI mass spectrum of $Zn_4O(OAc)_6$ showed the same peak pattern below m/z = 100 as was observed for $Zn(OAc)_2.2H_2O$. Above m/z = 100 additional peaks were observed which are recorded in table 4.1.2-B and shown in Fig. 4.1.2-B.

Mass	assignment
28	$[CO]^+$
32	$[O_2]^+$
44	$[CO_2]^+$
60	$[CH_3COOH]^+$
64[c]	$[Zn]^+$
205	$[Zn_2O(OAc)]^+$
235	unassigned
257	unassigned
389	$[Zn_3O(OAc)_3]^+$
469	$[Zn_4O_2(O_2CCH_3)_3]^+$
573	$[Zn_4O(OCCH_3)_5]^+$

Table 4.1.2-B The major peaks of the EI mass spectrum of $Zn_4O(OAc)_6$

1) M. K. Johnson, D. B. Powell and R. D. Cannon, *Spectrochim. Acta*, 1982, **38A, 2**, 125-131.
2) I. R. Beattie and T. Gilson, *J. Chem. Soc.*, 1961, 2585-6.
3) W. P. Griffith, *J. Chem. Soc.(A)*, 1969, 2270-73.

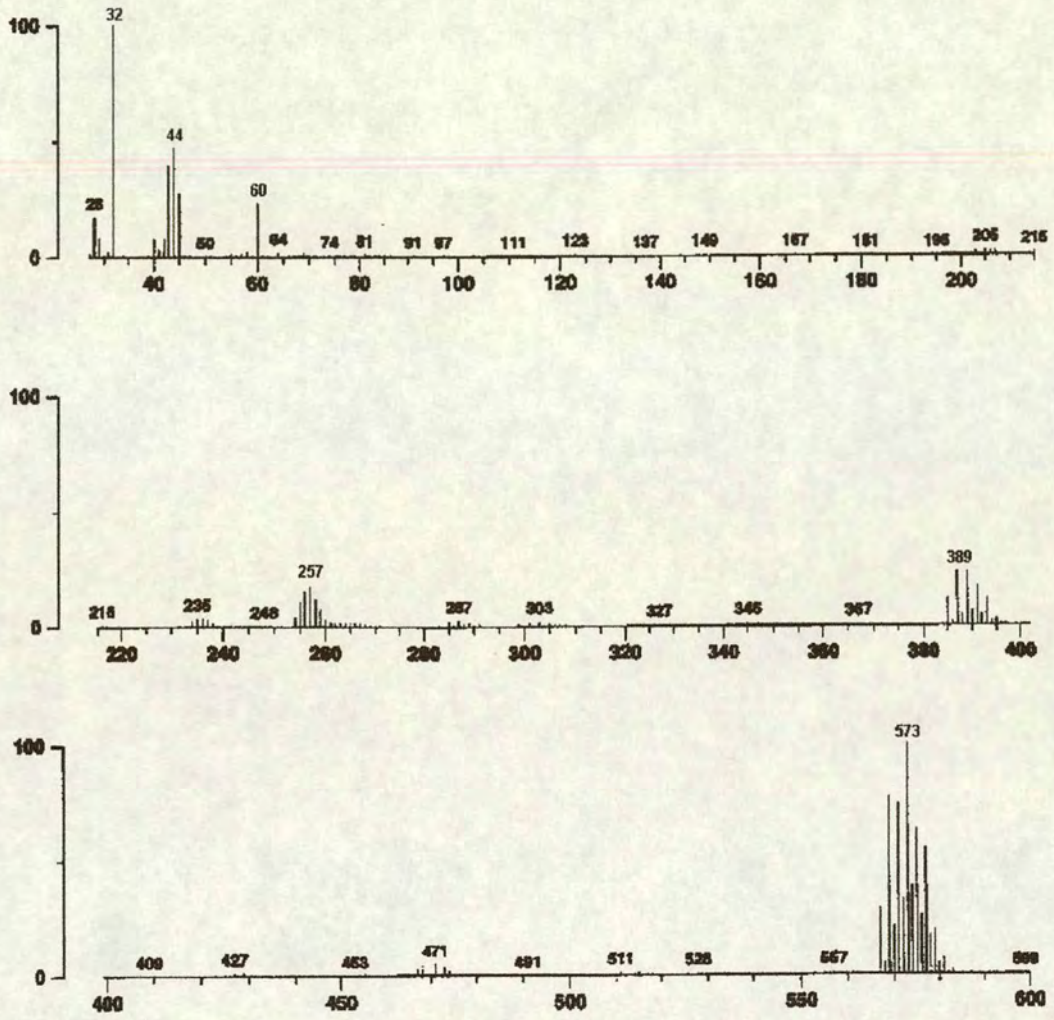

Figure 4.1.2-B EI mass spectrum of $Zn_4O(OAc)_6$

As reported by other authors,[4,5] the parent ion, $[Zn_4O(O_2CCH_3)_6]^+$, at m/z = 631.79 was not observed. The first daughter ion observed is that of $[Zn_4O(O_2CCH_3)_5]^+$ (m/z = 572.74), derived from the loss of the acetate radical ($CH_3CO_2^{\bullet}$, m/z = 59.04) from the parent ion. Further fragmentation is mainly through the loss of the even electron species like: $Zn(CH_3CO_2)_2$ (m/z = 183.47); and $(CH_3CO)_2O$ (m/z = 102.09) generating the peaks at m/z = 389.27, due to $[Zn_3O(O_2CCH_3)_3]^+$ and at m/z = 470.65,

4) L. Hiltunen, M. Leskelä, M. Mäkelä and L. Niinistö, "Crystal Structure of μ_4-oxo-hexakis(μ-acetato)tetrazinc and Thermal Studies of its Precursor, Zinc Acetate Dihydrate", *Acta. Chem. Scand.*, 1987, **A41**, 548-555.

5) J. Charalambous, R. G. Copperthwaite, S. W. Jeffs and D. E. Shaw, "Mass spectra of Tetracobalt(II) and Tetrazinc(II) μ_4-Oxo-hexa-μ-carboxylates (Basic Cobalt and Zinc Carboxylates)", *Inorg. Chim. Acta*, 1975, **14**, 53-58.

due to $[Zn_4O_2(O_2CCH_3)_3]^+$. These processes are analogous to those observed in the corresponding beryllium species.[6]

Two additional ions were observed at *m/z* = 235 and 257 which have not been observed by other authors. The strength of the ion signal for the ion at *m/z* = 257 was relatively large, suggesting a stable fragment. The only peaks larger than it were at *m/z* = 573 and 389, which are both parent ion derivatives. However, it has not been possible to propose any rational fragment losses from the parent ion which would account for their presence.

The FAB mass spectrum of $Zn_4O(OAc)_6$ in the range $0 < m/z < 200$ was dominated by peaks from the matrix reagent 3-nitrobenzaldehyde (3-NOBA). The only discernible non-matrix peak was that of CO_2 at *m/z* = 44. In the region $200 < m/z < 600$, peaks centred at *m/z* = 389, 429, 469 and 573 were observed; of these, the peak at *m/z* = 429 was not observed in the EI mass spectrum. This ion is assigned as a decomposition fragment of the $[Zn_4O_2(CH_3CO_2)]^+$ ion through loss of ketene (see Fig. 4.1.2-C) to form $[Zn_4O_2(O_2CCH_3)_2(OH)]^+$, *m/z* = 428.62.

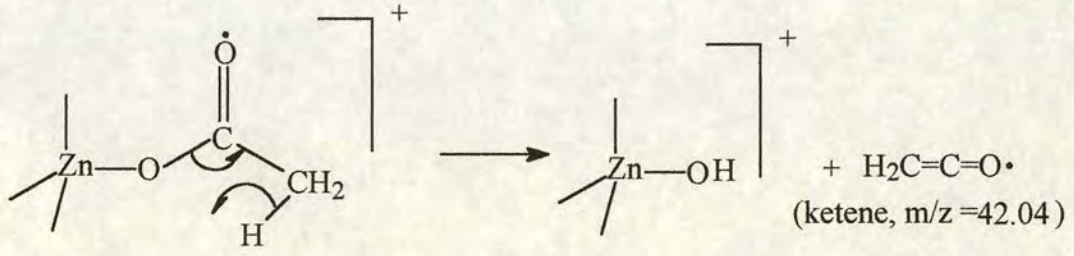

Figure 4.1.2-C The elimination of ketene from a $[Zn_xO_y(O_2CCH_3)_z]^+$ fragment

Above *m/z* = 600 fragments were observed which were indicative of the breakdown of higher nuclearity clusters. Whilst other authors have commented upon these, none have attempted to assign them. The following tentative assignments are made, based upon the hypothesis that basic zinc carboxylates generate higher nuclearity basic carboxylates within an FAB mass spectrometer. Also, that these higher nuclearity carboxylates are structurally analogous to those formed by beryllium (see section 2.3.1), such as $Zn_6O_2(O_2CCH_3)_8$ and $Zn_8O_3(O_2CCH_3)_{10}$. If the analogy holds true,

6) J. G. Vogel and B. G. Hobrock, *153rd A.C.S. Meeting, Miami Beach, Florida*, April, 1967.

then *m/z* values for theoretical break-down fragments may be predicted and compared with observed *m/z* values. In assessing whether an observed ion actually matches its predicted chemical formula accurate mass determinations may be obtained and compared with predicted accurate mass determinations. In order to assess the 'goodness of fit' between the data sets three criteria are commonly employed.

Peak matching criteria

The first is obtained by calculating the deviation between predicted and actual peaks. The deviation in ppm is calculated thus:

$$\frac{\text{found mass - calculated mass}}{\text{found mass}} \times 10^6 \text{ ppm} \qquad \text{Eqn. 4.1.2-A}$$

Differences of ± 20 ppm are regarded as within a safe margin of error regarding formulae assignment.[7] The second criterion regards the outline shape of the peak distribution pattern or the peak 'shell-patterns' (that is the pattern of the line connecting the peaks). This should correlate between the predicted and actual peaks. In the cases of Zn_x clusters where $x \geq 4$, it may be observed that the peaks form an inner and outer 'shell'. These shell-patterns can be seen in section 2.3.3, pp. 97-99; the inner shell is created by the outline of the peaks between each of the 'outer-shell' peaks. The form of these two shell-patterns is, roughly, a skewed bell-shape in each case. The observation of such double shell-patterns in the mass spectral patterns of zinc complexes is further corroboration that the fragment is that of a multi-nuclear cluster with four or more zinc metal centres.

The final criterion in assessing the 'goodness of fit' is the ratio of peak intensities, within a peak cluster. These should be the same in the observed peaks as they are in the predicted peaks. However, it is sometimes found that the intensity of the peaks in the inner-shell may be enlarged due to multiplier gain or probe phenomena.[7] Caution is therefore required when applying this criterion.

---

7) Private communication with A. Taylor, mass spectrometer technician, Department of Chemistry, University of Edinburgh.

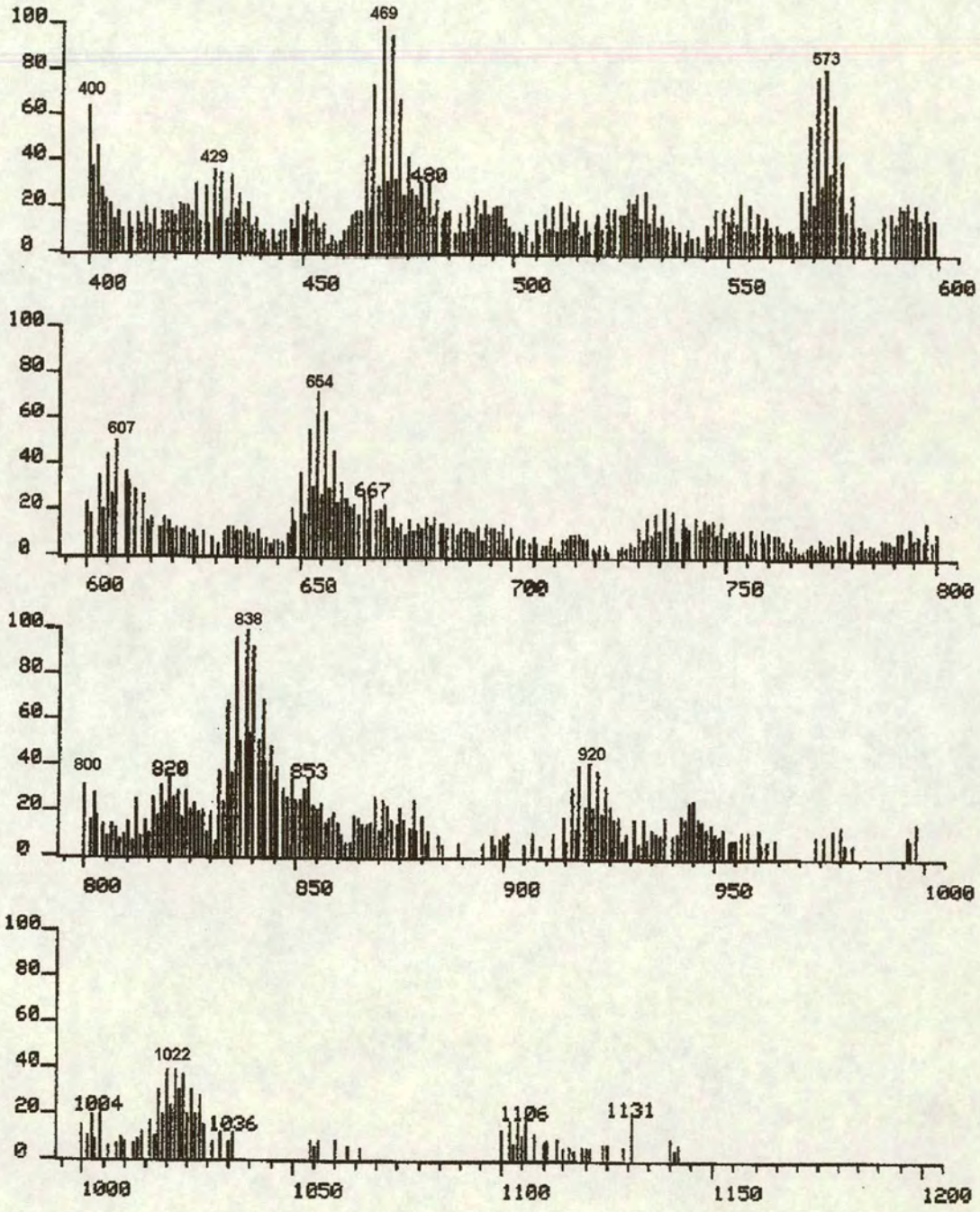

Figure 4.1.2-D FAB mass spectrum of $Zn_4O(OAc)_6$

Considering the observed peaks and assuming the formation of the species $Zn_8O_3(OAc)_{10}$ (m/z = 1161.48), the first peak would be expected at to appear at m/z = 1102 due to loss of acetate radical. However, this was not observed. The first actual peak observed with a sufficient degree of structure in its fragmentation pattern to corroborate its existence as a multi-nuclear zinc derivative occurred at m/z = 1022, and may be formulated as $[Zn_7O_2(O_2CCH_3)_9 + 1]^+$ for which m/z = 1022.06. In FAB mass spectroscopy it is not uncommon to find ions of charge M + 1, M + 2 (and even M + 3 in rare cases). This phenomenon is believed to be due to addition of protons, yet the m/z value for the ion is only altered in its mass, not in its charge. Such anomalous behaviour is commonly witnessed but not understood.[7] However, analysis of the accurate mass spectrum for this peak did not support this hypothesis.

In contrast, the next largest peak was successfully matched on studying the accurate mass spectrum. This peak occurred at m/z = 920 and was assigned to $[Zn_7O_3(O_2CCH_3)_7]^+$, which has m/z = 918.97 (see table 4.1.2-C for peak matches). The subsequent peak at m/z = 838 may be assigned to $[Zn_6O_2(O_2CCH_3)_7]^+$ (with m/z = 837.59), subsequent water loss yielding $[Zn_6O_2(O_2CCH_3)_7 - H_2O]^+$ which accounts for the peak observed at m/z = 819.58. The next sufficiently structured, prominent peak was observed at m/z = 654. This was assigned to the species $[Zn_5O_2(O_2CCH_3)_5]^+$ (m/z= 654.12), which may be a fragment of the ion $Zn_8O_3(OAc)_{10}$ or formed by the loss of the even-electron species $Zn(OAc)_2$ and an acetate radical CH_3COO from the hypothetical parent ion $Zn_6O_2(OAc)_8$. No feasible assignment could be formulated for the subsequent peak at m/z = 607.

Predicted peaks were calculated for the ions at m/z =654, 838, 920 and 1022. Of these, the assignments for the peaks at m/z = 654 and 920 were confirmed. The discrepancies in the degree of matching for the other two rendered them unacceptable as assignments.

For the ion at m/z = 920 the peak matching analysis is sufficient to confirm the assignment as due to a species of chemical formula $Zn_7C_{14}H_{21}O_{17}$. The actual

structural formulation, $[Zn_7O_3(O_2CCH_3)_7]^+$, may only be speculated at by chemical analogy to related materials.

$[Zn_7O_3(O_2CCH_3)_7]^+$ $Zn_7C_{14}H_{21}O_{17}$ (M_R = 918.97)		
Actual Mass	Predicted Mass	Deviation/ppm
912.59130	912.57537	-17.46
913.60119	913.57873	-24.58
914.59204	914.57427	-19.43
915.59148	915.57337	-19.78
916.57105	916.57117	0.13
917.58303	917.57227	-11.73
918.56064	918.56807	8.09
919.57934	919.56917	-11.06
920.55305	920.56497	12.95
921.56693	921.56807	1.24
922.53156	922.56387	35.02
923.55576	923.56497	9.97

Table 4.1.2-C MS peak matches for the fragment $[Zn_7O_3(O_2CCH_3)_7]^+$

$[Zn_5O_2(O_2CCH_3)_5]^+$ $Zn_5C_{10}H_{15}O_{12}$ (M_R = 654.12)		
Actual Mass	Predicted Mass	Deviation/ppm
646.69686	646.70185	7.72
647.74439	647.70521	-60.49
648.69450	648.69875	6.55
649.73396	649.69985	-52.5
650.69796	650.69765	-0.48
651.71464	651.69675	-27.45
652.69310	652.69255	-0.84
653.69371	653.69365	-0.09
654.68170	654.68945	11.84

Table 4.1.2-D MS peak matches for the fragment $[Zn_5O_2(O_2CCH_3)_5]^+$

For the ion at *m/z* =654 there are discrepancies with the 'fits' at *m/z* = 647.7, 649.7 and 651.7, however, the remainder of the peaks show good agreement for the assignment $Zn_5C_{10}H_{15}O_{12}$ for which the structure $[Zn_5O_2(O_2CCH_3)_5]^+$ is proposed. A summary of the final proposed assignments is given in table 4.1.2-E, below.

Observed mass	Assignment
44	$[CO_2]^+$
389	$[Zn_3O(OAc)_3]^+$
429	$[Zn_4O_2(O_2CCH_3)_2(OH)]^+$
469	$[Zn_4O_2(O_2CCH_3)_3]^+$
573	$[Zn_4O(OCCH_3)_5]^+$
607	unassigned
654	$[Zn_5O_2(O_2CCH_3)_5]^+$
820	$[Zn_6O_2(O_2CCH_3)_7 - H_2O]^+$
838	$[Zn_6O_2(O_2CCH_3)_7]^+$
920	$[Zn_7O_3(O_2CCH_3)_7]^+$
1022	$[Zn_7O_2(O_2CCH_3)_9 + 1]^+$

Table 4.1.2-E The major peaks of the FAB mass spectrum of $Zn_4O(OAc)_6$

Figures 4.1.2-E and 4.1.2-F show the graphical results of the above peak-matching analyses.

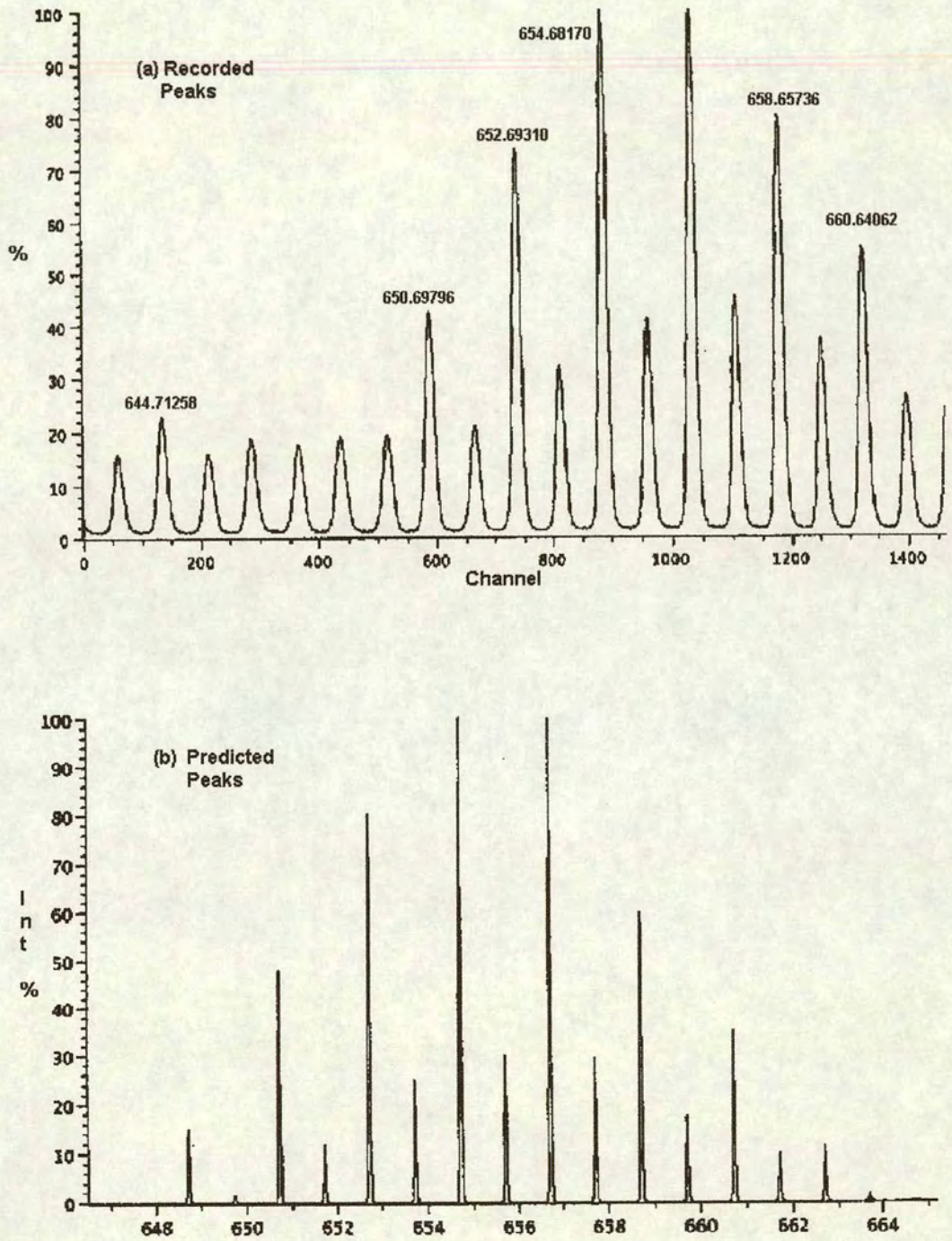

Figure 4.1.2-E Accurate mass FAB mass spectrum for the fragment $[Zn_5O_2(O_2CCH_3)_5]^+$ *m/z* = 654 (a) actual peaks, (b) predicted peaks

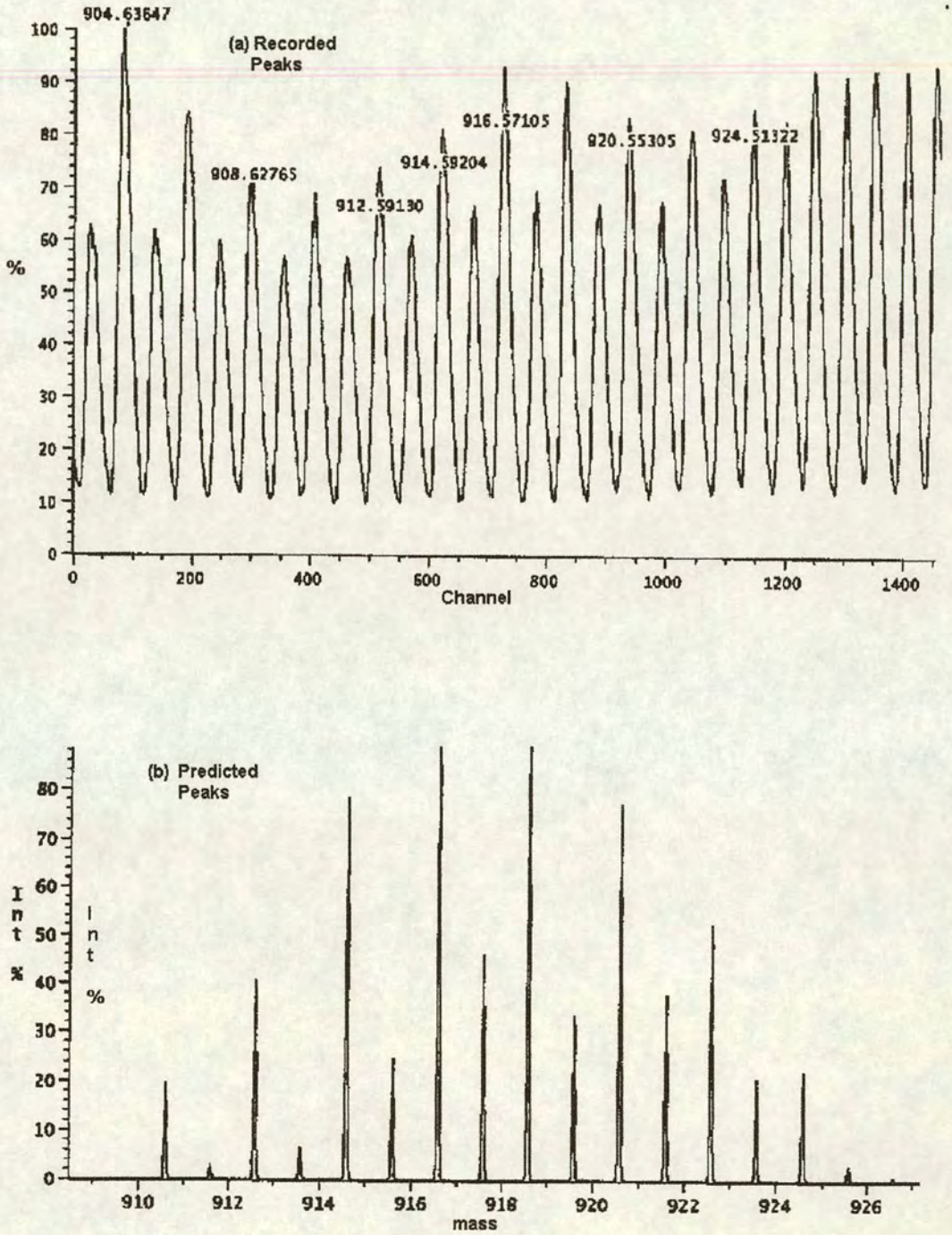

Figure 4.1.2-F Accurate mass FAB mass spectrum for the fragment $[Zn_7O_3(O_2CCH_3)_7]^+$ *m/z* = 920 (a) actual peaks, (b) predicted peaks

4.1.2(iv) X-Ray Powder Diffraction Data for $Zn_4O(O_2CCH_3)_6$

The XRPD pattern for $Zn_4O(OAc)_6$ has not previously been reported. It is included below, since it was frequently used as a means of corroborating the presence of this material, especially when intractably mixed products were obtained.

2θ	d	Relative peak height	Peak height order
9.72	9.1	100	1st
12.17	7.27	26	4th
18.27	4.86	29.7	3rd
19.02	4.67	41.7	2nd
21.97	4.05	24.5	5th
23.97	3.71	21.9	8th
26.82	3.32	20.3	9th
32.47	2.76	17.7	10th
32.95	2.72	22.9	7th
36.52	2.46	23.4	6th

Table 4.1.2-F XRPD Data for $Zn_4O(OAc)_6$

4.1.3 New Materials Found as Result of Preparation of $Zn_4O(O_2CCH_3)_6$

As described earlier, hitherto unreported materials were observed in the preparation of $Zn_4O(OAc)_6$. These are referred to as Z2, Z8, ZY, ZL, and ZN and are discussed below.

The attempted preparation of these materials was repeated more than thirty times. In only about half of these experiments was there sufficient of the products ZN, Z2 and Z8 formed to perform IR analysis. In only half these cases again were these products isolated from contaminants such as $Zn(OAc)_2.2H_2O$ and $Zn_4O(OAc)_6$. In those cases where the patches of Z2 and Z8 collected in isolated regions of the 'S'-tube they usually consisted of entirely amorphous material, often barely enough to run an IR spectrum and one or two mass spectral analyses. However, on three occasions, crystals of sufficient quality to be possible candidates for X-ray crystal structure determination, were found amidst the amorphous material. Disappointingly, none of the samples obtained diffracted strongly enough to obtain a complete crystal structure. Nevertheless, it was possible to obtain the unit cell dimensions, from which it was ascertained that these materials were indeed novel.

4.1.3(i) Analysis of Z2

The infrared spectrum of the amorphous, white solid Z2, is shown below. No useful mass spectral data could be obtained from this material. Despite repeated attempts to produce crystals of this material the best result achieved was a mere 8 reflections after 20 hours data collection. From this the unit cell was established. Z2 crystallizes in the orthorhombic form with cell dimensions: 3.8, 7.1 and 11.9Å, V = 321.06Å^3 and that it has a novel structure.

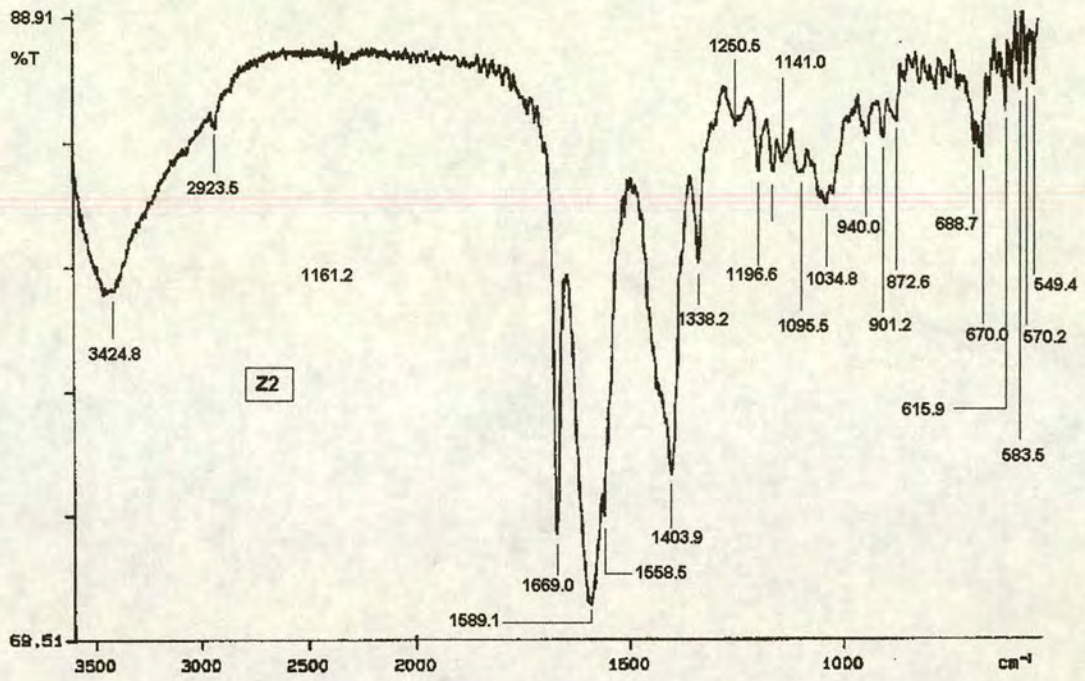

Figure 4.1.3-A Infrared spectrum of Z2 recorded as KBr pressed disk

Interpretation of the crystallographic data provides some direction regarding the nature of Z2. A reasonable estimate of the total number of non-hydrogen atoms in the structure may be obtained by dividing the volume (321.06 $Å^3$ in this case) by 18 and allowing for the number of molecules in the unit cell (Z). For an orthorhombic crystal $a \neq b \neq c$, $\alpha = \beta = \gamma = 90^{\circ}$ and Z = 1, giving $321 \div 18 \approx 17.8$. From this it may be inferred that there are *ca.* 18 non-hydrogen atoms within the unit cell. It is sensible to propose that the structure will consist of zinc atoms and acetate ligands or derivatives thereof. An acetate ligand comprises 4 non-hydrogen atoms; accordingly there are predicted to be no more than four acetate groups present ($18 \div 4 = 4.5$). If this is the case, there would be two remaining atoms, which could be accounted for by zinc. This would accord with the assignment $Zn_2(CH_3CO_2)_4$. Examining the plausibility of this assignment, one may consider the existence of analogous M^{2+} materials. In its +2 oxidation state, copper forms $Cu_2(OAc)_4$ with its renowned 'lantern' structure. Trivalent boron forms $B_2O(OAc)_4$ which has effectively a 'half-lantern' structure with a central μ_2 oxygen (see section 2.3.1). Furthermore, zinc

forms $Zn_2(OAc)_3(OCH_3)$.[1] Structurally this lacks a fourth bidentate ligand and is therefore prevented from forming the 'lantern' type structure of copper (II) acetate, instead of forming a three-dimensional polymeric structure. From the above, one may suggest that $Zn_2(OAc)_4$ is also a plausible chemical formula for Z2 and that, by analogy, it may also have a 'lantern' structure.

In its infrared spectrum very strong carbonyl stretches were observed with bands occurring at 1589.7 cm^{-1} (νCOO_{AS}) and 1403.9 cm^{-1} (νCOO_S), giving a high $\Delta\nu$ value of 185.8 cm^{-1}. Such a high value of $\Delta\nu$ is suggestive of a unidentate acetate bonding. If the structure does consist of a 'lantern' arrangement then there would be bridging acetate groups present. This evidence therefore appears to counter the suggestion that it comprises a 'lantern' structure. However, copper (II) acetate monohydrate,[2] $[Cu(OAc).H_2O]_2$, itself has a near identical $\Delta\nu$ value to that of Z2, having νCOO_{AS} = 1603cm^{-1}, νCOO_S = 1418cm^{-1} and $\Delta\nu$ = 185cm^{-1}. The $\Delta\nu$ value for anhydrous copper (II) acetate,[3] $[Cu(OAc)]_2$, is also quite high having: νCOO_{AS} = 1591cm^{-1}, νCOO_S = 1420cm^{-1} and $\Delta\nu$ = 171cm^{-1}. This demonstrates, once again, the fallibility of assigning bonding modes of carboxylates on the basis of $\Delta\nu$ values alone and also serves to further support the proposition that Z2 possesses a 'lantern' structure.

In addition to the above infrared features there is also a very sharp, strong absorption at 1669 cm^{-1} which is unusually high for any form of carboxylate ligand, although it is in the correct region for a carbonyl group. A similar feature appears in the infrared spectrum of Z8 at 1667.8 cm^{-1}. There is also a small, sharp shoulder at 1558.5 cm^{-1} on the $\nu(COO)_{AS}$ band at 1589.7 cm^{-1}. This may be $Zn(OAc)_2.2H_2O$ impurity which has a strong $\nu(COO)_{AS}$ at 1558.3 cm^{-1} (see Fig. 4.1.1-A). Although, $Zn_2(OAc)_3(OCH_3)$[1] shows a strong absorption at 1557cm^{-1} (in addition to bands at

---

1) C. D. Chandler, G. D. Fallon and B. O. West, "Synthesis and Molecular Structure of $[Zn_2(CH_3COO)_3(OCH_3)]$", *Polyhedron*, 1993, **12**, No. 16, 2001-2004.
2) K. Nakamoto, Y. Morimoto and A. E. Martell, *J. Am. Chem. Soc.*, 1961, **83**, 4528.
3) G. Costa, E. Pauluzzi and A. Puxeddu, *Gazz. Chim. Ital.*, 1957, **87**, 885.

1604 and 1542cm^{-1} in the ν_{AS} region and at 1445, 1417 and 1405cm^{-1} in the ν_S region) and so it may still be a genuine feature of Z2.

From the data obtained it was not possible to make a clear structural assignment. However, there is a good deal of evidence to support the proposition that it is $Zn_2(CH_3CO_2)_4$ and has a 'lantern' structure.

4.1.3(ii) Analysis of Z8

The FAB mass spectrum of Z8 (Fig. 4.1.3-B) shows the characteristic peaks of $[Zn_3O(OAc)_3]^+$ at *m/z* = 389 and $[Zn_4O(OAc)_5]^+$ at *m/z* = 574. These peaks are normally associated with the presence of $Zn(OAc)_2$ or $Zn_4O(OAc)_6$. However, comparison of their infrared spectra (Figs. 4.1.1-A and 4.1.2-A respectively) with that of Z8, Fig. 4.1.3-C, shows that it is clearly neither of these.

In the infrared spectrum of Z8, strong, sharp absorptions in the carbonyl region were observed at 1667.8, 1606.5 and 1595.0cm^{-1} in the ν_{AS} region and at 1393.7 cm^{-1} in the ν_S region. These values give $\Delta\nu$ = 212.8cm^{-1} (using ν_{AS} = 1606.5cm^{-1} and ν_S = 1393.7 cm^{-1}). As with Z2 this value is rather high, but not unheard of. For example, $Cu_2(pdp)_2(BrCH_2CO_2)_4$[4] has: νCOO_{AS} = 1630cm^{-1}, νCOO_S = 1418cm^{-1} and $\Delta\nu$ = 212cm^{-1} (where pdp = 1-phenyl-2,3-dimethyl-5-pyrazolone). Medium strength, low-frequency vibrations were also observed at 526.2 and 509.7 cm^{-1}. From this it is proposed that the structure comprises a Zn_xO_y framework, as such metal framework vibrations occur in this region.

The X-ray crystallographic data indicates that the material crystallizes in the monoclinic P space-group with sides a = 14.07, b = 7.07 and c = 38.6Å, hence, V = 3823.9 Å; from which it is estimated that there are 212 non-hydrogen atoms in the unit cell. Since the crystal is monoclinic, Z = 4 and therefore there would be 212 ÷ 4 = 53 non-hydrogen atoms in the molecule. From the above evidence and comparison

4) M. Melník, *Finn. Chem. Lett.*, 1974, 142.

with beryllium analogues, the tentative assignment $Zn_8O_3(OAc)_{10}$ is proposed. This contains 51 non-hydrogen atoms.

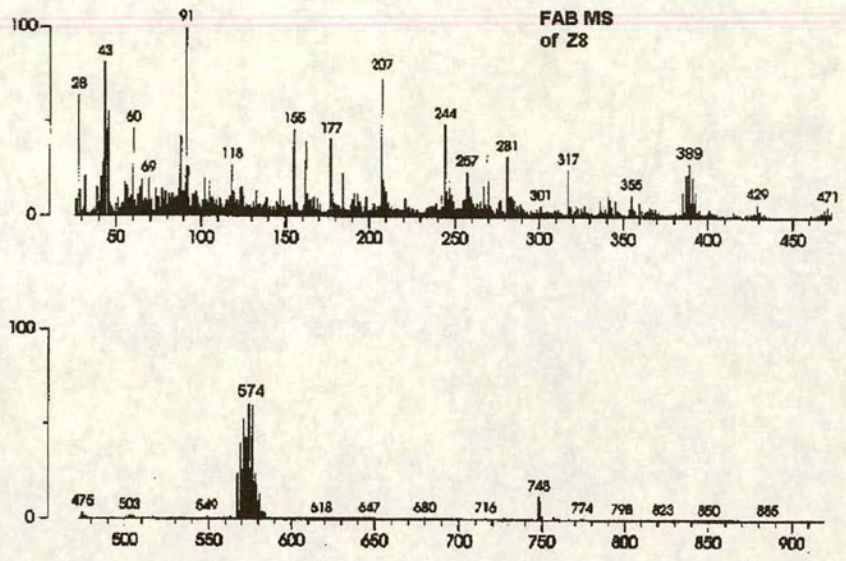

Figure 4.1.3-B FAB mass spectrum of Z8

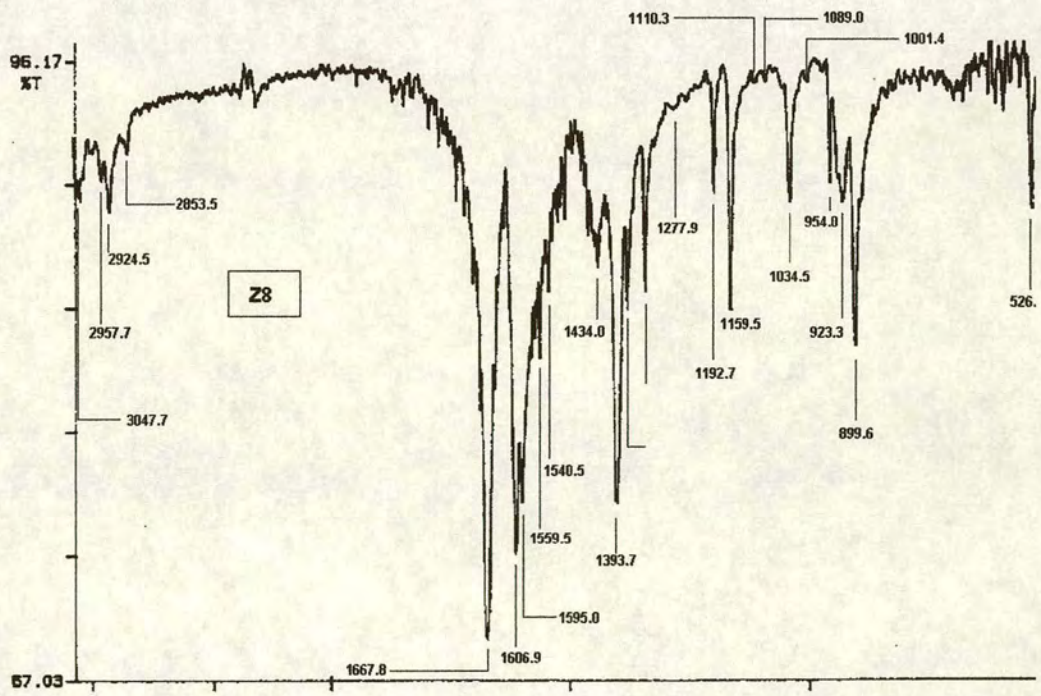

Figure 4.1.3-C Infrared spectrum of Z8

4.1.3(iii) Analysis of ZY

ZY is a yellow powder. It is known that ZnO forms a yellow powder upon heating. However, ZnO regains its white colour upon cooling again, whereas ZY did not, it remained yellow. Infrared and mass spectral analysis of ZY gave an identical spectra to $Zn_4O(OAc)_6$. This assignment was confirmed by elemental analysis. Insufficient sample could be collected for X-ray powder analysis. It is curious that this material should be yellow. It has been pointed out that ZnO and $Zn_4O(OAc)_6$ have similar Zn-O bond distances (section 2.3.3) and, consequently, certain similarities in their UV spectra. Thus, the observed colour change of $Zn_4O(OAc)_6$ may be due to effects similar to those observed for ZnO (see section 2.4.1). However, this material kept its colour on cooling, which suggests that a permanent structural alteration must have occurred if this effect is the result of a band gap variation due to structural changes. Finally, Goldschmied and Rae[5] have observed that the isomorphous incorporation of a small amount of Co^{2+} in anhydrous Zn(II) acetate, propionate and butyrate gave a blue colour; which suggests that the Zn atoms in these compounds have a tetrahedral coordination. Another explanation is, therefore, that the colour change in $Zn_4O(OAc)_6$ is due to the incorporation of trace metal ions from some part of the apparatus. Since this product, Z2, was observed in all the $Zn(OAc)_2$ sublimation reactions the contaminant ion would have to have been ubiquitous, perhaps present in the glassware used for the experiments.

4.1.3(iv) Analysis of ZL

On allowing the liquid nitrogen trap to warm to room temperature the three coloured fractions present merged to form a clear yellow/orange liquid (about 0.25mL was normally collected). The mass spectrum of this liquid gave no useful information. The infrared spectrum of ZL shows an absorption at 1710cm^{-1} indicating the presence of a carbonyl group. Aldehyde absorptions usually occur in the region 1720-1740cm^{-1} and esters in the region 1735-1750cm^{-1}; this suggests that it is due to a ketone or a carboxylic acid functional group. The odour of the material was

5) E. Goldschmied and A. D. Rae, "The Crystal Structure of Zn^{II} Propionate $(C_6H_{10}O_4Zn)_n$", Acta. Cryst., 1977, **B33**, 2117-2120.

ketonic in character. There are several absorptions in the 900-1300cm^{-1} region, suggesting the presence of C-O group(s). Absorptions in the 2800-3000cm^{-1} region suggest the presence of alkyl groups, whilst those between 300-3300cm^{-1} suggest the presence of alkene groups. The strong broad absorption at 3467.3cm^{-1} indicates the presence of OH groups. Due to the high volatility of the sample, elemental analysis could not be performed with any acceptable degree of accuracy. Consequently, no assignment was made for this material.

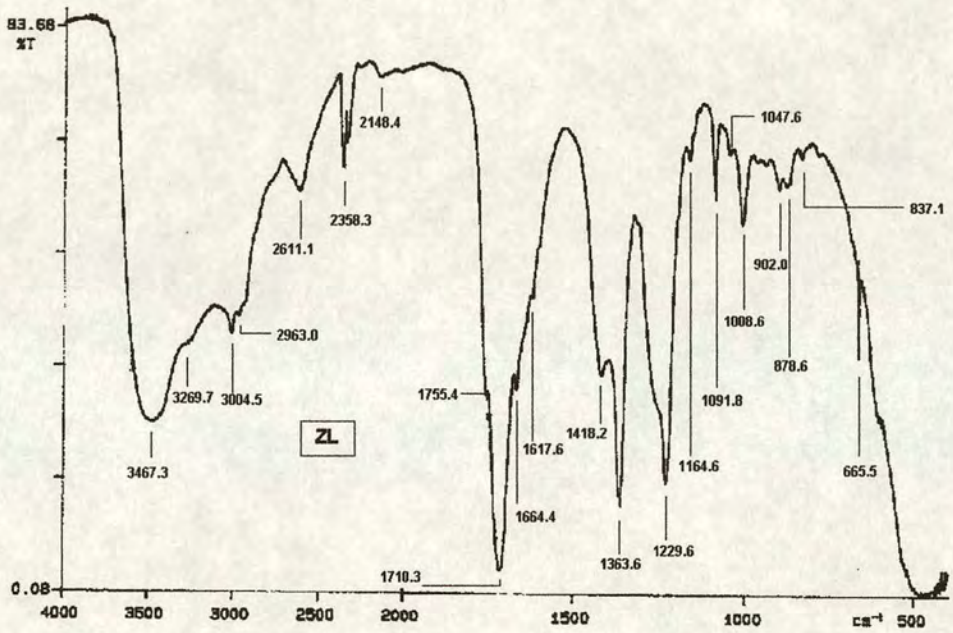

Figure 4.1.3-D Infrared spectrum of ZL

4.1.3(v) Analysis of ZN

The orange, roughly needle-shaped solid collected was found to smell the same as ZL. The infrared spectrum of ZN showed peaks common to $Zn_4O(OAc)_6$ and ZL. From this it was inferred that the needles were composed of $Zn_4O(OAc)_6$ coated with the volatile liquid ZL. On standing in air for several hours the needles gradually lost their colour and formed an amorphous pale yellow solid. Thus, it is most likely that

ZN is nothing more than $Zn_4O(OAc)_6$ coated in a layer of ZL, which evaporates on standing to leave a sample of yellow $Zn_4O(OAc)_6$ This material has been described previously in the section on ZL.

Conclusions

The thermal processes involved in the sublimation of $Zn(OAc)_2$ have been re-examined and it has been proposed that multiple reaction pathways are possible. The overall pathway is, to some extent, determined by the physical parameters of the sublimation apparatus, since these affect the diffusion rate of out-going volatiles. This, in turn, affects the preferred reaction pathway. This proposal unifies the previously contradictory evidence of other workers in this area.

The sublimation of $Zn(OAc)_2$ leads to the formation of products previously unnoticed by other researchers in this area. There is good evidence to support the assertion that these are $Zn_2(CH_3CO_2)_4$ and $Zn_8O_3(OAc)_{10}$. In addition, a yellow form of $Zn_4O(OAc)_6$ was found and a mixture of yellow/orange ketonic liquids was formed.

Future work

The use of *in vacuo* X-ray studies on a 'hot-plate' arrangement would allow the enhanced study of the sublimation of $Zn(OAc)_2$ and a great understanding of the decomposition pathways occurring during the process.

Low frequency infrared spectroscopic studies on Z2 and Z8 would yield more structural information should it not be possible to obtain adequate crystals for X-ray structural determination. However, time allowing, the repetition of the sublimation of $Zn(OAc)_2$, under appropriate conditions, should eventually yield suitable crystals.

Wet routes to Z8 may also be attempted, such as those used by Sipachev and Grigor'ev for the preparation of $Be_6O_2(OAc)_6$.[6]

---

6) A. I. Grigor'ev, V. A. Sipachev and A. V. Novoselova, "The Polymorphism of Beryllium Dioxide Acetate $Be_6O_2(OCOCH_3)_8$ ", *Russ. J. Inorg. Chem.*, 1972, **17(2)**, 297-298 and references therein.

Preparation of sufficient quantity of ZY would allow XRPD which may shed light onto the nature of its yellow coloration.

Finally, the use of GCMS (this facility was not available during the course of the research) to study ZL should resolve the nature of its contents.

4.1.4 Analysis of Hydrated Zinc(II) Propionate, $Zn(O_2C_2H_5)_2.2H_2O$

Preparation of this material led to the formation of a microcrystalline white solid. Several crystals were extracted over the course of the repeated preparations. Unfortunately, none of these was of sufficient quality to obtain any X-ray crystallographic information. The melting point was measured to be 201-202^{O}C (cf. that obtained by Gordon and Silver[1] 200-202^{O}C).

4.1.4(i) CHN and AAS Data for $Zn(O_2C_2H_5)_2.2H_2O$

Bassi *et al.*[2] claim to have prepared monohydrated zinc propionate, $Zn(C_2H_5COO)_2.H_2O$, by the stepwise addition of zinc (II) carbonate to propionic acid until effervescence ceased. Their analytical data are reproduced in table 4.1.4-A.

$Zn(O_2CC_2H_5)_2.H_2O$ = $C_6H_{12}O_5Zn$			
M_R = 229.54	C	H	Zn
Calculated	31.4	4.3	28.5
Found	31.3	4.5	28.6
% Error	0.32	4.65	0.35

Table 4.1.4-A Analytical Data for Preparation of Hydrated Zinc Propionate by Bassi *et al.*[14]

There are inconsistencies with the above data. Calculation of percentage elemental content for monohydrated zinc(II) propionate, $Zn(O_2CC_2H_5)2.H_2O$, shows that the value for hydrogen should be 5.3%, not 4.3% as stated in their paper. Using this value gives a percentage error of 15.1% which is extremely high, even for hydrogen (which usually suffers from decreased accuracy over other elements). This casts doubt upon the assignment of the molecular formula as a monohydrate. The elemental analysis obtained by this author (table 4.1.4-B) shows that the material formed is in fact a dihydrate, having the molecular formula $Zn(O_2CCH_2CH_3)_2.2H_2O$.

---

1) R. M. Gordon and H. B. Silver, "Preparation and properties of tetrazinc μ_4-oxohexa-μ-carboxylates (basic zinc carboxylates)", *Can. J. Chem.* ,1983, **61**, 1218-1221.

2) P. S. Bassi, H. S. Jamwal and B. S. Randhawa, "Comparative Study of the Thermal Analysis of Some Transition Metal(II) Propionates. Part 1", *Thermochimica Acta*, 1983, **71**, 15-24.

$Zn(O_2CC_2H_5)_2.2H_2O = C_6H_{14}O_6Zn$			$M_{AC} = 246.008183758$	
$M_R = 247.55$	C	H	N	Zn
Calculated	29.11	5.70	0.00	26.41
Found	29.72	5.47	0.00	26.65
% Error	2.1	3.8	0.00	0.47

Table 4.1.4-B Analytical Data for zinc propionate dihydrate obtained by this author

4.1.4(ii) Infrared Data for $Zn(O_2CC_2H_5)_2.2H_2O$

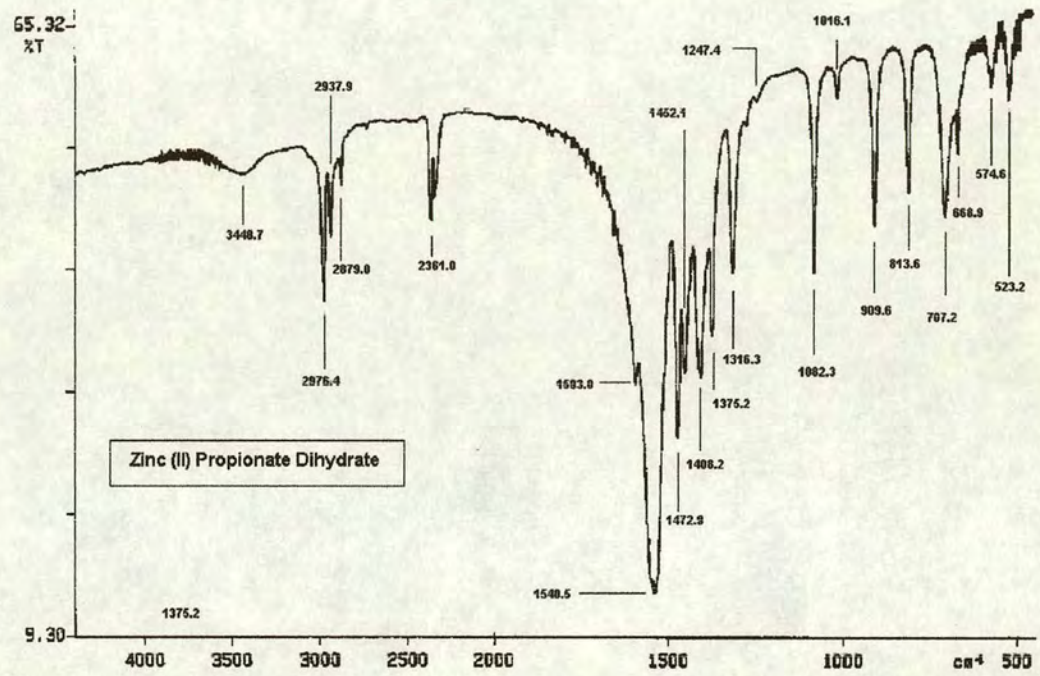

Figure 4.1.4-A Infrared data for zinc propionate dihydrate

4.1.4(iii) Mass Spectral Data for $Zn(O_2CC_2H_5)_2.2H_2O$

The FAB mass spectrum showed no substantial peaks below *m/z* = 400. Peaks showing structure indicating that they were zinc cluster fragments were found at *m/z* = 431, 513 and 725. These were assigned to $[Zn_3O(O_2CC_2H_5)_3]^+$, $[Zn_4O_2(O_2CC_2H_5)_3]^+$ and $[Zn_5O(O_2CC_2H_5)_5]^+$ respectively. They are predicted to have been formed by the same reaction sequences as described for the analogous acetates. Confirmation of the assigned formulae was obtained through accurate peak matching.

4.1.5 Analysis of Basic Zinc(II) Propionate, $Zn_4O(O_2C_2H_5)_6$

Formation of the sublimate $Zn_4O(OPp)_6$ did not result in the formation of additional side-products as occurred with the sublimation of $Zn(OAc)_2$. Sublimation was observed at *ca.* 180°C at which point the $Zn(OPp)_2$ began to melt and then boiled rapidly as a viscous liquid at *ca.* 190°C. A 3cm wide band of amorphous, white sublimate ($Zn_4O(OPp)_6$) condensed approximately two-thirds the way up the tube. Immediately below this was a fine ring (*ca.* 2mm wide) of *ca.* 20 transparent crystals of the basic propionate. In the base of the apparatus a grey-brown residue was formed. No other products were observed, in contrast to the large number of additional products found in the vacuum sublimation of $Zn(OAc)_2.2H_2O$.

4.1.5(i) CHN and AAS Data for $Zn_4O(O_2C_2H_5)_6$

$Zn_4O(O_2CCH_2CH_3)_6$ = $C_{18}H_{30}O_{13}Zn_4$			M_{AC} = 709.885223030	
M_R = 715.95	C	H	N	Zn
Calculated	30.20	4.22	0.00	36.63
Found	29.87	4.31	0.00	36.66
% Error	1.09	2.13	0.00	0.08

Table 4.1.5-A CHN and AAS analysis of $Zn_4O(O_2CCH_2CH_3)_6$

4.1.5(ii) Infrared Data for $Zn_4O(O_2C_2H_5)_6$

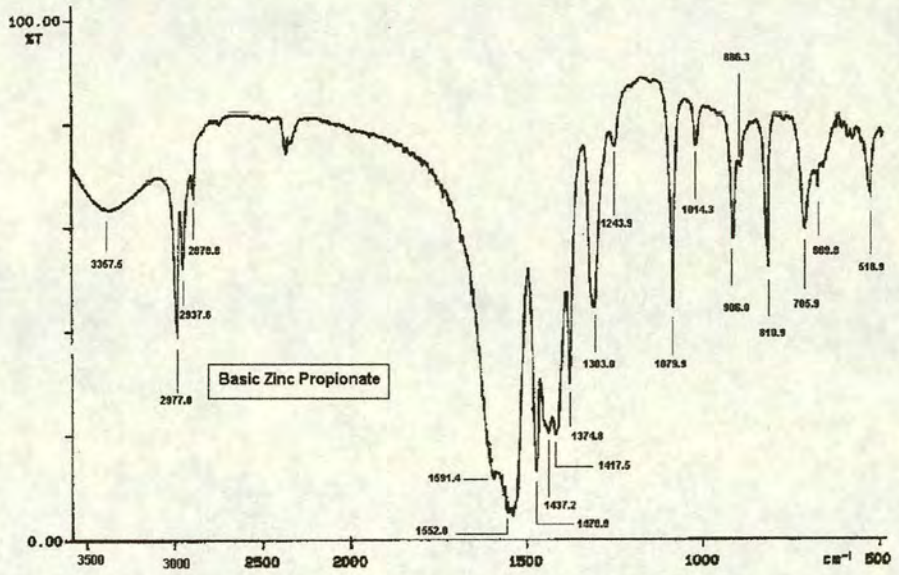

Figure 4.1.5-A Infrared data for basic zinc propionate $Zn_4O(OPp)_6$

4.1.5(iii) Mass Spectral Data for $Zn_4O(O_2C_2H_5)_6$

The EI mass spectrum for $Zn_4O(OPp)_6$ is shown in Fig. 4.1.5-B. The fragmentation pattern is analogous to that of the EI mass spectrum of $Zn_4O(OAc)_6$; the peaks at *m/z* = 431 and 643 being due to the ions $[Zn_3O(O_2CC_2H_5)_3]^+$ and $[Zn_4O(O_2CC_2H_5)_5]^+$, respectively. In the FAB mass spectrum additional peaks were observed at *m/z* = 936 and 723. These were assigned to $[Zn_6O_2(O_2CC_2H_5)_7]^+$ and $[Zn_5O_2(O_2CC_2H_5)_5]^+$, respectively, and confirmed by exact peak matching (see tables 4.1.5-B and 4.1.5-C respectively).

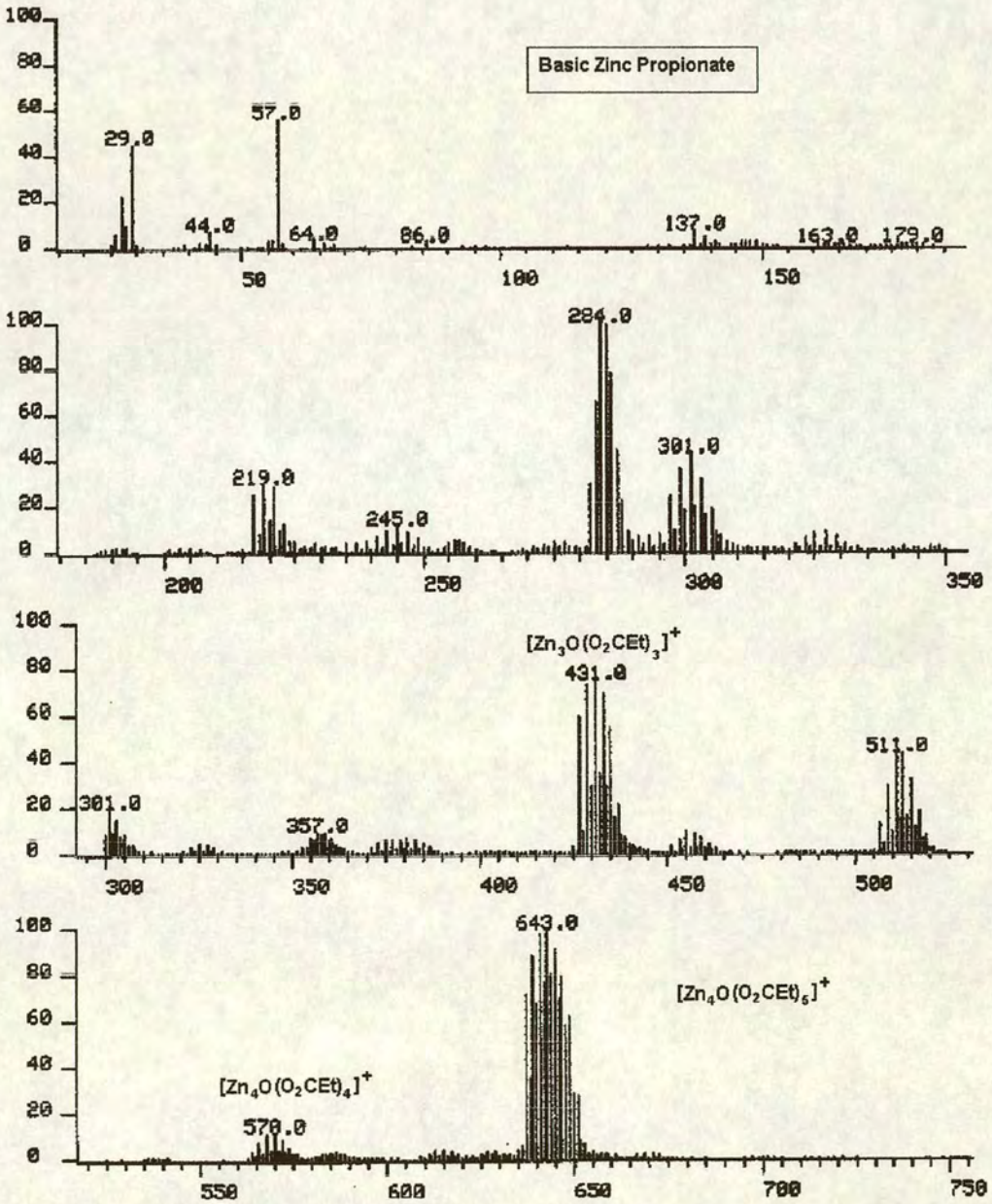

Figure 4.1.5-B EI mass spectrum for basic zinc propionate $Zn_4O(OPp)_6$

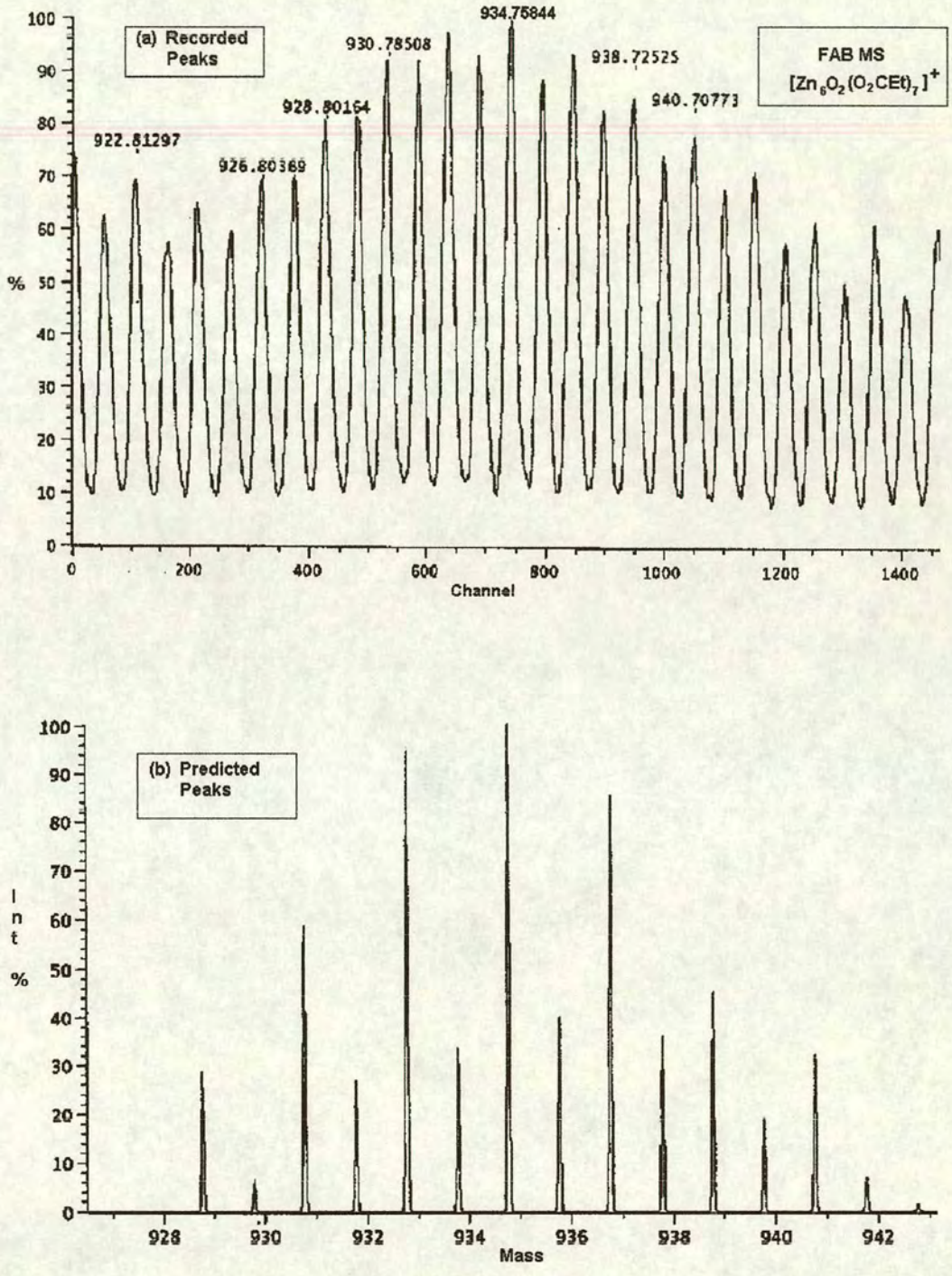

Figure 4.1.5-C Accurate mass FAB mass spectrum for the fragment $[Zn_6O_2(O_2CC_2H_5)_7]^+$ *m/z* = 934 (a) actual peaks, (b) predicted peaks

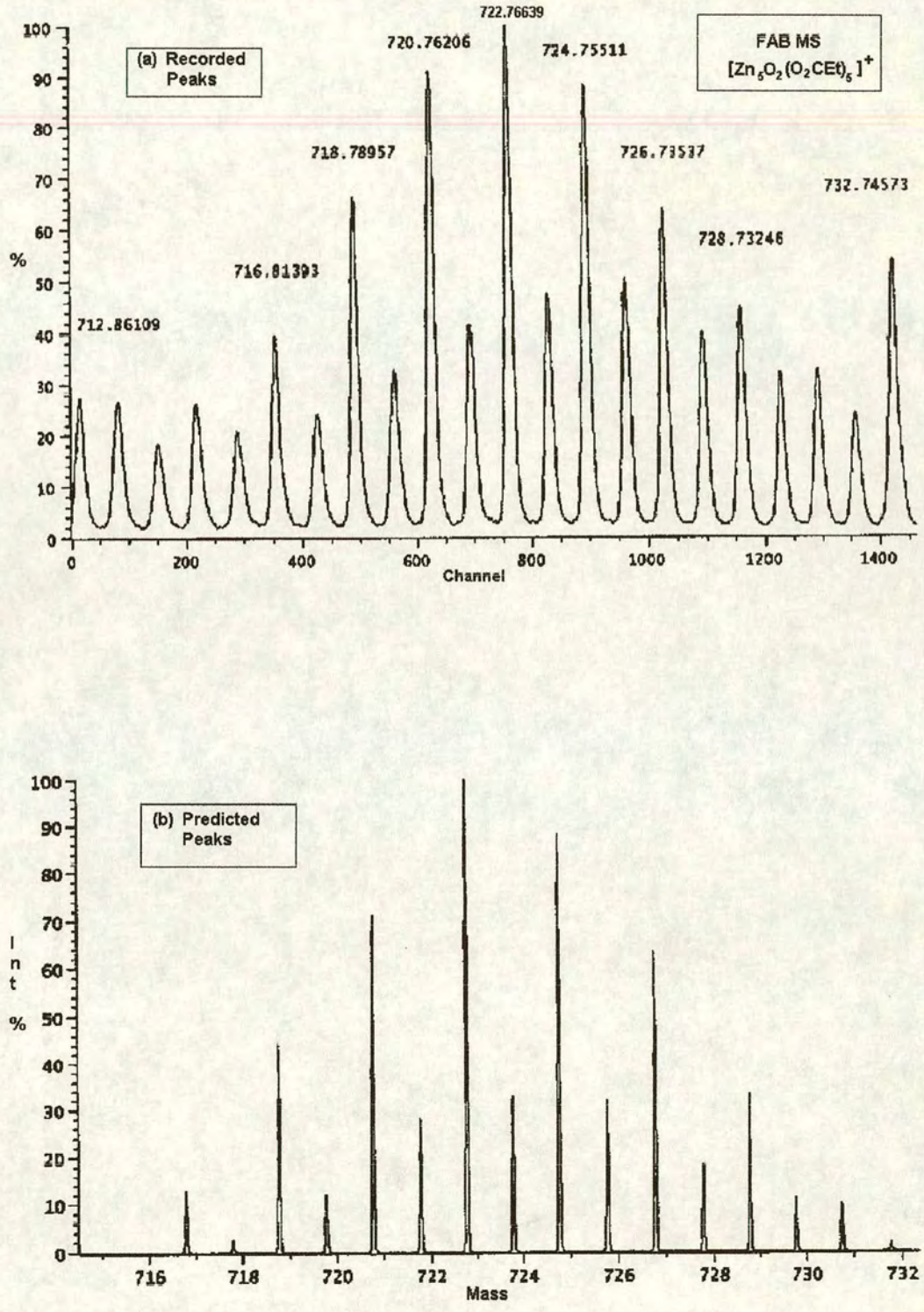

Figure 4.1.5-D Accurate mass FAB mass spectrum for the fragment $[Zn_5O_2(O_2CC_2H_5)_5]^+$ *m/z* = 724 (a) actual peaks, (b) predicted peaks

$[Zn_6O_2(O_2CCH_2CH_3)_7]^+$ $Zn_6C_{21}H_{35}O_{16}$ (M_R = 935.78)		
Actual Mass	Predicted Mass	Deviation/ppm
932.77957	932.75981	-21.18
933.79272	933.75891	-36.21
934.75844	934.75671	-1.85
935.76809	935.75781	-10.99
936.74255	936.75361	11.81
937.7526	937.75471	2.25
938.72525	938.75251	29.04
939.73485	939.75361	19.96

Table 4.1.5-B MS peak matches for the fragment $[Zn_6O_2(O_2CCH_2CH_3)_7]^+$

$[Zn_5O_2(O_2CCH_2CH_3)_5]^+$ $Zn_5C_{15}H_{25}O_{12}$ (M_R = 724.26)		
Actual Mass	Predicted Mass	Deviation/ppm
718.78957	718.77700	-17.49
719.80519	719.78036	-34.5
720.76206	720.77390	16.43
721.79918	721.77500	-33.5
722.76639	722.77280	8.87
723.78969	723.77616	-18.69
724.75511	724.76970	20.13
725.76347	725.77080	10.1

Table 4.1.5-C MS peak matches for the fragment $[Zn_5O_2(O_2CCH_2CH_3)_5]^+$

4.1.5(iv) X-Ray Powder Diffraction Data for $Zn_4O(O_2CCH_3)_6$

2θ	d	Relative peak height	Peak height order
9.37	9.44	16.7	7th
19.17	4.63	42.4	4th
21.1	4.21	20.6	8th
21.47	4.14	19.8	10th
23.34	3.81	100	1st
26.67	3.34	20.2	9th
36.52	2.46	17.5	6th
37.57	2.39	25.7	2nd
38.77	2.32	39.7	3rd
44.47	2.04	22.2	5th

Table 4.1.5-D X-ray powder diffraction data for $Zn_4O(OPp)_6$

4.1.5(v) X-Ray Crystal Structure Data for $Zn_4O(O_2CCH_3)_6$

The structure of the basic propionate was determined using X-ray diffractometer data collected at 293 K. The compound crystallizes in the monoclinic space group $P2_1/n$ with a = 16.945(5), b = 9.762(3) and c = 19.053(5) Å, $\alpha = \gamma = 90^O$ and β = 116.149(19)^O, V = 2829 Å^3 and Z = 4. Anisotropic refinement gave R_1 = 0.1381, wR_2 = 0.2939 and S = 0.247 for 354 reflections corrected for absorption. The $Zn_4O(O_2CCH_2CH_3)_6$ molecule has a central oxygen atom which is tetrahedrally coordinated to four zinc atoms. Each zinc atom is tetrahedrally surrounded by four oxygen atoms: three from different bidentate propanato groups [Zn-O = 1.92(8)Å], with the fourth one being the central oxygen [1.93(7)Å].

The tables of crystal data are given in appendix A 5.1.4-A.

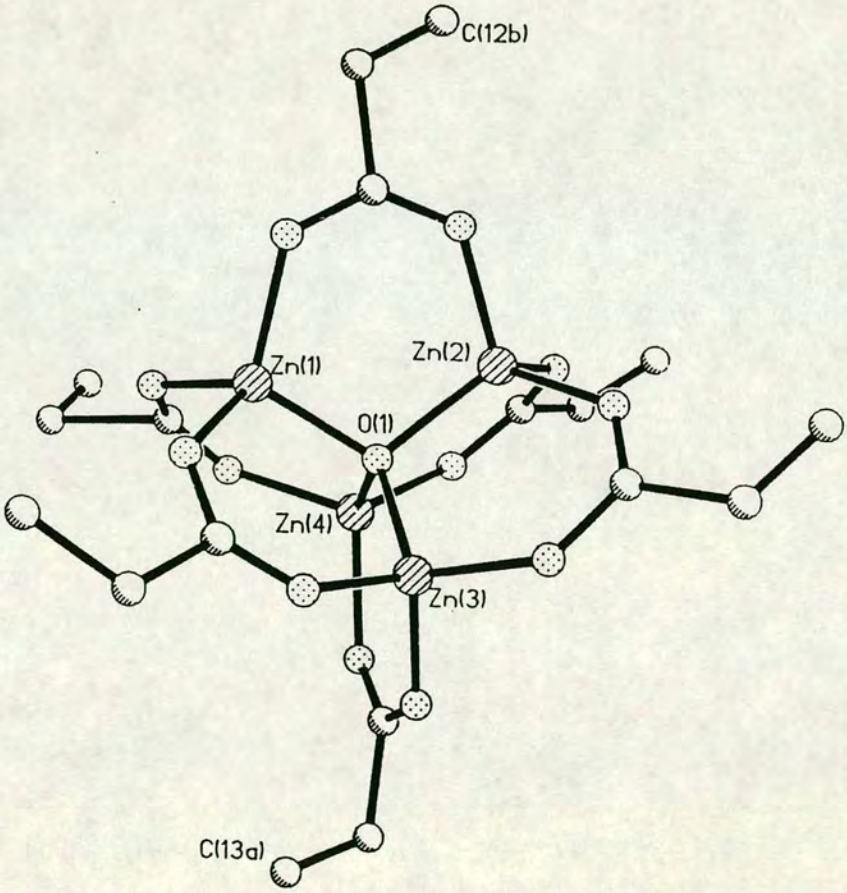

Figure 4.1.5-E Schematic representation of $Zn_4O(O_2CCH_2CH_3)_6$; hexakis[μ-(propanato-O:O')]-$μ_4$-oxotetrazinc

Conclusions

The preparation of the neutral propionate of zinc (II) leads to the formation of the dihydrated salt, $Zn(O_2CCH_2CH_3)_2 2H_2O$ contrary to previous reports which claim that the preparation leads to the formation of the monohydrated salt. Sublimation of this neutral salt yields $Zn_4O(OPp)_6$ in fairly low yield (55%). The crystal structure and X-ray powder diffraction patterns have not previously been reported and are given here. Evidence of the presence of higher nuclearity clusters, analogous to those formed by $Zn_4O(OAc)_6$, was observed in the mass spectral data. Exact peak matching was used to assign the peaks to the fragments $[Zn_6O_2(O_2CCH_2CH_3)_7]^+$ and $[Zn_5O_2(O_2CCH_2CH_3)_5]^+$. However, there was no evidence of the formation of additional higher nuclearity species in the sublimation apparatus.

Future work

In spite of various attempts to recrystallize the neutral salt, $Zn(OPp)_2.2H_2O$, to provide crystals of adequate quality for X-ray crystallographic analysis, none were grown forthcoming. Other methods should be considered in an attempt to obtain suitable crystals, in order to obtain the crystal structure of this materail and demonstrate unambiguously its structure as a dihydrate.

Experiments to examine the possibility of generating higher nuclearity clusters of zinc (II) propionate should be conducted.

4.1.6 Analysis of Zinc (II) Methoxide, $Zn(OMe)_2$

Twelve attempts were made to prepare zinc (II) methoxide. Standard Schlenk techniques were carried out under flowing nitrogen. The entire preparation from drying solvents and starting materials to collecting the final product took three to four days.

4.1.6(i) CHN and AAS Data for $Zn(OCH_3)_2$

$Zn(OCH_3)_2 = C_2H_6O_2Zn$			$M_{AC} = 125.965924902$	
$M_R = 127.45$	C	H	Cl	Zn
Calculated	18.85	4.75	0.00	51.30
Found	18.12	4.53	0.95	50.45
% Error	3.87	4.63	---	1.65

Table 4.1.6-A CHN and AAS Data for $Zn(OCH_3)_2$

In spite of repeated washing of the sample no better result could be obtained than that above. The enormous difficulty in removing chloride anion (present at almost 1%) meant that this material could not be considered as a potential precursor for hydrolysis. No further work was done with this material.

4.1.7 Analysis of ε-Zinc (II) Hydroxide, ε-$Zn(OH)_2$

4.1.7(i) CHN and AAS Data for ε-$Zn(OH)_2$

$Zn(OH)_2 = H_2O_2Zn$			$M_{AC} = 97.934624754$	
$M_R = 99.39$	C & N	H	Na	Zn
Calculated	0.00	2.03	0.00	65.78
Found	0.00	2.08	0.00	65.62
% Error	0.00	2.46	0.00	0.24

Table 4.1.7-A CHN and AAS Data for $Zn(OH)_2$

4.1.7(ii) DRIFTS Data for ε-$Zn(OH)_2$

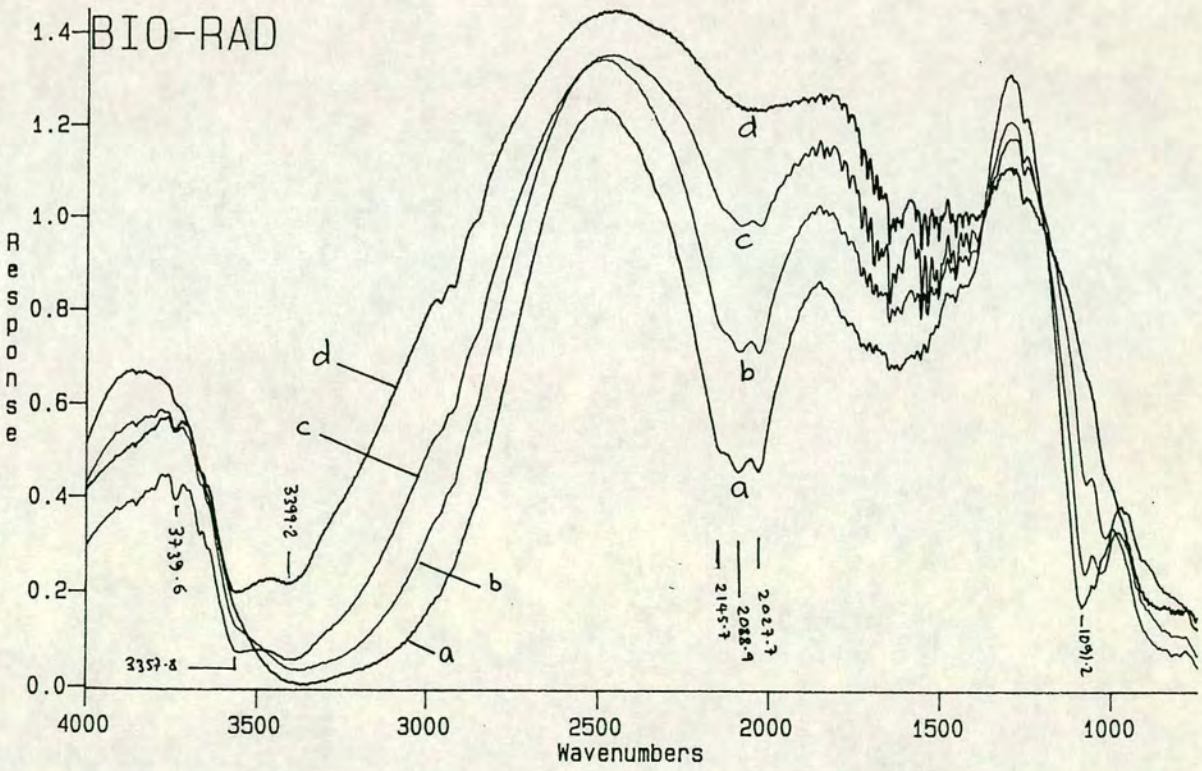

Figure 4.1.7-A The DRIFTS spectra of ε-$Zn(OH)_2$; (a) at 100°C for 1hr; (b) at 110°C for 10min; (c) 115°C for 5 min; (d) 120°C for 5 min. NB the spectrum at room temp. is identical to spectrum (a)

The most important point to arise from the DRIFTS analysis of the prepared sample of ε-$Zn(OH)_2$ is that the surface is not clean. As such it is of no use for analysis of the behaviour of a pure $Zn(OH)_2$ surface with H_2S.

The DRIFTS spectrum is dominated by the hydroxyl feature but the carbonate features are very strong too. The features around 1500cm^{-1} are almost identical to those observed by other authors[1,2] for carbonate species on ZnO surfaces. However, the features between 2077 and 2145cm^{-1} have not been reported before.

To investigate their nature, thermal decomposition of the sample was conducted with simultaneous analysis of the exiting gas phase. It was found that the sample began to decompose above 110^{O}C, but that it was perfectly stable up to *ca.* 100^{O}C. During the decomposition of the hydroxide the peaks centred at 2100cm^{-1} diminished and there was concomitant detection of CO_2 in the gas phase, indicating that these features are some form of carbonate feature. The typical range of carbonate features is 1100-1900cm^{-1}, whereas that of bicarbonates typically show absorptions at 1646, 1438 and 1230cm^{-1}.[3] Interestingly, whilst definitely due to carbon dioxide related species, these features show much higher absorption frequencies than typical of this type of species.

Thermal treatment up to 120^{O}C was sufficient to remove most of the 2100cm^{-1} feature but the carbonate features around 1500cm^{-1} were little diminished. Clearly, the structure of the $Zn(OH)_2$ has been altered as may be observed by the changes in the νOH region. Of interest in the νOH region is the free hydroxyl species shown by the absorption at 3739.6cm^{-1}. This feature is lost upon heating beyond 120^{O}C. From this it is inferred that samples of $Zn(OH)_2$ must be maintained below *ca.* 100^{O}C if studies are to reflect the true nature of its surface behaviour. Thus, heating the

---

1) K. Atherton, G, Newbold and J. A. Hockey, "Infra-red Studies of Zinc Oxide Surfaces", *Disc. Farad. Soc.*, 1971, **52**, 33-54.
2) K. Sohail, Ph.D. Thesis, Dept. Of Engineering, University of Edinburgh, 1992.
3) C. Morterra, A. Zecchina, S. Coluccia and A. Chiorino , "I.r. Spectroscopic Study of CO_2 Adsorption on η-Al_2O_3", *J. Chem. Soc., Farad. Trans.*, 1977, **73(2)**, 1544-1559 and references therein.

sample in an attempt to generate a clean $Zn(OH)_2$ surface is counter productive since it alters the very structure under investigation.

4.1.7(iii) X-Ray Powder Diffraction Data for ε-$Zn(OH)_2$

The XRPD data from the prepared sample is shown below. The results are compared with literature values, shown in red.[4]

Order	2θ	d	d_{ref}	d_{ref} order
1	20.92	4.266	4.268	3
2	27.12	3.288	3.28	2
3	20.32	4.37	4.41	1
4	40.7	2.217	2.208	8
5	32.9	2.722	2.718	5
6	27.87	3.201	3.198	4
7	60.5	1.53	---	---
8	36.6	2.454	2.458	6
9	39.4	2.287	2.288	7

Table 4.1.7-B X-ray powder diffraction data for ε-$Zn(OH)_2$

Conclusions

The standard routes to $Zn(OH)_2$, as anticipated, incorporate ambient CO_2 into their structure as carbonate features. Heat treatment to remove these features alters the structure under investigation.

Future work

Investigate air-free preparative routes to $Zn(OH)_2$. Test the resultant material for H_2S absorption activity. Investigate the nature of the species which shows absorption bands centred at 2100cm^{-1}.

4) *Powder Diffraction File, Inorganic Phases*, JCPDS International Centre for Diffraction Data, 1601 Park Lane, Swarthmore, Pennsylvania 19081 USA, 1982.

4.2 Potential Absorbents for the Desulphiding Reaction

4.2.1 Analysis of Products of the Hydrolysis of $Zn_4O(OAc)_6$

The hydrolysis of $Zn_4O(OAc)_6$ (referred to as TP7) led to the formation of two white, gelatinous products: one of which sank (TP7HS) and the other of which floated (TP7HF). When 1g of $Zn_4O(OAc)_6$, occupying *ca.* 1mL, was initially hydrolysed with *ca.* 20mL of water *ca.* 5mL of TP7HF was produced and *ca.* 3mL of TP7HS.

On examining the products with a glass rod, TP7HF was found to be viscous and gel-like, clinging to the glass rod as it was pushed through its bulk. On passing into TP7HS, this material was found to be even more gelatinous and almost 'glue-like'. The end of the glass rod had to be shaken vigorously to dislodge the attached TP7HS. However, in so doing TP7HS broke into tiny globules which then dispersed to the extent that virtually no TP7HS was visibly remaining.

If the sample was allowed to stand then the sinking product gave rise to increasingly more floating product until almost all the product was TP7HF. Infrared analysis of the remaining washed TP7HS material showed it to be mainlyZnO. Unfortunately, due to the highly dispersed nature of the product, XRPD data could not be obtained for it. DRIFTS analysis of this material showed it to be highly reactive with air (see Fig. 4.2.1-B). However, if a sample of TP7HF was taken and then reacted with water it generated, again, two products, one which floated and one which sank. Similarly for TP7HS.

The proposed reason for the above behaviour was due to the fact that the hydrolysis proceeds very slowly leading to several intermediate species with varying degrees of hydration. Infrared and XRPD analysis of the samples show that the intermediate stages contain unreacted $Zn_4O(OAc)_6$. Once the concentration of $Zn_4O(OAc)_6$ decreased below a threshold value the gelatinous material mixed with it is sufficient to cause it to float. Shaking either of the materials (TP7HF or TP7HS) with more

water forms more of the two products as both have small quantities of unreacted $Zn_4O(OAc)_6$within them and this reacts further to form two new layers.

Ultimately, after about four hours of repeated shaking and settling only TP7HF remains. CHN and AAS analysis of this material shows it to be $Zn(OH)(O_2CCH_3)$. Figure 2.4.1-A shows the DRIFTS spectrum of the $Zn(OH)(O_2CCH_3)$ formed. Note the $\Delta\nu$ value of $163cm^{-1}$ which is almost identical to the value for the free ion ($164cm^{-1}$). No XRPD data could be obtained for this material.

$Zn(OH)(O_2CCH_3)$ = $C_2H_4O_3Zn$			M_{AC} = 139.94518	
M_R = 141.44	C	H	N	Zn
Calculated	17.15	2.88	0.00	45.68
Found	16.97	2.89	0.00	46.23
% Error	1.04	0.35	0.00	1.20

Table 4.2.1-A CHN and AAS Data for $Zn(OH)(O_2CCH_3)$

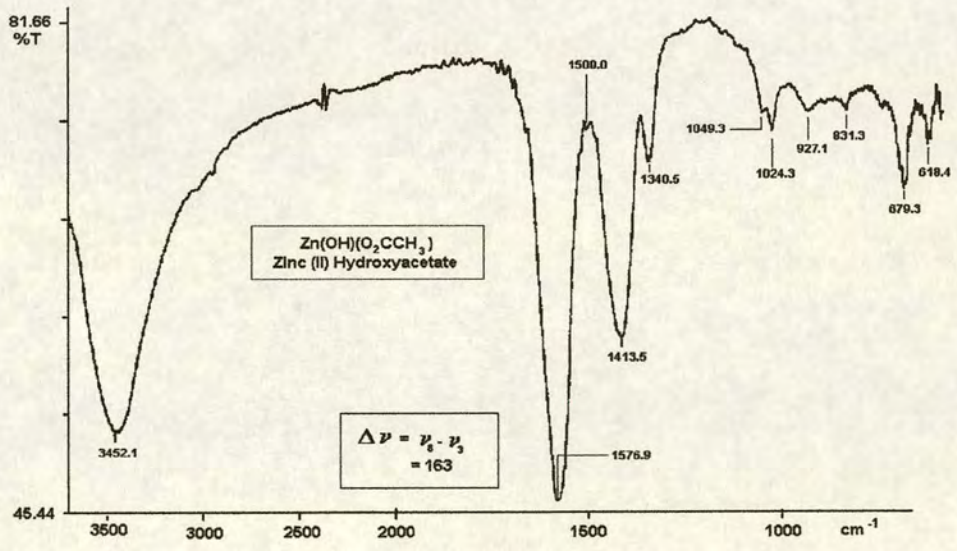

Figure 4.2.1-A Infrared spectrum of zinc(II)acetate, $Zn(OH)(O_2CCH_3)$

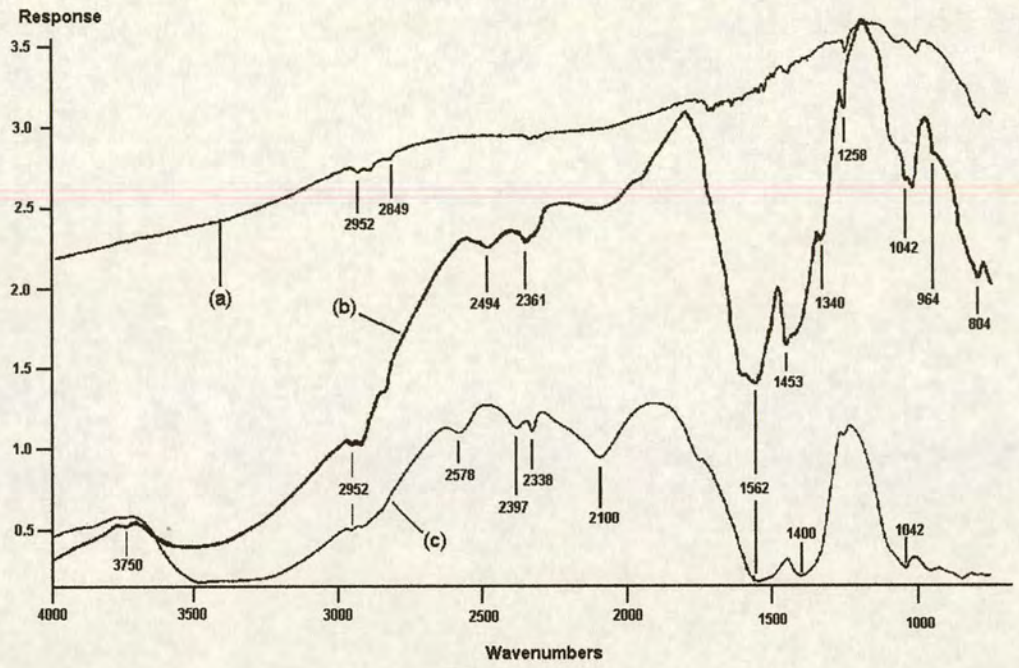

Figure 4.2.1-B The DRIFTS spectrum of TP7HS: (a) product of the hydrolysis of $Zn_4O(OAc)_6$ under flowing nitrogen; (b) the same material exposed to air for 20 minutes; (c) spectrum of $Zn_5(CO_3)_2(OH)_6$ for comparison

The DRIFTS spectrum shown if Fig. 4.1.2-B shows the reactivity of TP7HS to air in reacting with ambient CO_2 and H_2O to produce a material almost identical to $Zn_5(CO_3)_2(OH)_6$. This behaviour suggests that this material may be highly active as an absorbent for H_2S.

Future work

Further testing of the material TP7HS using H_2S should be conducted. In addition, the analysis of the reaction of TP7HS with nitrogen gas stream dosed with CO_2 and/or H_2O would be of academic interest.

CHAPTER 5: APPENDICES

Appendix A2.2.1-A Composition of the Atmosphere[1]

component	percentage by volume
nitrogen	78.08
oxygen	20.95
argon	0.934
carbon dioxide	0.0314
water	0.1-5 (normal range 1-3)
neon	1.818×10^{-3}
helium	5.24×10^{-4}
krypton	1.14×10^{-4}
xenon	8.7×10^{-6}
Trace gases	not listed

Appendix A2.2.1- B The Vapour Pressure of Water

Water vapour itself exerts a partial pressure which requires a correction (slight at lower temperatures) in calculating gas solubilities. The solubility of gases is affected by temperature, decreasing with increasing temperature as shown by the Clausius-Clapeyron equation, where C_1 and C_2 denote the gas concentrations in water at absolute temperatures of T_1 and T_2 respectively; ΔH is the heat of solution and R is the gas constant.

$$\log \frac{C_1}{C_2} = \frac{\Delta H}{2.303\ \mathrm{R}} \left\{ \frac{1}{T_1} - \frac{1}{T_2} \right\}$$

The Clausius Clapeyron Equation

Appendix A2.2.1-C Partial Pressure of Water at Different Temperatures[2]

T, ^{0}C	P_{H_2O}, torr	P_{H_2O}, atm
0	4.579	0.00603
25	23.756	0.03126
50	92.51	0.12172
100	760	1.00000

1) F. Verniani, "The Total Mass of the Earth's Atmosphere", *J. Geophys. Res.*, 1966, **71**, 385-391.
2) S. E. Manahan, "Environmental Chemistry", 4th edn., Lewis Pubs., London, 1990.

Appendix A2.2.1-D Derivation of the Distribution Species Diagram for the CO_2-HCO_3^--CO_3^{2-} System in Water

The H_2CO_3*-HCO_3^--CO_3^{2-} system in water has been described in section 2.3.1-A distribution of species diagram for this system may be prepared with pH as the master variable. Such a diagram shows the major species present in solution as a function of pH. For CO_2 in aqueous solution, the diagram is a series of plots of the fractions present as H_2CO_3*, HCO_3^- and CO_3^{2-} as a function of pH. These fractions, designated as α_x, are given by the following expressions:

$$\alpha_{H_2CO_3^*} = \frac{\left[H_2CO_3^*\right]}{\left[H_2CO_3^*\right]+\left[HCO_3^-\right]+\left[CO_3^{2-}\right]} \quad \text{(i)}$$

$$\alpha_{HCO_3^-} = \frac{\left[HCO_3^-\right]}{\left[H_2CO_3^*\right]+\left[HCO_3^-\right]+\left[CO_3^{2-}\right]} \quad \text{(ii)}$$

$$\alpha_{CO_3^{2-}} = \frac{\left[CO_3^{2-}\right]}{\left[H_2CO_3^*\right]+\left[HCO_3^-\right]+\left[CO_3^{2-}\right]} \quad \text{(iii)}$$

Substitution of the expressions for $[H_2CO_3^*]$, $[HCO_3^-]$ and $[CO_3^{2-}]$ (Eqns. 2.2.1-L, M and N respectively) into the expressions for α_x (Eqns. A2.2.1-D i, ii and iii) gives the fractions of species as a function of acid dissociation constants and hydrogen ion concentration:

$$\alpha_{H_2CO_3^*} = \frac{\left[H^+\right]^2}{\left[H^+\right]^2 + K_1\left[H^+\right] + K_1K_2} \quad \text{(iv)}$$

$$\alpha_{HCO_3^-} = \frac{K_1\left[H^+\right]}{\left[H^+\right]^2 + K_1\left[H^+\right] + K_1K_2} \quad \text{(v)}$$

$$\alpha_{CO_3^{2-}} = \frac{K_1 K_2}{\left[H^+\right]^2 + K_1\left[H^+\right] + K_1 K_2} \qquad \text{(vi)}$$

Examination of the above expressions for fractions of species reveals some basic characteristics of the distribution of species diagram. There are several "landmark points" which make construction of the diagram relatively easy; they are found at:

pH = pK_1 = 6.35, where $\alpha_{CO_2} = \alpha_{HCO_3^-}$;

pH = ½(pK_1 + pK_2) = 8.34, the pH at which $\alpha_{HCO_3^-}$ has its highest value; and

pH = pK_2 = 10.33, where $\alpha_{CO_3^{2-}} = \alpha_{HCO_3^-}$

The significance of these points can be seen in Fig. 2.2.1-A, in chapter 2.

Appendix A2.2.1-E Calculation of the Equilibrium Concentration of CO_2 in Water

Assume that pure air is allowed to come into equilibrium with pure water at 25°C. Since the water is neutral (pH 7) the dissolved carbon dioxide will exist almost exclusively in the forms H_2CO_3* and HCO_3^- and so only the equilibria for these species need be considered. The concentration of H_2CO_3*, HCO_3^- in water may be calculated as follows. The value of [H_2CO_3*] in the water is readily obtained from Henry's Law, given that in dry air[1] the volume fraction of CO_2 is 0.0314%, the vapour pressure of water is 0.0313 atm at 25°C (see appendix A2.2.1-C) and Henry's Law constant for CO_2 is 3.38×10^{-2} L^{-1} atm^{-1} at 25°C [2]

$$P_{CO_2} = (1.0000 \text{ atm} - 0.0313 \text{ atm}) \times 3.14 \times 10^{-4} = 3.04 \times 10^{-4} \text{ atm} \qquad \text{(vii)}$$

$$[H_2CO_3^*] = H_{CO_2} \times P_{CO_2}$$

$$\therefore [H_2CO_3^*] = (3.38 \times 10^{-2} \text{ L}^{-1} \text{ atm}^{-1}) \times (3.04 \times 10^{-4} \text{ atm})$$

$$\therefore \mathbf{[H_2CO_3^*] = 1.028 \times 10^{-5} M} \qquad \text{(viii)}$$

given $M_R(CO_2)$ = 44 $gmol^{-1}$ then [H_2CO_3*] = 4.523×10^{-4} gL^{-1}

Carbon dioxide (as H_2CO_3*) then dissociates partially in water to produce equal concentrations of H^+ and HCO_3^-

$$H_2CO_3^* \overset{K_1}{\rightleftharpoons} HCO_3^- + H^+ \qquad K_1 = \frac{[HCO_3^-][H^+]}{[H_2CO_3^*]} = 4.45 \times 10^{-7} \quad \text{(A2.2.1-F)}$$

The concentrations of H^+ and HCO_3^- are calculated from K_1, the acid dissociation constant for CO_2 (by rearranging Eqn. A2.2.1-F)

$$\therefore [H^+] = \{[CO_2] \times K_1\}^{1/2}$$

$$\therefore [H^+] = \{(1.028 \times 10^{-5}) \times (4.45 \times 10^{-7})\}^{1/2}$$

$$\therefore [H^+] = \mathbf{2.14 \times 10^{-6}\ M = [HCO_3^-]} \qquad \text{(ix)}$$

given $M_R(CO_2) = 44\ gmol^{-1}$ then $[HCO_3^-] = 9.416 \times 10^{-5}\ gL^{-1}$

$$\text{also, } \underline{pH} = -\log[H^+] = -\log(2.14 \times 10^{-6}) = \underline{5.67} \qquad \text{(x)}$$

Thus, the total amount of CO_2 from air dissolving in 1.00 litre of pure water is the sum of $[H_2CO_3^*]$ and $[HCO_3^-]$

$$[H_2CO_3^*] + [HCO_3^-] = (1.028 \times 10^{-5}M) + (2.14 \times 10^{-6}\ M)$$

$$= 1.242 \times 10^{-5}\ mol\ L^{-1}$$

$$\triangleq 0.55\ mg\ L^{-1}$$

$$\triangleq 0.55\ p.p.m.$$

A4.1.5-A Crystal data and structure refinement for $Zn_4O(O_2CC_2H_5)$

Table A4.1.5-A(a)

Identification code	zn4opr
Empirical formula	$C_{18}H_30O_{13}Zn_4$
Formula weight	715.90
Temperature	293(2) K
Wavelength	0.71073 Å
Crystal system	monoclinic
Space group	P21/c
Unit cell dimensions:	
a	16.945(5) Å
b	9.762(3) Å
c	19.053(5) Å
alpha	90 deg.
beta	116.15(2) deg.
gamma	90 deg.
Volume	2829.1(14) $Å^3$
Z	4
Calculated density	1.681 Mg/m^3
Absorption coefficient	3.406 mm^{-1}
F(000)	1448
Crystal size	0.47 x 0.31 x 0.16 mm^3
Theta range for data collection	2.68 to 22.48 deg.
Index ranges	-18<=h<=16, 0<=k<=10, 0<=l<=20
Reflections collected / unique	4154 / 3686 [R(int) = 0.0344]
Refinement method	Full-matrix least-squares on F^2
Data / restraints / parameters	3654 / 150 / 354
Goodness-of-fit on F^2	1.108
Final R indices [I>2sigma(I)]	R1 = 0.0870, wR2 = 0.2318
R indices (all data)	R1 = 0.1382, wR2 = 0.2940
Largest diff. peak and hole	0.702 and -0.655 $e.Å^{-3}$

Table A4.1.5-A(b): Atomic coordinates (x 10^4) and equivalent isotropic displacement parameters ($Å^2$ x 10^3) for $Zn_4O(O_2CEt)_6$. U(eq) is defined as one third of the trace of the orthogonalized U_{ij} tensor.

atom	x	y	z	U(eq)
Zn(1)	5812(1)	601(2)	8534(1)	80(1)
Zn(2)	5554(1)	-2166(2)	7591(1)	76(1)
Zn(3)	3895(1)	-636(2)	7541(1)	81(1)
Zn(4)	4967(2)	655(3)	6699(1)	90(1)
O(1)	5063(6)	-392(10)	7607(6)	64(3)
C(11)	4652(17)	2512(27)	10135(14)	167(12)
C(21)	3985(14)	1714(25)	9451(11)	122(8)
C(31)	4336(13)	1028(20)	8949(11)	87(5)
O(11)	3823(9)	272(15)	8415(8)	98(4)
O(21)	5143(9)	1162(15)	9086(7)	98(4)
C(12A)	1595(43)	883(60)	4990(33)	209(38)
C(22A)	2311(37)	1795(52)	5567(37)	129(24)
C(12B)	2084(31)	2751(53)	5628(31)	170(25)
C(22B)	2245(34)	1324(58)	5404(30)	167(29)
C(32)	3071(15)	950(28)	6092(12)	115(8)
O(12)	3007(9)	132(19)	6599(9)	121(5)
O(22)	3762(11)	1232(19)	6090(8)	128(6)
C(13)	3976(19)	-6165(22)	7609(23)	232(21)
C(23)	3533(15)	-4809(20)	7543(20)	163(12)
C(33)	4018(13)	-3523(22)	7586(12)	98(6)
O(13)	4766(9)	-3631(13)	7610(8)	100(4)
O(23)	3604(10)	-2428(16)	7584(10)	116(5)
C(14)	5971(25)	-3502(25)	5414(18)	229(19)
C(24)	5764(18)	-2004(25)	5422(13)	137(9)
C(34)	5628(14)	-1610(27)	6114(12)	100(6)
O(14)	5725(9)	-2443(14)	6658(8)	101(4)
O(24)	5346(11)	-392(18)	6072(8)	123(5)
C(15A)	8263(24)	-1574(41)	10466(19)	149(18)
C(25A)	7859(24)	-2376(41)	9707(24)	141(19)
C(15B)	8206(43)	-3389(65)	9649(41)	140(28)
C(25B)	7945(35)	-1947(74)	9764(34)	117(35)
C(35)	7076(12)	-1683(26)	9098(13)	100(6)
O(15)	6804(8)	-519(16)	9200(7)	103(4)
O(25)	6650(9)	-2419(16)	8490(9)	109(4)
C(16)	7035(20)	4322(33)	7289(19)	213(16)
C(26)	6596(23)	4162(23)	7812(19)	187(15)
C(36)	6218(20)	2753(23)	7706(25)	140(9)
O(16)	5717(12)	2270(16)	7026(11)	122(5)
O(26)	6268(11)	2264(17)	8281(12)	128(5)

Table A4.1.5-A(c): Bond lengths [Å] and angles [deg] for $Zn_4O(O_2CEt)_6$.

Bond	Bond Length	Bond	Bond Length
Zn(1)-O(1)	1.922(10)	Zn(1)-O(21)	1.935(12)
Zn(1)-O(15)	1.937(13)	Zn(1)-O(26)	1.95(2)
Zn(1)-Zn(4)	3.140(3)	Zn(2)-O(25)	1.907(14)
Zn(2)-O(1)	1.927(10)	Zn(2)-O(14)	1.942(12)
Zn(2)-O(13)	1.968(13)	Zn(2)-Zn(3)	3.148(3)
Zn(2)-Zn(4)	3.158(3)	Zn(3)-O(23)	1.83(2)
Zn(3)-O(12)	1.915(14)	Zn(3)-O(11)	1.938(13)
Zn(3)-O(1)	1.943(9)	Zn(4)-O(24)	1.89(2)
Zn(4)-O(22)	1.935(15)	Zn(4)-O(16)	1.95(2)
Zn(4)-O(1)	1.953(10)	C(11)-C(21)	1.511(10)
C(21)-C(31)	1.489(10)	C(31)-O(11)	1.25(2)
C(31)-O(21)	1.28(2)	C(12A)-C(22A)	1.516(11)
C(22A)-C(32)	1.484(10)	C(12B)-C(22B)	1.516(10)
C(22B)-C(32)	1.482(10)	C(32)-O(22)	1.20(3)
C(32)-O(12)	1.29(3)	C(13)-C(23)	1.500(10)
C(23)-C(33)	1.482(10)	C(33)-O(13)	1.25(2)
C(33)-O(23)	1.28(2)	C(14)-C(24)	1.506(10)
C(24)-C(34)	1.485(10)	C(34)-O(14)	1.27(2)
C(34)-O(24)	1.27(2)	C(15A)-C(25A)	1.517(10)
C(25A)-C(35)	1.486(10)	C(15B)-C(25B)	1.520(11)
C(25B)-C(35)	1.482(10)	C(35)-O(15)	1.27(2)
C(35)-O(25)	1.28(2)	C(16)-C(26)	1.493(10)
C(26)-C(36)	1.493(10)	C(36)-O(26)	1.16(3)
C(36)-O(16)	1.29(3)	O(1)-Zn(1)-O(21)	109.6(5)
O(1)-Zn(1)-O(15)	110.4(5)	O(21)-Zn(1)-O(15)	110.5(6)
O(1)-Zn(1)-O(26)	111.5(6)	O(21)-Zn(1)-O(26)	106.9(7)
O(15)-Zn(1)-O(26)	108.0(7)	O(1)-Zn(1)-Zn(4)	36.2(3)
O(21)-Zn(1)-Zn(4)	120.8(4)	O(15)-Zn(1)-Zn(4)	125.2(4)
O(26)-Zn(1)-Zn(4)	75.3(6)	O(25)-Zn(2)-O(1)	111.0(6)
O(25)-Zn(2)-O(14)	109.0(6)	O(1)-Zn(2)-O(14)	112.2(5)
O(25)-Zn(2)-O(13)	106.8(6)	O(1)-Zn(2)-O(13)	110.6(5)
O(14)-Zn(2)-O(13)	107.0(6)	O(25)-Zn(2)-Zn(3)	126.3(5)
O(1)-Zn(2)-Zn(3)	35.7(3)	O(14)-Zn(2)-Zn(3)	122.0(4)
O(13)-Zn(2)-Zn(3)	75.0(4)	O(25)-Zn(2)-Zn(4)	123.2(5)
O(1)-Zn(2)-Zn(4)	35.8(3)	O(14)-Zn(2)-Zn(4)	76.5(4)
O(13)-Zn(2)-Zn(4)	126.0(4)	Zn(3)-Zn(2)-Zn(4)	60.31(7)
O(23)-Zn(3)-O(12)	107.5(8)	O(23)-Zn(3)-O(11)	106.2(6)
O(12)-Zn(3)-O(11)	107.8(6)	O(23)-Zn(3)-O(1)	113.6(6)
O(12)-Zn(3)-O(1)	111.7(6)	O(11)-Zn(3)-O(1)	109.7(5)
O(23)-Zn(3)-Zn(2)	78.4(5)	O(12)-Zn(3)-Zn(2)	122.4(5)
O(11)-Zn(3)-Zn(2)	125.8(4)	O(1)-Zn(3)-Zn(2)	35.4(3)
O(24)-Zn(4)-O(22)	110.0(7)	O(24)-Zn(4)-O(16)	106.5(7)
O(22)-Zn(4)-O(16)	108.9(8)	O(24)-Zn(4)-O(1)	111.0(5)
O(22)-Zn(4)-O(1)	109.7(6)	O(16)-Zn(4)-O(1)	110.7(6)
O(24)-Zn(4)-Zn(1)	125.5(4)	O(22)-Zn(4)-Zn(1)	121.0(5)
O(16)-Zn(4)-Zn(1)	75.2(5)	O(1)-Zn(4)-Zn(1)	35.5(3)
O(24)-Zn(4)-Zn(2)	75.8(5)	O(22)-Zn(4)-Zn(2)	125.1(6)
O(16)-Zn(4)-Zn(2)	121.9(5)	O(1)-Zn(4)-Zn(2)	35.2(3)
Zn(1)-Zn(4)-Zn(2)	60.35(7)	Zn(1)-O(1)-Zn(2)	110.7(5)
Zn(1)-O(1)-Zn(3)	111.2(4)	Zn(2)-O(1)-Zn(3)	108.9(5)
Zn(1)-O(1)-Zn(4)	108.2(5)	Zn(2)-O(1)-Zn(4)	108.9(4)
Zn(3)-O(1)-Zn(4)	108.8(5)		

Table A4.1.5-A(d): Symmetry transformations used to generate equivalent atoms; Anisotropic displacement parameters ($Å^2 \times 10^3$) for $Zn_4O(O_2CEt)_6$. The anisotropic displacement factor exponent takes the form:$-2\pi^2 [h^2 a^{*2} U11 + ... + 2 h k a^* b^* U12]$

Atom	U11	U22	U33	U23	U13	U12
Zn(1)	66(1)	92(2)	74(1)	-5(1)	25(1)	-5(1)
Zn(2)	70(1)	81(1)	78(1)	4(1)	35(1)	4(1)
Zn(3)	59(1)	102(2)	81(1)	-5(1)	30(1)	-3(1)
Zn(4)	89(2)	109(2)	75(1)	22(1)	40(1)	21(1)
O(1)	57(5)	78(7)	69(6)	-6(5)	39(5)	0(5)
C(11)	268(34)	137(22)	177(24)	-56(18)	174(25)	-40(22)
C(21)	154(20)	147(21)	99(15)	-15(14)	86(15)	13(16)
C(31)	77(12)	94(14)	85(13)	4(10)	32(10)	3(11)
O(11)	94(9)	130(11)	91(9)	-6(8)	62(8)	-13(8)
O(21)	93(8)	126(11)	76(8)	-16(7)	39(7)	2(8)
C(12A)	160(55)	221(72)	119(45)	29(43)	-55(37)	40(49)
C(22A)	119(32)	114(48)	107(38)	-20(26)	8(30)	82(37)
C(12B)	79(31)	191(46)	196(58)	77(43)	20(34)	35(31)
C(22B)	111(27)	162(46)	119(44)	27(35)	-48(35)	-20(35)
C(32)	84(12)	155(22)	71(13)	12(12)	3(11)	38(14)
O(12)	81(8)	178(15)	94(9)	25(10)	29(8)	30(9)
O(22)	104(9)	175(16)	92(10)	44(10)	30(8)	49(11)
C(13)	193(31)	128(18)	458(66)	-6(33)	219(41)	-43(21)
C(23)	111(18)	138(17)	296(38)	-2(24)	141(24)	-13(15)
C(33)	79(13)	123(14)	107(15)	-5(14)	55(12)	-14(11)
O(13)	101(9)	92(8)	127(11)	37(8)	68(8)	17(7)
O(23)	110(10)	115(10)	154(13)	-4(10)	88(11)	-14(8)
C(14)	372(56)	204(29)	202(34)	-65(28)	209(39)	-16(36)
C(24)	152(21)	173(23)	122(18)	3(18)	92(18)	8(20)
C(34)	104(15)	115(15)	107(15)	-11(13)	70(14)	-15(13)
O(14)	130(11)	100(10)	113(10)	6(8)	89(9)	16(8)
O(24)	162(14)	137(12)	83(9)	24(8)	66(9)	45(11)
C(15A)	107(28)	200(44)	99(25)	71(25)	9(20)	15(29)
C(25A)	60(19)	139(35)	161(37)	21(28)	-9(21)	9(18)
C(15B)	103(49)	174(56)	155(63)	52(47)	68(46)	70(42)
C(25B)	113(62)	159(63)	59(40)	27(35)	20(28)	49(52)
C(35)	76(13)	110(16)	100(14)	24(12)	25(10)	22(11)
O(15)	68(7)	131(11)	84(8)	1(8)	11(6)	9(7)
O(25)	86(8)	118(12)	103(10)	19(8)	24(7)	35(8)
C(16)	198(33)	165(31)	312(48)	57(31)	145(33)	-14(25)
C(26)	303(42)	94(18)	242(35)	-46(19)	192(33)	-69(22)
C(36)	120(21)	111(19)	222(27)	2(19)	103(22)	-28(15)
O(16)	145(14)	89(9)	163(13)	8(9)	95(12)	-16(9)
O(26)	110(11)	100(11)	178(15)	-3(10)	67(11)	-32(9)

Table A4.1.5-A(e): Hydrogen coordinates (x 10^4) and isotropic displacement parameters ($Å^2$ x 10^3) for $Zn_4O(O_2CEt)_6$.

Atom	x	y	z	U(eq)
H(11A)	4378(17)	2916(27)	10431(14)	80
H(11B)	5111(17)	1903(27)	10464(14)	80
H(11C)	4897(17)	3221(27)	9942(14)	80
H(21A)	3522(14)	2328(25)	9135(11)	80
H(21B)	3734(14)	1027(25)	9651(11)	80
H(12A)	1066(43)	1329(60)	4629(33)	80
H(12B)	1862(43)	419(60)	4706(33)	80
H(12C)	1455(43)	231(60)	5296(33)	80
H(22A)	2079(37)	2261(52)	5880(37)	80
H(22B)	2488(37)	2449(52)	5288(37)	80
H(12D)	1553(31)	3169(53)	5253(31)	80
H(12E)	2073(31)	2714(53)	6128(31)	80
H(12F)	2581(31)	3281(53)	5671(31)	80
H(22C)	2288(34)	1306(58)	4918(30)	80
H(22D)	1778(34)	736(58)	5376(30)	80
H(13A)	3588(19)	-6908(22)	7572(23)	80
H(13B)	4150(19)	-6237(22)	7194(23)	80
H(13C)	4487(19)	-6205(22)	8103(23)	80
H(23A)	3346(15)	-4772(20)	7950(20)	80
H(23B)	3013(15)	-4804(20)	7053(20)	80
H(14A)	6052(25)	-3688(25)	4956(18)	80
H(14B)	6496(25)	-3742(25)	5872(18)	80
H(14C)	5487(25)	-4034(25)	5399(18)	80
H(24A)	5246(18)	-1764(25)	4959(13)	80
H(24B)	6245(18)	-1476(25)	5428(13)	80
H(15A)	8787(24)	-1943(41)	10879(19)	80
H(15B)	8372(24)	-652(41)	10357(19)	80
H(15C)	7798(24)	-1575(41)	10625(19)	80
H(25A)	7731(24)	-3301(41)	9793(24)	80
H(25B)	8305(24)	-2378(41)	9525(24)	80
H(15D)	8737(43)	-3574(65)	10112(41)	80
H(15E)	7774(43)	-4073(65)	9592(41)	80
H(15F)	8325(43)	-3407(65)	9201(41)	80
H(25C)	8376(35)	-1258(74)	9826(34)	80
H(25D)	7829(35)	-1919(74)	10214(34)	80
H(16A)	7265(20)	5235(33)	7340(19)	80
H(16B)	7511(20)	3677(33)	7467(19)	80
H(16C)	6646(20)	4144(33)	6750(19)	80
H(26A)	6119(23)	4807(23)	7640(19)	80
H(26B)	6979(23)	4342(23)	8352(19)	80